Department of Mechanical Engineering

An Investigation into the Effects of Thermal Errors of a Machine Tool on the Dimensional Accuracy of Parts

Yuxia Lu

This thesis is presented for the degree of
Doctor of Philosophy
of
Curtin University

December 2012

CANDIDATE STATEMENT

To the best of my knowledge and belief, this thesis contains no material previously published by any other person except where due acknowledgement has been made.

This thesis contains no material which has been accepted for the award of any other degree or diploma in any university.

Signature:…….

Date:…….

ABSTRACT

The reduction of machining errors has become increasingly important in modern manufacturing in order to obtain the required quality of parts. Geometric error makes up the basic part of the inaccuracy of the machine tool at the cold stage; however, as the machine running time increases, thermally-induced errors start to play a major role in machined workpiece accuracy. Dimensional accuracy of machined parts could be affected by several factors, such as the machine tool's condition, the workpiece material, machining procedures and the operator's skill. Of these, the machine condition plays an important role in determining the machine's performance and its effects on the final dimensions of machined parts. The machine's condition can be evaluated by its errors which include the machine's built-in geometric and kinematic error, thermal error, cutting force-induced error and other errors.

This research represents a detailed study of the effects of thermal errors of a machine tool on the dimensional accuracy of the parts produced on it. A new model has been developed for the prediction of thermally-induced errors of a three-axis machine tool. By applying the proposed model to real machining examples, the dimensional accuracy of machined parts was improved. The research work presented in this thesis has the following four unique characteristics:

- Investigated the thermal effects on the dimensional accuracy of machined parts by machining several components at different thermal conditions of a machine tool to establish a direct relationship between the dimensional accuracy of machined parts and the machine tool's thermal status.
- Developed a new model for calculating thermally-induced volumetric error where the three axial positioning errors were modelled as functions of ball screw nut temperature and travel distance. The influences of the other 18 error components were ignored due to their insignificant influence.
- Employed a Laser Doppler Displacement Meter (LDDM) with three thermocouples, instead of the expensive laser interferometer and the large number of thermocouples required by the traditional model, to assess the thermally-induced volumetric errors of a three-axis CNC machining centre. The thermally-induced volumetric error predictions were in good agreement with the measured results.
- Applied the newly developed thermally-induced volumetric error compensation model for drilling operations to improve the positioning accuracy of drilled holes. The results show that positioning accuracy of the drilled holes was improved significantly after compensation. The absolute reduction of the positioning errors of drilled holes was an average 30.44 μm at the thermal stable stage, while the average relative reduction ratio of these errors was 77%. Therefore, the proposed thermally-induced volumetric error compensation model can be an effective tool for enhancing the machining accuracy of existing machine tools used in the industry.

ACKNOWLEDGEMENTS

The author gratefully acknowledges the assistance of the following people:

Dr. Nazrul Islam for all his guidance and generous help during the four years of study to complete this research.

The Department of Employment, Training, and Youth Affairs, Government of Commonwealth of Australia, for its financial support through the provision of an Australian Postgraduate Award to support this project.

Mr. John Murray, Lab Manager, Department of Mechanical Engineering at Curtin University, for arranging all the experiments performed during this research.

Messrs. David Collier, Pierre Bastouil, and Carl Lewis, Lab Technicians, Department of Mechanical Engineering at Curtin University, for their assistance in conducting the experimental work.

Finally, I especially thank my husband Guobin, my lovely daughter Shiwan and my son Allen for their encouragement and cooperation that inspired me to complete this thesis.

CONTENTS

LIST OF FIGURES

LIST OF TABLES

NOMENCLATURE

Notation for Chapter 3

D_x	Hole's centre positioning error along the x-axis
D_y	Hole's centre positioning error along the y-axis
T_p	Hole's position tolerance
Δx_3	Tolerance of linear dimension x_3
Δx_4	Tolerance of linear dimension x_4
Δx_{34}	Tolerance of linear dimension x_{34}

Notation for Chapter 4

$\delta_x(x)$	Positioning error when carriage moves in x-axis
$\delta_y(y)$	Positioning error when carriage moves in y-axis
$\delta_z(z)$	Positioning error when carriage moves in z-axis
$\delta_y(x)$	Horizontal straightness error when carriage moves in x-axis
$\delta_z(x)$	Vertical straightness error when carriage moves in x-axis
$\delta_x(y)$	Horizontal straightness error when carriage moves in y-axis
$\delta_z(y)$	Vertical straightness error when carriage moves in y-axis
$\delta_x(z)$	Horizontal straightness error when carriage moves in z-axis
$\delta_y(z)$	Vertical straightness error when carriage moves in z-axis
$\varepsilon_x(x)$	Roll error when carriage moves in x-axis
$\varepsilon_y(x)$	Pitch error when carriage moves in x-axis
$\varepsilon_z(x)$	Yaw error when carriage moves in x-axis
$\varepsilon_x(y)$	Pitch error when carriage moves in y-axis
$\varepsilon_y(y)$	Roll error when carriage moves in y-axis
$\varepsilon_z(y)$	Yaw error when carriage moves in y-axis
$\varepsilon_x(z)$	Pitch error when carriage moves in z-axis
$\varepsilon_y(z)$	Yaw error when carriage moves in z-axis
$\varepsilon_z(z)$	Roll error when carriage moves in z-axis
$\varepsilon_x(\mathrm{r})$	Squareness error of *yoz* plane
$\varepsilon_y(\mathrm{r})$	Squareness error of *xoz* plane

ε_z(r)	Squareness error of *xoy* plane
α	Coefficient of linear thermal expansion
T_{xnut}	*x*-axis nut temperature
T_{ynut}	*y*-axis nut temperature
T_{znut}	*z*-axis nut temperature
β_x, β_y, β_z	Multiplication factors in *x*-, *y*- and *z*-axis respectively
$x_0(T_{xnut})$	*x*-axis origin offsets
$y_0(T_{ynut})$	*y*-axis origin offsets
$z_0(T_{znut})$	*z*-axis origin offsets
X_d, Y_d, Z_d	Vector P_d along *x*-, *y*- and *z*-axis respectively
P_d (X_d, Y_d, Z_d)	Designed position vector
P_m (X_m, Y_m, Z_m)	Measured position vector
PC	Process capability
S	Magnitude of size dimension
IT	Standard tolerance grade number

Notation for Chapter 5

Δf	Frequency shift of the reflected laser beam (LDDM)
$\Delta\theta$	Phase shift of the retro reflector
Δv	Velocity of the retro reflector
Δz	Displacement of the retro reflector
f	Frequency of the laser
c	Speed of the light
a	Thermal expansion coefficient
T_{xnut}	*x*-axis nut temperature
T_{ynut}	*y*-axis nut temperature
T_{znut}	*z*-axis nut temperature.
β_x, β_y, β_z	Multiplication factors in *x*-, *y*- and *z*-axis respectively
T_{x0}	*x*-axis nut temperature at cold start
T_{y0}	*y*-axis nut temperature at cold start
T_{z0}	*z*-axis nut temperature at cold start

Notation for Chapter 6

X_i	A set of position measurements, i =1, 2, 3…N
N	Total number of measurements
X_d	Nominal value (designed position)
X_{avg}	Average position deviation from the designed position
S	Standard position deviation
t	Coefficient (student's t)
R_p	Repeatability
T_{xnut}	x-axis nut temperature
β_x	Multiplication factor in x-axis
T_{x0}	x-axis nut temperature at cold start
a	Thermal linear expansion coefficient
O_x	Origin deviations of work coordinate system
Δx	Thermal drifts of the origin of the MCS
E_{mw}	Travelling error from the origin of MCS to the origin of the WCS
$RErr_x(x, T_{xnut})$	Relative positioning error when the machine travels from the origin of the WCS to the target position at temperature T_{xnut}
$RErr_x(x, T_{x0})$	Relative positioning error when the machine travels from the origin of the WCS to the target position at the cold start (T_{x0}) of the machine
$Err_x(x, T_{xnut})$	Positioning error when the machine travels from the origin of the WCS to the target position at temperature T_{xnut}

Chapter 1

Introduction

1.1 General

Machining is a significant industrial process carried out in most economically developed countries. A country's level of machining activity is directly related to its level of technology and economic wealth. Typically, machining operations serve large manufacturing facilities such as automobile, railway, ship building, aircraft components, home appliance, consumer electronics and construction industries. The cost of machining amounts to more than 15% of the value of all manufactured products in all industrialized countries [1]. A survey to 28 principle producing countries found that the total production of new machine tools was $92.7 billion in 2011 [2]. The national consumption of new machine tools in the USA from April 2010 to April 2011 was about $4.618 billion according to a survey jointly conducted by the Association for Manufacturing Technology (AMT) and the American Machine Tool Distributors' Association (AMTDA) [3].

Machining is one of the most common manufacturing processes and can be applied to a wide variety of work materials such as metals, plastic and composites. Although ceramics are difficult to cut because of their high hardness and brittleness, most ceramics can be successfully cut by the abrasive machining processes. In addition, machining can be used to create any regular and irregular geometry, such as flat planes, round holes, cylinders, screw threads and T-slots. Machining can produce very close tolerance. Some conventional machining processes are capable of producing tolerance of ±0.025 mm [4], much more accurate than most other manufacturing processes. Machining is also capable of creating very good surface finishes; roughness values as low as 0.4 micron can be achieved in some conventional machining operations [4].

In today's highly competitive market, the quest for high productivity and workpiece quality has led to major developments in machining. The most significant revolution in the machining field in the last century is the development of the

Computer Numerical Control (CNC) machine tool. CNC is a form of programmable automation controlled by a program containing coded alphanumeric data. The data represent relative positions between a tool and a workpiece. The operating principle of the CNC is to control the motion of work head relative to the workpiece and to control the sequence of motions.

The machining efficiency and workpiece accuracy of a CNC system are far better than the conventional machine tool due to its feedback system. However, it is impossible to produce any error-free workpiece using any type of machine tool. In some cases, the error produced by a CNC machine tool can even be higher than what is expected, despite the high order of machine accuracy claimed by the CNC machine tool's manufacturer.

Workpiece accuracy can be affected by several factors of which the following are the most significant ones [5]:

(1) the type of material machined,

(2) the shape of the part, its rigidity and stability,

(3) the surface area or size of the surface machined,

(4) the number of operations required to finish machine the dimension,

(5) the condition of the machine and

(6) the skill of the machine operator.

The machine condition includes the machine tool's geometric and kinematic errors, thermal errors, cutting force-induced errors, and other errors. Geometric and kinematic errors comprise the basic component of machine errors which affect the machining accuracy in the cold stage. However, as the machine tool's running time increases, thermal expansion and distortion cause significant changes in the machine tool's condition. Thermally-induced errors could comprise 40%–70% of total dimensional and shape errors of a workpiece [6]. Therefore, in precision machining, the thermal effect plays an important role on workpiece accuracy, the investigation of which is the focus of this research.

1.2 Overview of Machining Technology

Machining is the broad term used for describing the removal of unwanted material from a workpiece in the form of chips. It is an industrial activity for changing the shape of raw material to create component parts. Due to its capability of producing

high tolerance and smooth surface finishes, machining is often performed after other manufacturing processes such as casting, forging and bar drawing to provide the final geometry, dimensions and surface finish. However, the two major drawbacks of machining processes are that it is relatively slow and it produces a large amount of waste in the form of chips.

There are various types of machining processes, each of which is capable of generating a certain part geometry and surface texture. The three most common types are: turning, drilling and milling. Other machining operations include shaping, planing, broaching and sawing. The common feature of different machining processes is the use of a cutting tool to form a chip removed from the workpiece. To perform this operation, relative motion is required between the tool and the workpiece. This relative motion is achieved in most machining operations by means of a primary motion, called the cutting speed, and a secondary motion, called the feed rate. These motions, together with the shape of the tool and its penetration into the work surface (depth of the cut), produce the desired shape of the work surface.

The three most important elements in a machining process are the machine tool, the cutting tool and the cutting conditions. The machine tool is used to hold the workpiece, position the cutting tool relative to the work and provide the power for the machining process. A cutting tool that has one or more sharp cutting edges is employed to form chips which are removed from the workpiece. The most commonly used tool materials are: high speed steel (HSS), cemented carbides, ceramics, cermets, cubic boron nitride (CBN) and diamond. Cutting conditions include cutting speed, feed rate, depth of the cut, and cutting fluid. A cutting fluid is often applied to the machining operation to cool and lubricate the cutting tool. Decisions on selecting the machine tool, the cutting tool and the cutting conditions must give due consideration to workpiece machinability, part geometry, surface finish, and so forth.

Machine tools available today can be classified into two categories: manual machine tools and CNC machine tools. Manual machine tools are tended by a human operator, who loads and unloads the workpieces, changes cutting tools and sets the cutting conditions. CNC tools are designed to accomplish their operation with a form of automation. Both systems have various errors built-in during the construction of the machine tool and produced during the machining. These errors have significant effects on machining accuracy.

1.3 Machining Accuracy

1.3.1 Accuracy and error

The accuracy is defined as the closeness of agreement between a test and the accepted reference value. Error is the amount by which a measured value deviates from its true value. It is closely associated with accuracy. In a machine system, accuracy is the maximum transitional or rotational error between the desired position and the actual position [7].

1.3.2 Machine accuracy

The machine accuracy of a CNC machine refers to the ability of the CNC machine to produce a component within the specified degree of accuracy. The machine accuracy of a CNC machine depends on the structure of the machine as well as on the NC system; therefore, it is the accuracy of the machine tool itself.

1.3.3 Machining accuracy

The machining accuracy, also known as the working accuracy, workpiece accuracy or dimensional accuracy of machined parts, is the accuracy achieved on the machined workpiece. It is obvious that machining accuracy will depend on machine accuracy. Machining accuracy (dimensional accuracy of machined parts) reflects the product quality. According to current dimensioning and tolerancing standards, product quality is evaluated through [8]:

(1) size tolerance,

(2) geometric tolerance, including form, orientation and location tolerance, and

(3) surface texture characteristics.

Size and geometric tolerances are known as dimensional tolerance, which determines dimensional accuracy. In turn, dimensional accuracy shows the degree of agreement of the measured dimension with its desired magnitude.

1.3.4 Why dimensional accuracy of parts is important

Dimensional accuracy of parts is the best way to judge the product's quality. High-quality products are capable of performing precision functions which are widely used in high-technology industries, such as aerospace, biomedical and precision instruments. Although high-accuracy machining increases manufacturing

costs, it may generate considerable savings in the long run. For instance, when a model aircraft's petrol (gasoline) engine is improved by machining parts to high accuracy, the gap between the piston and the cylinder can be made small enough that the piston ring can be eliminated, reducing the cost by 25%. Moreover, without piston rings, a great engine output is obtained because there is less frictional resistance, the wear is minimized, and the assembly or disassembly is easer [9, 10].

In general, machining a part to high accuracy is capable of [10]:

- Creating a highly precise movement
- Reducing the dispersion of the product's function
- Making the parts interchangeable so that corresponding parts made by other factories or firms can be used in their place
- Eliminating the need for adjusting mechanisms and making the assembly and/or adjustments for subsequent processes easier. Specifically, high-accuracy parts are capable of making automatic assembly possible
- Making functions independent of each other
- Maintaining the same level of relative accuracy when the miniaturization is introduced
- Reducing the number of required parts to minimize accumulated error and improving the probabilistic reliability
- Improving the efficiency of the machine
- Reducing the initial costs
- Reducing the running costs
- Extending the life span
- Miniaturizing parts for portability
- Proving initially the validity of a new design; once proven, the accuracy can be relaxed while monitoring performance to achieve the required productivity
- Enabling the design safety factor to be lowered

Therefore, it is imperative to move away from the wrong belief that high-accuracy machining is costly, and realize that high-accuracy machinery often increases product value. The difference in accuracy may be the factor that determines the product's success in today's competitive market.

To achieve high accuracy, it is important to learn all the factors that affect the dimensional accuracy of machined parts. As discussed in Section 1.1, there are six factors affecting the dimensional accuracy. This research will concentrate on the effects of machine conditions (or machine tool errors) on dimensional accuracy of machined parts.

1.4 Machine Tool Errors

In general, a machining centre consists of a bed, column, spindle, slide and various linear and rotary axes. Each of these elements contributes error components to the total errors of the system. The total errors of the machine system can broadly be classified as: geometric and kinematic errors, thermal errors, cutting force-induced errors and other errors.

1.4.1 Geometric and kinematic errors

Geometric and kinematic errors constitute the largest source of inaccuracy and are dominant under a machine's cold-start conditions. Their typical sources are:

(1) within the machine due to its design,

(2) inaccuracies built-in during assembly,

(3) results from tolerance of components used on the machine, and

(4) concerned with quasistatic accuracy of motion surfaces relative to each other.

The total geometric and kinematic errors include errors associated with axial movements of the carriages, such as positioning error, straightness error, pitch error, yaw error and roll error as well as errors associated with rotation of the spindle, such as spindle radial drifts, spindle inclination and spindle radial play. A detailed list of geometric and kinematic errors is shown in Table 1.1.

1.4.2 Thermal errors

As the machine running time increases, errors caused by thermal expansion and deformation play a key role in the inaccuracy of machining. The changes of thermal condition not only increase the level of basic geometric and kinematic errors in value, but also add more error components to the machine's error budget, such as spindle thermal deflection, column bending, workpiece and bed thermal deflection, etc.

1.4.3 Cutting force-induced errors

In recent years, cutting force-induced errors have become more and more severe due to the application of extreme cutting conditions, such as high speed machining. In such conditions, the part is machined from its raw form directly to the finished shape which involves deep depths of cuts and single operations. Therefore, cutting forces as well as temperature become an important source of part distortion and subsequently dynamic or quasistatic errors.

Other errors in CNC machine systems could include the fixture error, controller error, etc. Table 1.1 shows an accurate list of machine errors.

Table 1.1: Error Types [7]

Geometric and Kinematic Errors	**Thermal Errors**
Positioning errors	Spindle axial growth
Straightness errors of each axis in its perpendicular axes	Spindle radial drift
Pitch angular error	Spindle thermal deflection
Roll angular error	Distortion of the spindle region
Yaw angular error	Expansion of the lead screw drive
Abbé error	Expansion and bending of machine column
Reversal errors	Expansion and bending of machine base
Backlash errors	Workpiece and bed thermal deflection
Squareness errors between two axes	Thermal parasitic errors
Contouring error of each axis	**Cutting Force-Induced Errors**
Hysteresis errors	Material instability errors
Non-perpendicularity of axes	Vibration
Spindle radial drift	Workpiece and bed elastic deflection
Spindle axial deviation	Instrumentation errors
Acceleration of axes	Tool wear
Spindle inclination (tilt or wobble errors)	Spindle elastic deflection
Spindle radial play (run-out error)	Cutting force parasitic errors
Friction and stick-slip motion errors	**Fixture Errors**
Inertia force errors while braking/accelerating	Axes offset error
Machine assembly errors	Workpiece slippage
Parasitic movements	Workpiece fixture deformation
	Controller Errors
	Servo errors
	Interpolation algorithmic errors
	Mismatch of position loop gain
	Instrumentation errors
	Noise

1.5 Problem Statement

The performance of machine tools in terms of accuracy is defined by the error of the relative movement between the cutting tool and the workpiece. This relative error is commonly known as volumetric error. Volumetric error includes all the errors presented in the machine tool error budget listed in Table 1.1. However, some error components are not included in the mathematical model because their effects are insignificant. The traditional model for a three-axis machine tool includes 21 error

components, the details of which are given in Chapter 4.

The traditional volumetric error model is effectively applied to a machine's cold start stage. As the machine running time increases, the machine's thermal expansion and distortion become the main contributors to volumetric errors. The traditional volumetric error model no longer effectively demonstrates the real error produced between the cutting tool tip and the designed workpiece dimension. The key deficiencies of the traditional model are:

(1) the 21 geometric error components included in the traditional model are constant values which do not vary with the thermal status of a machine tool, and

(2) measuring thermal variations of the 21 geometric errors at different thermal statuses requires a high-accuracy and costly measuring instrument, such as a laser interferometer.

During measurement, the laser interferometer has to be located in the proximity of the machine tool, and a large number of thermocouples must be attached at different locations which makes it complicated, costly and time-consuming. As a result, in spite of numerous researches published in this area, the findings cannot be applied in the industry to improve the dimensional accuracy of machined parts.

1.6 Objective of the Thesis

The objective of this research is to investigate the effects of thermal errors of a machine tool on the dimensional accuracy of machined parts. To achieve this goal, first a new model will be developed for calculating thermally-induced volumetric error by combining the dominant thermal error components into the traditional geometric error-based volumetric error model. Subsequently, the proposed model will be simplified to make it suitable for industrial applications. Finally, the newly developed model will be verified for its accuracy and applied for improving dimensional accuracy of component parts.

1.7 Layout of the Thesis

The specific objectives and relevance of each chapter of this thesis to the achievement of the main objective are stated below:

Chapter 1: The objectives of this introductory chapter are to introduce the topic

and to justify the reason for undertaking this research.

Chapter 2: The objectives of this chapter are to understand the state of the art regarding thermal error modelling and compensation and to apply the acquired knowledge in formulating the future direction of this research.

Chapter 3: The objective of this chapter is to perform a preliminary study to investigate the relationship between dimensional accuracy of the workpiece and the machine tool's thermal status. A number of workpieces will be machined at different thermal statuses while the machine tools and their dimensional accuracies will be measured offline.

Chapter 4: The objective of this chapter is to develop a new model for predicting the effects of thermally-induced errors of a machine tool on the dimensional accuracy of machined parts. The model should be suitable for application in today's industry.

Chapter 5: The objective of this chapter is to validate the newly developed thermally-induced error model by performing practical experiments in a CNC machining centre. The error components of the machined tool will be measured using a precision measuring instrument, and the predicted values will be compared with the measured values.

Chapter 6: The objective of this chapter is to apply the newly developed thermally-induced volumetric model for error compensation during machining to demonstrate the effectiveness of the model developed in this research.

Chapter 7: The objective of this chapter is to highlight the achievement of this research, to draw conclusions from the whole project and to propose areas of future research interest in thermal errors.

Chapter 2

Literature Review

2.1 Introduction

As indicated in Chapter 1, machine errors originating from the condition of a machine tool have significant effects on the dimensional accuracy of the component parts produced on it. Consequently, extensive researches have been carried out in this area. The objective of this literature review was to identify the state of the art and apply the acquired knowledge in formulating the future direction of this study. From the extensive literature review, it has been established that temperature-induced error has the most significant effects on the dimensional accuracy of machined parts after continuous usage of the machine tool. Therefore, an investigation of thermally-induced machine errors and their influences on the dimensional accuracy of machined parts is of particular interest to today's industry.

This chapter summarizes the research efforts on the effects of three major types of machine tool errors on the dimensional accuracy of parts, *viz.* (1) geometric and kinematic errors, (2) cutting force-induced errors, and (3) thermal errors. Brief introductions of geometric and cutting force-induced error research are given in Sections 2.2 and 2.3, respectively. Section 2.4 presents detailed treatment of the effects of thermal errors, which is the focus of this thesis. Finally, the limitations of previous research are highlighted in the concluding remarks.

Over 100 publications were reviewed during this study and have been classified into three groups according to the error type (as described in Section 1.4). The list of publications presented in Table 2.1 demonstrates the research progress in the field of machine errors.

Table 2.1: Summary of Literature Survey

Group No	Research Area	References
1	Geometric & Kinematic Errors	[11], [12-25], [97], [100], [101]
2	Cutting Force-Induced Errors	[11], [26], [100], [101]
3	Thermal Errors	[6], [27-111]

2.2 Research on Geometric and Kinematic Errors

Geometric errors are those errors that are extant in a machine on account of its basic design, the inaccuracies built-in during assembly and as a result of the components used on the machine. Kinematic errors are concerned with the relative motion errors of several moving machine components that need to move in accordance with precise functional requirements [11]. These errors are particularly significant during the combined motion of different axes; therefore, such errors are more pronounced during actual machining.

Geometric and kinematic errors form the basic inaccuracy of the machine tool in its cold start stage. These errors can be broadly grouped into two classes: one is errors associated with the axial movement of carriages, such as positioning errors, straightness errors, pitch error, yaw error, roll error, contouring errors and machine assembly errors; the other is errors associated with the spindle rotation, such as spindle radial drift, spindle axial deviation and spindle inclination. A detailed list of these errors is given in Table 1.1. The most popular way dealing with these error components is through volumetric error compensation, but not all of the error components are included in the volumetric error compensation model. For a three-axis machine tool, the commonly applied compensation model includes 21 error components [12-17]. Further treatment of volumetric error can be found in Chapter 4.

The first geometric error model was developed in 1977 by Schultschick [18] who formulated a geometric error model for a three-axis jig boring machine. Shortly after, Ferreira and Liu [19] developed a general method for modelling the geometric error of a three-axis machine based on the homogeneous co-ordinate transformation. Subsequently, extensive researches [20-25] have been carried out in this area. The current most common method is modelling the whole machine as a rigid body consisting of a series of linkages. Each linkage has its own error components. Since the whole machine slide system is a chain of moving linkages, tool position can be obtained by multiplying linkage error transformation matrices. The three transitional errors (linear error and straightness errors) and three rotational errors (roll, pitch and yaw) are described by a 4 x 4 transformation matrix for a typical carriage as T_x, T_y, and T_z. Similarly, squareness errors are also represented by a 4 x 4 transformation matrices as T_{xz} and T_{yz}. The total position error, E, due to the carriage movement can

be represented by the equation Eq. 2.1 [13]:

$$E = T_{xz} + T_{yz} + T_x + T_y + T_z \tag{2.1}$$

Measurement of the error components in a three-axis machine tool is typically carried out with the help of a laser interferometer that is capable of measuring most of the errors. However, the angular roll of the axes is measured by an electronic level [13]. In some cases, error measurement is conducted by a master block and a set of gauge blocks [20]. Measurement of the error components is also often done off-line where each error component is measured individually. Ni and Wu [14] devised a special optical system that could simultaneously track on-line up to five errors on each axis. In addition to measurements using the laser interferometer and gauge blocks, certain other tests like contouring accuracy and circular tests are conducted in order to identify the contouring accuracy of the machine and the backlash in each axis respectively [15, 16].

2.3 Research on Cutting Force-Induced Errors

Errors in the workpiece could be caused by excessive deformation at the cutting tool and the workpiece interface due to cutting action [11]. This type of error is one of the major sources of error in metal-cutting machines as the force involved in the cutting action is considerable. As a result of the cutting force, the position of the tool tip with respect to the workpiece varies on account of the distortion of the various elements of the machine. Depending on the stiffness of the structure under the particular cutting conditions, the accuracy of the machine tool would vary.

While real time compensation techniques for geometric and thermal errors have successfully improved machine tool accuracy, most of the current error compensation research has not considered the errors generated due to cutting forces. The argument that has been put forward for neglecting cutting force-induced errors is that, in finish machining, the cutting force is relatively small; as a result, the resultant deflection could be neglected. However, in some cases, the cutting force could be very large and therefore should not be neglected. Forces usually are measured by piezoelectric sensors, strain gauges or dynamometers. The compensation system reads the forces from the sensors in real time and the slide positions from the linear scales or

encoders before applying the mathematical models to calculate the cutting force-induced error components. These errors are then synthesised, and the compensation values for each of the axes are calculated. The values are then transferred into the CNC of the machine to effect the desired compensation [26].

2.4 Research on Thermal Errors

The accuracy of the workpiece produced in metal cutting machine tools is largely influenced by deviations from the planned relative movement between the tool and the workpiece. The deviations might be caused by the thermal expansion and deformation of the machine structure. Continuous usage of a machine tool generates heat at the moving elements, which causes expansion of the structural linkages of the machine that leads to the inaccuracy of positioning the tool. Such errors are called thermal errors and constitute a significant portion of the total error in a machine tool [27].

2.4.1 Identification of thermal errors

The effects of thermal errors on machining accuracy were first recognized by researchers in around 1960. In a 1967 CIRP (International Academy for Production Engineering) keynote paper, Bryan [28] reported the state of thermal error research. Since then, numerous researches in the manufacturing field have been reported [29-41]. In 1990, Bryan [6] summarised observations of CIRP members in another CIRP keynote paper. Opitz reported that the errors caused by thermal deformations have the same or higher order of magnitude as those errors due to the kinematic accuracy and the static and dynamic compliance [6]. Mottu reported that 50% to 60% of errors in precision parts result from thermal errors [6]. Peklenik suggested that the percentage of error from thermal effects may lie between 40% and 70% [6].

As the machine tool accuracy, tooling and cutting performance improve, thermal effects become more critical in their contribution to workpiece quality. Therefore, many researchers believe that the problem related to thermal errors will be one of the most important and troublesome problems in dimensional metrology and precision engineering in the upcoming decades. Bryan [6] observed that the increasing application of automatic manufacturing systems may necessitate a wider investigation into thermal-induced errors. Moore and Victory [32] reported that

thermal expansion is capable of causing troublesome dimensional changes in both workpieces and machines; therefore, the potential reduction in accuracy is neither insignificant nor inevitable. Bryan [28] concluded that the reduction of the thermal sensitivity of machine tools is of great importance and should be the topic of future research activities. Bryan [6] reported that machining accuracy is more often governed by thermal deformation of the structure than by dynamic stiffness.

Since 1967, some significant developments have taken place for improving tolerance capabilities of machine tools, such as the introduction of computers, laser interferometers, diamond turning machines and co-ordinate measuring machines (CMMs). However, in spite of all of these developments and some excellent research work in this field, not much has changed in industry. There were several versions of explanation about this phenomenon; most researchers agree that both the high cost of temperature control and the lack of education in industry theories are responsible for this. Bryan [6] believes that the problem is lack of education rather than cost. His theory was supported by a very common fact that the sun was allowed to shine directly on machine tools and measuring machines in a majority of factories and even in university research laboratories in that time period. Therefore, he suggested that the researchers who understand the real situation should make a sufficiently strong effort to explain this knowledge to industry workers.

The situation changed in the 1990s when the machine tool manufacturers indicated an increasing willingness to collaborate on research to minimize the influence of thermal effects [6]. With the cooperation of the industry and the improvement of computer technology and high-accuracy measuring instruments, the research of thermal error reduction and its application in industry made significant progress by the end of the 20th century.

2.4.2 Classification of thermal problems

The overall thermal problems could be divided into two major categories: (1) the effects of uniform temperature other than the standard temperature of 20ºC, and (2) the effects of non-uniform temperatures, such as temperature gradients and temperature variations, as shown in Fig. 2.1. For every measuring and machining operation, there are three elements, namely, the machine frame, the part and the master (or scale), affected by thermal deformation [6].

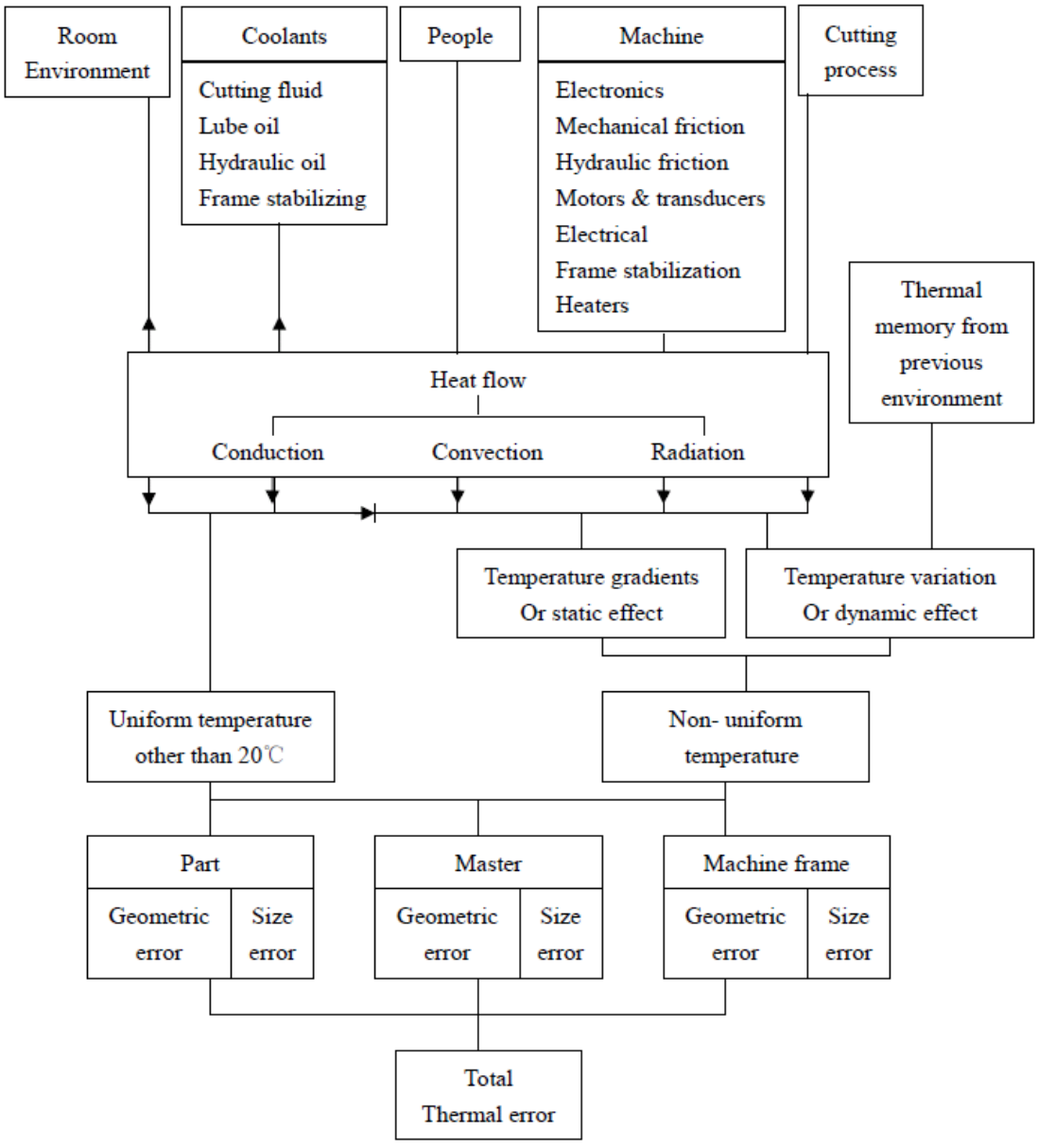

Figure 2.1: Thermal Effects Diagram [6]

Six heat sources are diagnosed in a machine tool [6], as shown in Fig. 2.1: (1) heat generated from the cutting process; (2) heat generated by the machine; (3) heating and cooling influence provided by the various cooling systems; (4) heating or cooling influence provided by the room; (5) the effect of the people; and (6) thermal memory from any previous environment. Room environment and coolant systems are the only influences that can create uniform temperatures other than 20°C. The remaining heat sources will cause either steady-state temperature gradients or temperature variation. Therefore, thermal error is a time and space variant error source.

All sources affect the three-element system through the three possible modes of heat transfer: conduction, convection and radiation, as shown in Fig. 2.1.

2.4.3 Thermal error reduction

The measures proposed by the researchers to reduce the thermal influence fall into three categories [42-47][49-67]: (1) control of heat flow into the machine system, (2) redesign of the frame and scale to reduce their sensitivity to heat flow, and (3) compensation through controlled relative motions within the frame.

Temperature-controlled rooms, boxes and insulation on sensitive elements of the machine are examples of the first type of measures, i.e. controlling heat flow into the frame. As people in industries have begun to realize the thermal influence of the environment on machining accuracy, some progress has been made on temperature-controlled rooms (clean rooms) in recent years. The clean rooms industry is now a mature business with good standards, test methods and design principles. Nevertheless, the temperature-controlled rooms of the best quality available are not good enough to do justice to a large percentage of the world's existing precision engineering equipment. Air and liquid showered boxes are necessary to allow the potential repeatability of this equipment to be revealed and exploited. Boxes consume less energy, they are cheaper than rooms, and they can be moved with the machine if necessary [6].

The feasibility of special boxes has been demonstrated on liquid showered diamond turning machines [46], liquid showered production machines [39], and air showered diamond turning machines [47]. Wirtz [6] kept his Co-ordinate Measuring Machine (CMM) working at 20±0.1°C by building a box around it and installing an air shower inside. With this machine enclosed in a temperature-controlled box, he

was able to (1) save energy; (2) provide better temperature control than before for the machine that greatly needed it; (3) isolate the machine from the operator's body heat; and (4) provide more comfortable temperature control for the students and faculty that utilise the rest of the laboratory for thermally less critical measurements such as surface finish. Fig. 2.2 shows individual precision gear grinding machines enclosed in temperature-controlled boxes in a big industry.

Figure 2.2: Temperature-Controlled Box for Gear Grinding Machine [48]

The selection of aluminium beams for the slide ways of a measuring machine is an example of the second type of measures, i.e. redesigning the frame to reduce sensitivity to heat flow. The high conductivity of aluminium minimizes the temperature difference between the top and bottom of the beam which in turn minimizes the thermal distortions and consequent angular motion and Abbé error [49]. Some researchers [50-54] also suggested using less sensitive to heat materials like cement concrete, fibre-reinforced plastics, etc. in the construction of machine tools. Spindle thermal growth caused by spindle friction is another source of errors in a machine tool. As such, a number of researchers [55-57] have dealt with the spindle friction problem. Instead of the more typical steel, the spindle was made of carbon fibre [55]. Spindle growth was reduced from 30 microns for steel to 2 microns for carbon fibre at 5000 rpm. Weck [6] selected ceramics in the design of aerostatic and

hydrostatic spindles. The ceramic air bearing had axial displacements of only one micron at 1200 rpm for five hours. If one ignores the cost and concentrates on the solution, optimizing the design of the machine tool is the most effective measure. Design measure alone is insufficient; however, to completely avoid thermal displacements, compensation techniques (the thermal error reduction measures presented in the third group) are necessary for increasing the working accuracy especially of numerically controlled machine tools [52]. Trapet and Waldele [49] also predicted that "…in the future, temperature-related errors will be reduced by combined approaches comprising numerical correction and thermo-mechanically advanced construction…"

2.4.4 Compensation techniques

Error compensation is defined as "a method of cancelling the effect of the error by predicting it using a model built for the purpose" [6]. There are two basic approaches to error compensation: (1) pre-calibrated error compensation and (2) active error compensation. The pre-calibrated error compensation technique is based on the assumption that the errors and the measurements are repeatable. In active error compensation, the identification of the error and its control are done simultaneously during machining. There are two general approaches to the identification of errors for active compensation: (1) through an in-process (on-line) gauging and (2) with a mathematical prediction.

Active error compensation through in-process gauging is difficult to implement because it needs highly effective on-line sensors. Due to the developments of sensing, modelling and computer techniques, real time error compensation based on the software approach (mathematical prediction) has received wide attention to further improve the machine accuracy through cost-effective measures [68].

The common procedure for the software approach is: (1) measure the temperatures of critical points on the whole machine space and also the errors induced in the machine at these temperature conditions; (2) match the thermal error data with the temperature readings in order to arrive at a generalized error model that could predict the error depending on the measured temperature values during actual machining; and (3) combine the predicted thermal error values into the individual geometric error components with the help of homogeneous transformation matrices to calculate the compensation data. The compensation data is then transferred to the

CNC controller that carries out the actual compensation. These activities, namely collection of temperature data, collection of encoder feedback signals from the machine, generation of temperature-thermal error map, evaluation of the compensation to be carried out at each axis and interfacing of this data to the machine, are all carried out by an externally situated PC. Compensation is done either by interrupting the encoder feedback and adding/subtracting quadrature pulses or by shifting the origin of the axes during cutting. Thus real time compensation of thermal errors could be achieved.

Measurement of temperature and errors. Measurement of the temperature and error components is the first step towards the goal of improving the accuracy of machine tools. It is also an important requirement for accurate modelling and compensation.

Measurement of temperatures has generally been carried out through thermocouples, which are mostly of foil type construction, either T-type or J-type. Some researchers also used platinum resistance thermometers and thermistors to measure the temperature [69]. The sensors are pasted onto the surface of the heat source and the data monitored periodically. However, the accuracy of surface temperature measurements is greatly reduced by a host of factors, such as: (1) the distortion of the temperature field at the surface area; (2) the presence of a surface coating (e.g., paints) which acts as an additional thermal barrier; (3) imperfect contact between the thermocouple and the surface; and (4) the uncertainty associated with the exact location of the effective junction of the thermocouple [70].

A laser interferometer is widely used to measure the position and orientation errors between the tool and the workpiece, while an electric level is used for the angular roll, the capacitance probe and the optical probes for the spindle drift [71].

Modelling of the thermal error. For effective error compensation, accurate modelling is essential. Homogeneous transformation matrices (HTM) have been applied to model the geometric errors of the machine tool. A kinematic linkage chain of the machine tool is established between the various linkages (axes) and the tool. Thermally-induced errors are typically modelled by various techniques, such as the finite element method (FEM) [72-74], artificial neural networks (ANN) [75, 76] and multi-variant regression (MRA) [75, 77].

FEM is an analytical technique which attempts to capture the entire temperature profile from a finite number of temperature measurements. According to some

researchers' experience [52], analytical techniques such as the finite element or differential method are suitable only for a qualitative description of the thermal behaviour of machine tools because of unknown boundary conditions. Empiric equations have to be utilized for calculating the amount of thermal energy as well as the convective coefficients, as these values cannot be calculated by analytical methods.

ANN is a popular method to develop empirical models between discrete temperature measurements and thermal errors. The MRA model has the advantage that the physical meaning of the model can be easily interpreted. The advantage of the ANN model over the MRA model is that multiple thermal errors could be easily modelled, and thus complex models could be automatically learned. However, the physical meaning of the ANN model is difficult to interpret from the error model.

2.4.5 Research progress on thermal error compensation

Extensive researches have been done in thermally-induced error measurement, error modelling and error compensation. Representative examples of the works carried out in these areas are listed herein. These research works have been classified into three categories according to the machine operating condition during the experiment: (1) temperature and related thermal errors are measured under air cutting (idle running the machine); (2) temperature and related thermal errors are measured under real cutting (i.e. real machining); and (3) complete compensation systems.

Air cutting. Most researchers [77-89] conducted their experiments under idle running conditions, commonly known as "air cutting". It is convenient for measurement and also saves material cost. Yoshida et al. [78] analysed the effect of thermal deformation on the accuracy of a cylindrical grinding machine. The temperature distribution of the grinding machine was determined at about 50 points by means of thermistors. Test stands were built around the machine, and strain gauges were mounted at the 30 measuring points to measure the thermal displacements. The distortion of slide ways was calculated using simple regression equations constructed on the basis of temperature distribution and thermal displacement of the machine. The bed of the cylindrical grinding machine was assumed to be a simple beam. Thermal deflection of the beam was calculated under various kinds of temperature gradients. It was concluded that variation of the cylindrical accuracy of the workpiece was caused by the thermal deformation of the

bed of the grinding machine and that this error could be determined by measuring the temperature distribution or the thermal deformation of the machine.

Experiments conducted at the lab of Purdue University [79] have shown that thermal effects on the accuracy of NC machine tools could be predicted by monitoring the temperature of a few selected points on the machine. A laser interferometer was employed in the measurement of the error components. Four thermometers were mounted at points around the machine to monitor room temperature. Both the data acquisition system and the interferometer were interfaced to a microcomputer. Finite element techniques were employed to obtain the deformations. Their research showed that the accuracy of the machine tool could be predicted by measuring the temperature at a few points on the structure applying a finite element model.

Instead of applying multiple variable regression, Kim and Cho [72] used finite element methods (FEM) with the bilinear (quadrilateral, four nodes) type of elements to analyse the temperature distribution along a ball screw system. The proposed FEM model was based on the assumption that the screw shaft and nut are a solid and hollow shaft respectively. The problem was defined as transient heat conduction in a non-deforming media without radiation. The point temperatures were measured by T-type thermocouples, while the temperature distribution was measured with the help of an infrared radiation thermocouple. From the data obtained, it was found that the temperature distribution and thermal deformation of the ball screw shaft could be considered to vary only in the axial direction; both stop time at each end and the moving velocity affected the temperature rise.

Thermally-induced positioning errors of the cutting edge for a vertical machining centre result from a combination of spindle growth, cantilever-arm bending, *z*-axis expansion, etc. Chen [82] described a quick set-up measurement system consisting of on-machine probes and artefacts in order to calibrate these thermal errors. Spindle drift was calibrated by a spindle-mounted MP7 probe and gauge block fixed on the work table. Thermal expansion of the horizontal linear axis was determined by the variation of the calibrated length of a quartz tube put in parallel with the axis, while that of the vertical axis was achieved by using a granite height gauge. Column bending was calibrated by measuring the co-ordinates of a gauge block at two z levels. Four tests were carried out in order to study the characteristics of thermal errors under different cutting conditions. A three-layer ANN model with a supervised

back propagation algorithm was employed to map the thermal errors to temperature measurements.

Yang et al. [84] introduced a novel concept of thermal error mode analysis in order to develop a better understanding of the thermal deformation on a turning centre. The thermal error of the machine was treated as the superposition of a series of thermal error modes with corresponding mode shapes and time constants. Two basic thermal error modes are thermal expansion and thermal bending. Based on the basic thermal error modes, four key thermal error modes (base bending mode, base expansion mode, *x*-axis ball screw expansion mode and spindle column expansion mode) were identified for the radius error in the *x*-axis direction of the turning machine. A robust modelling approach was also proposed to minimize the errors due to temperature measuring noise and the adverse effect of environmental changes. Through the application of thermal error mode analysis and the robust modelling approach, the number of thermal sensors has been reduced from 16 to four.

A high-speed drive system generates more heat through friction at contact areas, such as the ball screw and the nut, thereby causing thermal expansion which adversely affects machining accuracy. Therefore, the thermal deformation of a ball screw is one of the most important objects to consider for high-accuracy and high-speed machine tools. Wu and Kung [88] conducted several experiments for a ball screw system to investigate its temperature distribution and thermal deformation after a long-term running. Eight thermocouples were attached to specified locations along the ball screw (front and rear bearing, surface of ball screw, etc.) to detect the temperature variations, a capacitance probe was installed next to the driven side of the ball screw with the direction perpendicular to the side surface to record the whole thermal deformation of the ball screw, and a laser interferometer (HP5528A) was deployed to measure the positioning error distribution along the ball screw. The finite element method was used to analyse the thermal behaviour of the ball screw.

Compared with the traditional and stable ball screw feed drive system, linear motors are efficient tools offering high speed and accuracy, which is very competitive in modern industry. The main obstacle to the application of linear motors is the heat generated in the linear motor while operating at high speed. Kim et al. [89] designed several experiments on a horizontal machining centre equipped with linear motors in the *x*-, *y*- and *z*-axes to investigate the important heat sources and resulting thermal errors. The dominant thermal error components were identified from the

thermal error analysis by applying the finite element method. In total, 32 T-type thermocouples were attached to specified locations of the machining centre, such as the linear motors, the linear scales, the linear guide ways, the column and the spindle to measure the temperature variations. The resultant thermal error was measured at the end of the spindle, which was considered the cutting point. The thermal error in the feed direction was measured using a laser interferometer (ML10, Renishaw). Two gap sensors (AEC5505, Applied Electronics) and a photo sensor (FIRH, Takenaka) were used to identify thermal errors in the remaining axes. The tests were conducted at different feed rates with and without coolant to investigate the effects of feed rate and coolant on the thermal behaviour of the machine tool.

Real cutting. The thermal error model for software compensation is typically established from air cutting experiments. The accuracy of the air cutting model in real cutting applications is often questioned. Some researchers think that the thermal profile generated by real cutting conditions cannot be addressed by air cutting because of additional factors such as hot chips, cutting load-induced friction, etc. The following works [90-94] developed thermal error models in real cutting conditions.

Chen [90] studied and compared a multi-variant regression analysis (MRA)-based error model and an artificial neural network (ANN)-based error model built from both air cutting and real cutting conditions. Because the cutting load and applied cutting coolant in real cutting conditions can produce significant thermal effects not explored by the air cutting test, patterns of temperature rises in real cutting are very different from those generated in air cutting. Consequently, the air cutting model performs well in air cutting, but becomes unacceptable in real cutting applications. In some cases, the air cutting model produces an output in the direction opposite to the actual error. On the other hand, the hybrid model established from the air cutting and real cutting data gives satisfactory accuracy in both air and real cutting conditions.

Chen and Ling [91] developed an on-line multi-error measurement system during real machining. In the study, 15 E type thermocouples were used, and the set-up was easy and quick. Seven measurement points were selected over the entire working zone, of which one point was on the centre of the artefacts. The various error components were measured at the different points on the artefacts. The thermal effects at any location of the working zone were then linearly interpolated between these seven points. Thus, error measurement was carried out using an on-machine

probe and with the set of artefacts. An artificial neural network (ANN) based model was applied to map the relationship between the thermal errors and the temperature measurements. A three-layer feed forward ANN applying the sigmoid function was employed. The network was trained by a training set consisting of 540 training pairs of the input vector (temperature) with the output vector (thermal error) collected from several cutting conditions.

Several experiments were carried out on a three-axis vertical machining centre [93]. Both air cutting and real machining tests were conducted on this machine to study the thermal behaviour of the *x*- and *z*-axes. Thirty-two T-type thermocouples of foil construction were glued to different critical machine elements. These sensors were mounted at critical locations like the ball screw end bearings, the ball screw nut, the axis feed motor, the spindle head and motor, the guide ways, etc. These thermocouples were connected to a data acquisition system which in turn was connected to the controller through the RS-232 interface. The results showed that there was a significant increase in the axis positioning error on account of an increase in the temperature of the machine elements due to continuous operation. The specific operating parameters of the test cycles carried out also significantly affected the positioning error, and different sets of operating parameters generated significantly different error values even though the temperature of the machine elements generated by those operating conditions was similar. Based on these phenomena, this paper analysed the thermal behaviour of a three-axis vertical machining centre under the influence of various operating parameters and, through the experimental results obtained, explained the effect of these parameters on the axis positioning errors. An improved modelling methodology based above analysis was presented separately in part II of this paper [94].

Complete compensation system. There are three loops of machine error compensation techniques [95], namely, (1) pre-calibrate and real time compensation, (2) intermittent probing and (3) post machining inspection. Early work on machine tool error compensation focused on post machining inspection. The post-process inspection results were used to modify the NC part program [96]. With the increase of computer capabilities, more research efforts are working towards predicting and compensating for the machine errors before the parts are being machined. In other words, current machine tool error compensation techniques focus on pre-calibrate and real time compensation. The main feature of this technique is the development of

a "Real Time Error Corrector" which intercepts the feedback signal from an encoder (or similar devices) and adds or extracts some pulses according to the compensation command before the feedback signal is sent to the CNC controller. The advantage of this approach is the fact that no intrusion into the CNC controller is necessary [97]. A number of publications [97-101] have described a complete procedure of the "real time error compensation technique," the details of which are given below.

Chen et al. [97] developed an error compensation system to enhance the time-variant volumetric accuracy of a three-axis machining centre by correcting the existing machine errors through sensing, metrology and computer control techniques. A unique form of volumetric error model has been proposed to combine in a single expression both the geometric and thermal errors of a three-axis machining centre. Instead of the well-known 21 geometric errors, 32 thermal and geometric error components have been synthesized by this volumetric error model. All the error components were estimated in real time during machining. Instead of directly identifying the thermal errors, some empirical models (multiple variable, nonlinear regression models) which relate the thermal errors to the temperature field of the machine have been pre-established and then the thermal errors can be estimated on-line utilising the empirical models by monitoring the machine temperature field. In this study, 17 thermocouples were mounted on the machining centre to monitor the temperature variations.

This paper [97] also presented a complete compensation scheme, as shown in Fig. 2.3. A off-line data bank identifies the 21 geometric errors of the machining centre. The temperature field of the machine is monitored on-line by a temperature measurement system. Based on measured temperatures and the co-ordinates of the slides, the pre-established empirical models estimate the thermal error components in real time. A kinematic model then synthesizes the thermal and geometric error components to determine the volumetric error under the current machine conditions. Based on the determined volumetric error, an interface module which consists of three digital I/O boards sends out the compensation signals to the I/O ports of the controller. The controller cyclically picks up the compensation signals from the I/O ports approximately every 10 ms and corrects the volumetric error by shifting the origin of each slide.

Yuan and Ni [100] depicted a general procedure for the compensation of geometric, thermal and cutting force-induced errors (Fig. 2.4). Seven error

components with column thermal deformation were identified in this paper, namely, two straightness components, pitch, yaw, roll errors of the *y*-axis and the squareness errors between the *x*-*y* and *y*-*z* pairs of axes. Employing the telescopic ball bar system, the volumetric errors were measured at some points in the working volume, and the error components were estimated utilising an inverse kinematic algorithm. A total of 19 sensors were needed for the seven error components. The method of origin shift was also included in this research in order to compensate for the error. Data regarding temperature, slide position, etc. were collected in real time, and the error components were estimated by the error models. The resultant errors between the tool tip and the workpiece were calculated by applying the error synthesis model. The compensation signals were then sent to the CNC controller and affected the origin shift. The block diagram of the real time error compensation system is shown in Fig. 2.5.

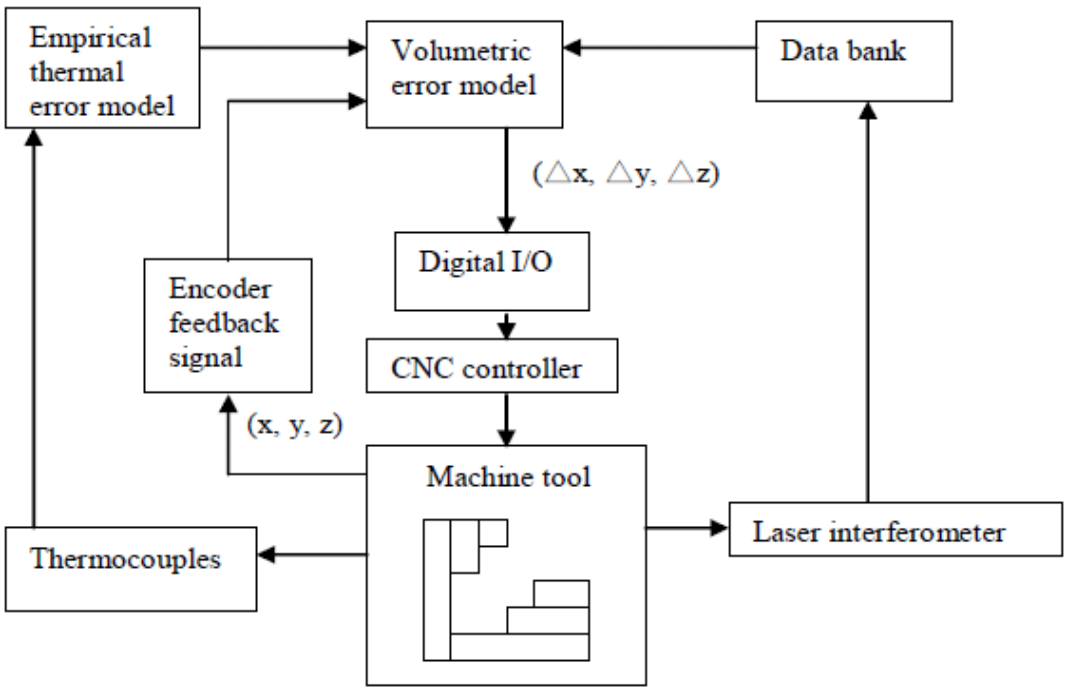

Figure 2.3: The Block Diagram of Error Compensation Scheme [97]

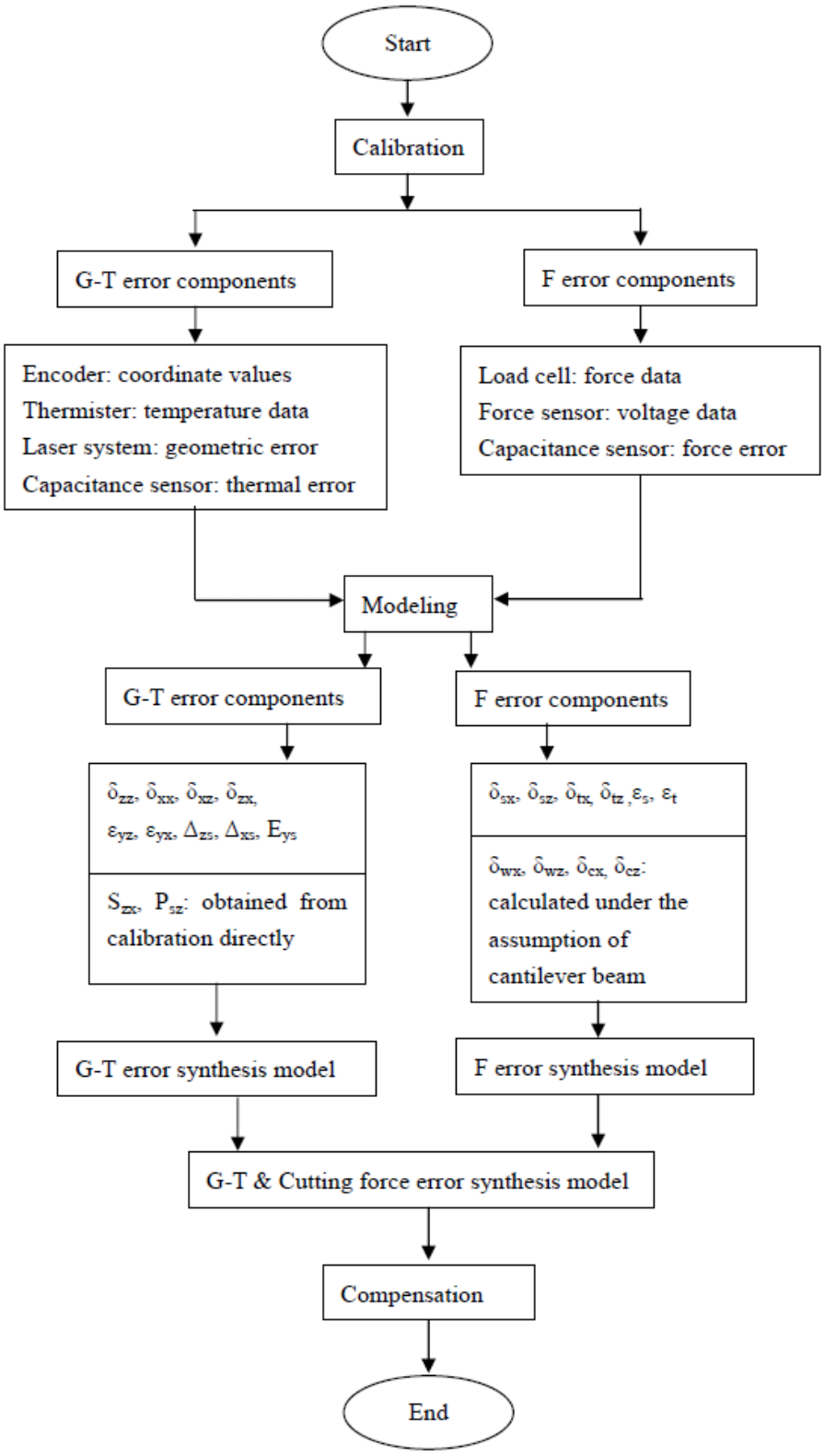

Figure 2.4: General Procedure for Geometric, Thermal and Cutting Force-Induced Error Compensation [100]

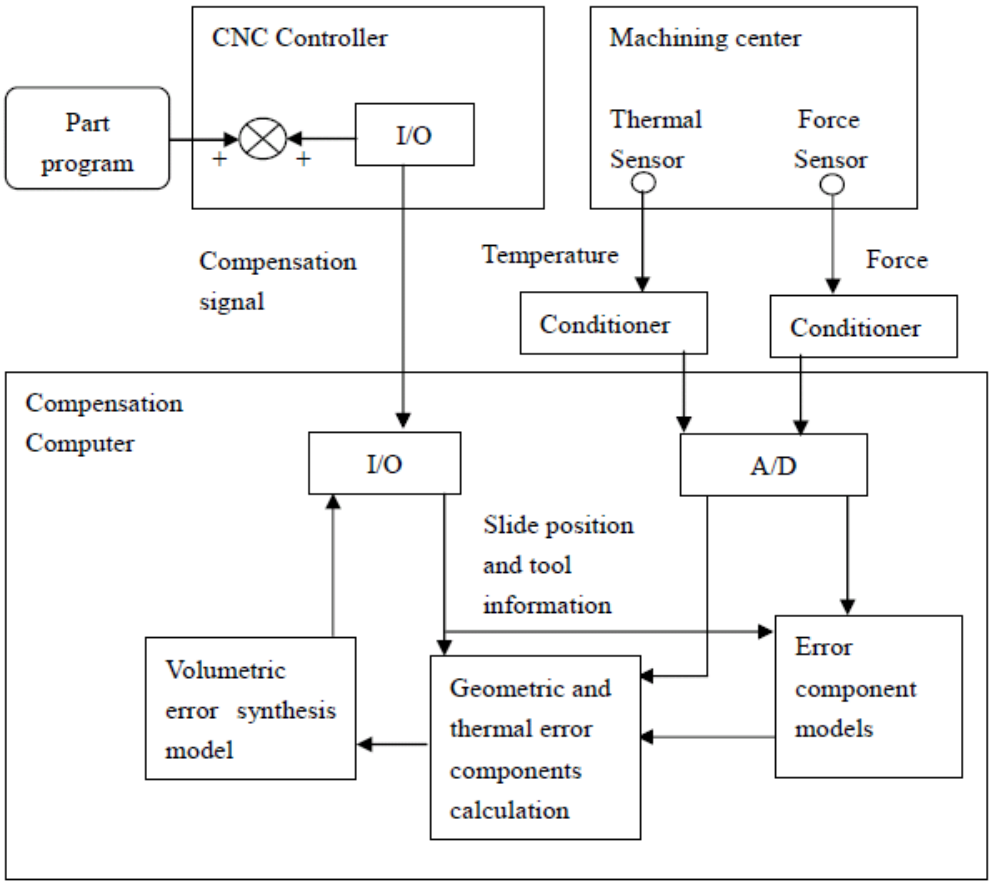

Figure 2.5: The Block Diagram of Real Time Error Compensation System [100]

2.5 Limitations of Previous Research

From this literature review, it appears that, despite a great number of previous works done in the thermal error research area; there are a number of issues that still remain to be addressed:

- Both analytical and empirical models require the measurement of temperature and related thermal error components that have to be obtained by time-consuming, expensive and difficult experiments. This is hard to achieve in ordinary industrial settings.
- Most of the modelling techniques employed in the analysis of thermal behaviour use the overall machine model to arrive at the volumetric error. This is complicated. Some researchers suggest that individual models for each major machine element should be developed and then superposed to get

the overall error model of the system.

- Most of the compensation systems available at present utilise an externally situated computer to perform the task of data acquisition and error modelling, and then the compensation values are fed back into the CNC system of the machine tool through the interface. This is also troublesome and hard to apply for many industries.

2.6 Concluding Remarks

From the literature review presented in this chapter, the following general remarks are drawn:

- Geometric and kinematic errors, thermal errors and cutting force-induced errors are three main contributors to the volumetric error of a machine tool. All of these errors have been modelled, measured and compensated respectively.
- In general, geometric and kinematic errors of a machine tool are modelled using a homogeneous transformation matrix. Measurement of the error components is usually carried out with a laser interferometer that is capable of measuring most of the errors. However, for the measurement of the angular roll of the axes, an electronic level is needed.
- Thermal errors are frequently modelled applying both analytical and empirical methods, namely FEM, ANN and MRA. Measurement of temperature variations are usually carried out by thermocouples, thermometers and thermistors. The corresponding error components are typically measured directly by a laser interferometer or a ball-bar.
- Cutting force-induced errors are calculated from a mathematical model which is the functions of cutting force. Cutting force can be measured by piezoelectric sensors, strain gauges and dynamometers.
- Completed real time error compensation for geometric and kinematic, thermal and cutting force-induced errors has been developed. However, cutting force-induced errors are usually neglected; therefore, the geometric-thermal synthesized model is mostly employed.

Chapter 3

Preliminary Study

3.1 Introduction

There have been numerous researches investigating the thermal behaviour of various machine tools and proposing various methods for reducing their detrimental effects on machining accuracy, typically by measuring and numerically modelling the machine errors. The problem of thermal effects on machining accuracy and its possible solution were first discussed in the CIRP keynote paper titled "International Status of Thermal Error Research" in 1967 [6]. Most researchers have concluded that the thermal error is the major source of error when the machine running time increases. However, to the best of the author's knowledge, no publication has yet investigated the actual relationship between workpiece dimensional accuracy and the machine tool's thermal status, which is a basic requirement for accurate modelling and subsequent reduction/compensation. Therefore, the objective of this chapter is to fulfil this gap.

This chapter describes the experimental work for achieving this goal. The experiment was conducted in the following sequence: (1) investigated the specified CNC machine tool's temperature distribution over the entire machine space under idle running conditions; (2) learnt the temperature rise pattern as the machine tool's running time increases; (3) made a number of test components at different thermal statuses of the machine tool; (4) inspected the dimensional accuracy of a machined workpiece using a precision instrument; and (5) showed the thermal effects on dimensional accuracy of a machined workpiece.

3.2 Experimental Work

3.2.1 Machine setup

All experimental work presented in this chapter were conducted on an EMCO F1 CNC milling machine (Fig. 3.1) manufactured by Emco Maier, Austria. It is a

three-axis machine with 180 x 90 x 170 mm axis strokes along the *x*-, *y*-, and *z*-axes respectively. It is fitted with a ball screw driving system that is capable of operating at a maximum feed rate of 400 mm/min along all axes. The maximum available spindle speed is 2000 rpm. 15 K-type thermocouples were attached to the machine tool to measure the temperature at the locations given in Table 3.1 and Fig. 3.2. A data logger system was employed to retrieve the temperature values from the thermocouples at 15-second intervals.

3.2.2 Temperature measurement

Thermocouples are widely used for measurement and control of temperature. They are inexpensive, interchangeable, supplied with standard connectors and can measure a wide range of temperatures. Thermocouple type K was employed in this experiment. As shown in Table 3.2, thermocouple type K is the most common general purpose thermocouple with a sensitivity of approximately 41 μV/°C. Because one of the constituent metals is nickel, which is magnetic, the K-type thermocouples may undergo a step change in output when the magnetic material reaches its Curie point (around 354°C). However, this was not a problem for this study as the range of temperature variation was far below the Curie point. All thermocouples were shielded and shorter than 40 meters to eliminate the noise effects. The standard limits of K-type thermocouples are one degree centigrade, based on the manufacturer's reports.

The heat sources can be classified into two categories: external and internal. Environment is probably the largest external heat source. The test machine was located in a large air-conditioned room, and no part of the machine was exposed to direct sunlight. To ensure stability of the environmental temperature, none of the other machine tools in the room were running when the experiments were performed. The testing machine was enclosed in a box, and two thermocouples (T14 and T15) were used to measure the ambient temperatures inside and outside the machine box, respectively. The internal heat sources were drive motors, bearings, ball screw nuts and the moving slide. A thermocouple was placed at each heat source. The thermocouples were glued to the machine using high-temperature epoxy. The epoxy held the thermocouple bead to the machine tool and had very high thermal conductivity.

Measurement of thermocouple voltages was performed by two 8-channel input

USB data loggers manufactured by PICO Technology. Measured voltages were converted to temperatures by the software related to this product.

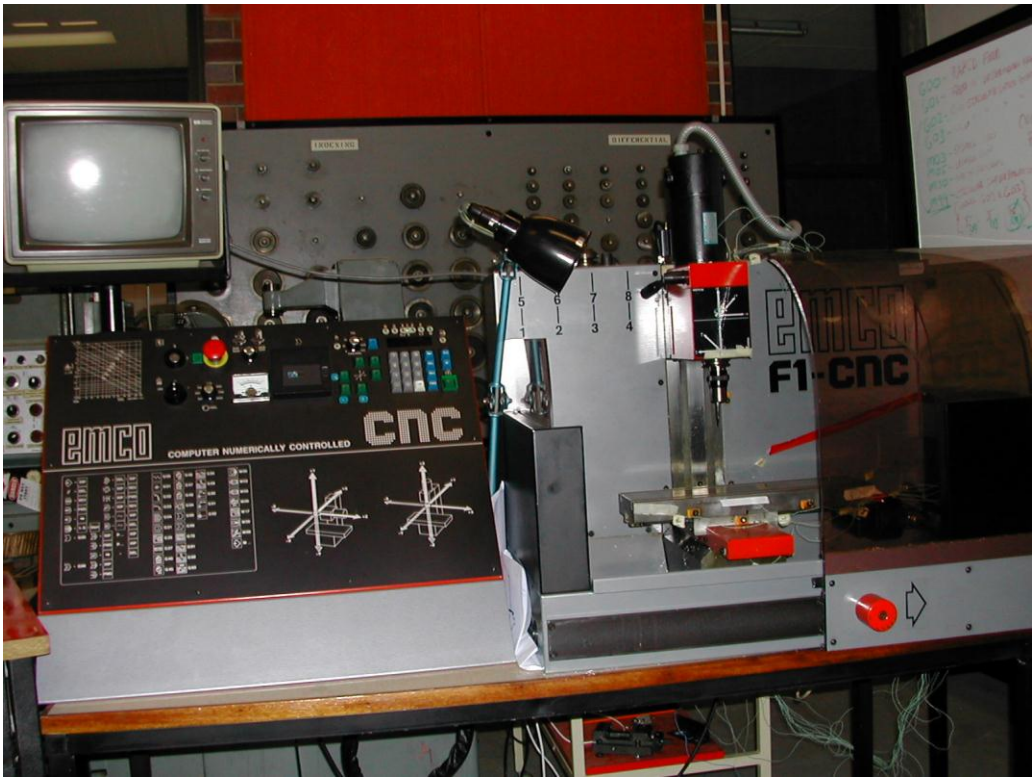

Figure 3.1: Test Machine Setup

Table 3.1: Thermocouple Locations

Sensor	Location on machine	Sensor	Location on machine
T1	Spindle nose	T8	*x*-axis feed motor
T2	Spindle side	T9	*x*-axis feed bearing
T3	*z*-axis feed motor	T10	*y*-axis slide base
T4	Spindle motor	T11	*x*-axis table end (near feed motor)
T5	*y*-axis feed motor	T12	*x*-axis table middle
T6	*z*-axis slide way top	T13	*x*-axis table end (far from feed motor)
T7	*z*-axis slide way bottom	T14 T15	Ambient temp inside of machine box Ambient temp outside of machine box

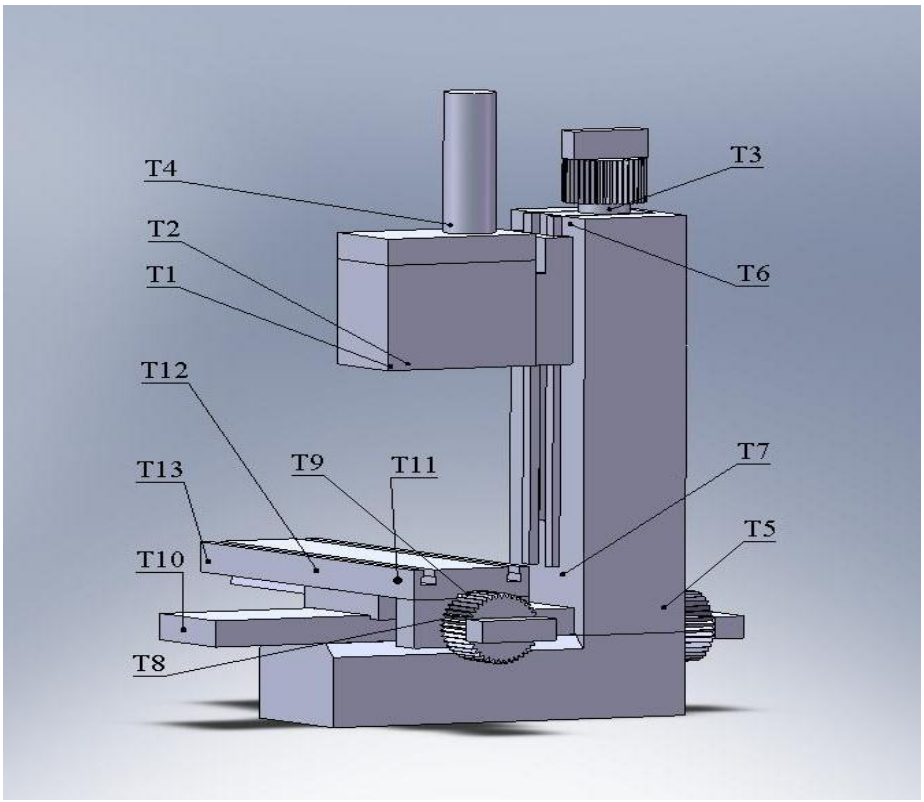

Figure 3.2: Thermocouple Locations

Table 3.2: Characteristics of K-Type Thermocouple

Type	K
Material	Chromel-alumel
Temp. range °C (continuous)	0 to +1100
Temp. range °C (short-term)	−180 to +1300
Tolerance class One (°C)	±1.5 between −40°C and 375°C ±0.004×T between 375°C and 1000°C
Tolerance class Two (°C)	±2.5 between −40°C and 333°C ±0.0075×T between 333°C and 1200°C
Curie point (°C)	354

3.2.3 Test components and cutting tool

A simple test component was designed for this experimental purpose (Fig. 3.3). Twenty-one specimens (120 x 50 x 50 mm) were prepared for these experiments. Seven of them were used for end milling of faces F1 and F2, another seven specimens were used for end milling of faces F3 and F4, and the remaining seven specimens were used for drilling holes H1, H2, H3 and H4. Planes A, B and C were machined with good surface finish so that they were suitable to be datum planes for CMM measurements.

Aluminium alloy 6061 was chosen as the workpiece material because it is readily available and widely used in the industry. It is also relatively easy to machine and capable producing a good surface finish. A high-speed steel (HSS) end mill of 10 mm diameter was used to machine faces F1, F2, F3 and F4. A HSS drill of 10 mm diameter was used to drill the holes denoted by H1 to H4, as shown in Fig. 3.3.

3.2.4 Experiment design

The experimental work described in this chapter was split into two stages. In the first stage, three idle running experiments were conducted before the real cutting tests to learn the machine's thermal behaviour and its influences. The applied cutting conditions are listed in Table 3.3. Experiments for each axis were performed separately to eliminate the combined effects on thermal behaviour when operating on multiple axes. The machine tool was operated at the maximum feed rate along each axis within the maximum stroke to get the machine's temperature distribution under extreme conditions. The spindle was rotating at a speed of 1000 rpm, which is a typical machining speed for this machine. The first experiment was conducted for more than three hours to let the temperature rise stabilise. It was found that the temperature rise slowed down to 1°C per hour after running for three hours. Consequently, following tests were all conducted for three hours for the sake of uniformity as well as for saving time and power consumption.

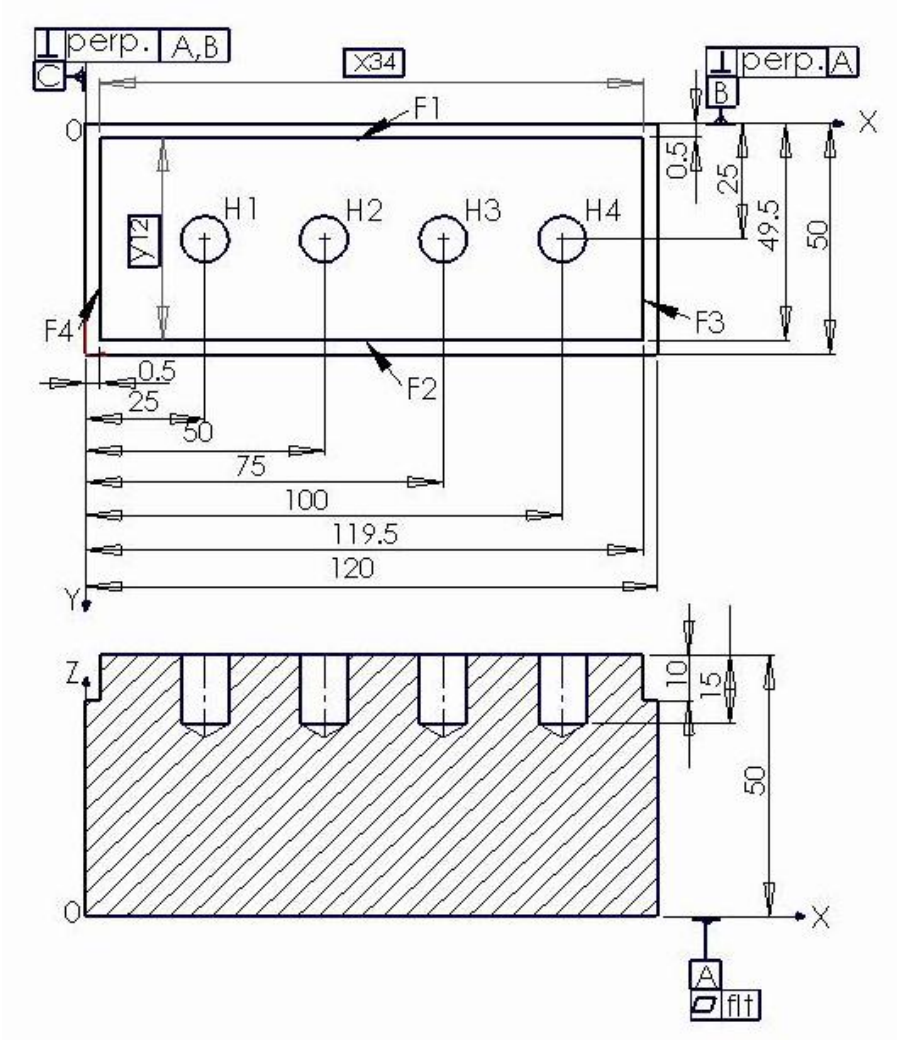

Figure 3.3: Test Component (unit: mm)

At the second stage, three real cutting tests (two end milling and one drilling) were conducted, and seven workpieces marked Part 1 to Part 7 were machined in each mode of machining respectively. Because the machine temperature rose rapidly within the first hour of the experiment, more readings were recorded during this period. In other words, the seven workpieces were machined in different machine thermal statuses (as shown in Table 3.4), corresponding to machine running time 0, 10, 20, 30, 60, 120 and 180 minutes, respectively. The real machining time is longer than the designed time due to the extra time required for loading and unloading the workpiece (as shown in Table 3.3). Recognizing the effect of the type of milling on the dimensional accuracy, the same type of milling (down milling) was chosen for machining all sides of the test component. Other cutting parameters (as shown in

Table 3.3), such as feed rate, spindle speed, radial depth of cut and axial depth of cut, were determined according to the requirement for good surface finish and the machine's machining capability.

The temperature value measured by thermocouple T9 was taken as the reference temperature. All tests were carried out on different days so that the machine had enough time to cool down to room temperature. Neither idle running nor real cutting tests used cooling systems so that the machining could be conducted among real thermal surroundings.

For the real cutting tests, datum planes B and C were set as the origin of the *x*- and *y*-axis, respectively. Consequently, the designed positions for machined elements were as follows: face F1: y_1 = 0.5 mm; face F2: y_2 = 49.5 mm; face F3: x_3 = 119.5 mm; face F4: x_4 = 0.5 mm; hole H1: x_{H1} = 25 mm, y_{H1} = 25 mm; hole H2: x_{H2} = 50 mm, y_{H2} = 25 mm; hole H3: x_{H3} = 75 mm, y_{H3} = 25 mm; hole H4: x_{H4} = 100 mm, y_{H4} = 25 mm.

Fig. 3.4 shows the details of machining operations for milling faces F1, F2, F3 and F4, and drilling holes H1, H2, H3 and H4. Datum planes A, B and C were chosen as the reference planes, and the same procedures were followed while doing the CMM inspection.

3.2.5 Workpiece inspection using CMM

The CMM used in this study is Discovery Model D-8, manufactured by Sheffield, UK (as shown in Fig. 3.5). It is structured with a moving bridge configuration, 508 x 609 x 406 mm measuring range, precision driving systems for all three axes, touch trigger probe, a microscopic grating scale, and the most popular and powerful metrology software *PC-DMIS*. The probes used were spherical probes with a star configuration, manufactured by Renishaw Electrical Ltd. A large number of points, 11x13 points for faces F1 and F2, 10x11 points for faces F3 and F4, were measured to determine geometric characteristics of each face, including position of the surface, that were later used to determine the distance between two machined surfaces. In addition, eight points were probed at a number of height levels (12 levels per hole) to determine the hole's centre position and diameter.

Table 3.3: Cutting Conditions

Exp. No.	Axis	Feed rate (mm/min)	Spindle (rpm)	Stroke (mm)	Time (min)	Mode of operation
1.1	X	400	0	180	180	Idle running
1.2	Y	400	1000	90	180	Idle running
1.3	Z	400	1000	170	180	Idle running
2.1	X, Y	X: 250 Y: 400	2000		220	Down milling face F1 and F2 Radial depth of cut: 0.5 mm Axial depth of cut: 10 mm Machine running time: 8, 28, 80, 115, 154, 188, 219 min
2.2	X, Y	X: 250 Y: 250	2000		207	Down milling face F3 and F4 Radial depth of cut: 0.5 mm Axial depth of cut: 10 mm Machine running time: 10, 25, 50, 82, 124, 165, 207 min
2.3	X, Y, Z	X, Y: 400 Z: 100	2000		258	Drilling hole H1, H2, H3 and H4 Machine running time: 10, 28, 62, 118, 167, 211, 258 min

Table 3.4: Thermal Status While Machining Parts

Part No.	Exp. No. 2.1		Exp. No. 2.2		Exp. No. 2.3	
	Time (min)	Temp. (T9: °C)	Time (min)	Temp. (T9: °C)	Time (min)	Temp. (T9: °C)
1	8	26.8	10	21.0	10	28.8
2	28	32.2	25	28.1	28	34.4
3	80	36.6	50	37.2	62	39.9
4	115	38.0	82	43.0	118	43.7
5	154	39.1	124	46.4	167	46.7
6	188	39.8	165	48.4	211	48.9
7	219	40.4	207	49.5	258	49.5

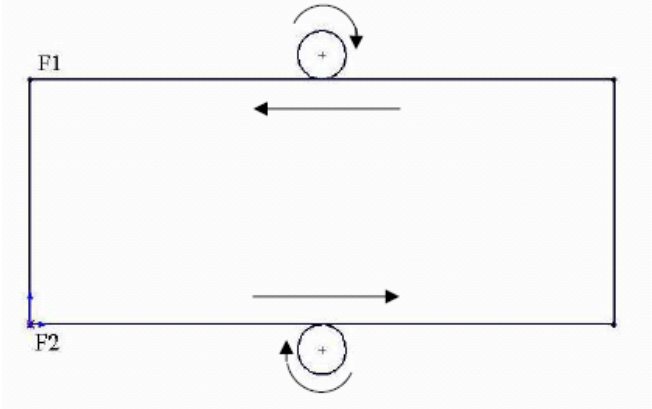

(a) Down Milling Faces F1 and F2 (Exp. No. 2.1)

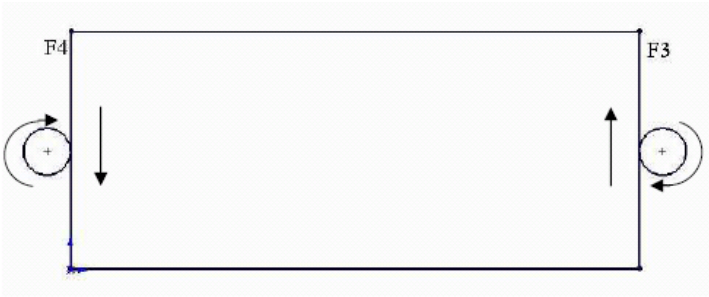

(b) Down Milling Faces F3 and F4 (Exp. No. 2.2)

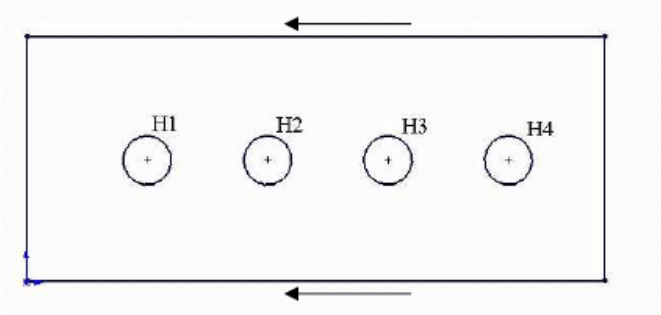

(c) Drilling Holes H1, H2, H3 and H4 (Exp. No. 2.3)

Figure 3.4: Details of Machining Operations: (a) Down Milling of Faces F1 and F2; (b) Down Milling of Faces F3 and F4; (c) Drilling of Holes H1, H2, H3, and H4

Figure 3.5: CMM Used in This Study [112]

3.3 Results and Analysis

3.3.1 Machine tool's thermal behaviour

Fig. 3.6 illustrates the variations of temperature monitored by all thermocouples when the machine tool moved along the *x*-axis, i.e. during Exp. No. 1.1, the details of which are given in Table 3.3. Three motor temperatures are in colour (Fig. 3.6a) to

emphasize the temperature variations of the main heat sources. To give a clear view, variations of temperature at different locations specifically related with *x*-axis movement are shown in Fig. 3.7. It can be observed that the *x*-motor temperature T8 gets the maximum temperature rise, followed by the *x*-axis end bearing temperature T9 and table end temperature T11, which are all close to the *x*-motor. End bearing T9 not only gets heat from the motor but also produces heat due to friction; therefore, the temperature variations of the end bearing are also significant. The temperature variation curves illustrated in Fig. 3.7 show that the temperature reduces as the position of the thermocouples moves away from the main heat source. This non-uniform temperature variation may have significant effects on the *x*-positioning error.

The variations of temperature monitored by all thermocouples when the machine tool moved along the *y*-axis (Exp. No. 1.2) are shown in Fig. 3.8. Three motor temperatures are in colour (Fig. 3.8a) to emphasize the temperature variations of the main heat sources. It demonstrates that the *y*-motor temperature T5 gets the maximum variations, followed by the *x*-motor temperature T8 and *z*-motor temperature T3. Fig. 3.9 compares the temperatures of the *y*-axis motor and the *y*-axis slide base. It indicates that the temperatures reduce along the *y*-axis from the motor to the slide base. This non-uniform temperature variation may have significant effects on the *y*-positioning error.

The variations of temperature monitored by all thermocouples when the machine tool moved along the *z*-axis (Exp. No. 1.3) are shown in Fig. 3.10. Three motor temperatures are in colour (Fig. 3.10a) to emphasize the temperature variations of the main heat sources. The variations of temperature at different locations specifically related with the movement along the column (i.e., *z*-axis movement) are illustrated in Fig. 3.11. It shows that the *z*-motor temperature T3 gets the highest value among all the machine elements, followed by the temperature of the *x*-motor T8, the *y*-motor T5 and the spindle motor T4. Temperature variation along the column is the main reason that causes column bending, which leads to spindle drifts and subsequently affects the dimensional accuracy of machined parts.

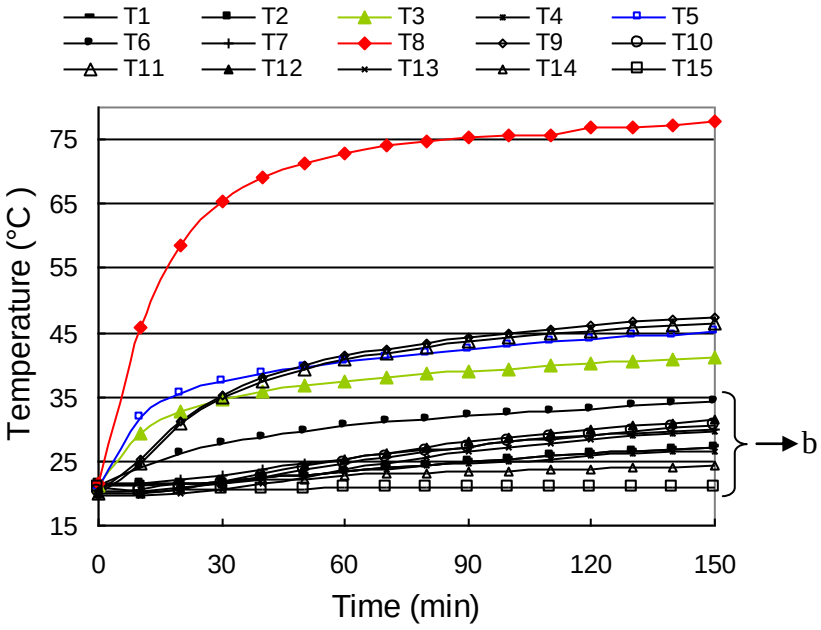

(a)

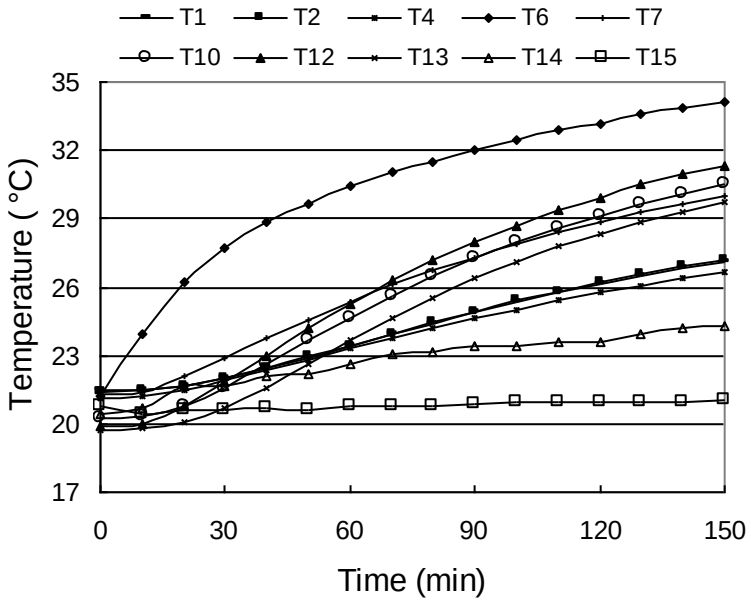

(b)

Figure 3.6: Temperature Variation vs. Machine Running Time for the *x*-axis (Exp. No. 1.1)

(a) Full Temperature Range (three motor temperatures are in colour) and

(b) Enlarged Temperature Range

The following observations can be made from the first stage of experimental investigations:

- All the motor temperatures (T3, T5 and T8) change abruptly during the first machine running hour, and then the changes in temperature gradually slow down. After about two-and-a-half hours, the temperature rise slows down to 1°C per hour.
- Variations of temperature at locations T1, T2, T6, T9 and T11, which are close to different motors, follow the same pattern as the motor temperature variation.
- While the machine moves in only one direction, the other two motors still produce heat that affects the thermal behaviour of the machine tool system.
- Significant temperature gradient is observed along the *x*-axis, *y*-axis and column respectively. These phenomena might significantly affect the positioning accuracy of the cutting tool tip to the designed dimension.

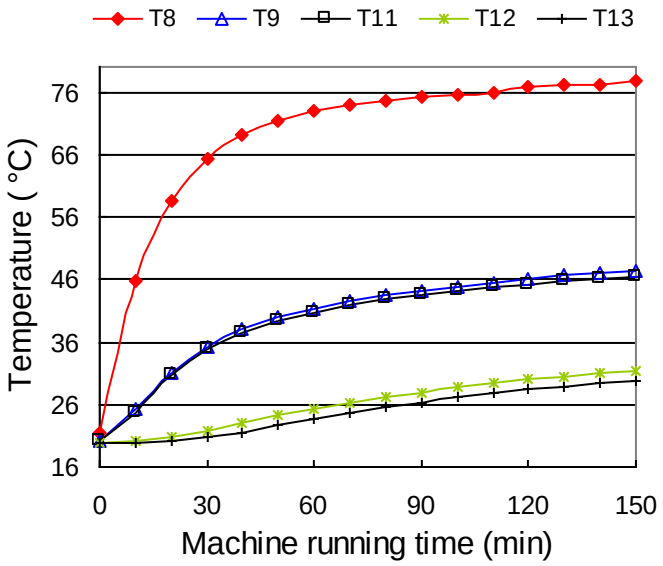

Figure 3.7: Variation of Temperature along *x*-axis (Exp. No. 1.1)

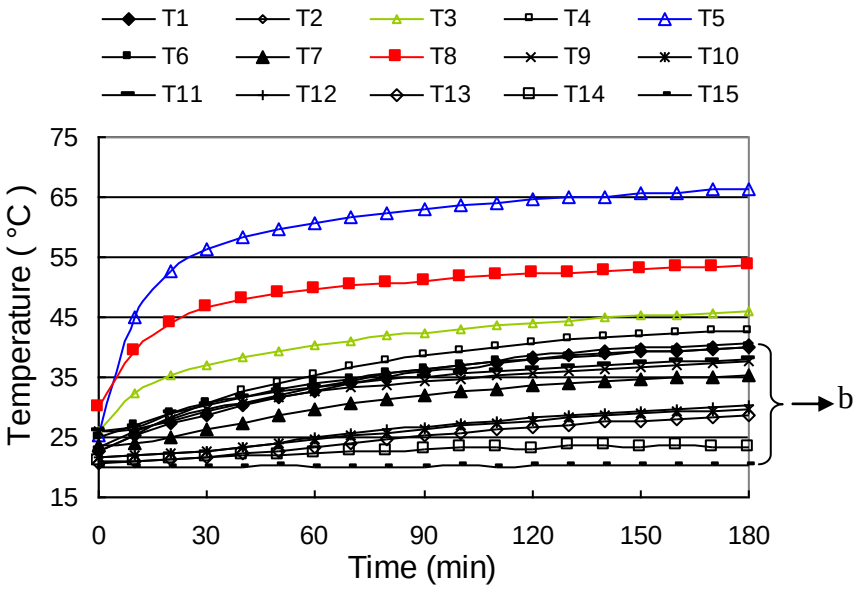

(a)

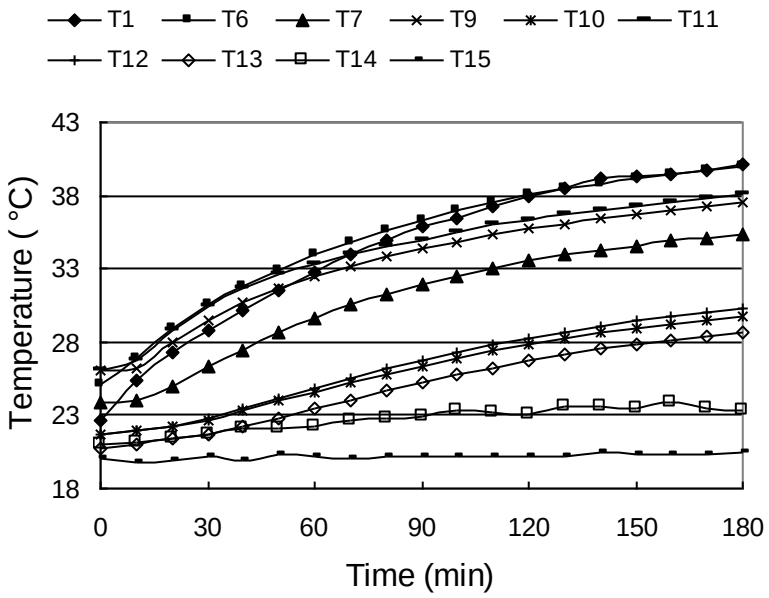

(b)

Figure 3.8: Temperature Variation vs. Machine Running Time for the *y*-axis (Exp. No. 1.2)

(a) Full Temperature Range (three motor temperatures are in colour) and

(b) Enlarged Temperature Range

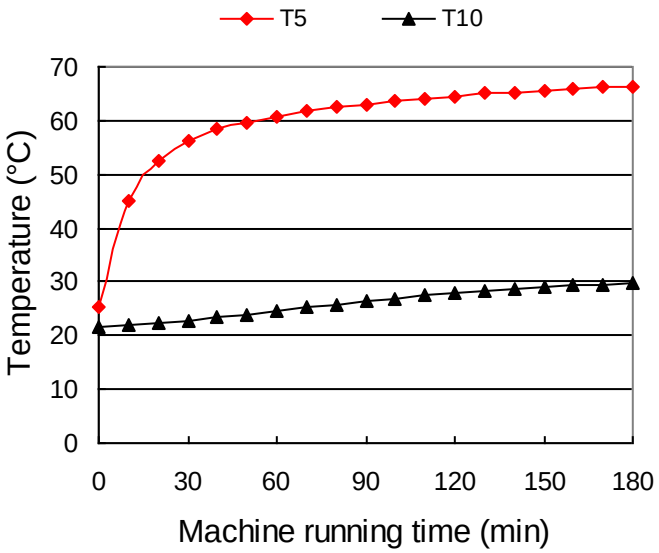

Figure 3.9: Variation of Temperature along *y*-axis (Exp. No. 1.2)

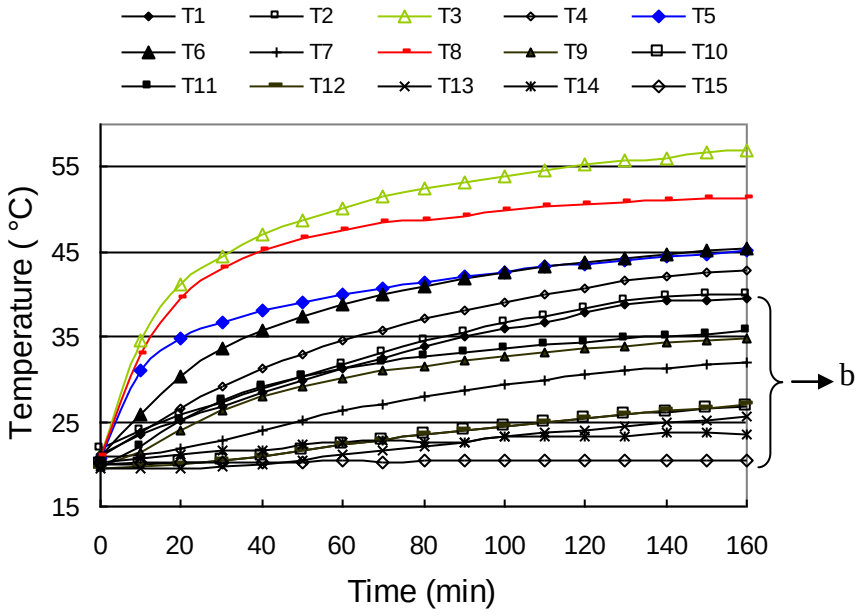

(a)

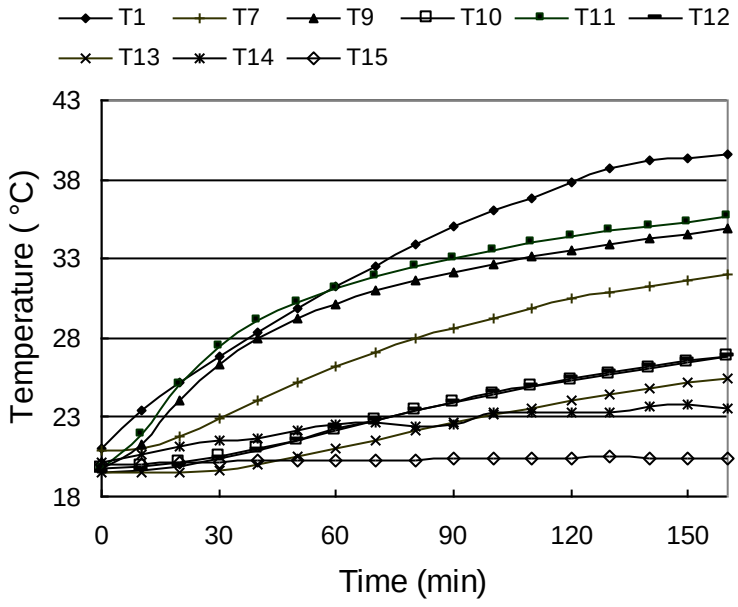

(b)

Figure 3.10: Temperature Variation vs. Machine Running Time for the *z*-axis (Exp. No. 1.3)

(a) Full Temperature Range (three motor temperatures are in colour) and

(b) Enlarged Temperature Range

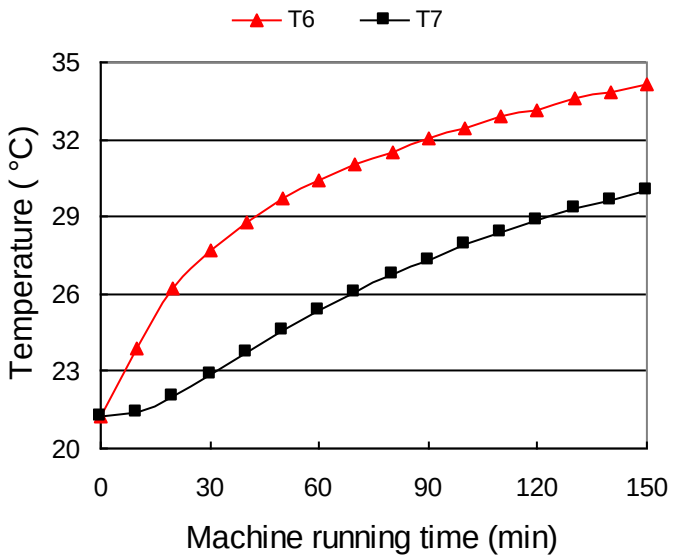

Figure 3.11: Variation of Temperature along *z*-axis (Exp. No. 1.3)

3.3.2 Thermal effects on dimensional accuracy

Flatness error. Flatness is one of the most important geometric characteristics of a plane that influences the dimensional accuracy of machined parts, especially when the plane is a datum plane. It may also influence the properties and performance characteristics of a finished component part. The flatness error is a measure of the difference between the highest and the lowest values in the frequency distribution of all points on a plane; thus, it specifies a tolerance zone defined by two parallel planes between which the entire surface must lie. The flatness errors of machined faces F1 and F2 at different thermal conditions of the machine tool are shown in Fig. 3.12. The figure demonstrates that the flatness errors of machined surfaces are greatly influenced during the machine tool's warm-up period due to the machine tool's thermally unstable conditions. During this period, the flatness errors are high; they stabilize to lower values when the machine tool enters thermally stable conditions. The flatness errors of faces F3 and F4 showed similar trends (Fig. 3.13).

The profiles of faces F1, F2, F3 and F4 machined during different thermal conditions of the machine tool are shown in Fig. 3.14 – Fig. 3.17. It can be seen that the face F1 of parts 5, 6 and 7 machined during the thermally stable stage is flatter than that of other parts produced during thermally unstable stages. It also shows that

the machine tool's thermal status has a significant influence on positioning errors (measured position minus designed position).

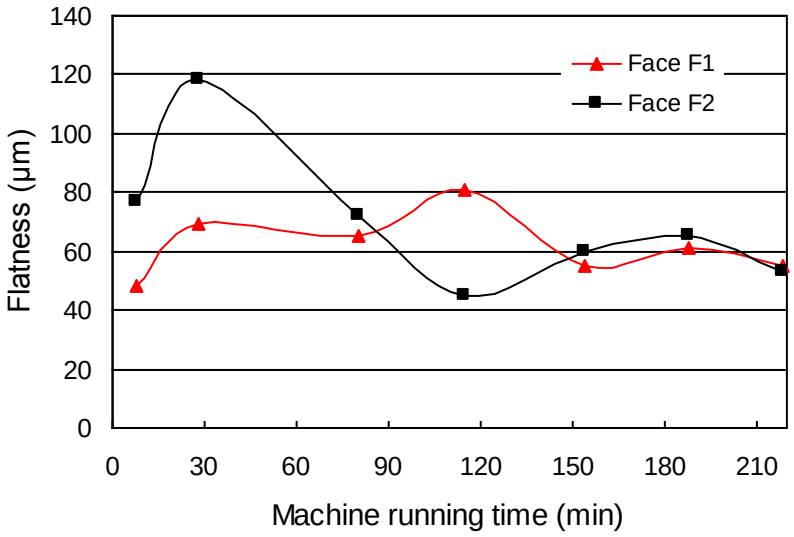

Figure 3.12: Variation of Flatness Error of Faces F1 and F2 (Exp. No. 2.1)

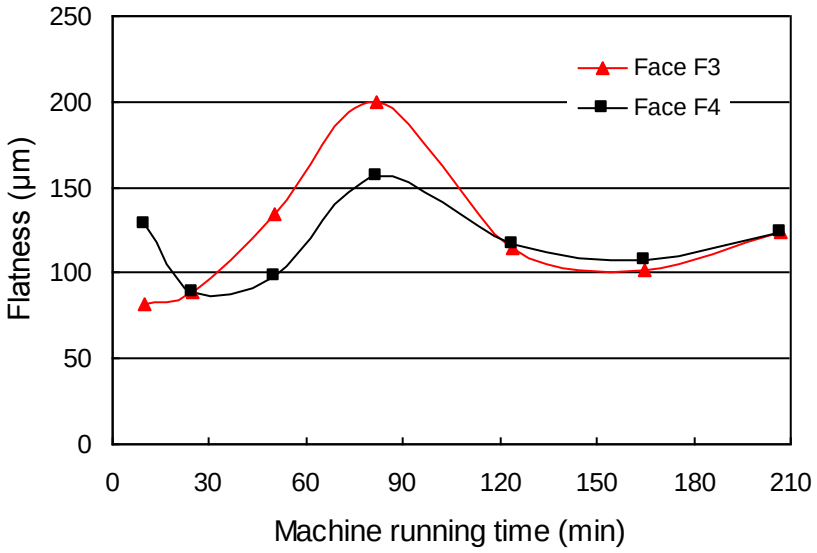

Figure 3.13: Variation of Flatness Error of Faces F3 and F4 (Exp. No. 2.2)

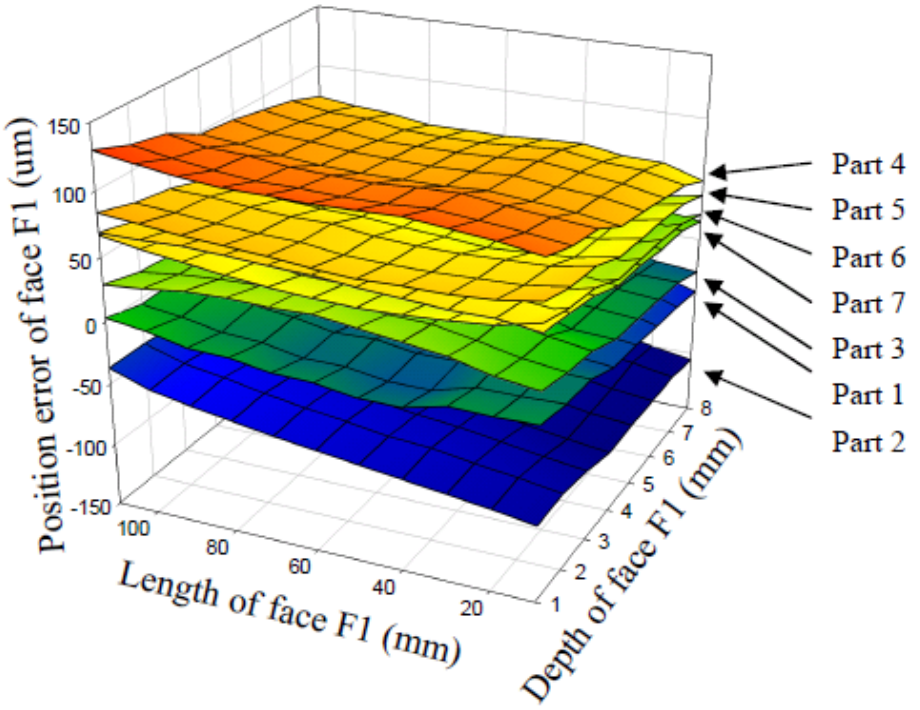

Figure 3.14: Profiles of Face F1 Machined at Different Thermal Statuses (Exp. No 2.1)

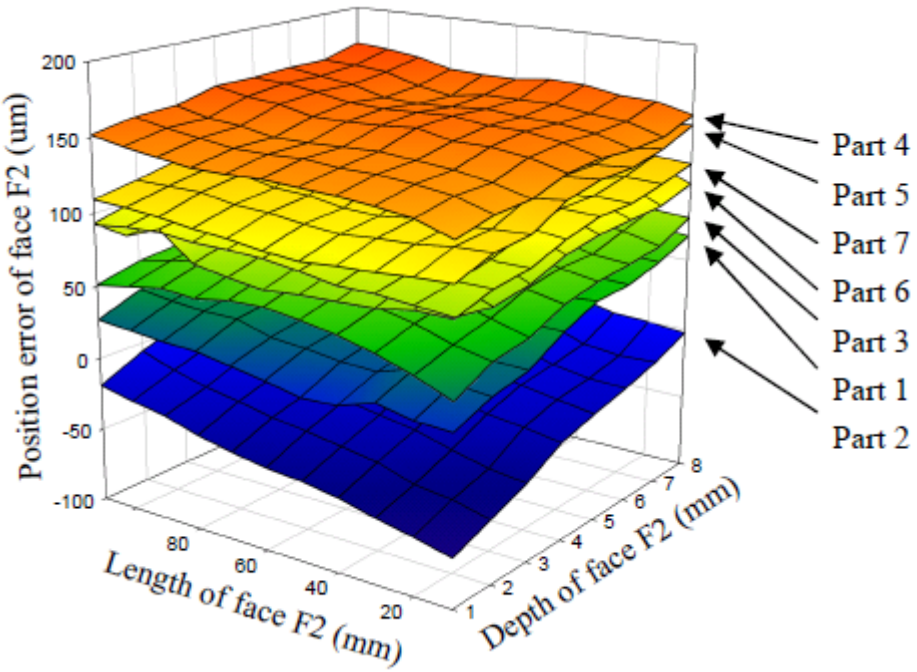

Figure 3.15: Profiles of Face F2 Machined at Different Thermal Statuses (Exp. No. 2.1)

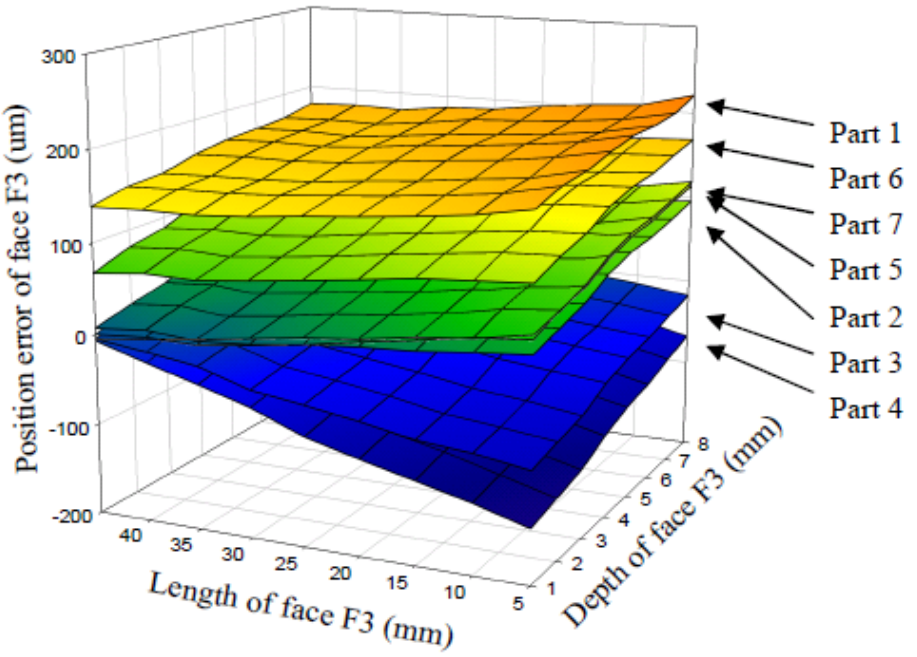

Figure 3.16: Profiles of Face F3 Machined at Different Thermal Statuses (Exp. No. 2.2)

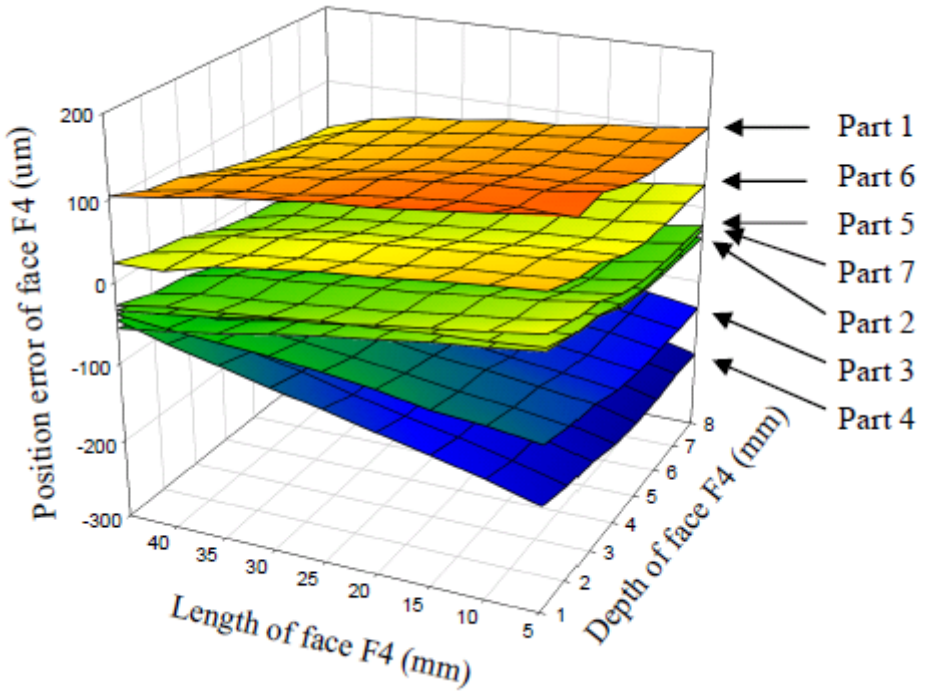

Figure 3.17: Profiles of Face F4 Machined at Different Thermal Statuses (Exp. No 2.2)

Positioning error. In real machining, due to the machine tool's volumetric error, the cutting tool tip cannot be placed at its designated position, causing the position to deviate from the designed value. The positioning error of a machined surface is defined as the difference between the measured position and the designed position. Fig. 3.18 and Fig. 3.19 show the positioning errors of faces F1, F2, F3 and F4, respectively. To depict the position value accurately, the average of 143 points is used for both faces F1 and F2 and 110 points for both faces F3 and F4. Three times standard deviations (3σ) are adopted to show the skater of measured points, as shown in Fig. 3.20 – 3.23. From these figures, the following observations can be attained:

With regard to the average position:

- During the warm-up period, the position of the machined surface changes significantly and gradually becomes stable when the machine tool enters a thermally stable stage.
- The relationship between the position and the machine tool's thermal status is nonlinear. The reason might be that various parts of the machine tool expanded differently, in both magnitude and direction. Only the combined effects of all these growing elements are reflected in the machined workpiece.
- Positioning error is accumulative and proportional to the travel distance. For example, the positioning error of face F2 is always larger than that of face F1, and the positioning error of face F3 is always larger than that of face F4.

With regard to the distribution of the measured value:

- During the warm-up period, the ranges of the distribution vary as the machine tool's thermal status changes, and subsequently, it gradually stabilizes close to the average value when the machine tool enters a thermally stable stage.
- When the machine tool is in the thermally stable stage, most of the points for faces F1, F2 and F3 are above the nominal value, whereas most of the points for face F4 are around the nominal value. This relates to the expansion direction of the moving axis.

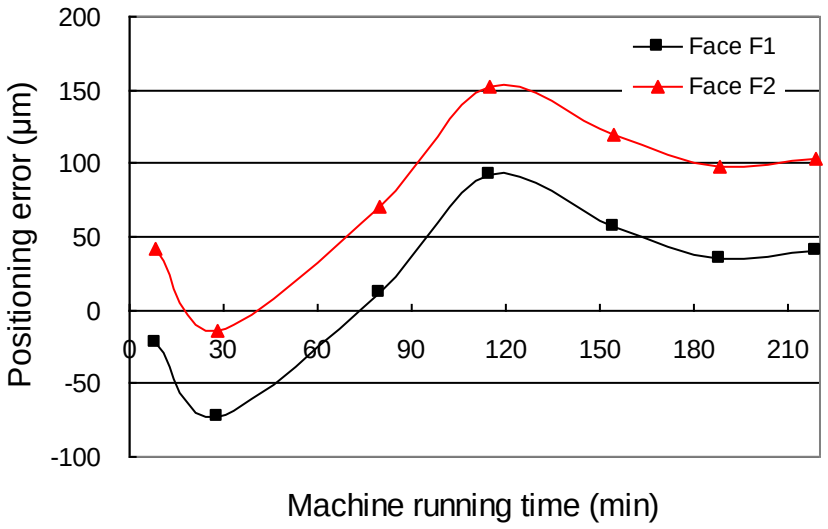

Figure 3.18: Positioning Errors of Faces F1 and F2 (Exp. No. 2.1)

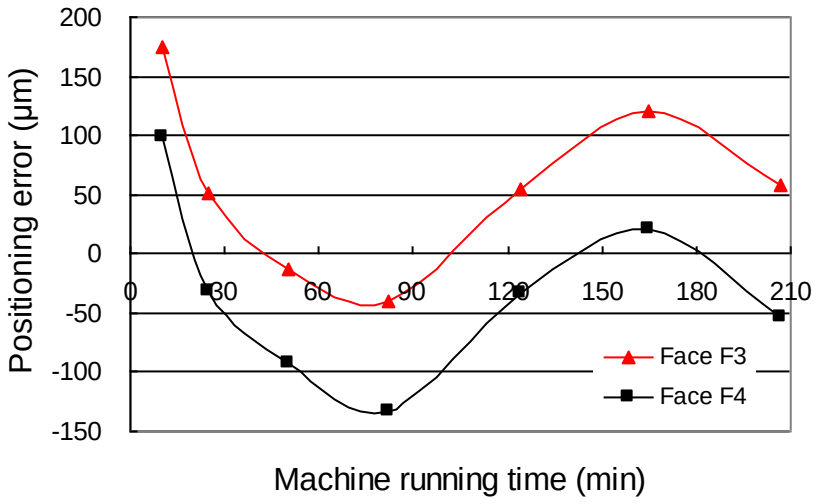

Figure 3.19: Positioning Errors of Faces F3 and F4 (Exp. No. 2.2)

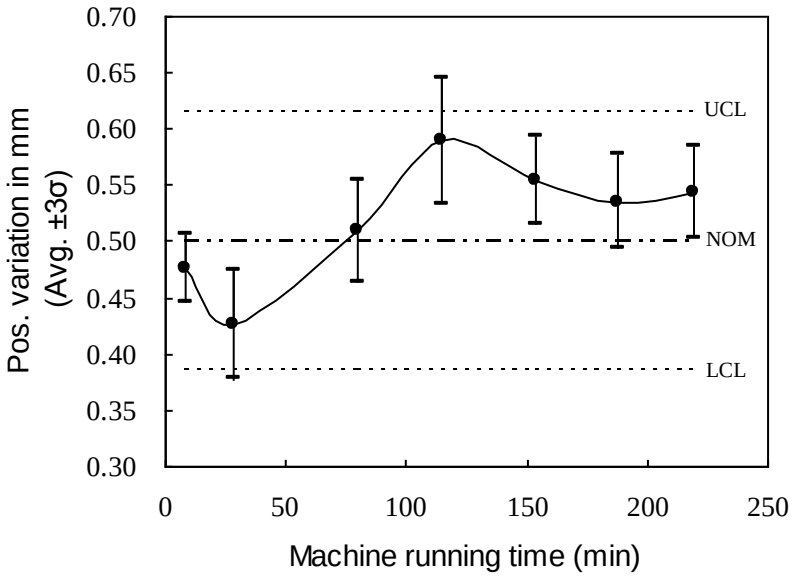

Figure 3.20: Variation of Position of Face F1 (Exp. No. 2.1)

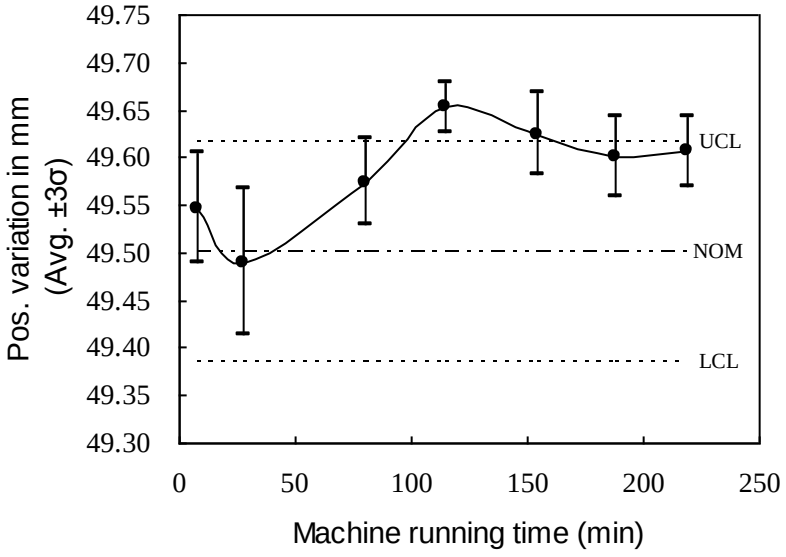

Figure 3.21: Variation of Position of Face F2 (Exp. No. 2.1)

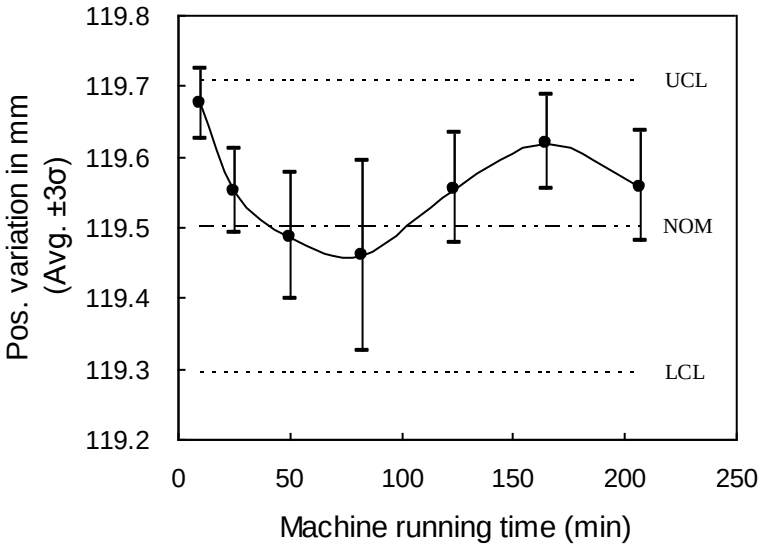

Figure 3.22: Variation of Position of Face F3 (Exp. No. 2.2)

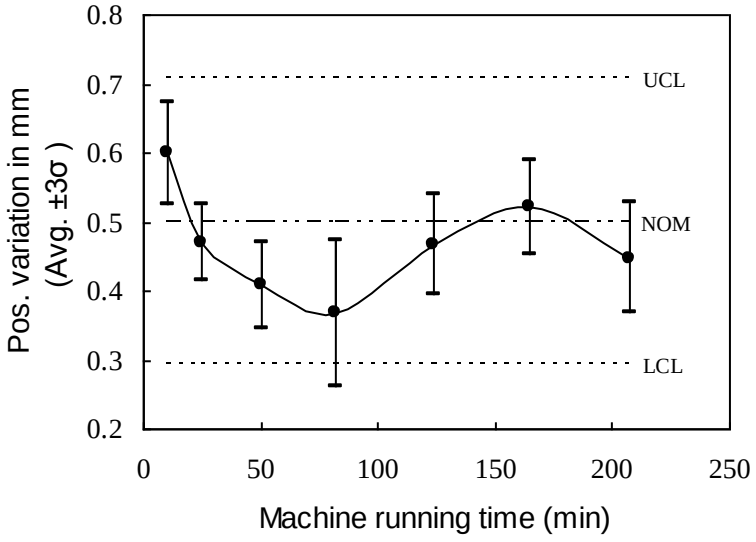

Figure 3.23: Variation of Position of Face F4 (Exp. No. 2.2)

Although the positioning errors of faces F1, F2, F3 and F4 all stabilize in the thermally stable stage, their variation trends during the warm-up period are not identical. The variation trends of faces F1 and F2 are similar, as they are machined applying the same process; the same applies to faces F3 and F4. On the other hand, the variation trends for faces F1 and F2 are different from the variation trends for faces F3 and F4. The reasons behind the differences are as follows: (1) they are machined applying different processes, and the warm-up programs during the machining interval are different; (2) the positioning errors of faces F1 and F2 demonstrate the *y*-axis's thermal feature, whereas the positioning errors of faces F3 and F4 are evidence of the *x*-axis's thermal attributes.

Variations of the centre of the hole's position with the machine's thermal status are shown in Fig. 3.24 – Fig. 3.29. It is observed that thermally-induced position variations in the drilling process are similar to those that occur in the end milling process.

Positioning tolerance. The positioning tolerance vector for each hole can be calculated using the following formula [113]:

$$T_p = 2\sqrt{D_x^2 + D_y^2} \tag{3.1}$$

where T_p is the position tolerance and D_x and D_y are centre positioning errors along the *x*- and *y*-axis, respectively. All of them are expressed in microns. The positioning tolerance calculated using Eq. 3.1 is an important parameter for the application of geometric dimensioning and tolerancing (GD&T) where the tolerance zone is specified as round rather than square as specified by traditional plus/minus tolerancing.

The variations of positioning tolerance for the centres of holes are illustrated in Fig. 3.30. The following observations can be made from this graph:

- Similar to the positioning errors, the centre of a hole's positioning tolerance also stabilizes after the machine tool runs for two-and-a-half hours (i.e., when it has reached a thermally stable stage).
- The centre of a hole's positioning tolerance machined in a thermally stable stage is at the same low level as one machined at the cold start. However, the holes drilled during the warm-up period have high position tolerances.

In the production of workpieces with the same dimensions, the lower is the position tolerance, the higher is the repeatability. Therefore, for a big industry where a large number of workpieces with the same dimensions are produced, it would be beneficial to avoid the machine's warm-up period and machine workpieces in the thermally stable stage to increase repeatability.

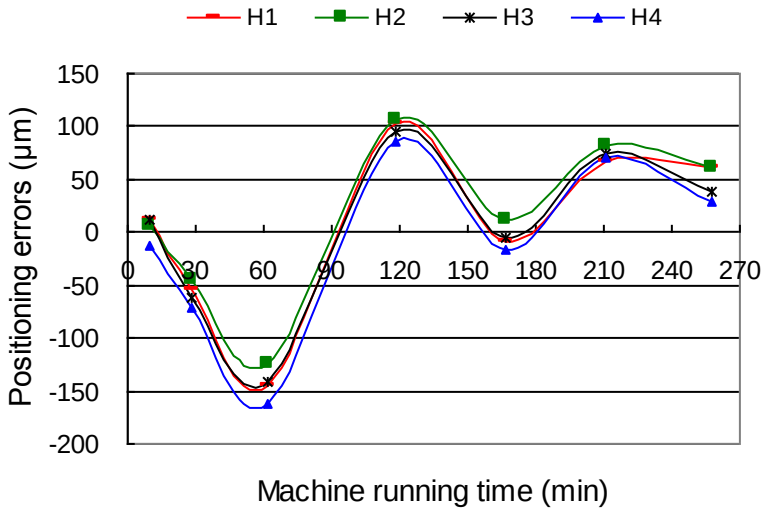

Figure 3.24: Positioning Errors of Hole Centres along the *x*-axis (Exp. No. 2.3)

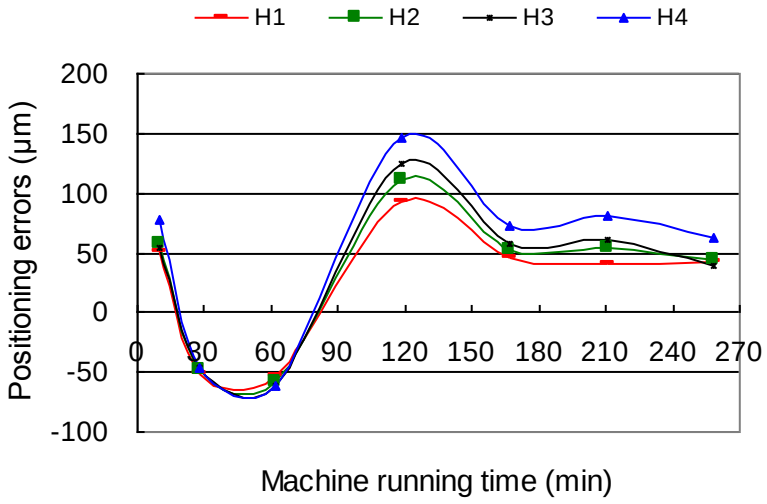

Figure 3.25: Positioning Errors of Hole Centres along the *y*-axis (Exp. No. 2.3)

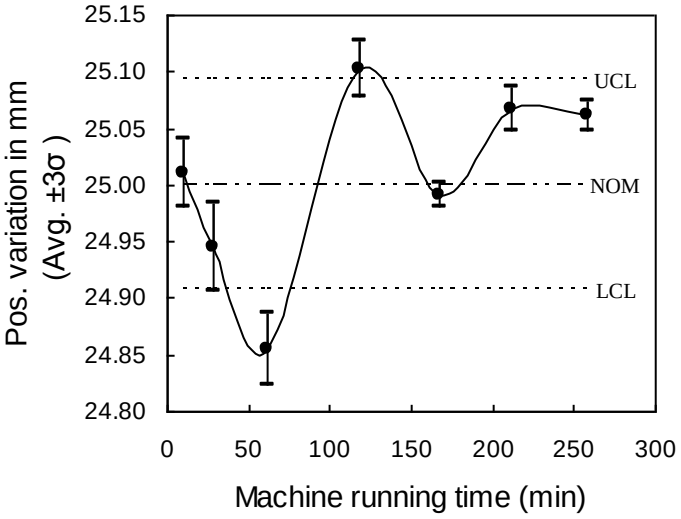

Figure 3.26: Variation of Position of Centre of H1 in *x*-axis (Exp. No. 2.3)

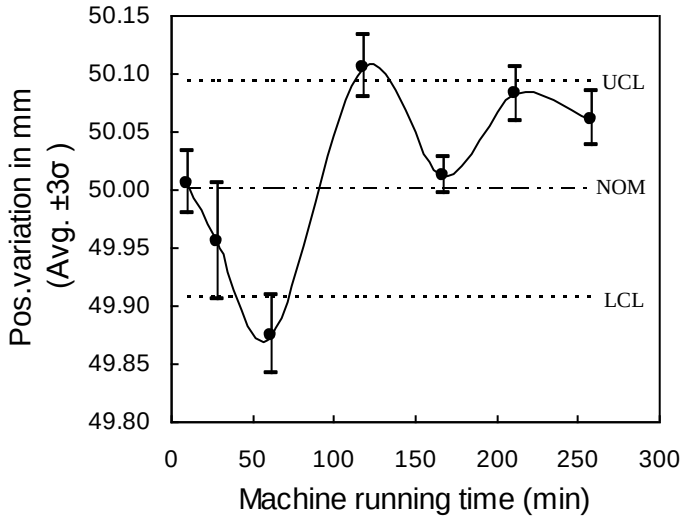

Figure 3.27: Variation of Position of Centre of H2 in *x*-axis (Exp. No. 2.3)

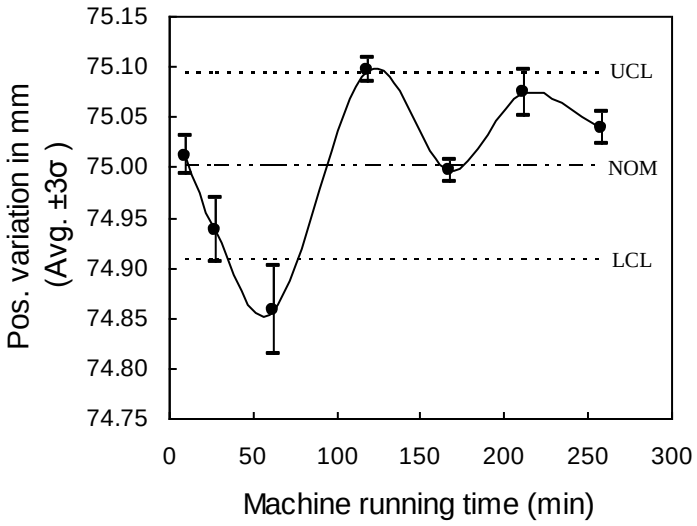

Figure 3.28: Variation of Position of Centre of H3 in *x*-axis (Exp. No. 2.3)

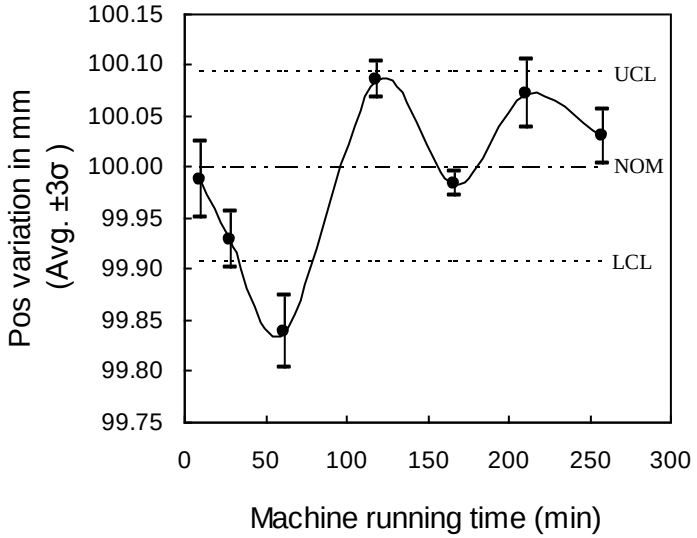

Figure 3.29: Variation of Position of Centre of H4 in *x*-axis (Exp. No. 2.3)

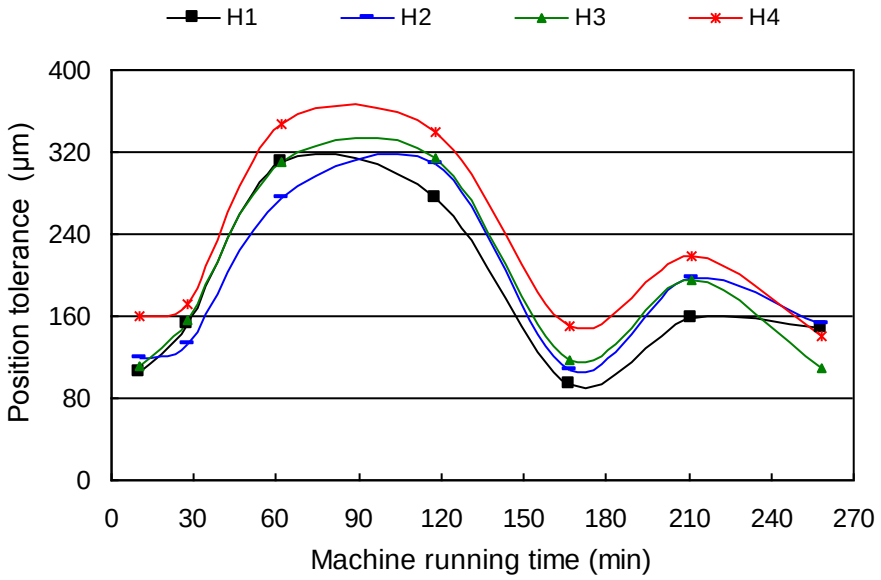

Figure 3.30: Variation of Position Tolerance for Hole Centres (Exp. No. 2.3)

Linear dimensional errors. Linear dimensions are also important when the workpiece is to be assembled or mated with other parts. Therefore, the accuracy of linear dimensions x_{34} and y_{12} (see Fig. 3.3) is also evaluated in this study. Designed values for these linear dimensions are as follows: x_{34} = 119 mm, y_{12} = 49 mm. The linear dimensions are defined by two parallel surfaces that are related to the dimension. For example, the linear dimension x_{34} is calculated by the following relationship:

$$x_{34} = x_3 - x_4 \tag{3.2}$$

where x_3 and x_4 are positions of faces F3 and F4 respectively. Due to the positioning error of the tool, the measured results of x_3 and x_4 deviated from their designed values; in consequence, the measured linear dimension x_{34} deviated from its designed value. As for the worst-case tolerance accumulation model, the tolerance of x_{34} is estimated by applying the following relationship:

$$\Delta x_{34} = \Delta x_3 + \Delta x_4 \tag{3.3}$$

where Δx_3 and Δx_4 are the tolerances of x_3 and x_4 respectively, defined as three times

the standard deviation.

Fig. 3.31 and Fig. 3.32 show the linear dimension variations as the machine tool's thermal status changes. It is observed that the thermal status does not have much effect on the average linear dimension value; however, the distribution of measured points appears more stable at the thermally stable stage.

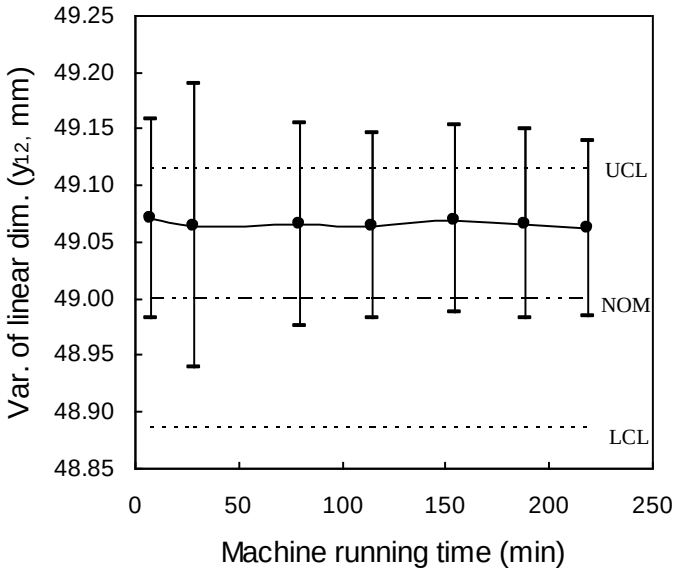

Figure 3.31: Variation of Linear Dimension y_{12} (Exp. No. 2.1)

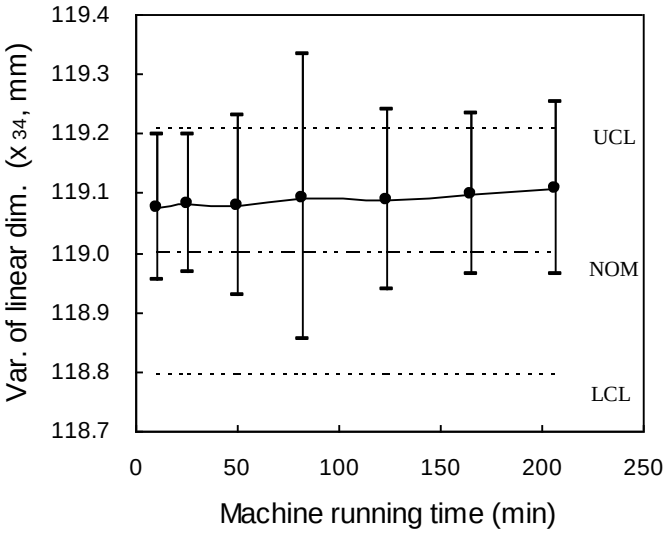

Figure 3.32: Variation of Linear Dimension x_{34} (Exp. No. 2.2)

3.4 Concluding Remarks

From this experimental investigation, the following conclusions can be drawn:

- The machine tool has a warm-up period before attaining its thermally stable status. The length of the warm-up period depends mainly on the machine tool's structure.
- During the warm-up period, the positioning error of the machine tool deteriorates significantly, which has detrimental effects on the repeatability of machined parts.
- Compared to the positioning error, a machine tool's thermal statuses do not have a significant effect on linear dimension errors.
- A machine tool's thermal statuses have effects on the flatness of a machined surface. When the machine reaches its thermally stable stage, the flatness tolerance of the machined surface also becomes stable and narrow.
- When the machine tool reaches the thermally stable stage, positioning errors also stabilize. This is the optimum stage to improve positioning accuracy and increase the repeatability of a machined workpiece using the compensation technique.

Machining after the warm-up period would be a good alternative for big factories where the machine tools usually run for the whole day. However, this decision should be made carefully, due to the extra wear and power wastage caused by the pre-warming of machine tools.

Chapter 4

Model Development

4.1 Introduction

Throughout the preliminary study described in Chapter 3, it has been shown that the thermal errors of a machine tool have significant effects on the dimensional accuracy of machined parts produced on it and that these effects vary with the thermal status of the machine tool. The aim of this research is to propose some control measures to eliminate or at least reduce the effects of these thermally-induced machine tool error components and thus improve the dimensional accuracy of component parts. To achieve this goal, in this chapter a new model is developed for calculating thermally-induced volumetric error developed by integrating the dominant thermal error components into the traditional geometric error-based volumetric error model.

The main problem with the traditional model for calculating thermally-induced volumetric error is that it requires the measurement of a large number of geometric error components and their variation data at different temperatures. Collecting these data is cumbersome and time-consuming, especially in an industrial setting. To overcome this difficulty, here a new model is proposed which is based on the variation of only three error components. The considered error components are the three axial positioning errors of the machine tool. This proposition is justified by the fact that, in comparison with the other geometric errors, the positioning errors and their thermal variations have the most significant effect on volumetric error for machine tools. This conclusion was drawn by analysing the data presented by Venugopal [79].

The positioning errors are modelled as functions of ball screw nut temperature

and travel distance. Therefore, when the thermal condition of a machine tool changes due to its continuous usage, only the ball-screw nut temperatures are needed to be monitored. The other input parameter for the model, the travel distance, is available from the CNC controller. Although some accuracy will be sacrificed due to the simplification, it can be a useful tool for industrial applications.

4.2 Volumetric Error Model

4.2.1 General model

A three-axis machine tool is typically composed of three linear moving elements that are designed to have only one degree of freedom in each moving direction. However, due to a number of factors, error-free movement is not possible, and the moving element has six degrees of freedom of movement. Or, to put it another way, six error components can occur. The six error components of a typical linear carriage designed to move in the x-direction are illustrated in Fig. 4.1, where $\delta_x(x)$ represents the x-positioning error and $\delta_y(x)$ and $\delta_z(x)$ represent the horizontal straightness error and vertical straightness error, respectively. The angular deviations during carriage motion (commonly known as roll, pitch and yaw) are represented by $\varepsilon_x(x)$, $\varepsilon_y(x)$ and $\varepsilon_z(x)$. Hence, for a three-axis machine tool, classification of 18 error components is possible. In addition to these errors, positioning of the machine tool can be influenced by the non-perpendicularity of the axes. For a three-axis machine tool, three such errors can occur (Fig. 4.2), leading to the identification of a total of 21 error components. These 21 error components include three positioning errors, six straightness errors, nine angular errors, and three orthogonal (squareness) errors.

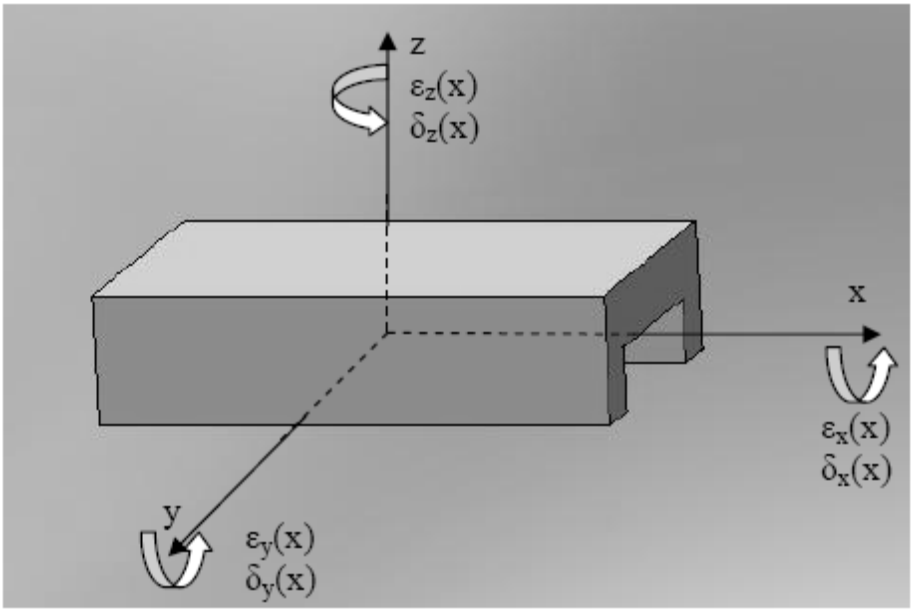

Figure 4.1: A Typical Linear Carriage with Six Degrees of Freedom

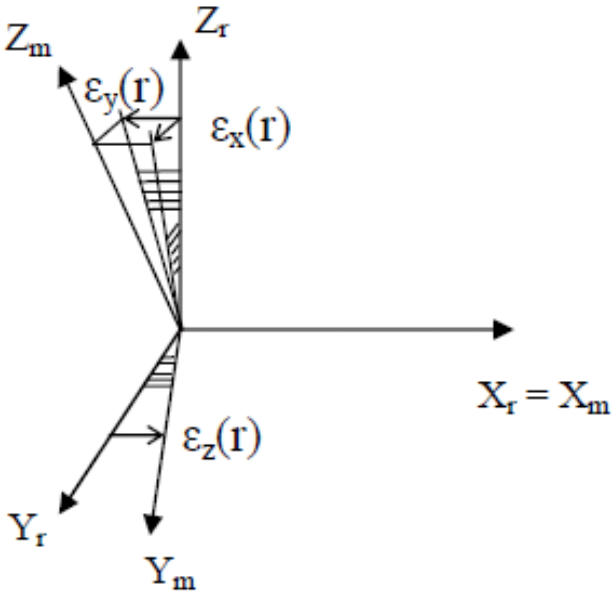

Figure 4.2: Non-Orthogonality Errors

In order to determine the combined effect of individual error components on the volumetric error, the following method based on the principle of *rigid body kinematics* can be applied. Consider an ideal co-ordinate system, called a space

co-ordinate system (or reference co-ordinate system), attached very close to the machine co-ordinate system. All initial co-ordinates refer to the space co-ordinate system, which is regarded as "perfect". The designated position of any point within the machine space is represented by a vector P_d (X_d, Y_d, Z_d). Due to geometric errors of the machine tool, carriage movement does not follow the space co-ordinate system, resulting in a change of position from the original designated position to the new position, which is then represented by vector P_m (X_m, Y_m, Z_m). As the space co-ordinate system and machine co-ordinate system may have translation and/or rotation, vector P_m (X_m, Y_m, Z_m) can be expressed using a homogeneous transformation of space T as:

$$P_m = T \cdot P_d \tag{4.1}$$

where T is the transformation matrix capable of translational and rotational transformations.

As for the linear carriage (Fig. 4.1), the error transformation matrix caused by roll error $\varepsilon_x(x)$ can be expressed by the following equation (Eq. 4.2), derived by the application of rigid body kinematics and small-angle approximation [99]:

$$Rollerror = Rot(x, \varepsilon_x(x)) = \begin{bmatrix} 1 & 0 & 0 & 0 \\ 0 & 1 & -\varepsilon_x(x) & 0 \\ 0 & \varepsilon_x(x) & 1 & 0 \\ 0 & 0 & 0 & 1 \end{bmatrix} \tag{4.2}$$

Similarly, the transformation matrix attributed to pitch and yaw errors can be represented using Eqs. 4.3 and 4.4:

$$Pitcherror = Rot(y, \varepsilon_y(x)) = \begin{bmatrix} 1 & 0 & \varepsilon_y(x) & 0 \\ 0 & 1 & 0 & 0 \\ -\varepsilon_y(x) & 0 & 1 & 0 \\ 0 & 0 & 0 & 1 \end{bmatrix} \tag{4.3}$$

$$Yawerror = Rot(z, \varepsilon_z(x)) = \begin{bmatrix} 1 & -\varepsilon_z(x) & 0 & 0 \\ \varepsilon_z(x) & 1 & 0 & 0 \\ 0 & 0 & 1 & 0 \\ 0 & 0 & 0 & 1 \end{bmatrix} \tag{4.4}$$

Translational transformation due to positioning error $\delta_x(x)$, horizontal straightness error $\delta_y(x)$ and vertical straightness error $\delta_z(x)$ is given by:

$$Trans(\delta_x(x), \delta_y(x), \delta_z(x)) = \begin{bmatrix} 1 & 0 & 0 & \delta_x(x) \\ 0 & 1 & 0 & \delta_y(x) \\ 0 & 0 & 1 & \delta_z(x) \\ 0 & 0 & 0 & 1 \end{bmatrix} \tag{4.5}$$

The homogeneous transformation of space T_x can then be represented by matrix multiplication of the rotational and translational matrices given in Eqs. 4.2 – 4.5.

$$T_x = Rot(x, \varepsilon_x(x)) \cdot Rot(y, \varepsilon_y(x)) \cdot Rot(z, \varepsilon_z(x)) \cdot Trans(\delta_x(x), \delta_y(x), \delta_z(x)) \tag{4.6}$$

Neglecting second order terms,

$$T_x = \begin{pmatrix} 1 & -\varepsilon_z(x) & \varepsilon_y(x) & \delta_x(x) \\ \varepsilon_z(x) & 1 & -\varepsilon_x(x) & \delta_y(x) \\ -\varepsilon_y(x) & \varepsilon_x(x) & 1 & \delta_z(x) \\ 0 & 0 & 0 & 1 \end{pmatrix} \tag{4.7}$$

This transformation matrix T_x takes into account six error components along the *x*-axis only. However, in a three-axis machine tool, the position of the tool within the machine space in general will depend on movement along the three axes. Therefore the homogeneous transformation of space *T* for the whole machine system can be represented by matrix multiplication along three axes:

$$T = T_x \cdot T_y \cdot T_z \tag{4.8}$$

where T_x, T_y and T_z can be expressed by Eqs. 4.7, 4.9 and 4.10, respectively.

$$T_y = \begin{pmatrix} 1 & -\varepsilon_z(y) & \varepsilon_y(y) & \delta_x(y) \\ \varepsilon_z(y) & 1 & -\varepsilon_x(y) & \delta_y(y) \\ -\varepsilon_y(y) & \varepsilon_x(y) & 1 & \delta_z(y) \\ 0 & 0 & 0 & 1 \end{pmatrix} \tag{4.9}$$

$$T_z = \begin{pmatrix} 1 & -\varepsilon_z(z) & \varepsilon_y(z) & \delta_x(z) \\ \varepsilon_z(z) & 1 & -\varepsilon_x(z) & \delta_y(z) \\ -\varepsilon_y(z) & \varepsilon_x(z) & 1 & \delta_z(z) \\ 0 & 0 & 0 & 1 \end{pmatrix} \tag{4.10}$$

where $\delta_x(x)$, $\delta_y(y)$ and $\delta_z(z)$ are the positioning errors;

$\delta_y(x)$, $\delta_z(x)$, $\delta_x(y)$, $\delta_z(y)$, $\delta_x(z)$ and $\delta_y(z)$ are the straightness errors; and

$\varepsilon_x(x)$, $\varepsilon_y(x)$, $\varepsilon_z(x)$, $\varepsilon_x(y)$, $\varepsilon_y(y)$, $\varepsilon_z(y)$, $\varepsilon_x(z)$, $\varepsilon_y(z)$ and $\varepsilon_z(z)$ are the angular errors.

Then Eqs. 4.7 – 4.10 can be substituted into Eq. 4.1 neglecting second order terms and denoting the following variables:

$$\begin{cases} \Sigma X = \varepsilon_x(x) + \varepsilon_x(y) + \varepsilon_x(z) \\ \Sigma Y = \varepsilon_y(x) + \varepsilon_y(y) + \varepsilon_y(z) \\ \Sigma Z = \varepsilon_z(x) + \varepsilon_z(y) + \varepsilon_z(z) \\ \Delta X = \delta_x(x) + \delta_x(y) + \delta_x(z) \\ \Delta Y = \delta_y(x) + \delta_y(y) + \delta_y(z) \\ \Delta Z = \delta_z(x) + \delta_z(y) + \delta_z(z) \end{cases} \tag{4.11}$$

Then the real position vector P_m (X_m, Y_m, Z_m) can be represented using the following equation:

$$\begin{bmatrix} X_m \\ Y_m \\ Z_m \\ 1 \end{bmatrix} = \begin{bmatrix} 1 & -\sum Z & \sum Y & \Delta X \\ \sum Z & 1 & -\sum X & \Delta Y \\ -\sum Y & \sum X & 1 & \Delta Z \\ 0 & 0 & 0 & 1 \end{bmatrix} . \begin{bmatrix} X_d \\ Y_d \\ Z_d \\ 1 \end{bmatrix} \tag{4.12}$$

where the error transformation matrix for the whole system is demonstrated by:

$$T = \begin{bmatrix} 1 & -\sum Z & \sum Y & \Delta X \\ \sum Z & 1 & -\sum X & \Delta Y \\ -\sum Y & \sum X & 1 & \Delta Z \\ 0 & 0 & 0 & 1 \end{bmatrix} \tag{4.13}$$

In the above analysis, it was assumed that the machine axes are "perfectly" perpendicular to each other, but in reality this may not be the case, which will obviously contribute to the volumetric error. In Fig. 4.2, the non-orthogonality error components are shown. For convenience, it is assumed that the *x*-axis of the machine tool (X_{m}) coincides with the *x*-axis of the space co-ordinate system (X_r). Considering the effect of non-orthogonality errors, Eq. 4.13 becomes:

$$T = \begin{bmatrix} 1 & -\sum Z & \sum Y & \Delta X \\ \sum Z & 1 & -\sum X & \Delta Y \\ -\sum Y & \sum X & 1 & \Delta Z \\ 0 & 0 & 0 & 1 \end{bmatrix} . \begin{bmatrix} 1 & -\varepsilon_z(r) & \varepsilon_y(r) & 0 \\ \varepsilon_z(r) & 1 & -\varepsilon_x(r) & 0 \\ -\varepsilon_y(r) & \varepsilon_x(r) & 1 & 0 \\ 0 & 0 & 0 & 1 \end{bmatrix} \tag{4.14}$$

where ε_x(r), ε_y(r) and ε_z(r) are orthogonal errors (squareness errors).

Neglecting second order terms yields Eq. 4.15:

$$T = \begin{bmatrix} 1 & -\sum Z - \varepsilon_z(r) & \sum Y + \varepsilon_y(r) & \Delta X \\ \sum Z + \varepsilon_z(r) & 1 & -\sum X - \varepsilon_x(r) & \Delta Y \\ -\sum Y - \varepsilon_y(r) & \sum X + \varepsilon_x(r) & 1 & \Delta Z \\ 0 & 0 & 0 & 1 \end{bmatrix} \tag{4.15}$$

The difference between the designed position and actual position is defined as volumetric error. The volumetric error *V* can then be expressed by:

$$[V] = [P_m] - [P_d] = [T] \cdot [P_d] - [P_d] \tag{4.16}$$

Or,

$$[V] = \begin{bmatrix} V_x \\ V_y \\ V_z \\ 1 \end{bmatrix} = \begin{bmatrix} X_m - X_d \\ Y_m - Y_d \\ Z_m - Z_d \\ 1 \end{bmatrix} = \begin{bmatrix} -Y_d \cdot [\sum Z + \varepsilon_z(r)] + Z_d \cdot [\sum Y + \varepsilon_y(r)] + \Delta X \\ -Z_d \cdot [\sum X + \varepsilon_x(r)] + X_d \cdot [\sum Z + \varepsilon_z(r)] + \Delta Y \\ -X_d \cdot [\sum Y + \varepsilon_y(r)] + Y_d \cdot [\sum X + \varepsilon_x(r)] + \Delta Z \\ 1 \end{bmatrix} \tag{4.17}$$

Then, the volumetric error vector in *x*, *y* and *z* directions for designed position P_d can be expressed by Eq. 4.18:

$$\begin{cases} V_x = (-Y_d) \cdot [\sum Z + \varepsilon_z(r)] + Z_d \cdot [\sum Y + \varepsilon_y(r)] + \Delta X \\ V_y = (-Z_d) \cdot [\sum X + \varepsilon_x(r)] + X_d \cdot [\sum Z + \varepsilon_z(r)] + \Delta Y \\ V_z = (-X_d) \cdot [\sum Y + \varepsilon_y(r)] + Y_d \cdot [\sum X + \varepsilon_x(r)] + \Delta Z \end{cases} \tag{4.18}$$

4.2.2 Proposed thermally-induced volumetric error model (TIVEM)

The general volumetric error model described previously includes 21 geometric error components. These components are each expected to vary (by different amounts) when the thermal status of the machine tool changes. However, analysis of the data given in Tables 4.1, 4.2 and 4.3 demonstrates that the three positioning errors and

their thermal variations have the most significant effect on volumetric error for machine tools (in comparison with the other 18 geometric errors). Less than 20% accuracy is sacrificed if variations from the other 18 geometric errors are ignored (Tables 4.4 and 4.5). It is worth pointing out that a high-resolution laser interferometer is needed to measure geometric error components, making the process costly, complicated and time-consuming. Conversely, the measurement of the positioning error components can be performed using a Laser Doppler Displacement Meter (LDDM). Considering the cost and time, reducing the accuracy of the proposed model by less than 20% is a justified trade-off.

Thermally-induced positioning error prediction. Thermally-induced positioning error is a result of the motion of the slide on a lead screw. The basic part of the motion error comes from the expansion of the lead screw. Assuming that the lead screw is a simple linear beam and the temperature is evenly distributed along the lead screw, according to the definition of a coefficient of linear thermal expansion, the expansion in any point of the lead screw can be calculated as:

$$\text{Expansion} = \alpha \cdot L \cdot (T - 20) \tag{4.19}$$

where α is the coefficient of linear thermal expansion, L is the location where the expansion is measured and T is the lead screw temperature.

Table 4.1: Geometric Error Components of the Three-Axis Horizontal CNC Machine (Cold Start*) [79]

***x*-axis(mm)**	**0**	**50**	**100**	**150**	**200**	**250**	**300**	**350**	**400**	**450**	**500**
$\delta_x(x)$:µm	3.42	8.10	9.22	15.78	15.45	17.43	21.21	23.63	25.93	32.68	39.20
$\delta_z(x)$:µm	34.13	31.70	32.65	33.70	34.48	35.23	34.37				
$\delta_y(x)$:µm	-0.22	0.17	2.29	1.89	0.44	-2.75	-0.27				
$\varepsilon_z(x)$: s	0.76	0.74	0.51	-0.10	-0.12	-0.40	-1.04	-1.32	-1.45	-1.34	-1.57
$\varepsilon_y(x)$: s	-0.28	0.26	1.31	2.70	4.30	5.86	7.50	9.31	11.13	12.79	13.32
$\varepsilon_x(x)$: s	1.87	2.08	2.07	1.83	2.08	1.73	1.57	1.23	1.53	1.30	1.17
***y*-axis(mm)**	**0**	**50**	**100**	**150**	**200**	**250**	**300**	**350**	**400**	**450**	**500**
$\delta_y(y)$:µm	10.33	-10.93	-7.97	-2.92	-3.62	-2.28	3.13	9.68	10.53		
$\delta_x(y)$:µm	-1.17	-0.48	-1.46	-1.93	-1.98	-1.86	-1.4				
$\delta_z(y)$:µm	-1.17	-0.34	-0.58	-0.60	0.53	-0.61	-1.10				
$\varepsilon_x(y)$: s	0.16	1.75	0.86	0.94	0.83	-0.71	-1.71	-2.11	0.45		
$\varepsilon_z(y)$: s	0.26	0.35	-0.11	-0.58	-1.10	-1.39	-2.05	-2.61	-2.51		
$\varepsilon_y(y)$: s	0.47	-1.58	-1.67	-1.90	-2.07	-1.75	-0.87	-1.07	-1.10		
***z*-axis(mm)**	**0**	**50**	**100**	**150**	**200**	**250**	**300**	**350**	**400**	**450**	**500**
$\delta_z(z)$:µm	-2.79	-4.47	-7.71	-5.74	-5.47	-7.48	-7.95	-3.36	-2.23	-1.03	1.31
$\delta_x(z)$:µm	-0.30	-0.48	-0.33	-0.05	-0.33	-0.23					
$\delta_y(z)$:µm	-5.83	-3.81	-4.78	-6.05	-6.93	-6.53					
$\varepsilon_x(z)$: s	-1.78	-1.87	-2.24	-2.58	-2.88	-3.20	-3.67	-4.13	-4.57	5.14	-5.69
$\varepsilon_y(z)$: s	-0.07	-0.09	0.01	0.09	0.35	0.51	0.83	1.54	2.07	2.02	2.43
$\varepsilon_z(z)$: s	0	-0.08	-0.07	-1.08	-1.92	-2.50	-3.83	-4.50	-5.25	-6.50	-7.00
* cold start: T*x*-nut = 24.56°C, T*y*-nut = 27.33°C, T*z*-nut = 25.72°C											

Table 4.2: Geometric Error Components of the Three-Axis Horizontal CNC Machine (Thermal Stable Stage*) [79]

***x*-axis(mm)**	**0**	**50**	**100**	**150**	**200**	**250**	**300**	**350**	**400**	**450**	**500**
$\delta_x(x)$:μm	-63.7	-55.3	-49.0	-36.9	-31.5	-26.0	-16.27	-9.32	-0.89	10.22	22.14
$\delta_z(x)$:μm	48.7	46.71	46.92	47.35	48.41	50.32	48.77				
$\delta_y(x)$:μm	17.42	19.58	19.36	19.63	19.22	18.17	17.5				
$\varepsilon_z(x)$: s	-12.7	-12.7	-13.5	-14.2	-14.2	-14.9	-15.7	-15.8	-16.0	-16.7	-16.9
$\varepsilon_y(x)$: s	-8.33	-7.73	-6.27	-4.42	-2.49	-0.56	1.46	3.74	5.95	7.81	8.32
$\varepsilon_x(x)$: s	-25.01	-25.2	-25	-25	-25.2	-25.1	-25.3	-25.4	-26	-25.8	-26
***y*-axis(mm)**	**0**	**50**	**100**	**150**	**200**	**250**	**300**	**350**	**400**	**450**	**500**
$\delta_y(y)$:μm	40.87	49.55	61.32	73.75	81.30	91.19	104.8	120.4	126.3		
$\delta_x(y)$:μm	-14.9	-14.6	-15.4	-16.1	-16.1	-16.0	-15.2				
$\delta_z(y)$:μm	14.88	15.55	15.56	16.27	16.03	15.58	14.90				
$\varepsilon_x(y)$: s	9.62	11.94	11.71	11.73	11.01	10.29	9.47	8.59	11.48		
$\varepsilon_z(y)$: s	-16.6	-17.2	-18.5	-19.8	-21.0	-22.0	-23.3	-24.4	-24.7		
$\varepsilon_y(y)$: s	9.62	11.94	11.71	11.73	11.01	10.29	9.47	8.59	11.48		
***z*-axis(mm)**	**0**	**50**	**100**	**150**	**200**	**250**	**300**	**350**	**400**	**450**	**500**
$\delta_z(z)$:μm	63.66	70.08	77.34	88.97	98.63	106.3	116.00	129.6	140.0	151.0	163.3
$\delta_x(z)$:μm	1.52	1.00	2.29	2.07	1.49	1.63					
$\delta_y(z)$:μm	20.00	19.94	18.75	19.39	19.96	20.13					
$\varepsilon_x(z)$: s	-8.39	-9.1	-9.09	-10.4	-11.0	-11.40	-12.1	-12.9	-13.4	-14.2	-15.1
$\varepsilon_y(z)$: s	1.20	1.47	1.90	1.91	2.10	2.15	2.38	2.68	3.04	3.23	3.34
$\varepsilon_z(z)$: s	1.0	0.92	0.5	0.0	0.0	0.0	1.0	-1.33	-2.08	-3.33	-3.92
* thermal stable stage: T*x*-nut = 31.86℃ T*y*-nut = 35.12℃, Tz-nut = 37.61℃											

Table 4.3: Axial Origin Offsets as Temperature Rises (Adapted from Venugopal [79])

X nut temp. (℃)	24.56	25.62	27.17	28.83	29.72	30.37	30.75	31.62	31.86	31.92
X origin offsets (μm)	3.42	-0.13	-32.20	-57.55	-71.54	-60.85	-52.9	-57.70	-63.70	-60.13
Y nut temp. (℃)	27.33	30.35	33.57	33.66	34.32	34.93	34.99	35.12	35.34	
Y origin offsets (μm)	-15.00	-8.00	20.85	13.67	25.80	45.77	44.58	40.87	40.85	
Z nut temp. (℃)	25.72	28.43	31.43	31.93	33.69	35.58	36.26	36.46	37.35	37.61
Z origin offsets (μm)	-2.79	21.84	33.94	57.37	55.07	60.95	75.95	57.37	75.33	63.66

Table 4.4: Error Variations between Cold Start and Thermal Stable Stage (Adapted from Venugopal [79])

Error components	x, y, z = 50 mm	x, y, z = 150 mm	x, y, z = 250 mm
	Err variations	Err variations	Err variations
Pos. $\delta_x(x)$: µm	**-73.60**	**-66.58**	**-59.33**
Hori. Str. $\delta_z(x)$: µm	7.50	7.40	7.67
Ver. Str. $\delta_y(x)$: µm	8.64	7.74	10.31
Pitch $\varepsilon_z(x)$: arcsec	-13.50	-14.06	-14.46
Yaw $\varepsilon_y(x)$: arcsec	-7.99	-7.12	-6.42
Roll $\varepsilon_x(x)$: arcsec	-27.28	-26.83	-26.83
Pos. $\delta_y(y)$: µm	**63.93**	**81.07**	**97.78**
Hori. Str. $\delta_x(y)$: µm	-14.12	-14.17	-14.14
Ver. Str. $\delta_z(y)$: µm	15.14	14.91	14.11
Pitch $\varepsilon_x(y)$: arcsec	10.19	10.79	11.00
Yaw $\varepsilon_z(y)$: arcsec	-17.52	-19.18	-20.59
Roll $\varepsilon_y(y)$: arcsec	13.52	13.63	12.04
Pos. $\delta_z(z)$: µm	**86.00**	**106.04**	**126.48**
Hori. Str. $\delta_x(z)$: µm	1.48	2.12	1.86
Ver. Str. $\delta_y(z)$: µm	5.40	5.17	5.43
Pitch $\varepsilon_x(z)$: arcsec	-7.23	-7.82	-8.20
Yaw $\varepsilon_y(z)$: arcsec	1.56	1.82	1.64
Roll $\varepsilon_z(z)$: arcsec	1.00	1.08	2.50
Note: When calculating the volumetric error, the units of angular errors have to be converted into radian. For example, roll error: -27.28 (*arcsec*) = (-27.28) · 4.848 e $^{-6}$ = 0.000132 (*rad.*)			

Table 4.5: Comparison of Volumetric Error Calculated Results (Adapted from Venugopal[79])

x, y, z (mm)	V (µm)	Vp (µm)	V-Vp (µm)	(V-Vp)/V
50	162.17	132.74	29.43	18.14%
100	160.45	132.69	27.79	17.32%
150	161.91	134.42	27.49	16.98%
200	161.84	136.74	25.1	15.51%
250	162.71	136.66	26.05	16.01%
*Volumetric error **Vp** in the thermal stable stage considers only the three positioning error variations; the remaining 18 geometric errors remain the same with cold start values. ** Volumetric error **V** in the thermal stable stage considers the variations of 21 error components.				

In reality, the temperature distribution along the lead screw is uneven. The frictional heat generated by the moving nut dominates the expansion of the lead screw, while the heat generated by the support bearing is another heat source leading to temperature increase [88].

An experiment was conducted to map the temperature distribution along a lead screw of a machine tool. The schematic structure of the lead screw and the locations of temperature measurement points are depicted in Fig. 4.3. The test results are illustrated in Fig. 4.4, which shows that the nut temperature (T1) has the most significant temperature increase during the 4 h of idle running, whereas the bearing temperature (T4) has the lowest degree of increase compared to other parts of the lead screw. These findings also show that the temperature at the contact surface between the nut and the lead screw (T2) is close to the temperature (T1) found at the nut. Similar results have been reported by Wu and Kung [88].

During the machining period, the nut is continuously moving along the lead screw, making it difficult to measure the temperature of the contact surface between the nut and the lead screw. Therefore, the temperature of the nut is used as the lead screw temperature for the calculation of lead screw expansion.

T−20 is used as the temperature rise since 20°C is the international standard temperature when describing the length of an object [114]. Apparently, according to Eq. 4.19, the error will be zero at axis origin. However, previous research [79] has demonstrated that the error at each axis origin has always been offset by a small amount. Therefore, modification of the positioning error prediction (Eq. 4.20) on the basis of Eq. 4.19 is proposed:

$$\begin{cases} E_x(x,T_{xnut}) = x_0(T_{xnut}) + \beta_x \cdot \alpha \cdot x \cdot (T_{xnut} - 20) \\ E_y(y,T_{ynut}) = y_0(T_{ynut}) + \beta_y \cdot \alpha \cdot y \cdot (T_{ynut} - 20) \\ E_z(z,T_{znut}) = z_0(T_{znut}) + \beta_z \cdot \alpha \cdot z \cdot (T_{znut} - 20) \end{cases} \tag{4.20}$$

where $E_x(x, T_{xnut})$, $E_y(y, T_{ynut})$ and $E_z(z, T_{znut})$ are the positioning errors along axes,

defined as the functions of axial travel distance and nut temperature;

$x_0(T_{xnut})$, $y_0(T_{ynut})$ and $z_0(T_{znut})$ are axis origin offsets, defined as the functions of nut temperature. They can be measured regularly and then stored in a databank together with basic geometric errors;

x, y and z represent axial travel distance;

T_{xnut}, T_{ynut} and T_{znut} represent nut temperature; and

β_x, β_y and β_z are multiplication factors in the x-, y- and z-axis, respectively.

A machine tool is a complicated structure, and the axis cannot expand freely like a simple beam. Therefore, it is essential to introduce a multiplication factor to each error prediction equation. Their values depend mainly on the machine's structure and thermal status.

Determination of multiplication factors. The axis origin offsets x_0 (T_{xnut}), y_0 (T_{ynut}) and z_0 (T_{znut}) in Eq. 4.20 can be determined from the pre-calibrated data stored in a databank, while nut temperature (T_{xnut}, T_{ynut}, T_{znut}) and axial travel distance (x, y, z) are taken from on-line measurement. The values of multiplication factors (β_x, β_y, β_z) can be calculated by the least squares method based on experiment data. The procedure is explained below, using the z-axis as an example.

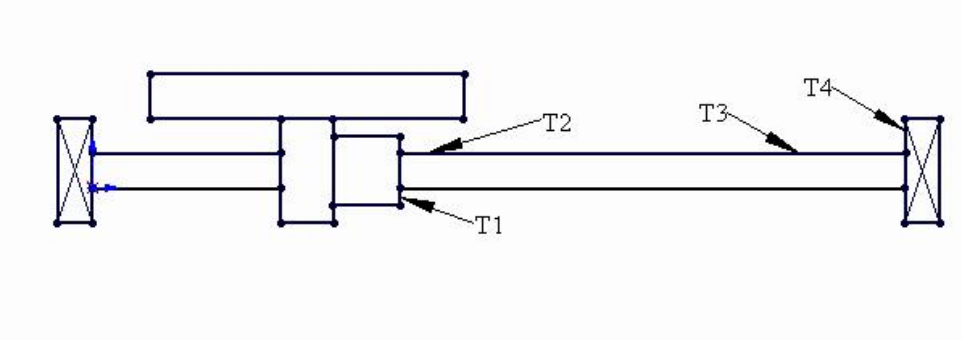

Figure 4.3: Location of Measured Points on a Lead Screw

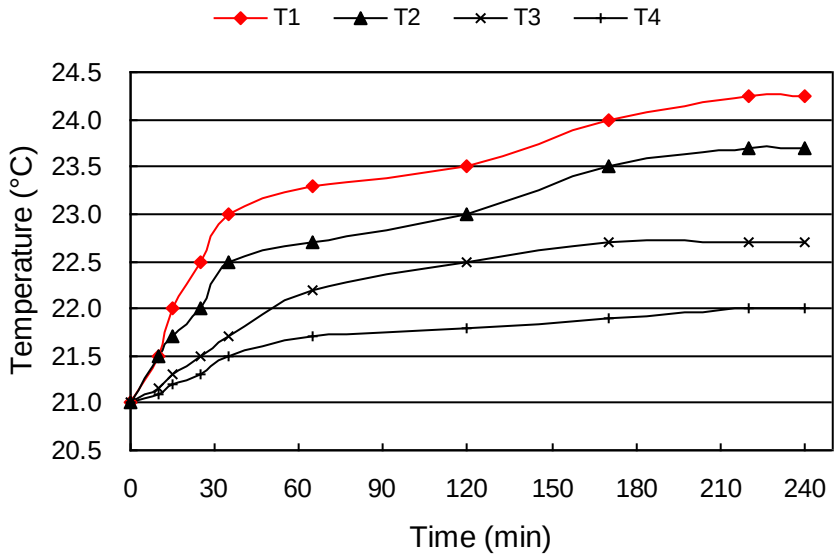

Figure 4.4: Measured Temperature Increase vs. Machine Running Time

Fig. 4.5 illustrates the *z*-axis positioning error data set (z_1, E_{z1}), (z_2, E_{z2}), ..., (z_n, E_{zn}). The fitting line ($f(z) = a + bz$) has the deviations d_1, d_2, ..., d_n calculated from each data point. The minimum least squares error equation is:

$$\prod_{\min} = d_1^2 + d_2^2 + ... + d_{n-1}^2 + d_n^2 = \sum_{i=1}^{n} d_i^2 = \sum_{i=1}^{n} [E_{zi} - f(z_i)]^2 \tag{4.21}$$

Solving the above equation, the line-of-best-fit equation for the *z*-axis can be obtained (Fig. 4.5):

$$f(z) = a + bz = 75.33 + 0.0002z \tag{4.22}$$

Eq. 4.23 can be derived by equating Eqs. 4.20 and 4.22. The unknown β_z can then be determined by solving Eq. 4.23:

$$75.33 + 0.0002z = z_0(T_{znut}) + \beta_z \cdot \alpha \cdot z \cdot (T_{znut} - 20) \tag{4.23}$$

It should be pointed out that Eqs. 4.22 and 4.23 result from the thermal stable stage; in other words, β_z not only depends on the axis structure of the machine tool, but also varies with its thermal status. Fig. 4.6 shows that, during the machine warm-up period, β_z changes significantly, reaching a stable value when the machine tool becomes thermally stable. As most compensation for volumetric error is performed at the thermal stable stage, the average value is taken from several calculations at this stage. For the tested machine tool, the multiplication factors for the *x*-, *y*-, and *z*-axes are calculated to be 0.97, 0.76 and 0.67, respectively.

So far, with regard to the prediction Eq. 4.20, the two variable components are nut temperature and axial travel distance. The positioning errors along each axis at a certain temperature can now be predicted using Eq. 4.20. Fig. 4.7 shows good agreement between the positioning error data predicted by Eq. 4.20 and experimental data.

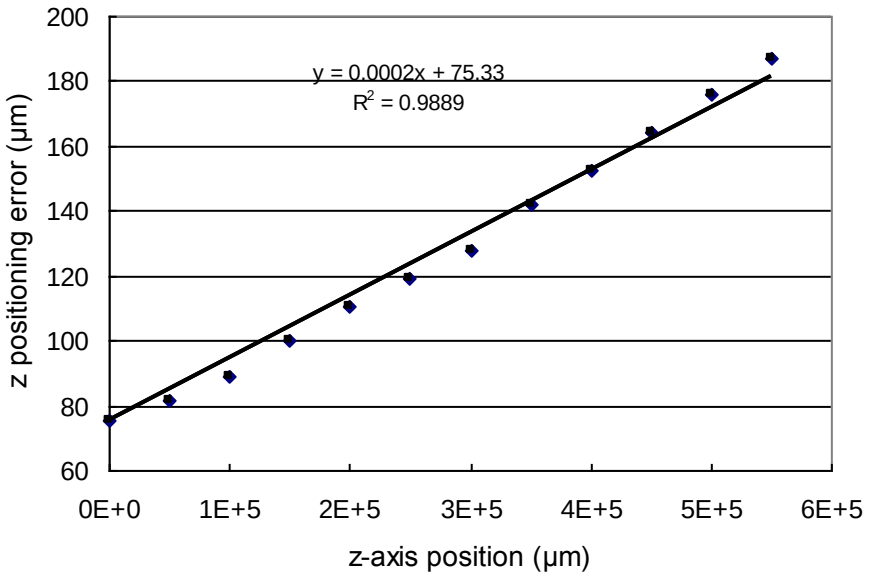

Figure 4.5: Curve Fitting for *z*-axis Positioning Errors at Nut Temperature (37°C)

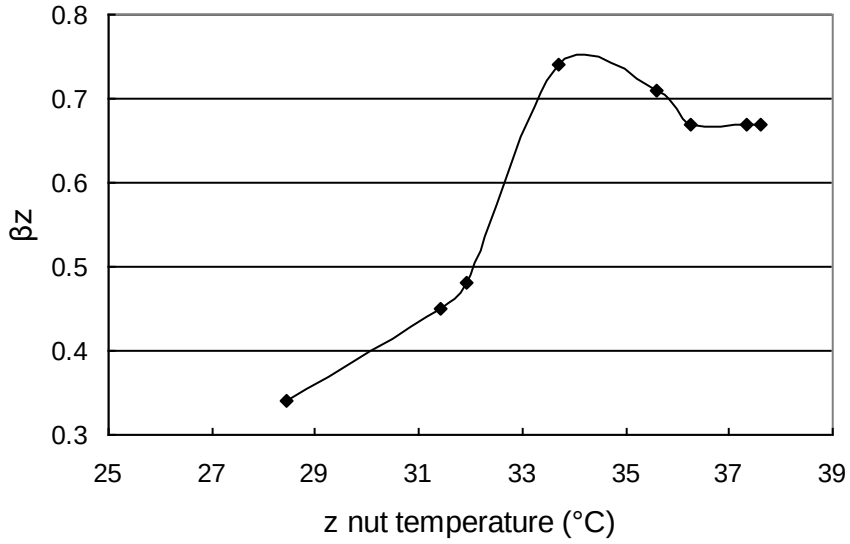

Figure 4.6: Variations of β_z with the Increase of z-axis Nut Temperature

Formation of TIVEM. The new thermally-induced volumetric error model can be formulated based on the general model from Eq. 4.11 assuming that the six straightness errors ($\delta_y(x)$, $\delta_z(x)$, $\delta_x(y)$, $\delta_z(y)$, $\delta_x(z)$, $\delta_y(z)$), nine angular errors ($\varepsilon_x(x)$, $\varepsilon_y(x)$, $\varepsilon_z(x)$, $\varepsilon_x(y)$, $\varepsilon_y(y)$, $\varepsilon_z(y)$, $\varepsilon_x(z)$, $\varepsilon_y(z)$, $\varepsilon_z(z)$) and three squareness errors ($\varepsilon_x(r)$, $\varepsilon_y(r)$, $\varepsilon_z(r)$) do not vary with the machine's thermal status. Replacing three positioning errors ($\delta_x(x)$, $\delta_y(y)$, $\delta_z(z)$) with thermally-induced positioning errors ($E_x(x, T_{xnut})$, $E_y(y, T_{ynut})$, $E_z(z, T_{znut})$) in Eq. 4.11, the following equation is derived:

$$\begin{cases} \Delta X = E_x(x, T_{xnut}) + \delta_x(y) + \delta_x(z) \\ \Delta Y = \delta_y(x) + E_y(y, T_{ynut}) + \delta_y(z) \\ \Delta Z = \delta_z(x) + \delta_z(y) + E_z(z, T_{znut}) \end{cases} \tag{4.24}$$

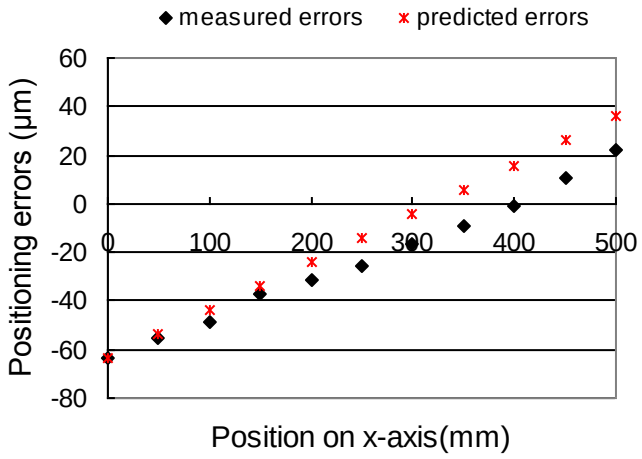

(a) *x*-axis

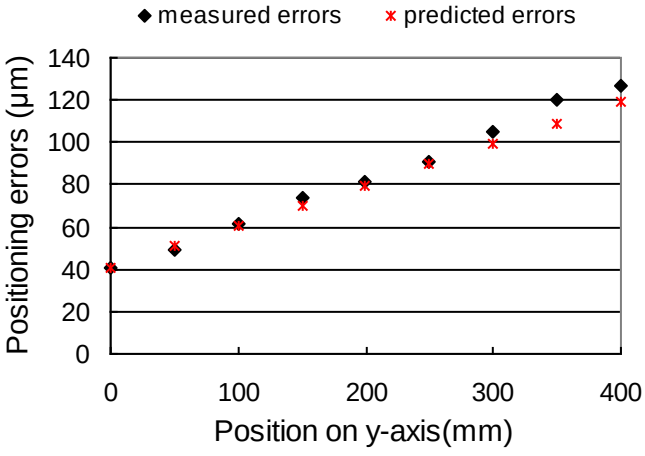

(b) *y*-axis

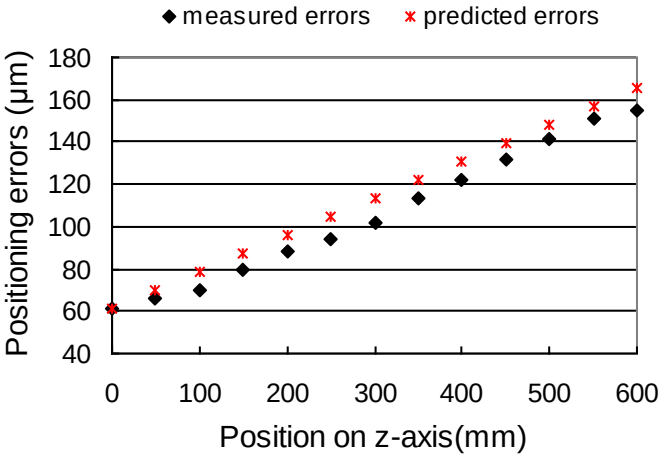

(c) *z*-axis

Figure 4.7: Comparisons of Measured [79] and Predicted Positioning Error Data: (a) *x*-axis, (b) *y*-axis, (c) *z*-axis

Substituting Eq. 4.24 to Eq. 4.18, the new model for thermally-induced volumetric error can be expressed through the following equations:

$$\begin{cases} V_x = (-Y_d)\cdot[\sum Z + \varepsilon_z(r)] + Z_d \cdot[\sum Y + \varepsilon_y(r)] + E_x(x, T_{xnut}) + \delta_x(y) + \delta_x(z) \\ V_y = (-Z_d)\cdot[\sum X + \varepsilon_x(r)] + X_d \cdot[\sum Z + \varepsilon_z(r)] + \delta_y(x) + E_y(y, T_{ynut}) + \delta_y(z) \\ V_z = (-X_d)\cdot[\sum Y + \varepsilon_y(r)] + Y_d \cdot[\sum X + \varepsilon_x(r)] + \delta_z(x) + \delta_z(y) + E_z(z, T_{znut}) \end{cases} \tag{4.25}$$

in which all geometric error components and variables have denotations that are the same as those for the general model.

4.3 Verification of TIVEM

4.3.1 Volumetric error calculation based on measured data

The 3D volumetric error for any given point at cold start and at the thermal stable stage of a three-axis machine tool can be calculated using the general volumetric error model (Eqs. 4.11 and 4.18) by applying measured geometric error data for the cold start and the thermal stable stage (Tables 4.1, 4.2 and 4.3) [79]. Comparing these two results, it is possible to find the magnitude of error induced by temperature increase in a machine tool.

4.3.2 Compensation point calculation by proposed TIVEM

For any nominal tool position P_d set by the CNC controller, its compensation point P_c can be calculated by applying the proposed TIVEM in conjunction with the algorithm proposed by Lee et al. [13]. According to this calculation procedure, at a certain thermal stage (e.g., the thermal stable stage), the CNC controller will set the cutting tool tip to the compensated point P_c instead of to point P_d to achieve high-quality machining. However, another error exists, $P_{c\text{-}newerror}$, which can be calculated by the general volumetric error model using geometric error data measured at the thermal stable stage [79]. After compensation, the resultant

volumetric error (V_c) can then be predicted as:

$$V_c = P_c + P_{c-newerror} - P_d \tag{4.26}$$

where $P_{c\text{-}newerror}$ is the error vector for point P_c at the thermal stable stage.

In the same way, the resultant linear displacement error ($\delta_{cx}(x)$, $\delta_{cy}(y)$, $\delta_{cz}(z)$) can be predicted after compensation as:

$$\begin{cases} \delta_{cx}(x) = P_{cx} + \delta_x(x) - X_d \\ \delta_{cy}(y) = P_{cy} + \delta_y(y) - Y_d \\ \delta_{cz}(z) = P_{cz} + \delta_z(z) - Z_d \end{cases} \tag{4.27}$$

where P_{cx}, P_{cy} and P_{cz} define vector P_c along x, y and z-axes respectively;

$\delta_x(x)$, $\delta_y(y)$ and $\delta_z(z)$ define axial positioning error at point P_c at the thermal stable stage; and

X_d, Y_d and Z_d define vector P_d along x-, y- and z-axes respectively.

Fig. 4.8 illustrates the flow chart for the calculation procedure. The databank consists of 21 geometric errors at different positions measured at the cold start stage [79] and a set of axial origin offsets with different thermal statuses. For any given point P_d (X_d, Y_d, Z_d) and on-line measured nut temperature (T_{xnut}, T_{ynut}, and T_{znut}), the 21 basic geometric errors at cold start and three origin offsets can be obtained directly from the databank or by the linear interpolation method.

4.4 Results and Analysis

Testing of a traditional model for thermally-induced volumetric error of a three-axis machine tool requires measurement of 21 geometric error components and their variation data at different temperatures. Obtaining these data is difficult and time-consuming. Hence, in this chapter, data presented in other published literature are used to demonstrate the effectiveness of the proposed model [79].

4.4.1 Volumetric error

The volumetric errors of a working zone of 210 x 210 x 210 mm in a typical three-axis horizontal CNC machine (Fig. 4.9) have been calculated to evaluate the spatial-based and thermal-based volumetric error variation before and after compensation. The working zone (Fig. 4.10) is from A_0 (40, 40, 40) to C_1 (250, 250, 250), units: mm.

Fig. 4.11 shows the thermally-induced volumetric error on plane $A_1B_1C_1D_1$ before compensation. The top layer shows the volumetric errors on this plane when the machine is at the thermal stable stage. The bottom layer shows the volumetric errors at cold start. The thermally-induced error on plane $A_1B_1C_1D_1$ increased from a minimum value 10 μm at cold start to a maximum value 208 μm at the thermal stable stage, a 198 μm increase.

Fig. 4.12 shows the spatial-variant volumetric errors in working zone $A_0B_0C_0D_0$ – $A_1B_1C_1D_1$. The top layer shows the volumetric errors in plane $A_0B_0C_0D_0$. The bottom layer shows the volumetric errors in plane $A_1B_1C_1D_1$. The spatial-variant error observed in this working zone at the cold start stage rose from a minimum value of 11 μm to a maximum value of 33 μm, i.e., a 22 μm increase. From this, it can be concluded that volumetric error caused by thermal distortion in a big industry, where the machine tool usually runs for the whole day, would be the major error source.

Fig. 4.13 shows the volumetric errors on plane $A_1B_1C_1D_1$ with and without compensation. The volumetric error rises from a minimum value of 10 μm (bottom layer) to a maximum value of 208 μm (second layer) without compensation, while the machine tool runs from the cold start stage to the thermal stable stage. The increase in volumetric error is reduced to 72 μm (64% decrease) when compensated for by the proposed model (third layer). If only compensated by the geometric model, the results might be worse (top layer), as the errors at high temperature might trend in different directions compared to their behaviour at the cold start stage. This phenomenon can be observed in Figs. 4.14, 4.15 and 4.16.

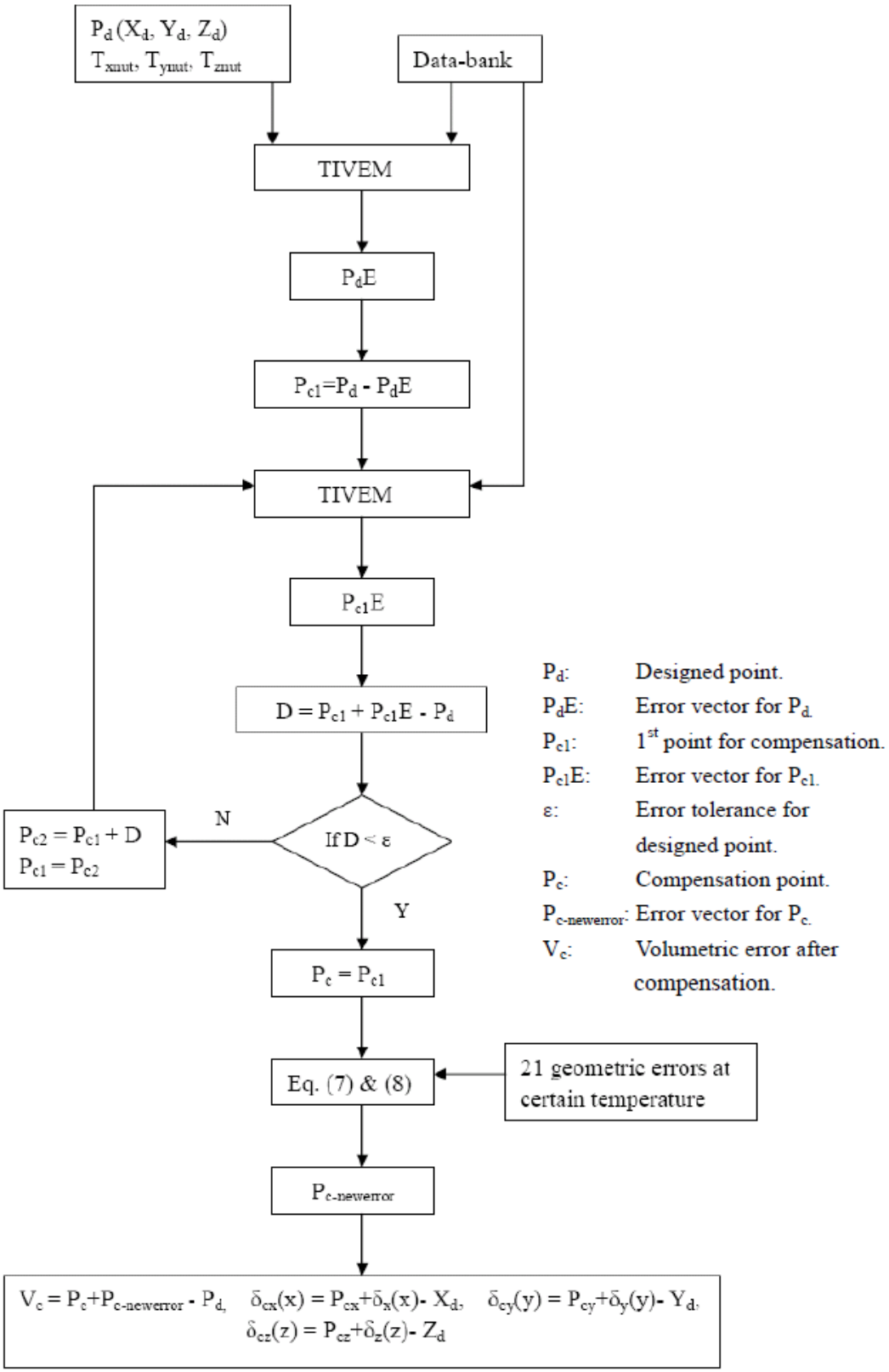

Figure 4.8: Flow Chart of Calculation Procedure

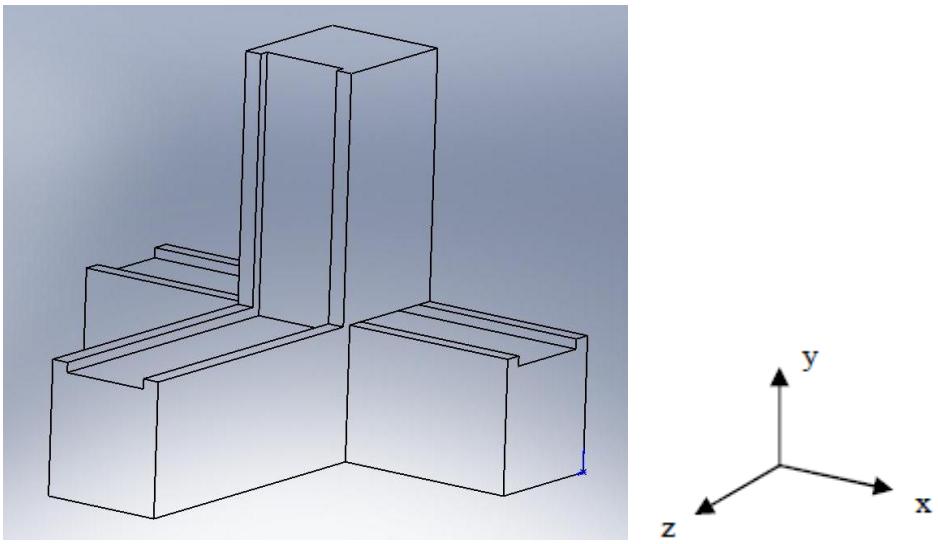

Figure 4.9: Test Machine Structure

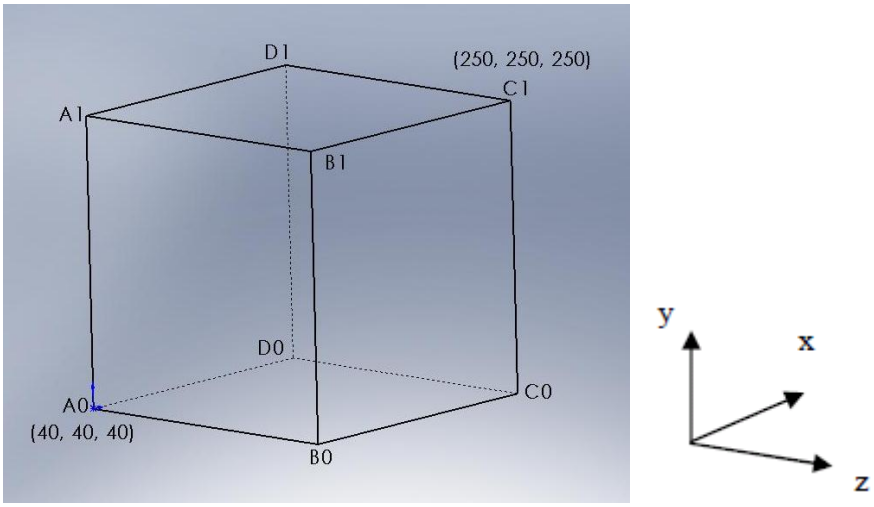

Figure 4.10: Work Zone

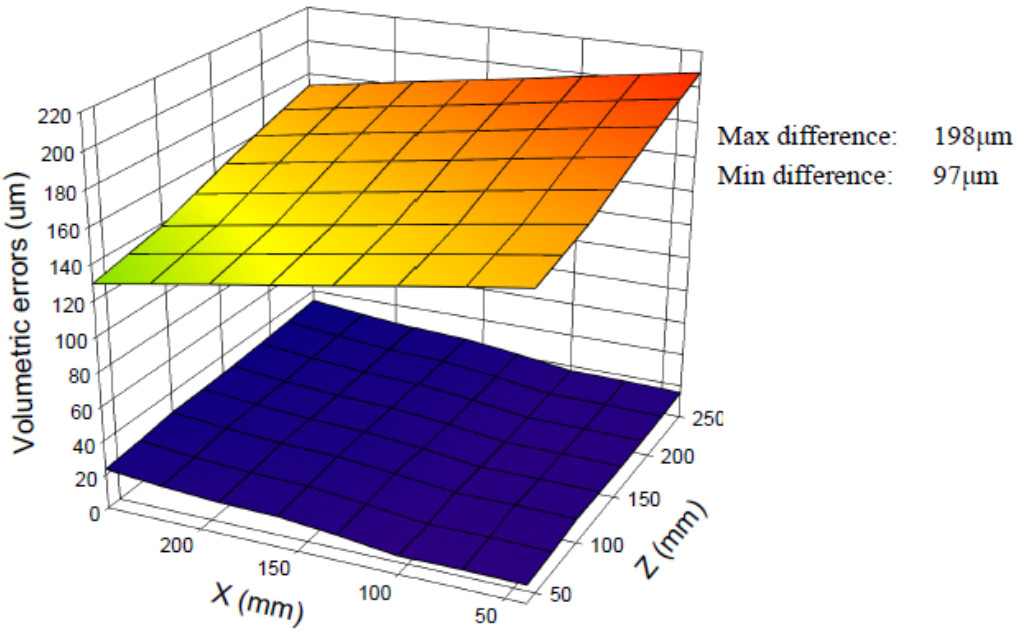

Figure 4.11: Thermally-Induced Volumetric Errors of Plane $A_1B_1C_1D_1$ before Compensation

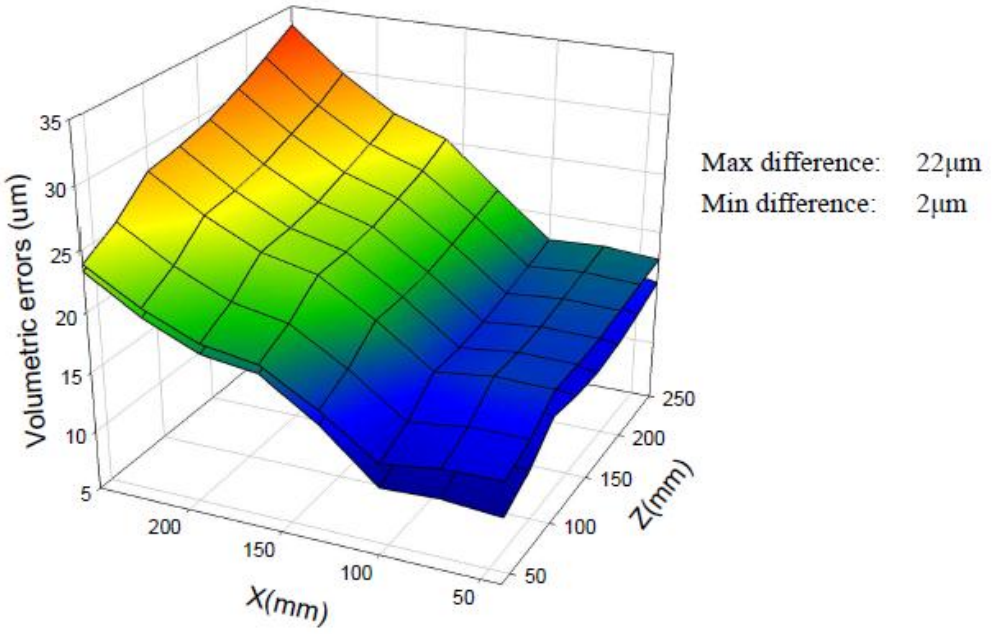

Figure 4.12: Spatially-Induced Volumetric Errors of Working Zone $A_0B_0C_0D_0 - A_1B_1C_1D_1$

4.4.2 Linear displacement error

The linear displacement errors along each axis have been calculated to evaluate the linear accuracy when the machine travels along the axial direction. Fig. 4.14 shows the linear displacement errors in the *z*-axis with and without compensation when the machine moves along line A_0B_0. It is observed that the maximum error, which is defined as the measured value minus the designed value, is reduced from 106.27 μm to -5.14 μm (95% reduction) at the thermal stable stage for the machine after compensation by the proposed model.

Fig. 4.15 shows the linear displacement error in the *x*-axis with and without compensation when the machine moves along line A_0D_0. The maximum error is reduced by 91% in total after compensation.

Fig. 4.16 shows the linear displacement error in the *y*-axis with and without compensation when the machine moves along line B_0B_1. The maximum error is reduced by 89% in total after compensation.

4.4.3 Prediction of the dimensional accuracy of cut workpiece

Two kinds of machining jobs have been simulated, and their results have been predicted. The first one is the milling of surface $A_0A_1D_1D_0$. Its positioning error and average depth difference between several machining situations have been calculated to evaluate the effectiveness of the compensation in the *z*-axis. The second job is the drilling of four holes in surface $A_0A_1D_1D_0$. The distance errors between holes are calculated to evaluate the effectiveness of compensation in the *x*-axis and *y*-axis.

Fig. 4.17 shows the positioning error distribution of milled surface $A_0A_1D_1D_0$ under different machining situations. The top layer shows the results machined under high temperature without compensation. The second one is machined under high temperature and then compensated by the proposed model. The third one shows the ideal position. The bottom one shows the results for cold start. It is evident that the positioning errors have been reduced. Fig. 4.18 illustrates the average depth difference of surface $A_0A_1D_1D_0$ with and without compensation. The surface jumps

between workpieces machined at different times have been reduced from 115.40 μm to 45.37 μm, for a total reduction of 61% after compensation.

Table 4.6 shows the distance errors between holes under different machining situations. The designed positions of the holes are shown in Fig. 4.19. The maximum distance error is reduced from 38.69 μm to -0.14 μm, for a total reduction of 99% after compensation.

4.5 A Simple Error Compensation Scheme

Based on the above discussion, a simple on-line volumetric error compensation system is proposed for existing machine tools, which will provide the opportunity for manufacturing high-precision parts without the purchase of new, more sophisticated machine tools. A block diagram of the proposed on-line volumetric error compensation system is given in Fig. 4.20. The figure shows that the 21 basic geometric errors (calibrated around 20°C) and temperature-related origin offsets only need to be checked regularly unless the machine has been remounted. Three thermocouples need to be attached to the machine to monitor the variations in nut temperature. A personal computer is also needed to do the calculations and communicate with the CNC controller. The proposed system is under development and will be presented as an extension of this work.

Table 4.6: Distance Errors* between Holes under Machine Tool's Different Thermal Conditions

Distance error (unit: μm)	Cold start	High temp.	Compensated by old model	Compensated by new model
Dis.O12	8.81	25.05	16.22	1.75
Dis.O23	5.41	27.31	21.91	-0.89
Dis.O34	9.45	26.08	16.63	2.16
Dis.O41	6.42	29.97	23.53	0.78
Dis.O13	8.80	37.98	29.17	2.84
Dis.O24	12.5	38.69	26.19	-0.14
* Distance error = measured distance – designed distance				

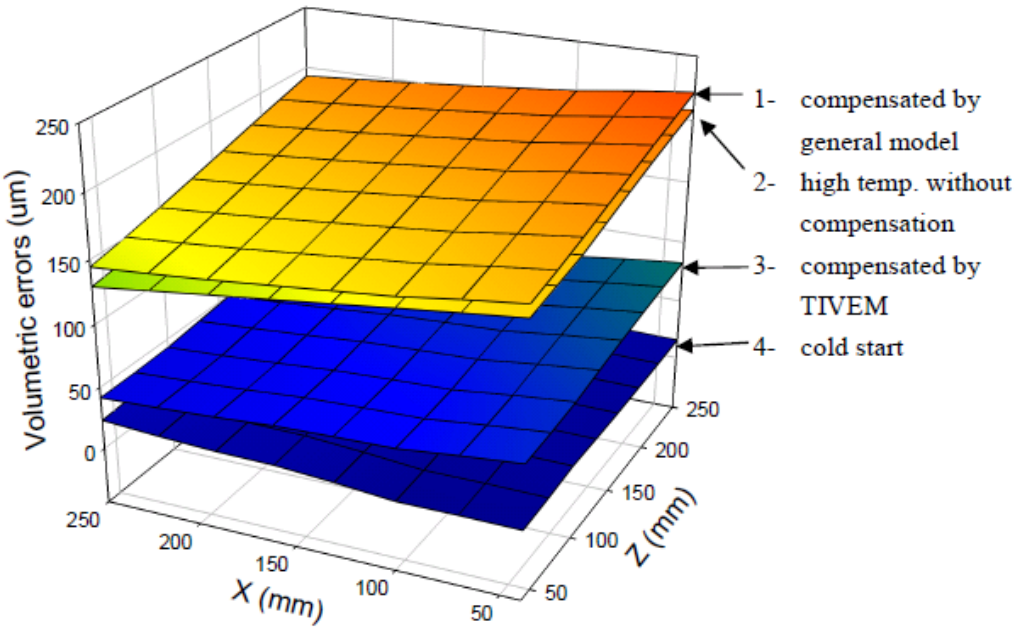

Figure 4.13: Thermally-Induced Volumetric Errors of Plane $A_1B_1C_1D_1$ with and without Compensation

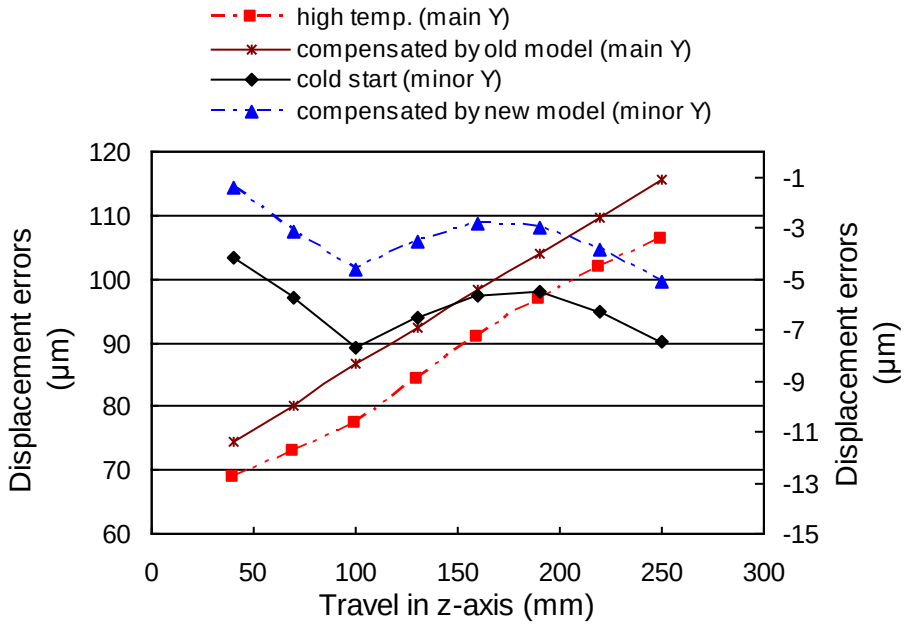

Figure 4.14: Linear Displacement Errors in *z*-axis When Machine Moves along Line A_0B_0

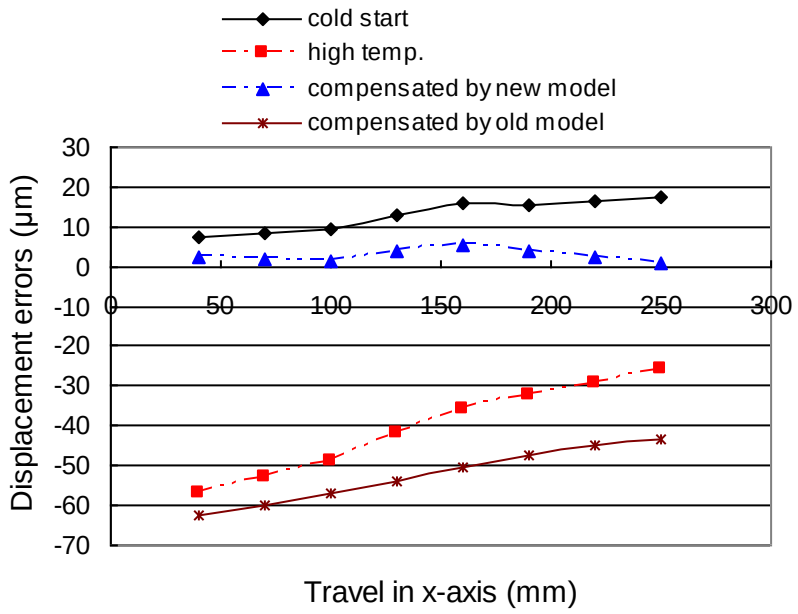

Figure 4.15: Linear Displacement Errors in *x*-axis When Machine Moves along Line A_0D_0

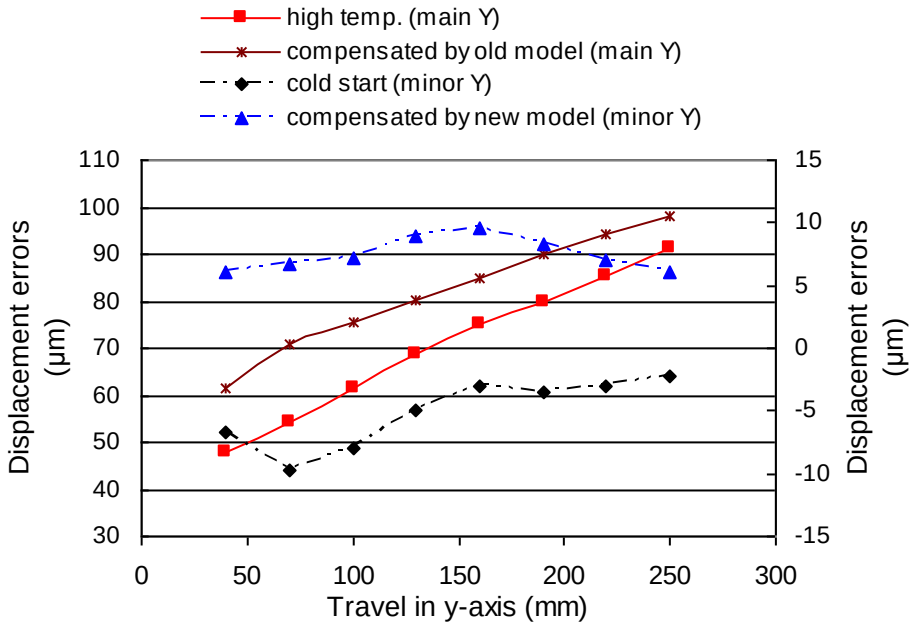

Figure 4.16: Linear Displacement Error in *y*-axis When Machine Moves along Line B_0B_1

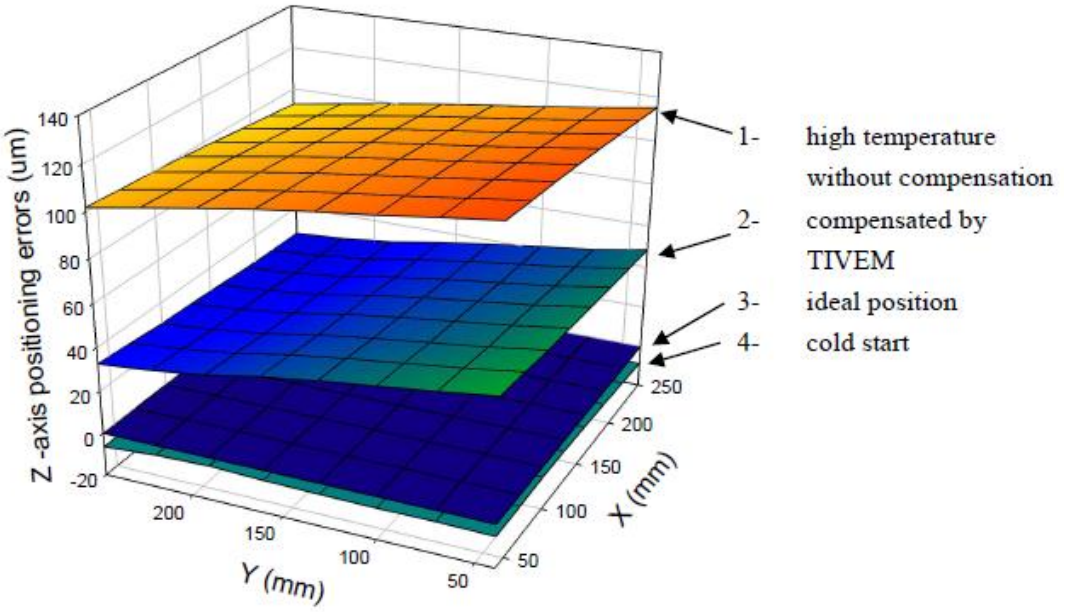

Figure 4.17: Positioning Error Distribution of Milled Surface $A_0A_1D_1D_0$ under Different Machining Situations

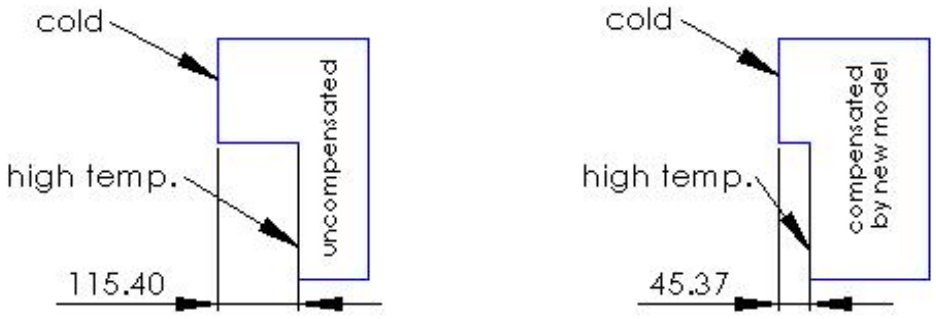

Figure 4.18: Average Depth Difference (μm) for Surface $A_0A_1D_1D_0$ with and without Compensation

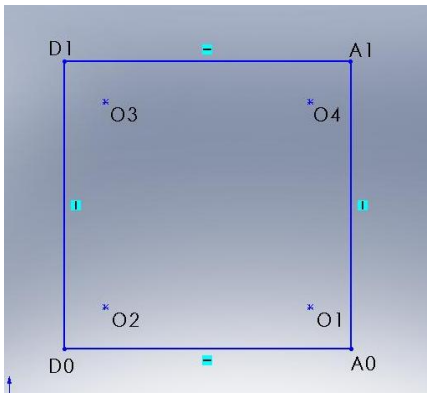

Figure 4.19: Positions of the Holes

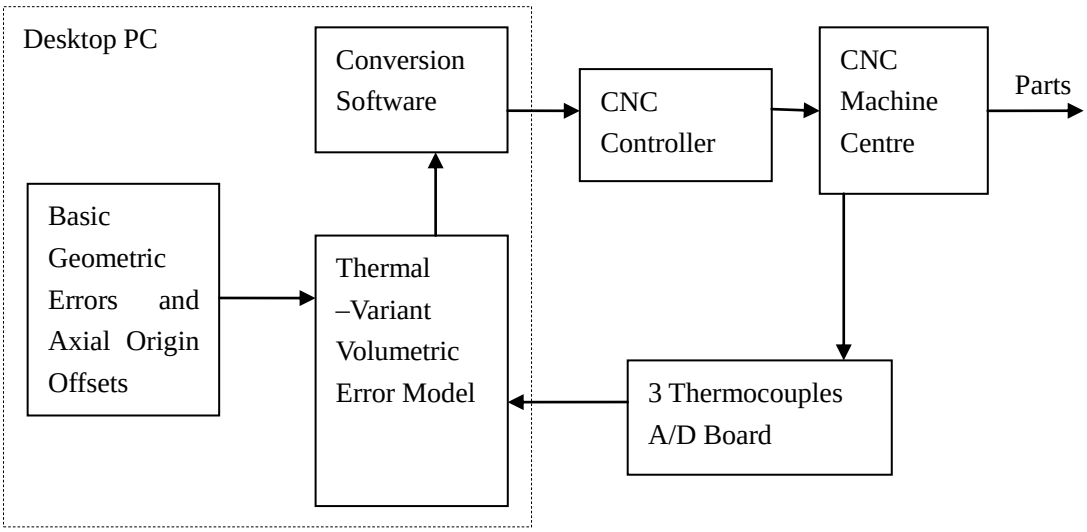

Figure 4.20: Block Diagram of On-line Volumetric Error Compensation System

4.6 Simplification of TIVEM

The main characteristic of the thermally-induced volumetric error model (TIVEM) developed so far is that it considers the changes of positioning errors only; the variations of the remaining 18 geometric error components are ignored. As a result, the need for monitoring the changes of 18 geometric error components with temperature is no longer required: thus, the large number of thermocouples required for the traditional model is reduced to three. However, the TIVEM still includes the same number of error components (21 geometric error components) as the traditional model. This sub-section attempts to further simplify the TIVEM for expanding its applications in general industry by ignoring angular errors, straightness errors, and squareness errors at the cold stage and compensating for volumetric error by considering only the thermally-induced positioning errors.

The simplified model can be expressed as Eq. 4.28 based on TIVEM (Eq. 4.25):

$$\begin{cases} V_x = E_x(x, T_{xnut}) = x_0(T_{xnut}) + \beta_x \cdot \alpha \cdot x \cdot (T_{xnut} - 20) \\ V_y = E_y(y, T_{ynut}) = y_0(T_{ynut}) + \beta_y \cdot \alpha \cdot y \cdot (T_{ynut} - 20) \\ V_z = E_z(z, T_{znut}) = z_0(T_{znut}) + \beta_z \cdot \alpha \cdot z \cdot (T_{znut} - 20) \end{cases} \tag{4.28}$$

To demonstrate the effectiveness of the simplified model, milling operations were simulated on a three-axis horizontal CNC machining centre (Fig. 4.9). Fig. 4.21 shows the prismatic component sized 280 x 50 x 50 mm, 150 x 25 x 25 mm, and 30 x 10 x 10 mm, respectively. Faces $A_0B_0C_0D_0$ and $A_1B_1C_1D_1$ were machined in the simulation.

For any nominal tool position P_d set by the CNC controller, its compensation point P_c and error-remains after compensation can be calculated by applying the simplified model in conjunction with the algorithm shown in Fig. 4.8. The calculation results and analysis are shown in following sections.

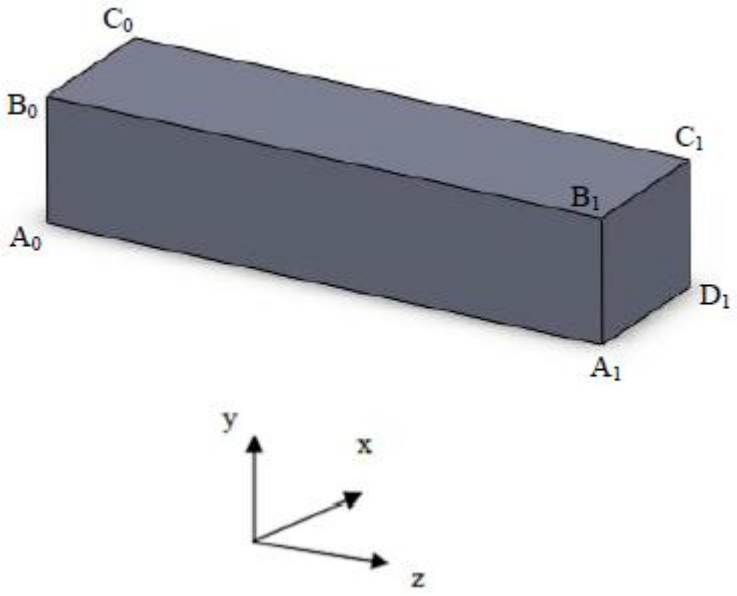

Figure 4.21: Simulated Machining Components

4.6.1 Volumetric errors

Fig. 4.22 illustrates the thermally-induced volumetric errors of plane $A_1B_1C_1D_1$ (workpiece size: 150 x 25 x25 mm) machined under different machine conditions. The top layer shows that the average volumetric error is calculated as 192 microns if machined at high temperature without compensation. The second layer shows that the average volumetric error is calculated as 82 microns if machined at high temperature and compensated by the simplified model, which is a 57.3% reduction from the uncompensated error. The third layer shows that the average volumetric error is calculated as 77 microns if machined at high temperature and compensated by TIVEM, which is a 59.9% reduction from the uncompensated error. The bottom layer depicts that the average volumetric error is calculated as 11 microns if machined at the cold start state, which does not require any thermal compensation. Therefore, the difference between the simplified model and the TIVEM is 5 microns or 2.6% of the uncompensated thermal error, which is negligible.

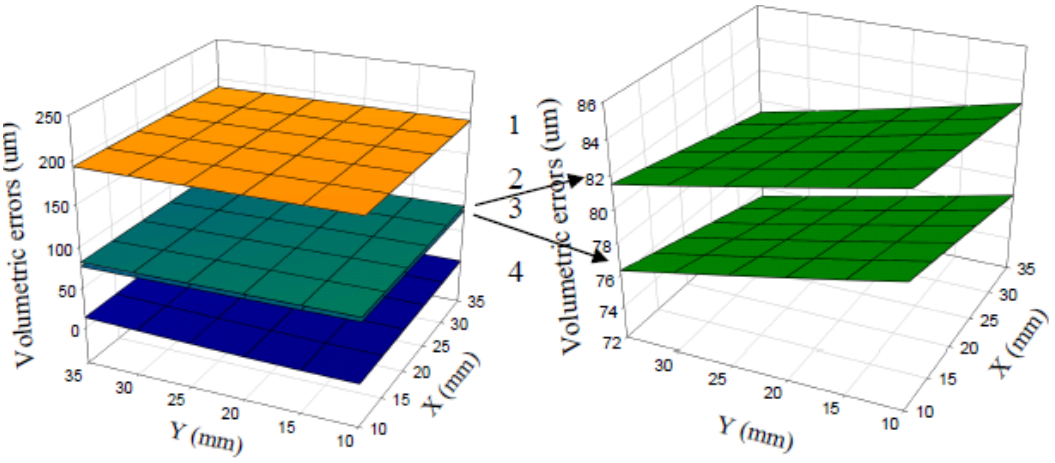

Figure 4.22: Thermally-Induced Volumetric Errors of Plane $A_1B_1C_1D_1$ (Workpiece Size: 150 x 25 x 25 mm) at Different Machining Conditions

Plot 1: High Temperature without Compensation

Plot 2: Compensated by Simplified Model

Plot 3: Compensated by the TIVEM Including All 21 Errors

Plot 4: Cold Start

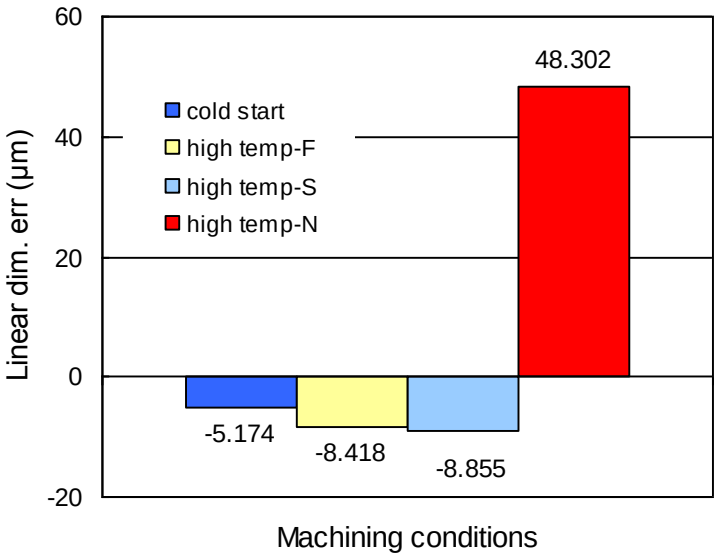

Figure 4.23: Linear Dimension Errors of a 280 x 50 x 50 mm Workpiece (Length: 280 mm)

F - Compensated by full error model TIVEM

S - Compensated by simplified model

N - Without compensation

4.6.2 Linear dimension errors

Linear dimension, the distance between planes $A_0B_0C_0D_0$ and $A_1B_1C_1D_1$, was calculated to evaluate the effectiveness of the simplified model on linear dimension compensation. The linear dimension error is defined as the measured value minus the designed value. Fig. 4.23 shows that the linear dimension error for a large workpiece increased by 0.437 microns (|(-8.855)-(-8.418)|) if compensated by the simplified model rather than the TIVEM. Similarly, for medium and small sized workpieces, the errors are increased by 0.107 and 0.004 microns, respectively, using the simplified model (Fig. 4.24 – Fig. 4.25). A comparison of linear dimension errors between different size workpieces (Fig. 4.26) confirms that the linear dimension error is proportional to the size of the workpiece.

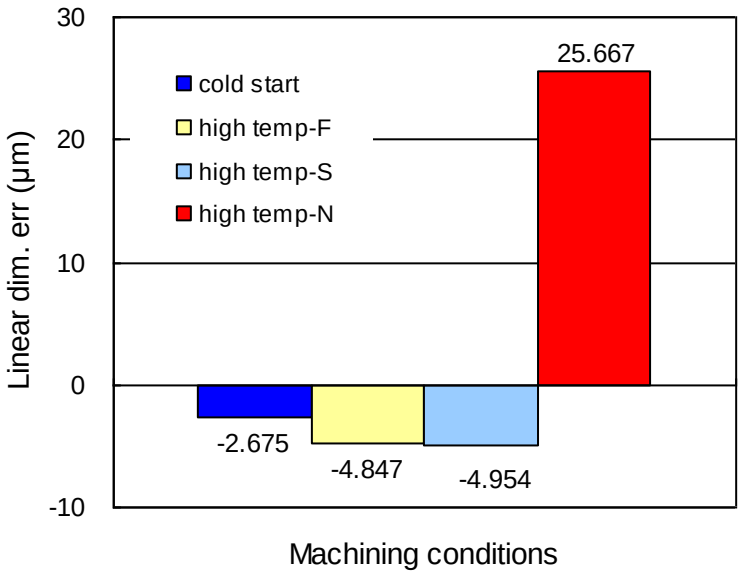

Figure 4.24: Linear Dimension Errors of a 150 x 25 x 25 mm Workpiece (Length = 150 mm)
F - Compensated by full error model TIVEM
S - Compensated by simplified model
N - Without compensation

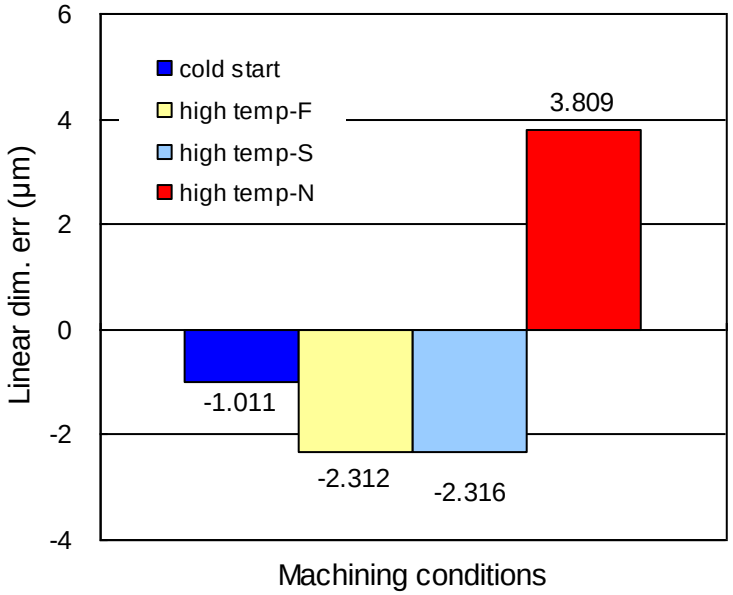

Figure 4.25: Linear Dimension Errors of a 30 x 10 x 10 mm Workpiece (Length = 30 mm)

F - Compensated by full error model TIVEM

S - Compensated by simplified model

N - Without compensation

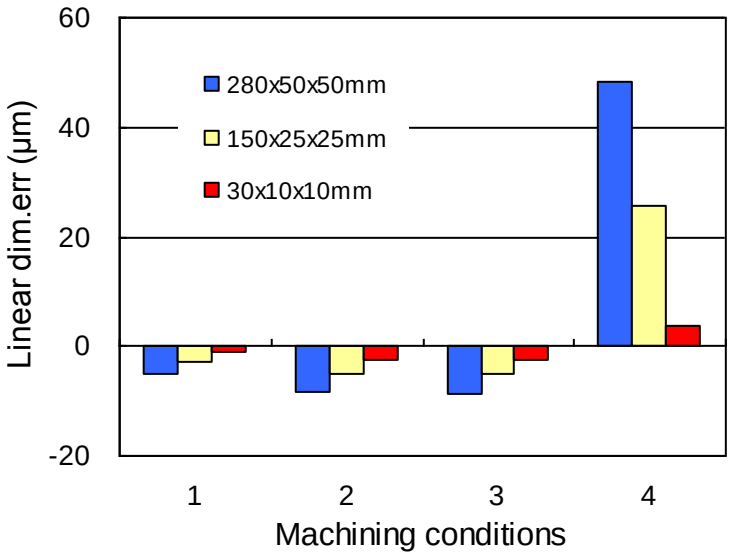

1-cold start 2-high temp-F 3-high temp-S 4-high temp-N

Figure 4.26: Comparison of Linear Dimension Errors of Different Workpiece Sizes

F - Compensated by full error model TIVEM

S - Compensated by simplified model

N - Without compensation

4.6.3 Assessment of compensation results by process capability data

It is worth comparing the results with process capability data because it is an indicator of real machining error. Process capability (also known as natural tolerance) is the smallest tolerance that can be maintained economically by a particular process; as such, it represents the precision of a process. The smaller the process capability value is, the more precise the process is, yielding a higher quality product with smaller variability in dimensions. Process capability data can be estimated by applying the following equation [105, 106]:

$$PC = (0.45\sqrt[3]{S} + 0.001S)10^{\frac{IT-16}{5}} \tag{4.29}$$

where PC represents process capability (mm); S presents magnitude of size dimension (mm); and IT presents international tolerance grade number.

The IT grade indicates the precision of a manufacturing process. Each manufacturing process is capable of producing an IT grade range. The actual process capability depends on a number of process factors. Farmer [5] proposed a method for calculating process capability considering six major factors: (1) type of material machined, (2) shape of the part, (3) surface area, (4) number of operations, (5) machine conditions and (6) skill of the operator. The method uses a scoring system, the details of which are available in Farmer [5]. The change in process capability value caused by machine conditions can be estimated by assuming the other five process factors remain the same.

Machine condition is affected by a number of factors, such as the built-in geometric and kinematic errors, thermally-induced errors, errors caused by the cutting process and other machine system errors. Considering other aspects unchanged, the dimensional error caused by the machine's temperature rise can be calculated from measured data. From this baseline, the percentage of error reduced by using the simplified compensation model out of the total dimensional error caused by machine conditions can be obtained.

The results show that thermally-induced dimensional error comprises 75.94% of

total dimensional errors caused by machine conditions (Fig. 4.27a). When compensated by the full-error model, 70.23% of total dimensional errors can be eliminated, which leaves 5.71% thermally-induced dimensional error remaining (Fig. 4.27b). When compensated by the simplified model, 69.46% of total dimensional errors can be eliminated, which leaves 6.48% thermally-induced dimensional error remaining (Fig. 4.27c). This suggests that only 0.77% of total dimension compensation accuracy will be sacrificed by adopting the simple and economical model proposed in this research instead of the traditional model.

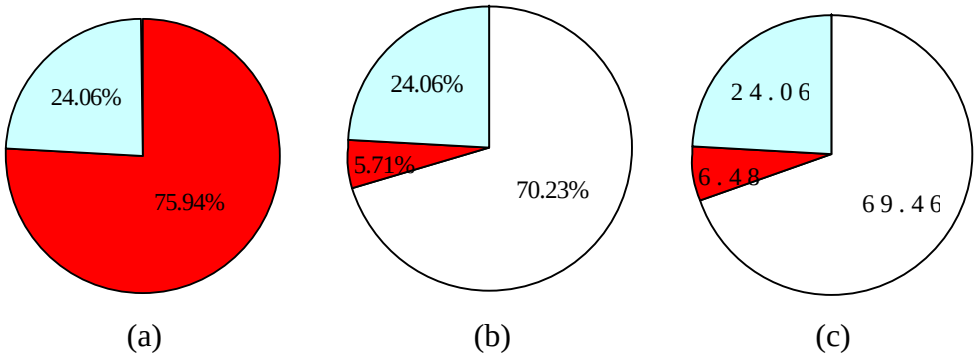

Figure 4.27: The Percentage of Thermally-Induced Dimensional Error with and without Compensation: Workpiece Size: 280 x 50 x 50 mm

(a) Thermally-induced dimensional error comprises 75.94% without compensation; 24.06% of total dimensional error is caused by other machine error

(b) Thermally-induced dimensional error is reduced by 70.23% if compensated by the TIVEM

(c) Thermally-induced dimensional error is reduced by 69.46% if compensated by the simplified model

4.7 Concluding Remarks

- A thermally-induced volumetric error model (TIVEM) has been developed to calculate the volumetric error at any time and at any given point in a three-axis CNC machining centre working zone.
- The proposed model was applied for two types of simulated machining jobs: milling and drilling. The results show that, by application of the proposed model, the thermally-induced volumetric error was reduced from 115.40 μm

to 45.37 μm for the milled surface, and the maximum distance error between drilled holes for the drilling operation was reduced from 38.69 μm to -0.14 μm.

- The model was simplified to take into account only the three axial positioning errors and their variations with temperature. The simulated machining results indicate that only a negligible amount of total dimensional accuracy will be sacrificed by adopting the simplified compensation model compared with the traditional model.
- The simplified model requires only measurement of the three axial positioning errors and their variations with temperature; therefore, a Laser Doppler Displacement Meter (LDDM) will be adequate to meet the accuracy requirement.

Chapter 5

Model Verification

5.1 Introduction

In Chapter 4, the validation of the developed model was completed using experimental data available in the literature reported by Venugopal [79]. This was necessary because a comparison with the traditional model was needed to demonstrate the effectiveness of the new model. However, the traditional model requires the measurement of 21 error components, the avoidance of which is the main objective of this project. In this chapter, the verification of the proposed model is done by applying new experimental data.

The proposed model requires the measurement of only three positioning error components; therefore, a Laser Doppler Displacement Meter (LDDM) was adequate for the error measurements. A number of tests were performed to observe the variations of the positional errors with temperature along the three axes separately. The effects of cutting operations on positioning errors were also analysed by performing two machining operations: drilling and milling. Finally, comparisons were made between measured and predicted errors to demonstrate the accuracy of the error prediction model.

5.2 Thermally-Induced Positioning Error

In Eq. 4.20, 20°C is used as the starting point for the temperature rise because it is the international standard temperature for describing the length of an object [114]. In practice, however, guaranteeing 20°C as the initial temperature is difficult to accomplish when measuring original lead screw errors. In Eq. 4.20, therefore, (T-20) is substituted by (T-T_0) in the subsequent prediction model, where T_0 is the actual starting temperature.

As described in Chapter 4, ball screw nut temperature was chosen as the temperature measurement point to demonstrate the lead screw expansion, and it

should be measured at a spot facing the driving motor and as close as possible to the nut–lead screw contact surface, as shown in Fig 5.1. This determination is based on the fact that the friction heat generated in the nut–lead screw contact surface dominates the lead screw expansion and the assumption that heat from friction between the nut and lead screw is equally dispersed to these two parts.

On the basis of the above-stated analysis, the prediction model for thermally-induced positioning error (Eq. 4.20) can be represented by the following equations:

$$\begin{cases} E_x(x,T_{xnut}) = E_x(x,T_{x0}) + \beta_x \cdot \alpha \cdot x \cdot (T_{xnut} - T_{x0}) \\ E_y(y,T_{ynut}) = E_y(y,T_{y0}) + \beta_y \cdot \alpha \cdot y \cdot (T_{ynut} - T_{y0}) \\ E_z(z,T_{znut}) = E_z(z,T_{z0}) + \beta_z \cdot \alpha \cdot z \cdot (T_{znut} - T_{z0}) \end{cases} \tag{5.1}$$

where $E_x(x, T_{xnut})$, $E_y(y, T_{ynut})$ and $E_z(z, T_{znut})$ are the positioning errors along axes that are functions of axial travel distance and nut temperature;

$E_x(x, T_{x0})$, $E_y(y, T_{y0})$ and $E_z(z, T_{z0})$ denote the original positioning errors, which can be measured before machine operation;

x, y, and z represent the axial travel distances;

T_{xnut}, T_{ynut} and T_{znut} are the nut temperatures; and

β_x, β_y and β_z are the adjustment factors in the x-, y- and z-axis, respectively. The adjustment factors are determined from data measured using the least squares method. The details of this procedure can be found in Chapter 4 of this thesis.

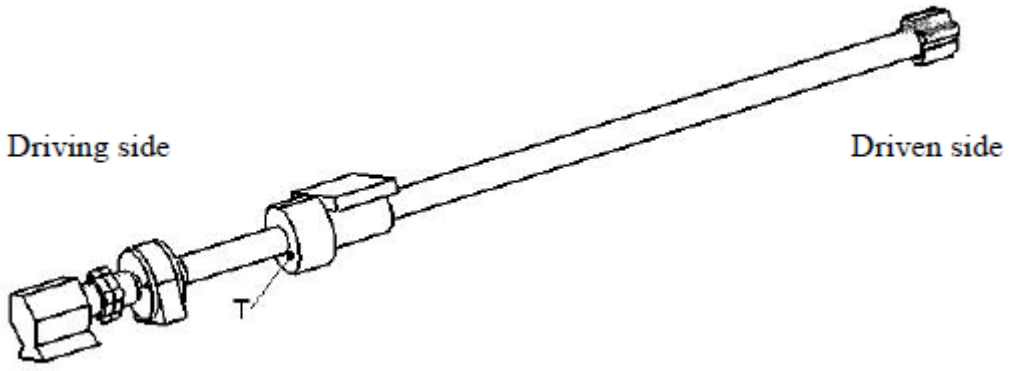

Figure 5.1: Location of Thermocouple (T) on *x*-axis Ball Screw Nut

5.3 Experimental Work

5.3.1 Test machine setup

The experiment was conducted on a CNC machining centre at the CAD/CAM lab of the Department of Mechanical Engineering, Curtin University. It should be pointed out that an EMCO F1 CNC milling machine was used in the preliminary study. EMCO F1 is a small CNC milling machine suitable for research and educational purposes. This machine was chosen for the preliminary study because of the ease of disassembly of its frame and setting up the thermocouples at various locations. As the simplified model no longer requires measurement of temperature at a large number of locations, all the validation tests described in this chapter were conducted on a bigger machine typically used in the industry, the Leadwell V30 manufactured by Leadwell, Taiwan. The Leadwell V30 (Fig. 5.2) is a three-axis vertical machining centre with maximum strokes 760 x 410 x 520 mm along the *x*-, *y*- and *z*-axes respectively. A ball screw driving system is fitted to each axis and is capable of operating at a maximum feed rate of 5000 mm/min along all axes. The maximum available spindle speed is 8000 rpm. The other specifications of the machine are listed in Appendix A [117]. A thermocouple with a magnetic end was attached to the nut to measure the temperature variations for each axis (Fig. 5.1).

5.3.2 Measuring instrument

Introduction of LDDM. The positioning error was measured by a Laser Doppler Displacement Meter (LICS-100) manufactured by Optodyne, Inc., USA. The LICS-100 system consists of three components: a laser head with processor module, a retro reflector and a notebook computer, as shown in Fig. 5.3. The technical specifications of LICS-100 are listed in Appendix B [118].

The LICS-100 monitors the displacement of the objective or target from an initial position where the display is zeroed to any final position within the range of the instrument. Displacement is shown continuously as the target moves. At the final position, the displacement of the target is displayed. The sign of the displayed number indicates positive or negative displacement.

Figure 5.2: V30 CNC Machine Centre

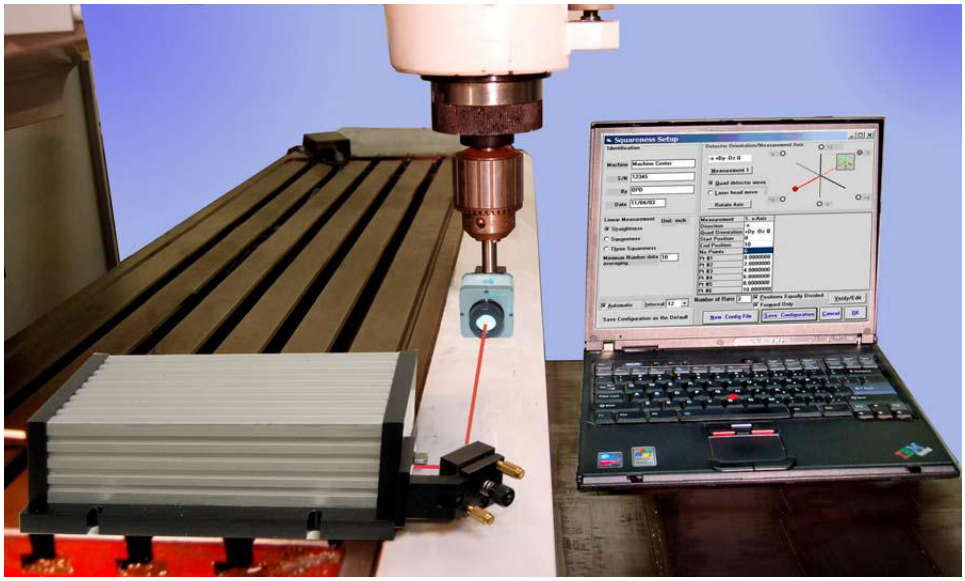

Figure 5.3: Laser Doppler Displacement Meter (LICS-100) [118]

LICS-100 uses an electro-optical device which detects the Doppler shift of a laser frequency caused by a moving target to measure displacement with a high degree of accuracy. The range may be from a few microns to several meters. Other precision displacement measuring devices use interferometric techniques, requiring a sophisticated laser that calls for critical, time-consuming alignments and causes additional expense. LDDM is based on the principles used in radar. Its construction is simpler, less costly and more rugged, and it is much easier to use than a conventional interferometer.

The frequency of the reflected laser beam is shifted by the motion of the retro reflector and is proportional to its velocity. The phase shift is proportional to the displacement. A phase-detector is used to sense the phase shift. For each half-wavelength of displacement, a counter is incremented. A microprocessor is used to read the counter and the phase angle before converting them to inches or centimetres.

The Doppler frequency shift can be expressed as:

$$\Delta f = (2f / c) \cdot \Delta v \tag{5.2}$$

or

$$\Delta \theta = 2\pi \cdot (2f / c) \cdot \Delta z \tag{5.3}$$

where Δf and $\Delta \theta$ are the frequency and phase shift, and Δv and Δz are the velocity and displacement of the retro reflector, respectively. The variable f is the frequency of the laser, and c is the speed of light.

A counter is used in conjunction with the phase detector to record the number of half-wavelengths ($\lambda/2$) detected. A microprocessor reads the counter and the phase angle and converts them to output units. Compensation for changes in the speed of light due to temperature, pressure and humidity variations is programmable.

Setup of the LDDM. Fig. 5.4 shows that the LDDM is set up for measuring *x*-axis positioning errors. The laser is launched from the laser head, which is secured on a stable surface. A 90° beam bender is attached to the laser head to reflect the laser beam to any desired direction from the incident beam. The laser beam is then returned by a retro reflector mounted on the moving parts. The reflected beam is detected near the laser source: the original and the reflected beams run the same

paths. After detection, the displacement information is calculated and sent to a notebook PC through a USB interface for displaying the reading, data collection and analysis. When measuring the *y*-axis positioning error, the laser head is fixed in the front of the machine; the reflector is still mounted on the table and facing the laser head. The white form board and box are used as temporary barriers to protect the LDDM from cutting coolant and flying chips.

Fig. 5.5 shows that the LDDM is setup for measuring *z*-axis positioning errors. The laser head is fixed on the table, which does not move during the measuring. A 90° beam bender bends the laser beam to the *z* direction. The reflector with the magnetic end is attached to the moving spindle (no rotations) to reflect the laser beam. Fig. 5.6 shows a screenshot during measuring.

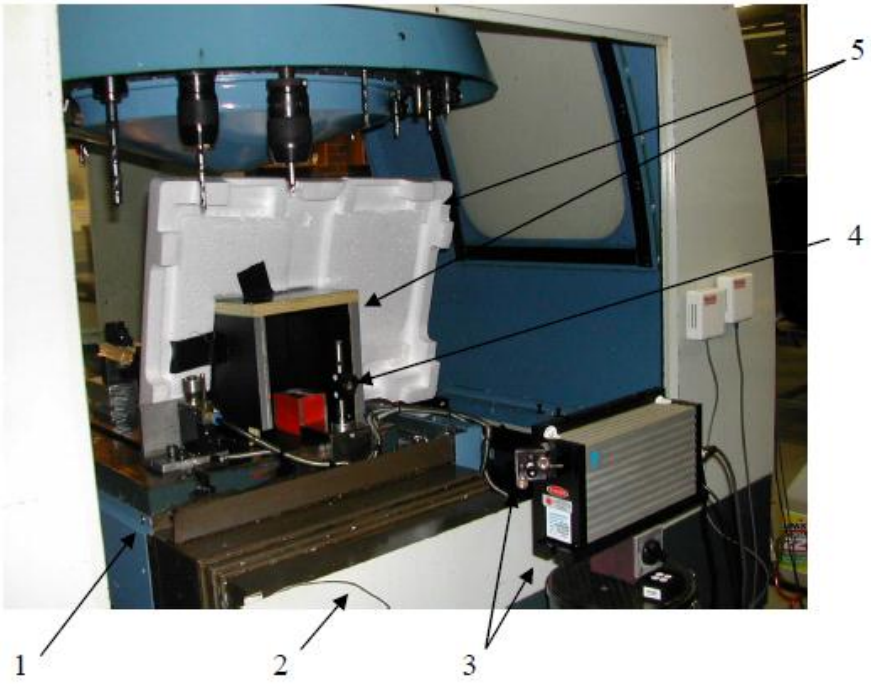

1: Moving table 2: Thermocouple 3: Laser head and beam bender
4: Retro reflector 5: Temporary barrier

Figure 5.4: Setup of LDDM in *x*-axis

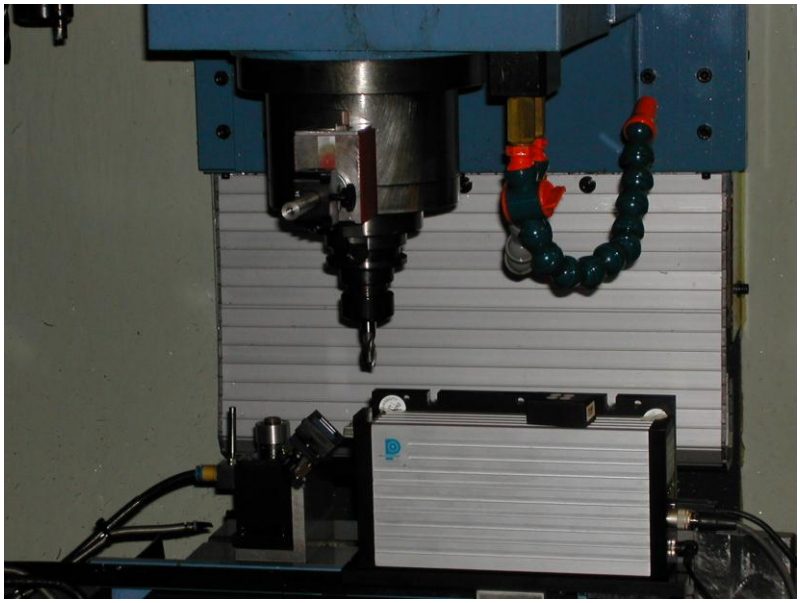

Figure 5.5 Setup of LDDM in *z*-axis

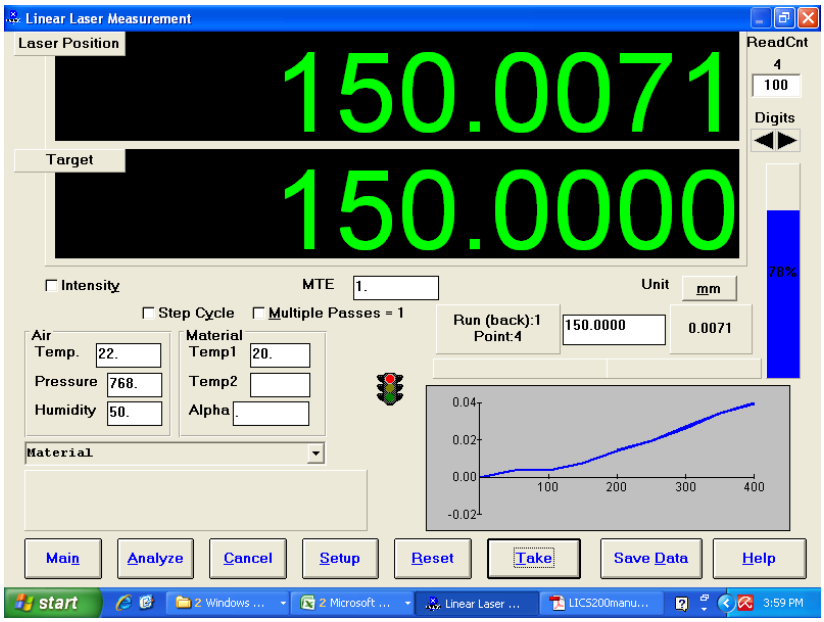

Figure 5.6: Screenshot during Measuring

5.3.3 Testing procedure

The aim of this experiment is to monitor the variations in the three-axis positioning errors of a CNC machine with temperature and the effects of operating conditions on positioning errors. The operating conditions considered in this research were idle run, end milling, and drilling. During an idle run, the machine does not cut any material; hence, this stage is called air cutting by some researchers. During air cutting, the machine was operated at the maximum feed rate and full stroke of the machine tool to simulate the load generated by the actual cutting process. A test component was designed for conducting the end milling and drilling operations (Fig. 5.7). Aluminium alloy 6061, which is readily available and widely used in industry, was chosen as the work material. It is also relatively easy to machine and is capable of producing a good surface finish.

Idle run was applied in the three axes separately to avoid the combined effects of the axes. Two operating modes were adopted in conducting positioning error measurements under the idle run condition. One was maintaining a constant idle run at the maximum feed rate along the full backward and forward strokes to generate heat and warm up the machine; the other mode was idle measurement. During idle measurement, the table was moved step by step (at an increment of 50 mm for each step); the positioning errors were measured and recorded during each step as the table was moved both ways (forward and backward) to inspect the hysteresis caused by backlash. The values were recorded at each step. Therefore, the machine was operated in a repeated procedure—idle measurement > constant idle run > idle measurement—until the temperature reached a steady state.

The idle measurement time is designed for machine run times of 0, 10, 20, 30, 60, 120 and 180 min as temperature increases rapidly in the first hour (Chapter 3). However, this measurement schedule cannot be sustained in practice because of the considerable time required to change the operating program. The actual measurement times are shown in Tables 5.1, 5.2 and 5.3, in which the operation column shows the first letter that defines the operation name (I: idle measurement; D: drilling; M: end milling), the second letter denotes the operating axis and the number represents the machine run time.

The actual cutting operations (drilling and end milling) were performed only on the *x*-axis. A high-speed steel (HSS) drill with a 12 mm diameter was used to drill

holes denoted as H1 to H10. Holes H1 to H5 were drilled under a low temperature (Table 5.1), and the test procedure was designated as DX15. Holes H6 to H10 were drilled at a high temperature, and the test procedure was designated as DX315. The positioning errors of the machine under the drilling operation were measured using the LDDM when the drill was moved from datum plane A to each hole.

An HSS end mill (12 mm diameter) was used to machine faces F1–F5. Each face requires four cuts to finish. The depth of each cut was 7, 7, 5 and 1 mm, respectively. The machine's positioning errors (travelling errors) under the end milling operation were measured when the end mill cut off material from datum plane A to faces F1 – F5. The positioning error for the rough cut (7 mm) and finish cut (1 mm) were recorded for further analysis.

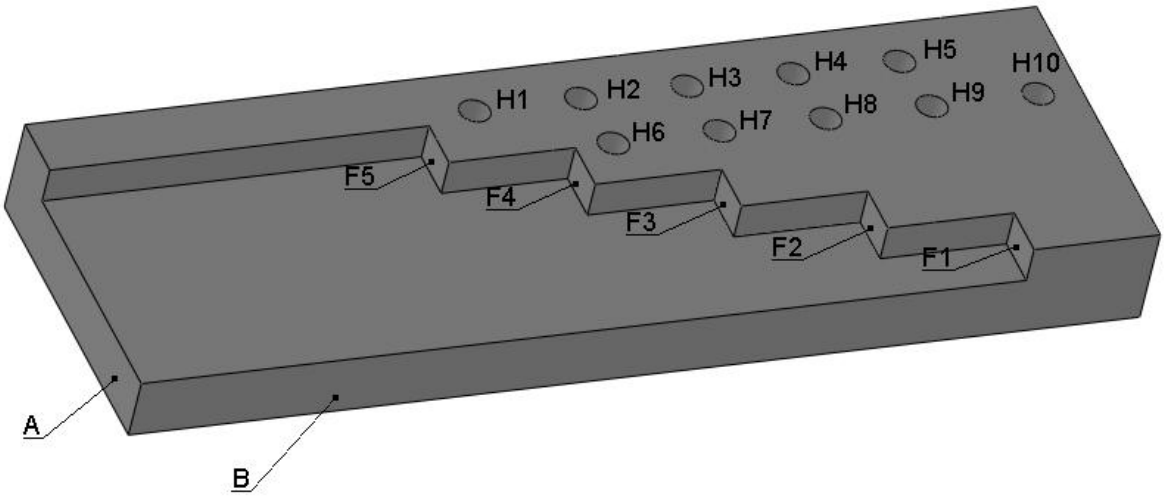

Figure 5.7: Test Component

Table 5.1: *X*-axis Testing Condition

Operations	Machine run time (min)	Ball screw nut temperature (°C)	Spindle speed (rpm)	Feed rate (mm/min)
IX0	0	22.5	0	4800
DX15*	15	22.6	4297	172
IX50	50	23	0	4800
IX105	105	24.95	0	4800
IX145	145	25.6	0	4800
IX185	185	26	0	4800
IX225	225	26.3	0	4800
IX285	285	26.5	0	4800
DX315*	315	25.6	4297	172
MX330	330	25.6	2202[§] 4005[†]	220[§] 417[†]

I---idle measurement; D---drilling; M---end milling; X---*x*-axis; the following number shows machine run time.

*Drilling method: G83 mode; [§] Rough cut, depths of cuts are 7, 7 and 5mm respectively; [†] Finish cut, depth of cut is 1mm.

During each measurement interval, the machine was heated up by idle run at 4800 mm/min feed rate.

Table 5.2: *Y*-axis Testing Condition

Operations	Machine run time (min)	Ball screw nut temperature (°C)	Feed rate (mm/min)
IY0	0	20.1	4800
IY18	18	21.7	4800
IY51	51	22.9	4800
IY85	85	24.4	4800
IY136	136	24.9	4800
IY194	194	25.9	4800

I---idle measurement; Y---*y*-axis; the following number shows machine run time.
During each measurement interval, the machine was heated up by idle run at 4800 mm/min feed rate.

Table 5.3: *Z*-axis Testing Condition

Operations	Machine run time (min)	Ball screw nut temperature (°C)	Feed rate (mm/min)
IZ0	0	22.6	4800
IZ16	16	23.6	4800
IZ45	45	24.5	4800
IZ75	75	25.3	4800
IZ138	138	26.1	4800
I---idle measurement; Z---*z*-axis; the following number shows machine run time. During each measurement interval, the machine was heated up by idle run at 4800 mm/min feed rate.			

5.4 Results and Analysis

5.4.1 Machine tool's thermal behaviour

Temperature variations with the machine run time. Fig. 5.8 shows the variations in the *x*-axis ball screw nut temperature during the entire testing (11 h from 7:00 am to 6:00 pm). Preparing the measurement program and setting up the measurement system took more than 3 h, which increased the nut temperature from 21°C to 22.5°C. The first series of idle measurements (IX0) were initiated at 10:15 am, which is considered the zero point in the timeline for calculating machine run time (Fig. 5.8 and Table 5.1). This point was taken as the reference in plotting all the graphs for machine run time in the *x*-axis. Fig. 5.8 also shows that during the first 30 min, the machine was in the idle measurement mode, paused, and then proceeded with the drilling process to measure the original errors. The nut temperature did not vary much (22.5°C) during this period. When a constant idle run was initiated, the temperature abruptly increased until it reached a thermal stable stage; this process took around 2 h for the test machine used in this study. Subsequently, the rate of temperature increase gradually slowed down (1°C increase during the next 2 h). This stage was assumed to be a thermal stable stage. After the constant idle run, the machine returned to the normal milling and drilling process, and the temperature quickly decreased. The trends of the temperature variations indicate that the machine usually works in a thermal state below the highest temperature even in large-scale industries, where machines are operated the entire day. When the workers pause to reload the workpiece, clean the chips, and so on, the machine goes into a

running–pausing cycle. Therefore, it does not reach the highest thermal stable stage. The actual temperature value depends on room temperature and the machining process.

Temperature variations of *y*- and *z*-axis ball screw nut with the machine run time are shown in Fig. 5.9 and Fig. 5.10, respectively. The test in the *y*-axis started from the second morning, and the measuring system was set up in the first evening; therefore, the ball screw nut temperature started from cold (20°C), as shown in Table 5.2. The test in *z*-axis was conducted in the afternoon when the machine was in a warm condition; therefore, the start temperature was 22.6°C, as shown in Table 5.3.

Three operations, idle run, drilling and end milling, were all performed in the *x*-axis test; therefore, the *x*-axis test time lasted for 450 minutes. The *y*- and *z*-axis tests performed only the idle run tests; therefore, each of these tests stopped when the temperature and thermal growth were close to stable.

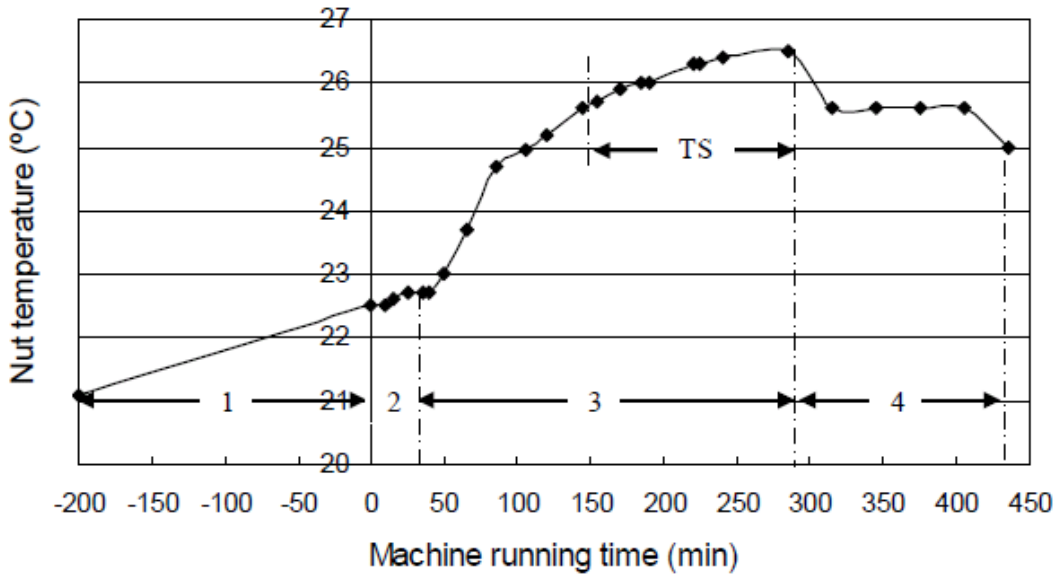

1 --- Measurement system setup
2 --- Cold stage idle measurement (IX0) and drilling (DX15)
3 --- Idle run and idle measurement (IX50 – IX285)
4 --- Drilling and milling at high temperature (DX315, MX330)
TS ---Thermal stable stage

Figure 5.8: Ball Screw Nut Temperature Variations with Machine Running Time (*x*-axis)

Maximum thermal growth. Fig. 5.11 shows the maximum thermal growth of the *x*-, *y*- and *z*-axis lead screw under idle run operating conditions when they reach the thermal stable stage. The maximum thermal growth for the *x*-axis lead screw is close to 55 μm (*y*: 48μm, *z*: 43 μm). It can be observed that the lead screw thermal growth is strongly related to the nut temperature. In the first hour and a half, the temperature increased abruptly (Fig. 5.8 – Fig. 5.10), as did the thermal growth. When the temperature increased slowly, the rate of the thermal growth also slowed down. In fact, the lead screw expansion is related to the temperature of the lead screw. The reason to choose the nut temperature as the alternative has been depicted in Section 5.2.

Thermal effects on positioning errors. Fig. 5.12 – Fig. 5.14 show the average positioning error variations with the temperature in three axes respectively. It is observed that the positioning error increases when the nut temperature (or machine run time) increases. The legend about the testing conditions shown in these graphs and the following graphs coincides with Table 5.1 – Table 5.3.

Fig. 5.15 – Fig. 5.21 show the positioning error variations when the table moves in both ways along the *x*-axis at several thermal statuses. It is observed that the positioning errors are proportional to the travel distance; the *x*-axis movement of this test machine is stable as the lines are pretty close to straight lines even in high temperatures.

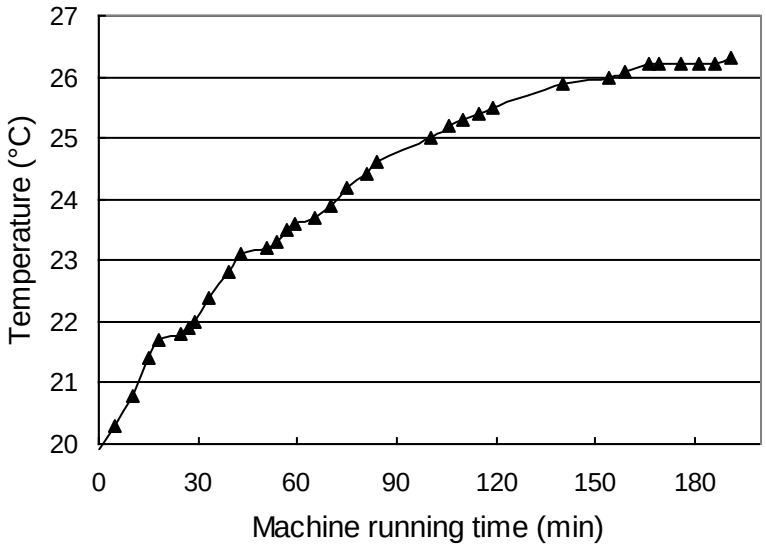

Figure 5.9: Ball Screw Nut Temperature Variations with Machine Running Time (*y*-axis)

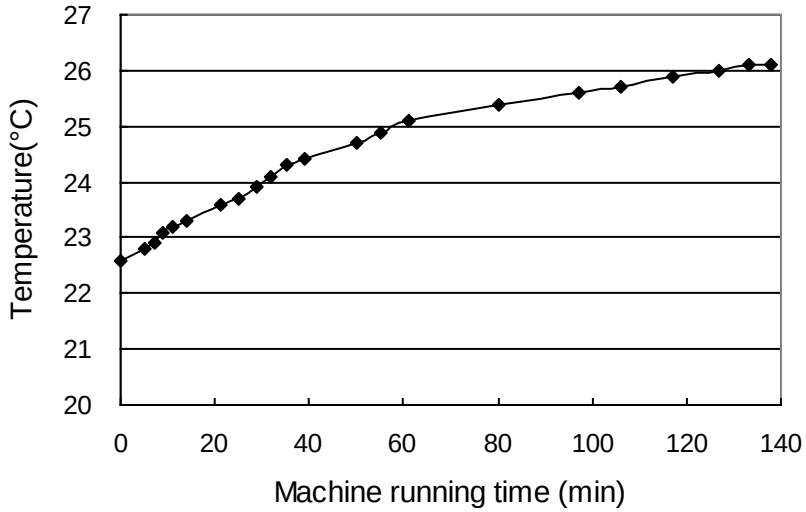

Figure 5.10: Ball Screw Nut Temperature Variations with Machine Running Time (*z*-axis)

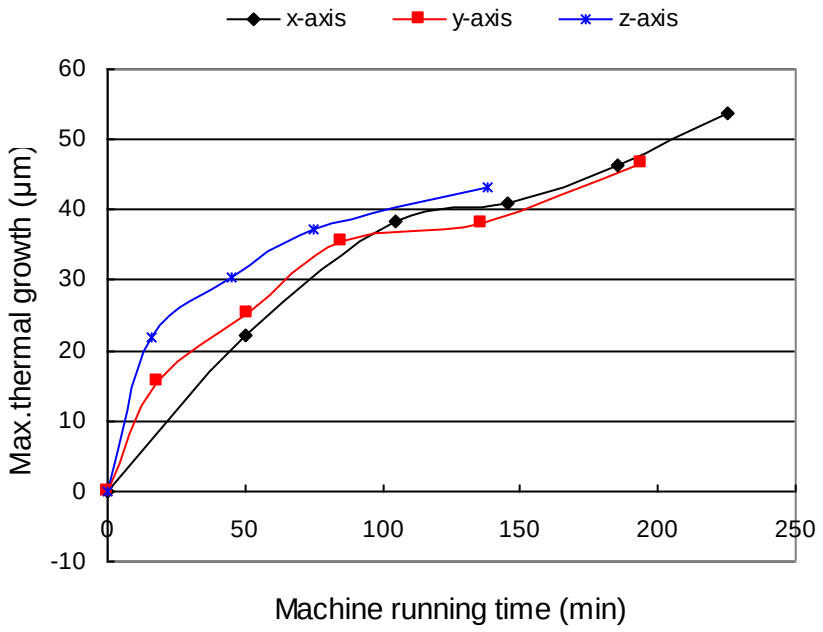

Figure 5.11: Maximum Thermal Growth in Three Axes Directions

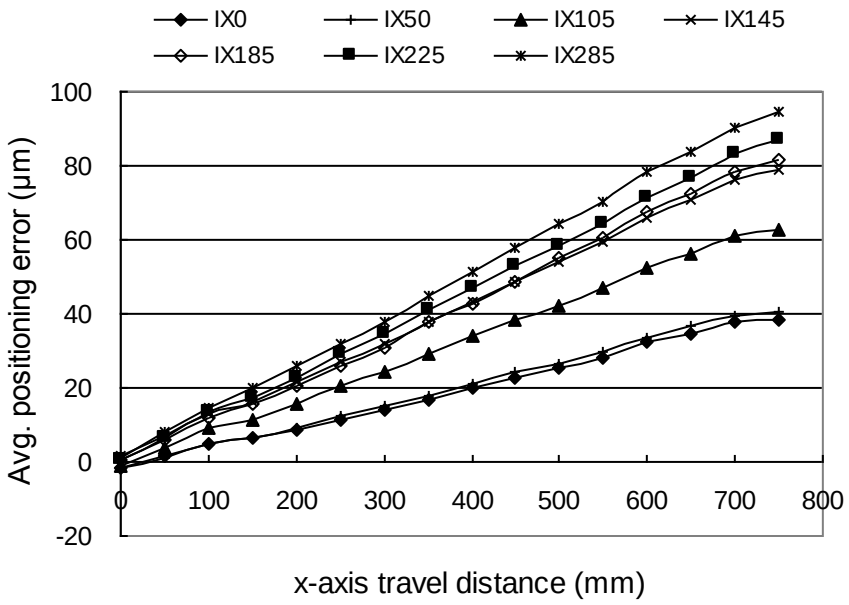

Figure 5.12: Positioning Error Variations with Temperature (*x*-axis)

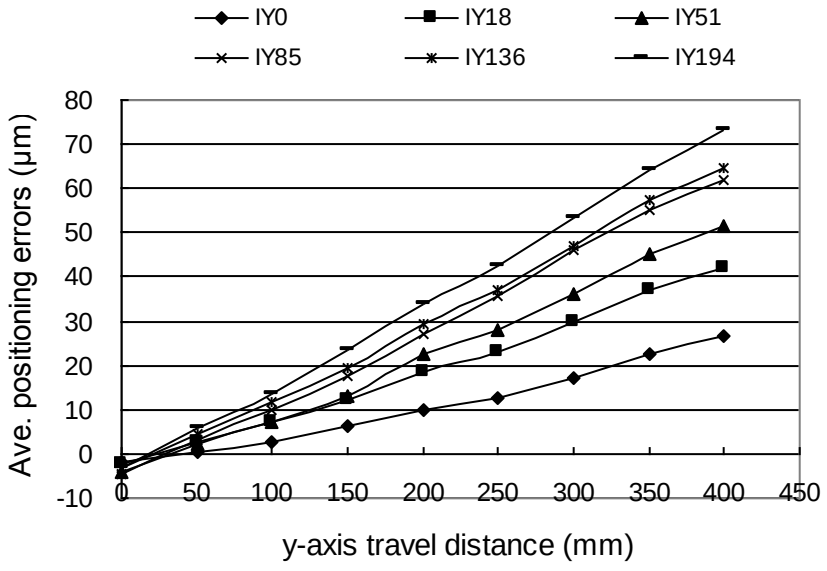

Figure 5.13: Positioning Error Variations with Temperature (*y*-axis)

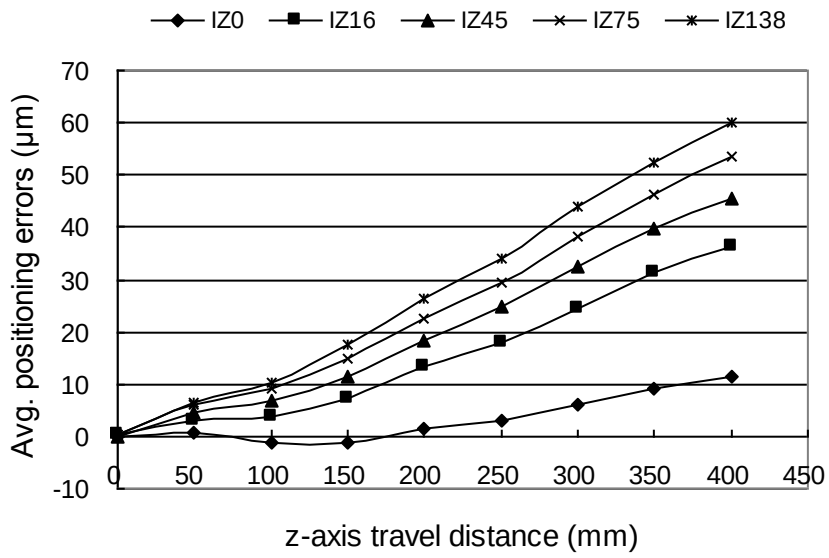

Figure 5.14: Positioning Error Variations with Temperature (*z*-axis)

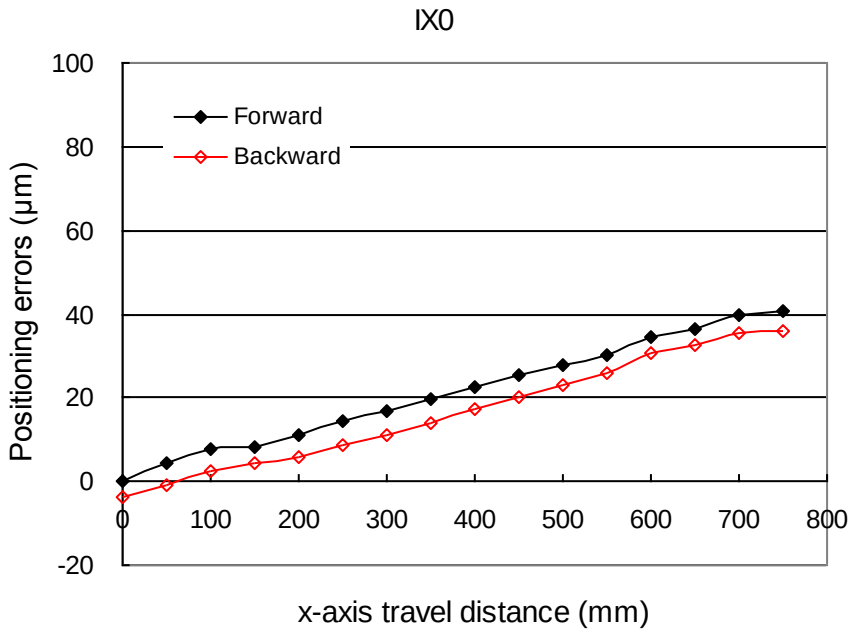

Figure 5.15: Positioning Errors When Machine Moves in *x*-axis (22.5°C)

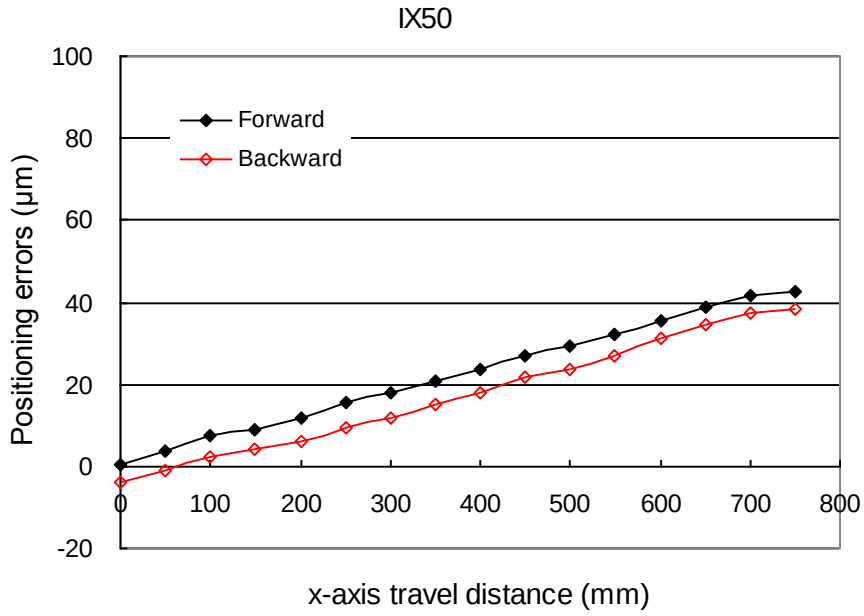

Figure 5.16: Positioning Errors When Machine Moves in *x*-axis (23°C)

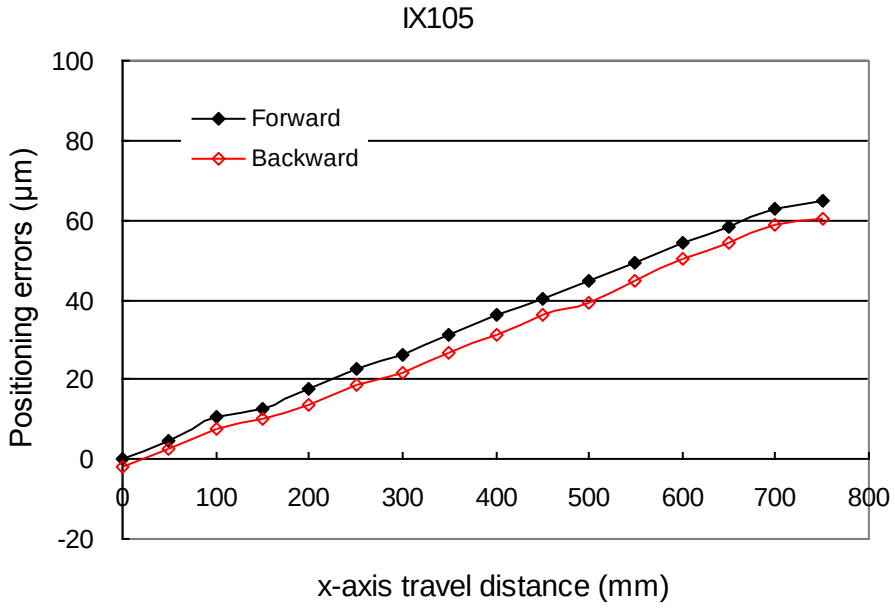

Figure 5.17: Positioning Errors When Machine Moves in *x*-axis (24.95°C)

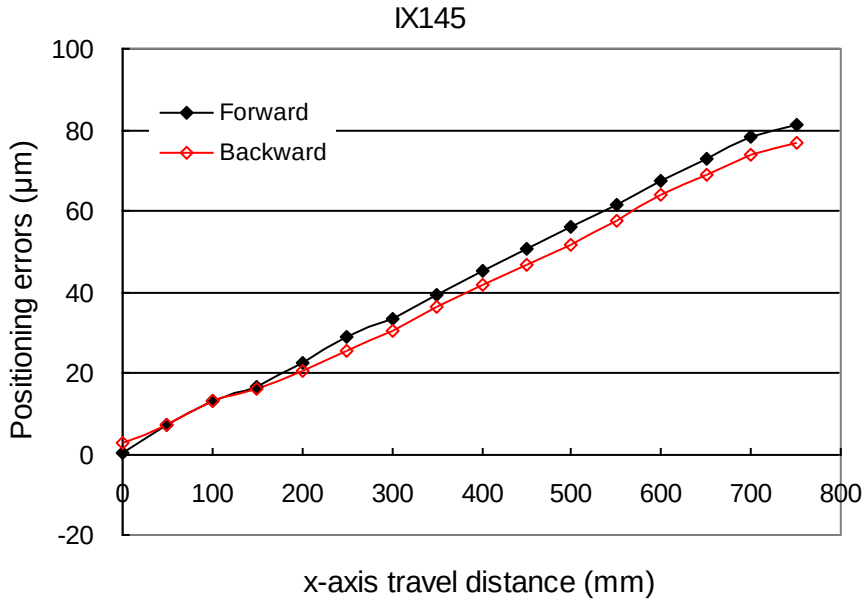

Figure 5.18: Positioning Errors When Machine Moves in *x*-axis (25.6°C)

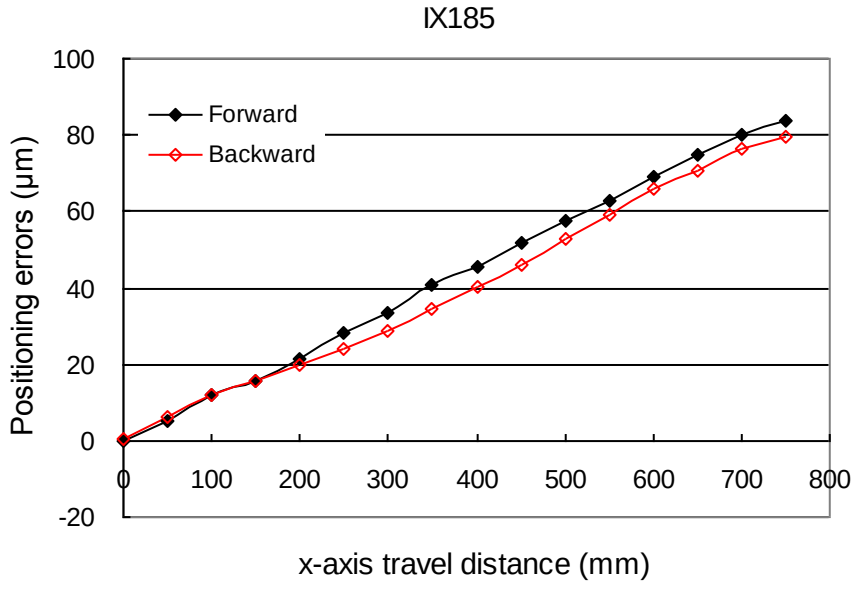

Figure 5.19: Positioning Errors When Machine Moves in *x*-axis (26°C)

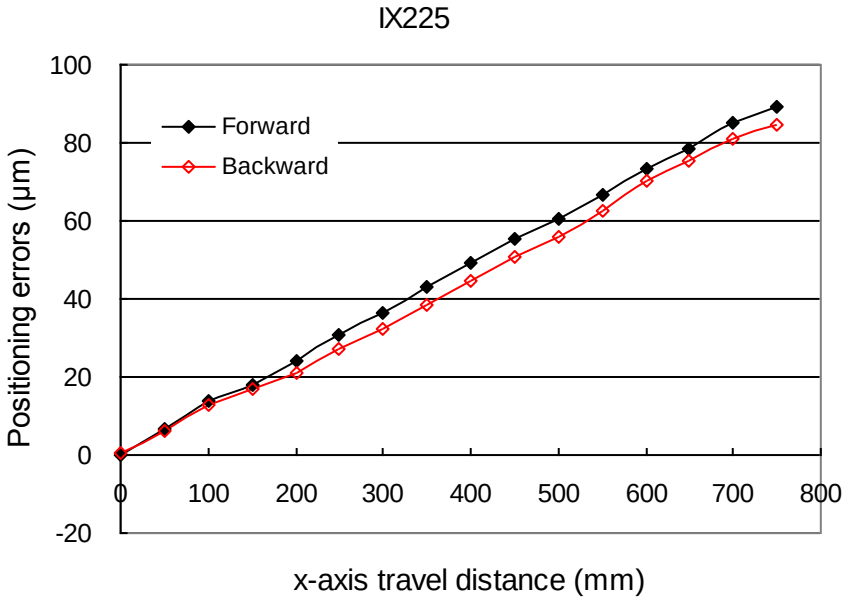

Figure 5.20: Positioning Errors When Machine Moves in *x*-axis (26.3°C)

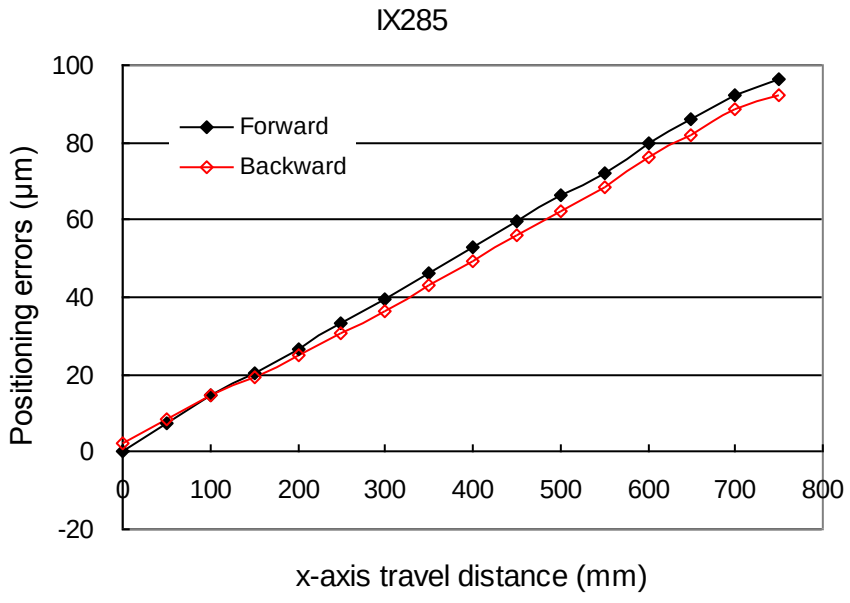

Figure 5.21: Positioning Errors When Machine Moves in *x*-axis (26.5°C)

Fig. 5.22 – Fig. 5.27 show the positioning error variations when the table moves in both ways along the *y*-axis at several thermal statuses. Similar phenomena about the positioning error variations can be observed from these figures.

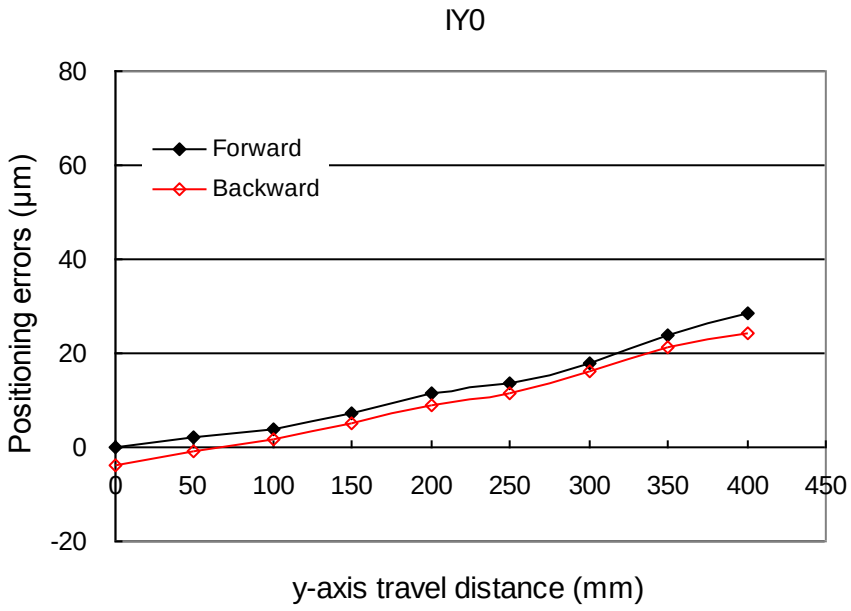

Figure 5.22: Positioning Errors When Machine Moves in *y*-axis (20.1°C)

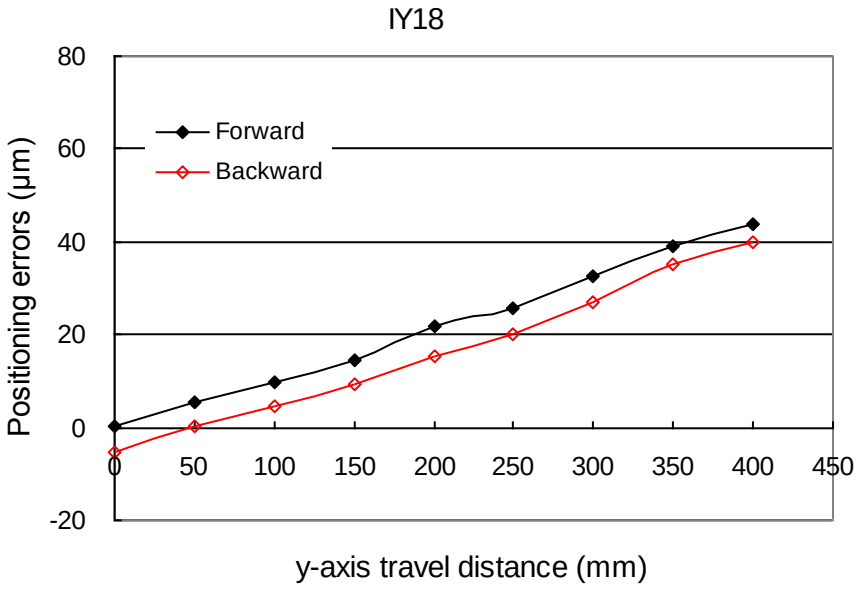

Figure 5.23: Positioning Errors When Machine Moves in *y*-axis (21.7°C)

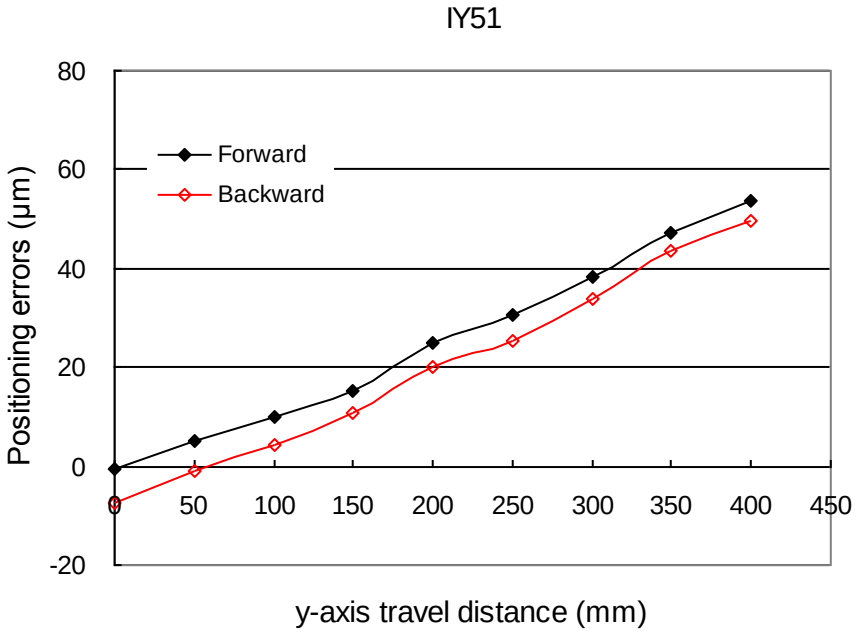

Figure 5.24: Positioning Errors When Machine Moves in *y*-axis (22.9°C)

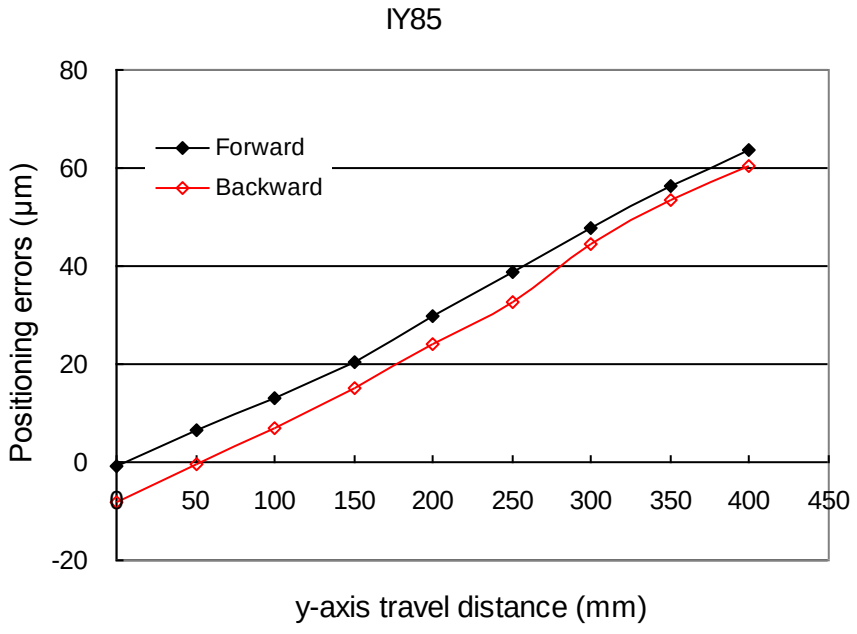

Figure 5.25: Positioning Errors When Machine Moves in *y*-axis (24.4°C)

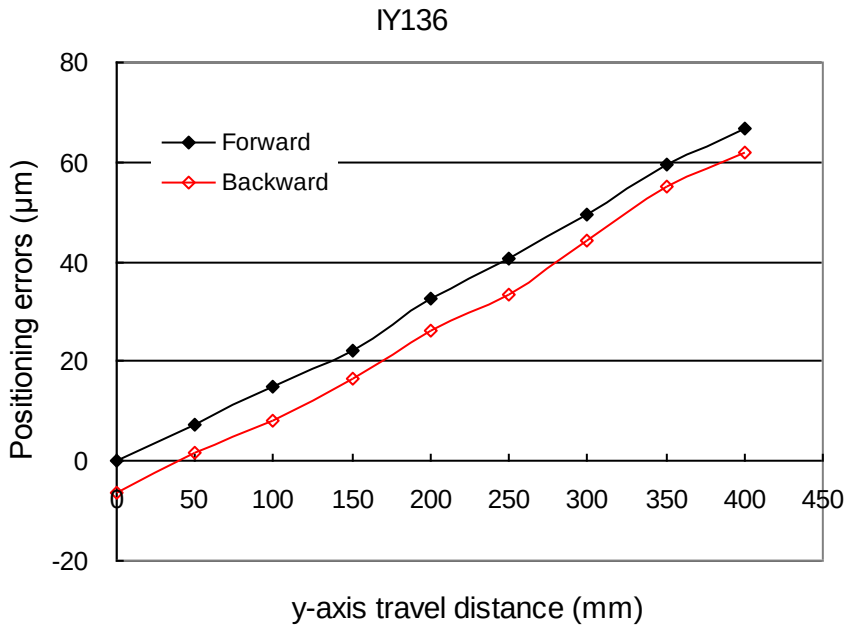

Figure 5.26: Positioning Errors When Machine Moves in *y*-axis (24.9°C)

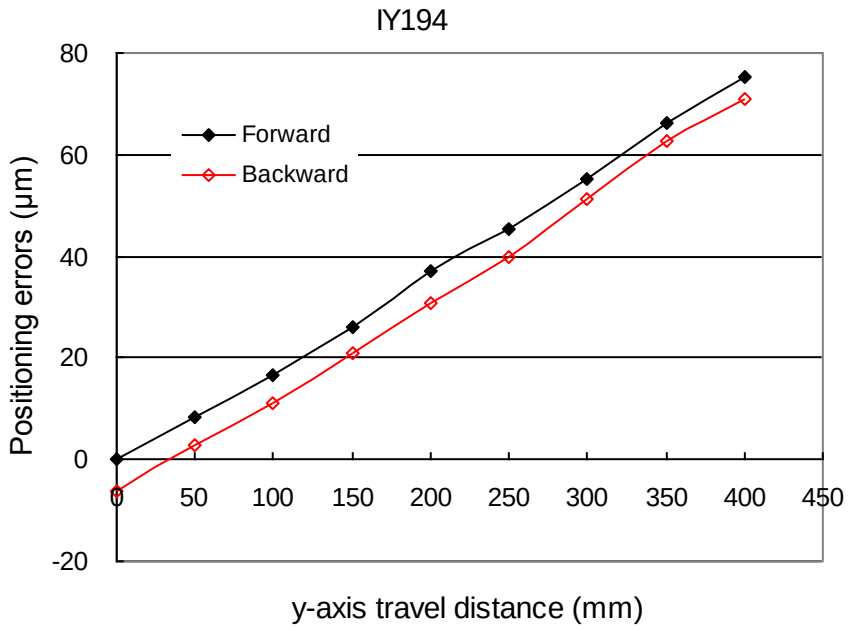

Figure 5.27: Positioning Errors When Machine Moves in *y*-axis (25.9°C)

Fig.5.28 – Fig. 5.32 show the positioning error variations when the table moves in both ways along the *z*-axis at several thermal statuses. The difference between the forward moving and backward moving is close to zero. This will be further analysed in Section 5.4.2.

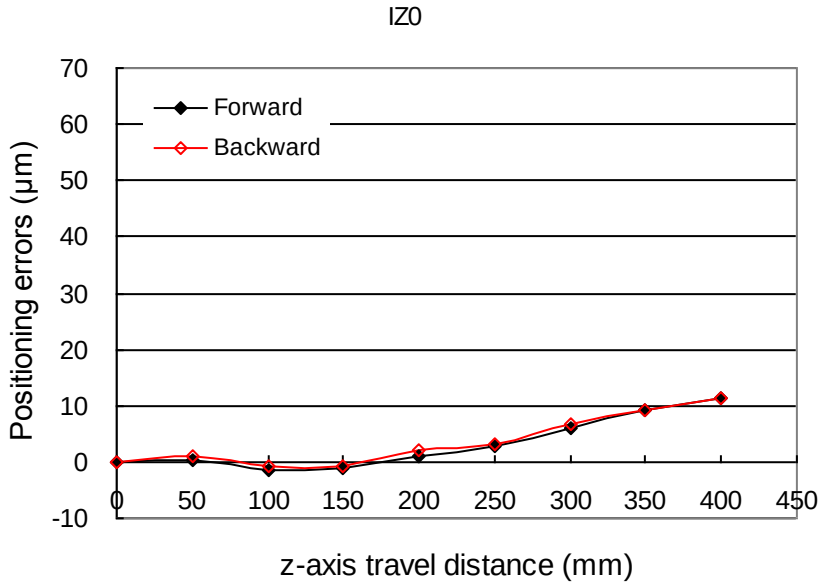

Figure 5.28: Positioning Errors When Machine Moves in *z*-axis (22.6°C)

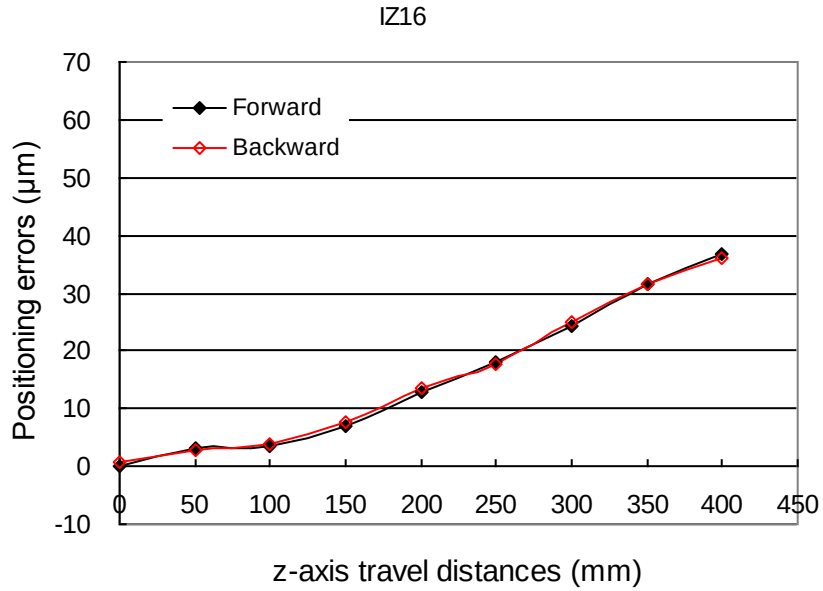

Figure 5.29: Positioning Errors When Machine Moves in *z*-axis (23.6°C)

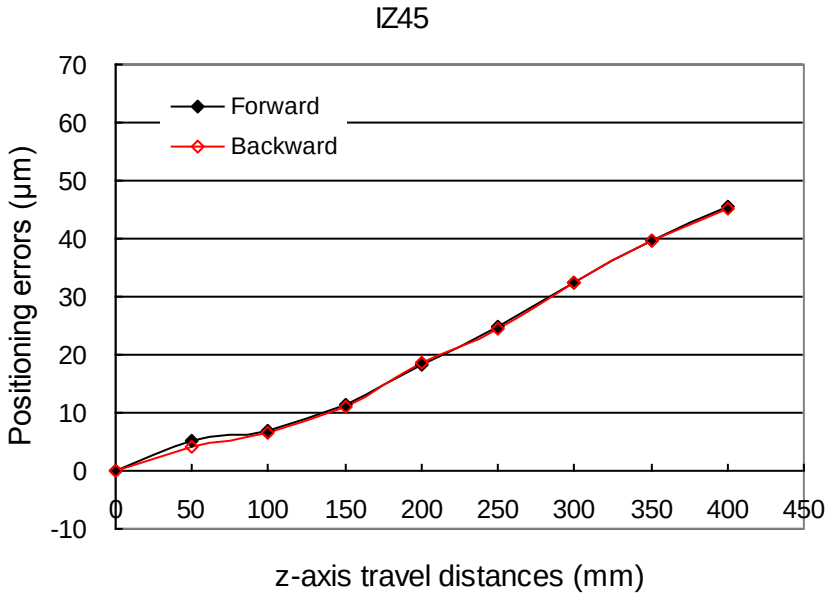

Figure 5.30: Positioning Errors When Machine Moves in *z*-axis (24.5°C)

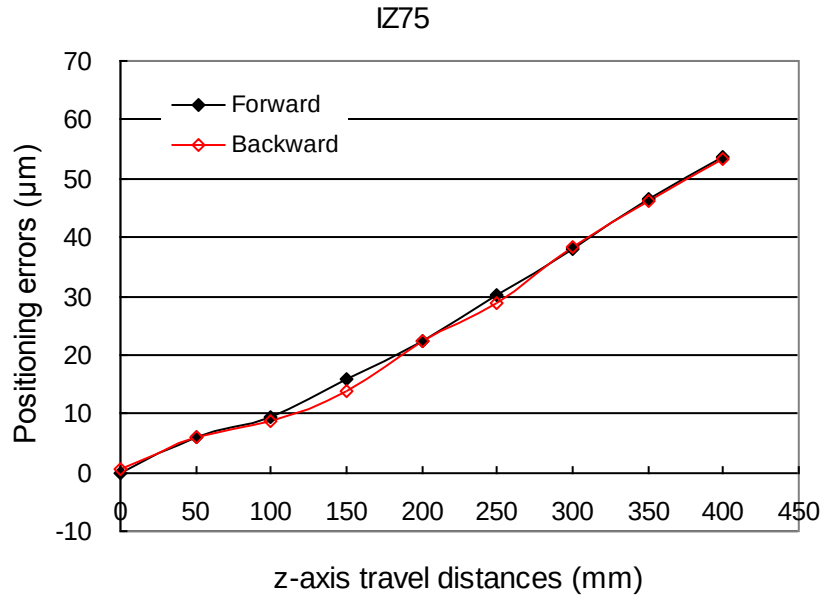

Figure 5.31: Positioning Errors When Machine Moves in *z*-axis (25.3°C)

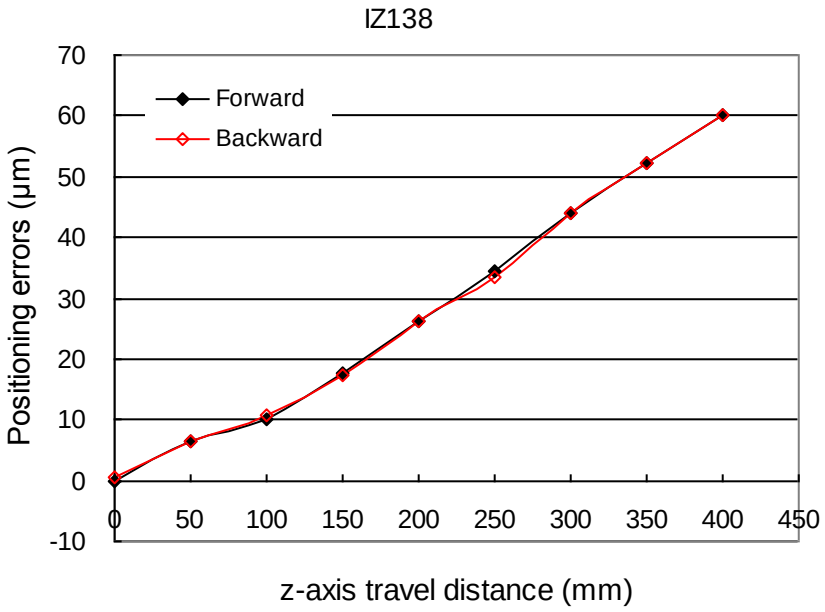

Figure 5.32: Positioning Errors When Machine Moves in *z*-axis (26.1°C)

5.4.2 Thermal effects on hysteresis

The error difference between forward and backward movements (hysteresis) is primarily caused by backlash. The hysteresis on the *x*-axis was reduced while the lead screw expanded because the gap between the forward and backward movements shrank under high temperature (Fig. 5.15 – Fig. 5.21). Fig. 5.33 further demonstrates that the hysteresis on the *x*-axis diminished significantly at the point of origin, but varied less at another end as machine run time increased. This phenomenon can be attributed to the structure of the *x*-axis. In CNC machine tools, one end of the lead screw is usually connected to the driving motor and is supported by a thrust bearing. This end can be considered fixed, whereas the other end supported by a ball bearing can be regarded as a free end, i.e., free to expand in an axial direction. Therefore, temperature had significant effects on the hysteresis in the free end (point of origin of the test machine). Conversely, the effect on the *y*-axis hysteresis was insignificant because the origin of the *y*-axis is at the fixed end (Fig. 5.34). The *z*-axis hysteresis was close to zero at any thermal state because this axis moves in a vertical direction, thereby eliminating hysteresis through the natural weight of the spindle head (Fig. 5.35).

The original data about positioning errors, average positioning errors and hysteresis under different thermal statuses are presented in Appendix C – Appendix

E.

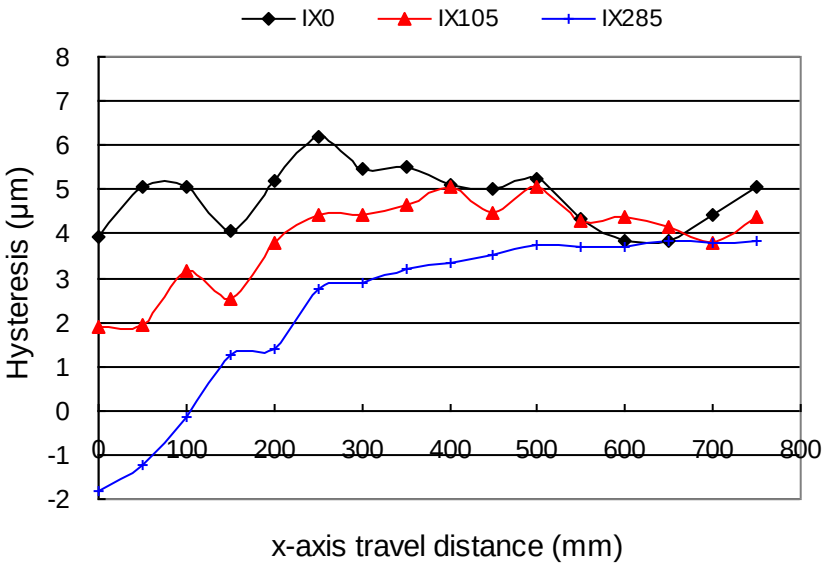

Figure 5.33: Thermal Effects on Hysteresis in *x*-axis

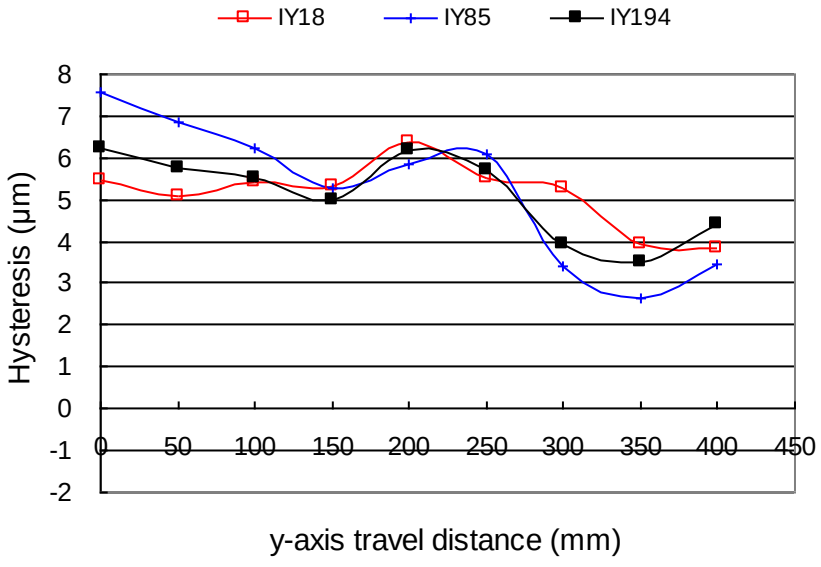

Figure 5.34: Thermal Effects on Hysteresis in *y*-axis

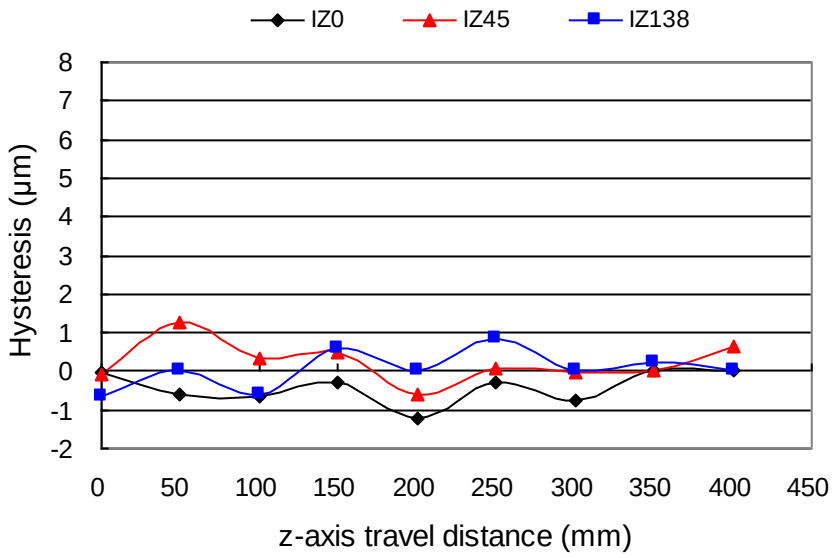

Figure 5.35: Thermal Effects on Hysteresis in *z*-axis

5.4.3 Effects of cutting operations on positioning errors

Idle run experiments are usually employed to simulate cutting load under actual cutting conditions. Nonetheless, this approach is not universally accepted [11] [27]. In this research, a series of actual cutting experiments were conducted to determine the influence of ideal and actual machining operations at the same thermal conditions.

Fig. 5.36 compares the positioning errors produced under the idle run (IX145) and end milling (MX330) operations. The ball screw nut temperature for these two operations was the same (25.6°C), as shown in Table 5.1. The positioning errors produced during the milling-rough cut operation were slightly higher (maximum difference, 3 µm) than those produced under the idle run (IX145) and milling-finish cut operations. However, this difference is insignificant; thus, the errors can be considered similar.

Fig. 5.37 shows the comparison of the positioning errors produced under the idle run and drilling operations at normal and high temperatures, respectively. Under a normal temperature, the positioning errors produced in drilling process DX15 were similar to those generated in idle run IX0 because the temperature for both operations was the same (22.5°C). Under a high temperature, the errors produced in drilling process DX315 were slightly lower (maximum difference, 8 µm) than those generated in idle run IX145, even though the temperature for these operations was

the same (25.6°C). This result may be attributed to the fact that the drilling was a point-to-point operation and did not exert much load on travel distance compared with the milling operations. This phenomenon indicates that the positioning errors produced in actual machining operations can be approximately simulated by a high feed rate idle run operation as long as the thermal statuses of the machine tools are similar, especially in low temperature ranges.

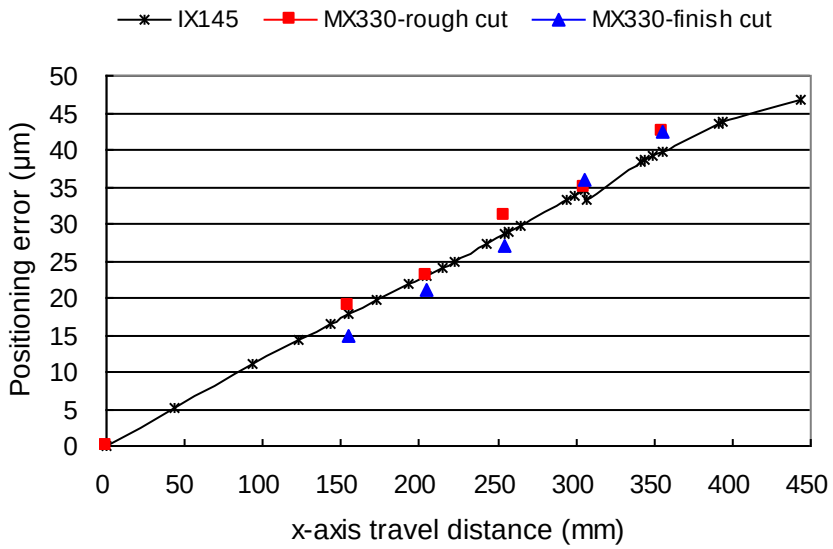

Figure 5.36: Comparison of Positioning Errors between Idle Running and End Milling

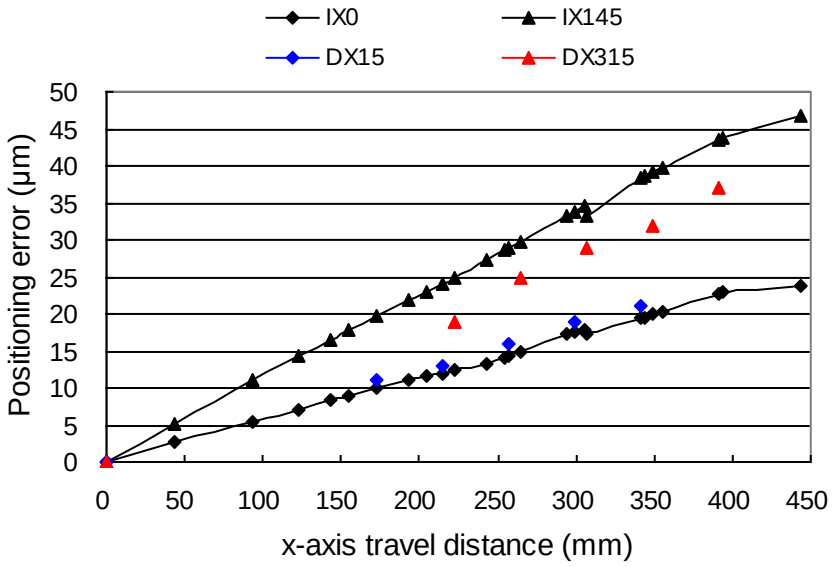

Figure 5.37: Comparison of Positioning Errors between Idle Running and Drilling

5.4.4 Modification of thermally-induced positioning error prediction model

Based on the test results, the thermally-induced positioning error prediction model for Leadwell V30 in *x*, *y* and *z* directions is modified from Eq. 5.1 to the following form. The adjustment factors are determined based on measured data by applying the least squares method as described in Chapter 4.

X-axis positioning error prediction model (tests were conducted between 22.5°C and 27°C):

$$\begin{cases} \text{When } T_{xnut} \le T_{x0} = 22.5 \\ RE_x(x, T_{xnut}) = RE_x(x, T_{x0}) \\ \text{When } T_{x0} < T_{xnut} \le 27 \\ RE_x(x, T_{xnut}) = RE_x(x, T_{x0}) + \beta_x \cdot \alpha \cdot x \cdot (T_{xnut} - T_{x0}) \qquad \beta_x = 0.96 \\ \text{When } T_{xnut} > 27 \\ RE_x(x, T_{xnut}) = RE_x(x, 27) \end{cases} \tag{5.4}$$

Y-axis positioning error prediction model (tests were conducted between 20.1°C and 26°C):

$$\begin{cases} \text{When } T_{ynut} \le T_{y0} = 20.1 \\ RE_y(y, T_{ynut}) = RE_y(y, T_{y0}) \\ \text{When } T_{y0} < T_{ynut} \le 26 \\ RE_y(y, T_{ynut}) = RE_y(y, T_{y0}) + \beta_y \cdot \alpha \cdot y \cdot (T_{ynut} - T_{y0}) \qquad \beta_y = 1.13 \\ \text{When } T_{ynut} > 26 \\ RE_y(y, T_{ynut}) = RE_y(y, 26) \end{cases} \tag{5.5}$$

Z-axis positioning error prediction model (tests were conducted between 22.6°C and 27°C):

$$\begin{cases} \text{When } T_{znut} \le T_{z0} = 22.6 \\ RE_z(y, T_{znut}) = RE_z(z, T_{z0}) \\ \text{When } T_{z0} < T_{znut} \le 27 \\ RE_z(z, T_{znut}) = RE_z(z, T_{z0}) + \beta_z \cdot \alpha \cdot z \cdot (T_{znut} - T_{z0}) \qquad \beta_z = 2.27 \\ \text{When } T_{znut} > 27 \\ RE_z(z, T_{znut}) = RE_z(z, 26) \end{cases} \tag{5.6}$$

5.4.5 Comparison of measured and predicted positioning errors

The predicted positioning errors along three directions are calculated by equations 5.4, 5.5 and 5.6 respectively. Fig. 5.38 – Fig. 5.43 show the comparison between measured and predicted positioning errors in the *x*-axis under different thermal conditions. The predicted positioning error agrees well with the measured values. However, the agreement level from Fig. 5.38 to Fig. 5.43 is not the same. The predicted value for IX185 is closer to the measured value than is the predicted value of other test conditions. This result is attributed to the averaging of adjustment factor β in Eq. 5.4 – Eq. 5.6 for different thermal conditions (Chapter 4). The prediction results for the *y*-axis (Fig. 5.44 – Fig. 5.48) and the *z*-axis (Fig. 5.49 – Fig. 5.52) show similar phenomena. Table 5.4 – Table 5.6 show the relative difference between the measured and predicted positioning errors in three axes at normal and high temperatures, respectively.

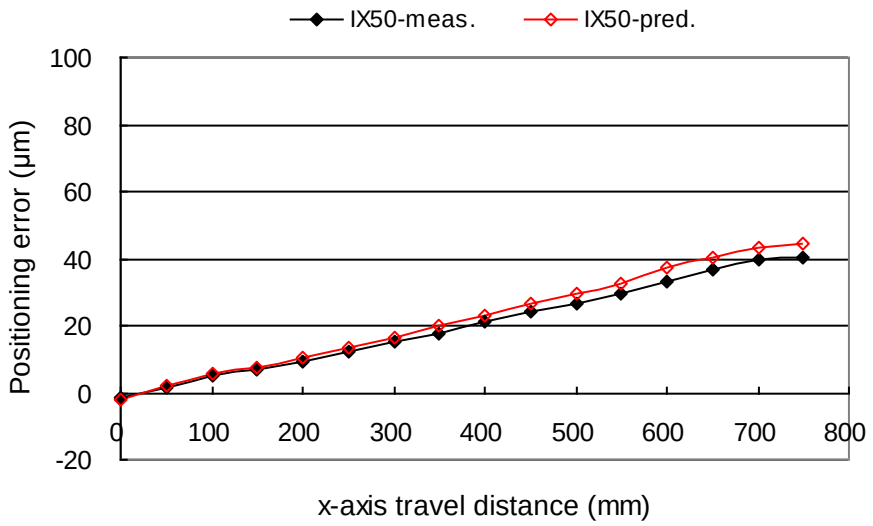

Figure 5.38: Comparison of Measured and Predicted Positioning Errors (*x*-axis, 23°C)

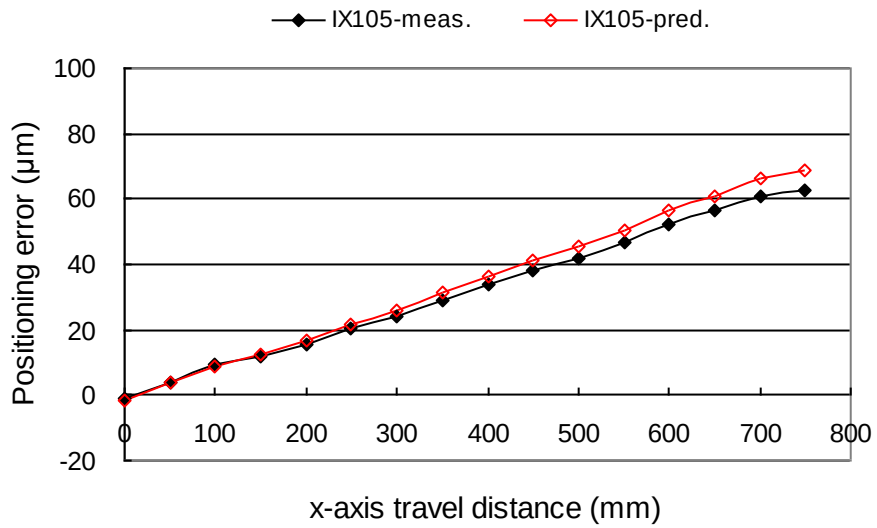

Figure 5.39: Comparison of Measured and Predicted Positioning Errors (*x*-axis, 24.95°C)

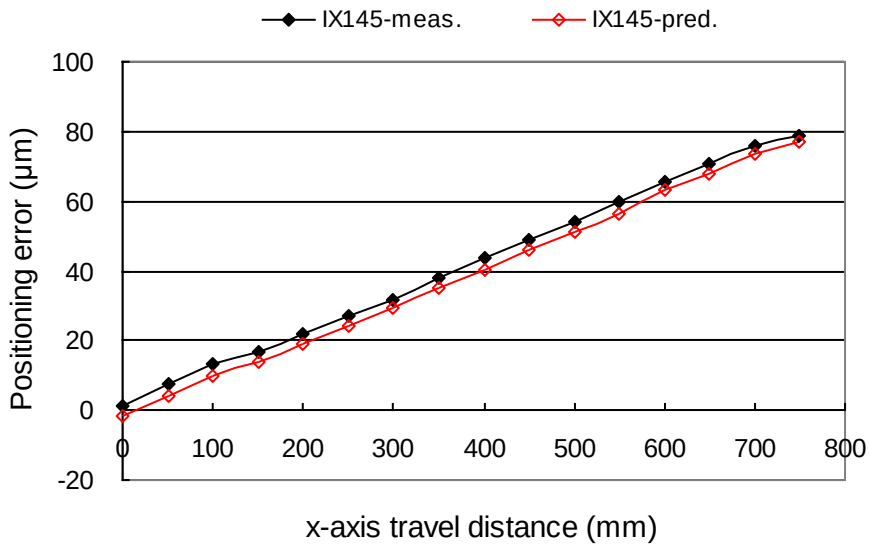

Figure 5.40: Comparison of Measured and Predicted Positioning Errors (*x*-axis, 25.6°C)

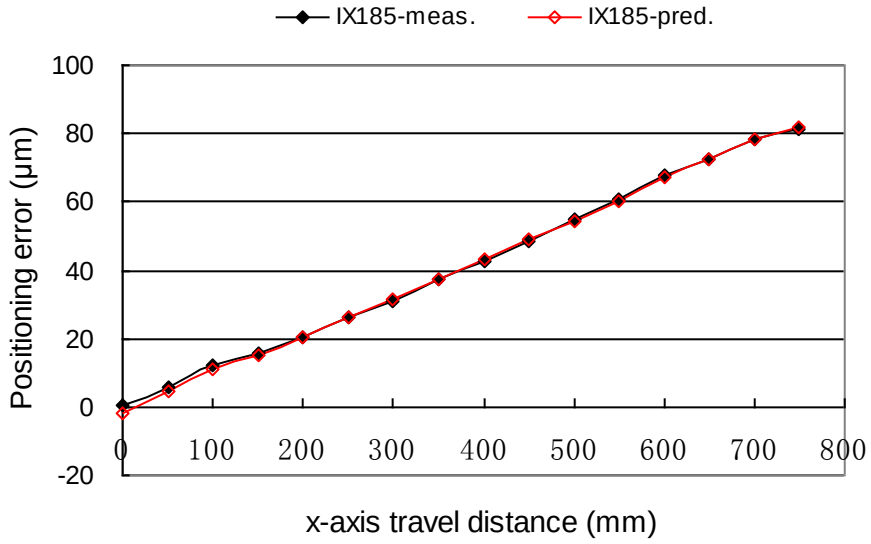

Figure 5.41: Comparison of Measured and Predicted Positioning Errors (*x*-axis, 26°C)

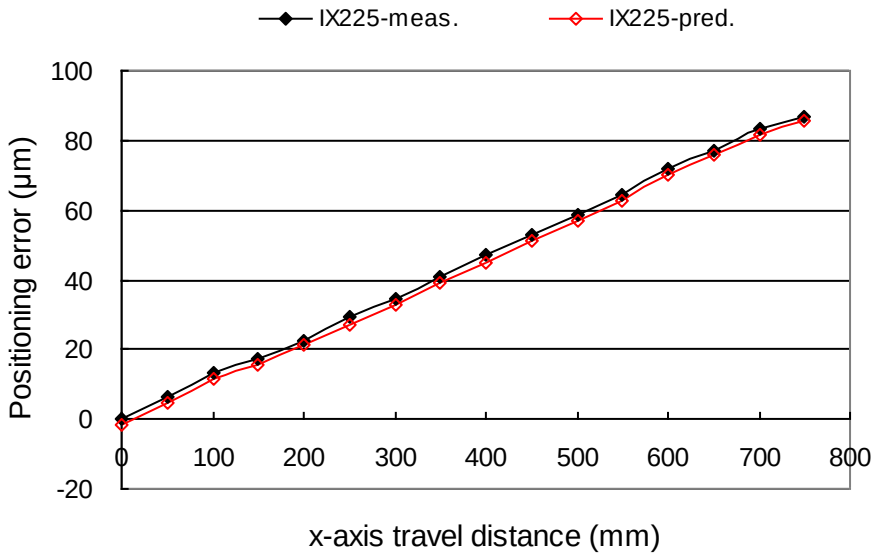

Figure 5.42: Comparison of Measured and Predicted Positioning Errors (*x*-axis, 26.3°C)

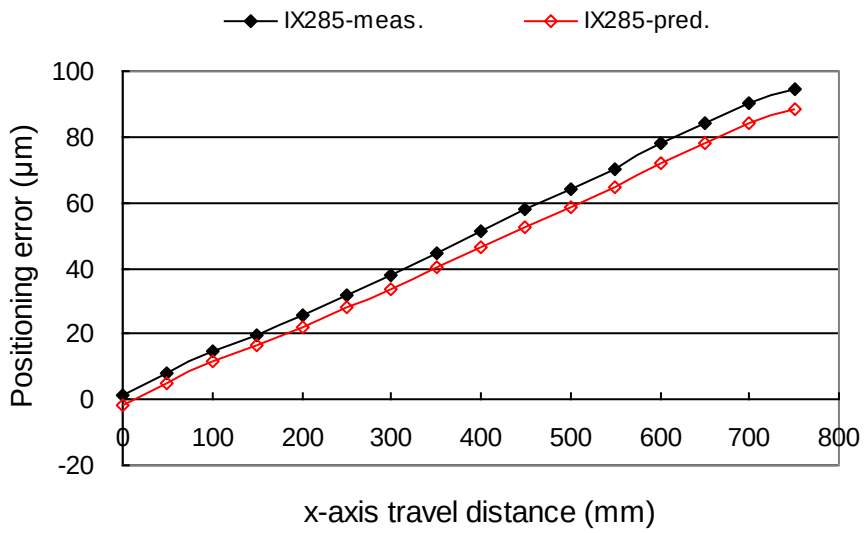

Figure 5.43: Comparison of Measured and Predicted Positioning Errors (*x*-axis, 26.5°C)

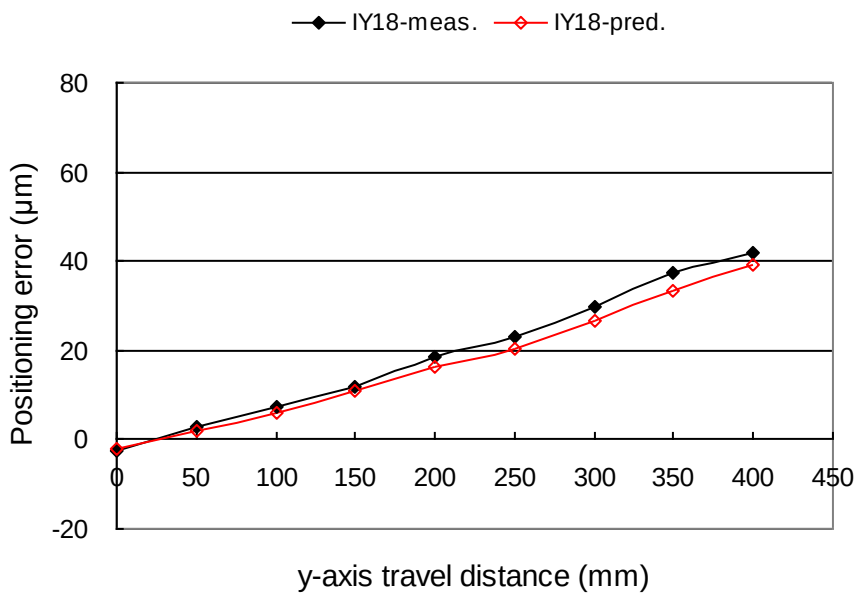

Figure 5.44: Comparison of Measured and Predicted Positioning Errors (*y*-axis, 21.7°C)

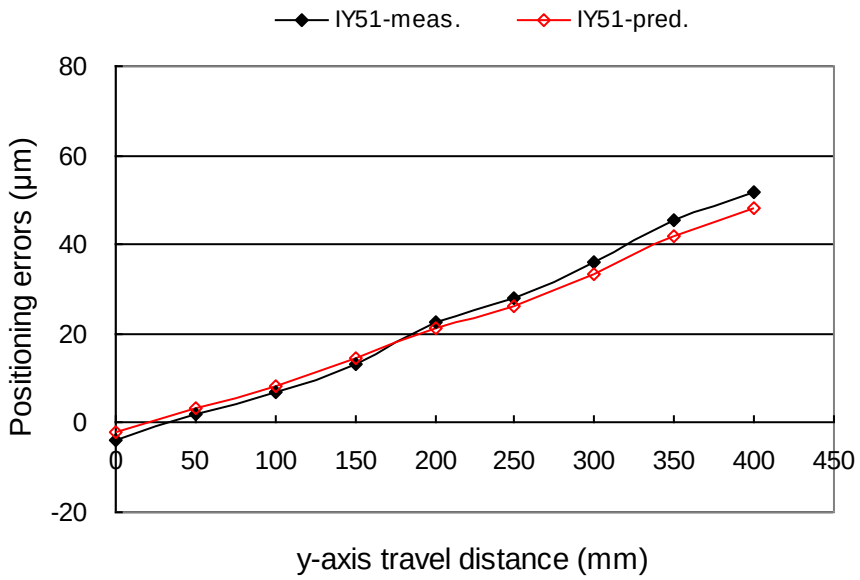

Figure 5.45: Comparison of Measured and Predicted Positioning Errors (*y*-axis, 22.9°C)

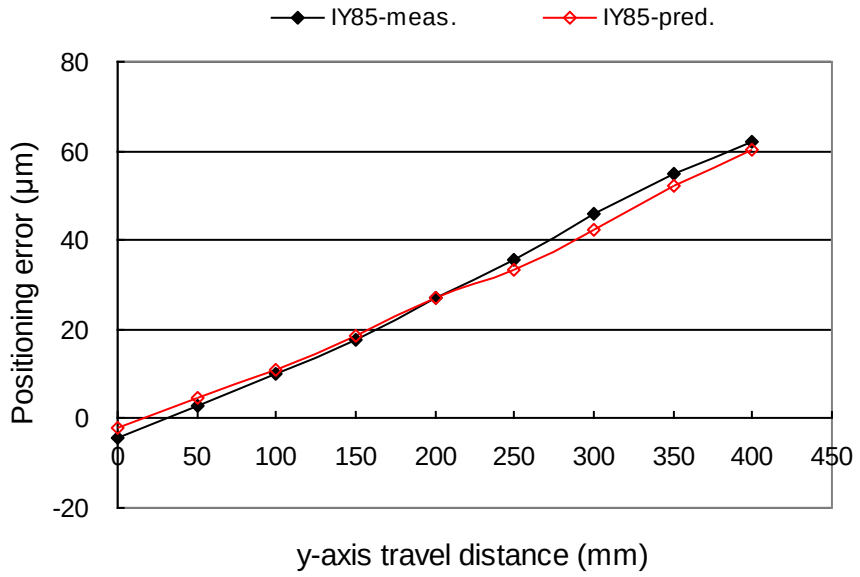

Figure 5.46: Comparison of Measured and Predicted Positioning Errors (*y*-axis, 24.4°C)

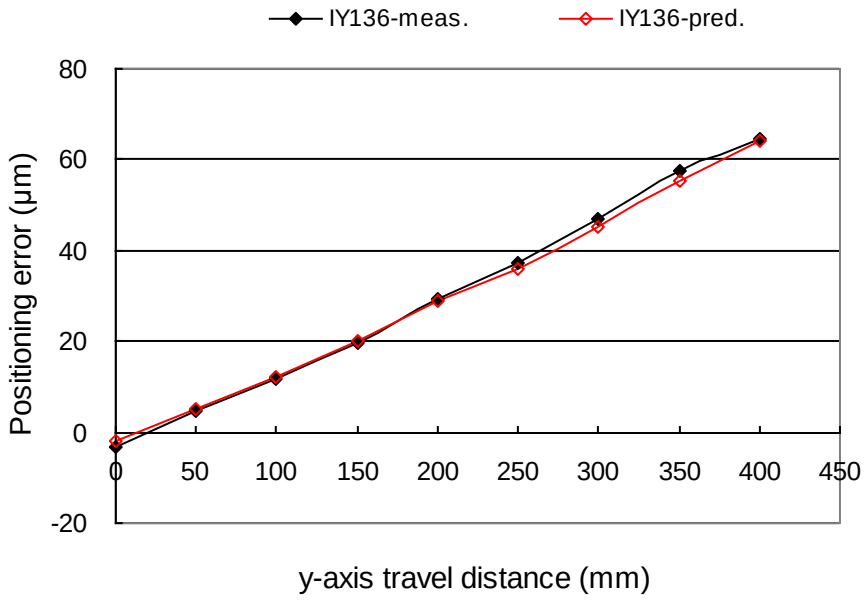

Figure 5.47: Comparison of Measured and Predicted Positioning Errors (*y*-axis, 24.9°C)

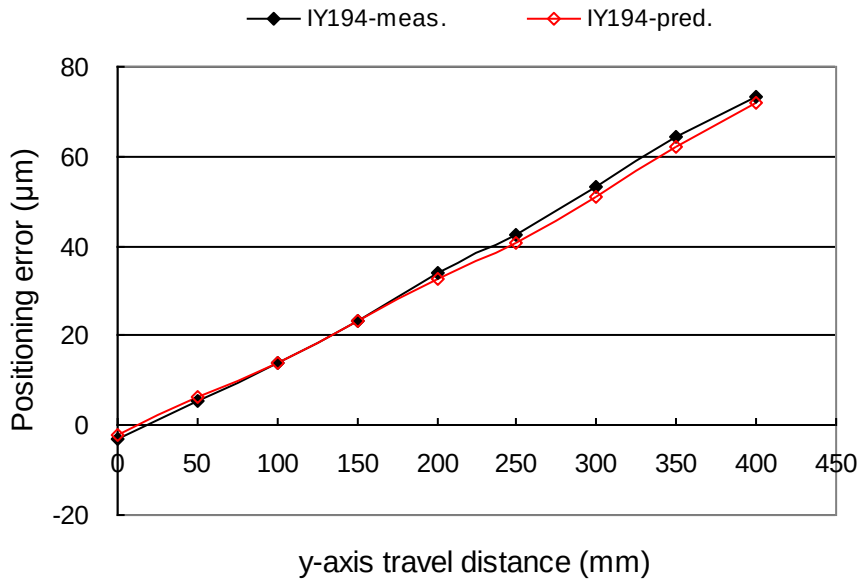

Figure 5.48: Comparison of Measured and Predicted Positioning Errors (*y*-axis, 25.9°C)

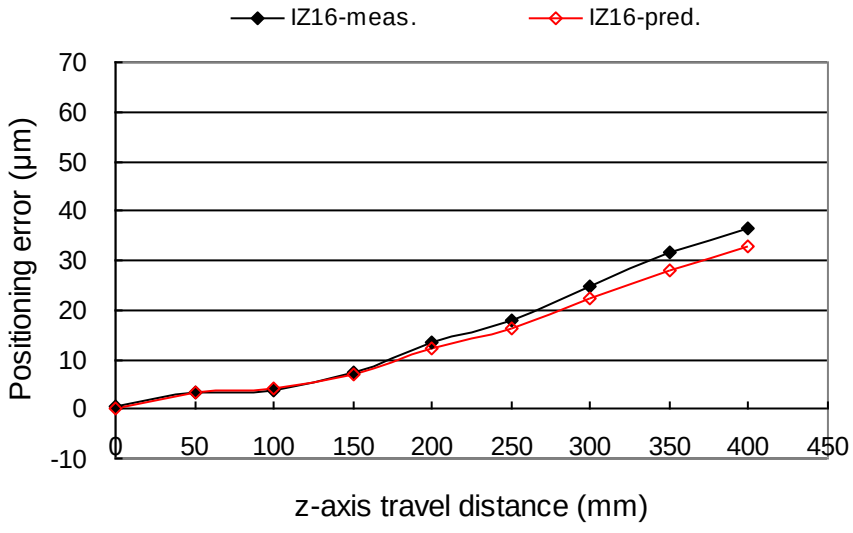

Figure 5.49: Comparison of Measured and Predicted Positioning Errors (*z*-axis, 23.6°C)

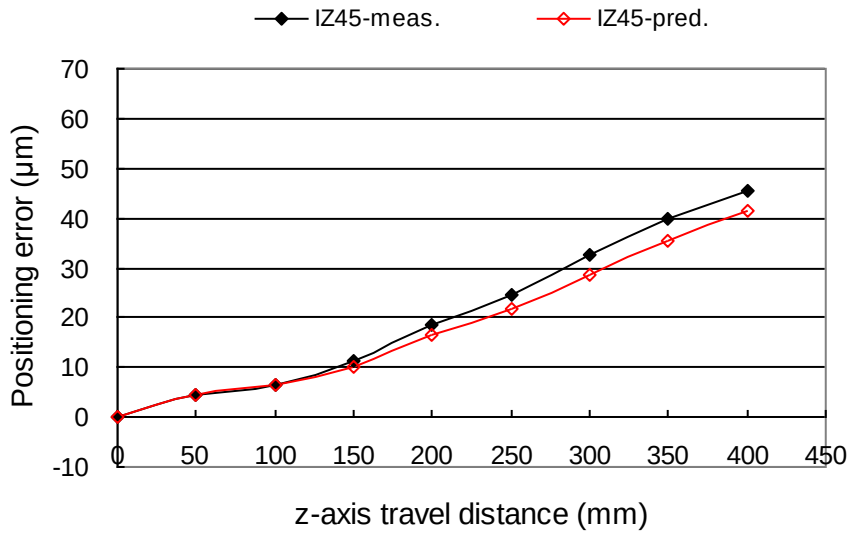

Figure 5.50: Comparison of Measured and Predicted Positioning Errors (*z*-axis, 24.5°C)

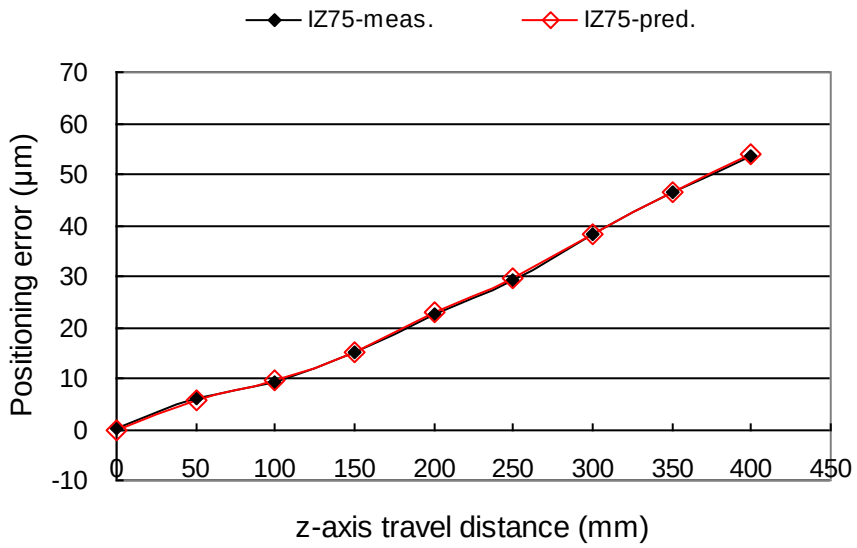

Figure 5.51: Comparison of Measured and Predicted Positioning Errors (*z*-axis, 25.3°C)

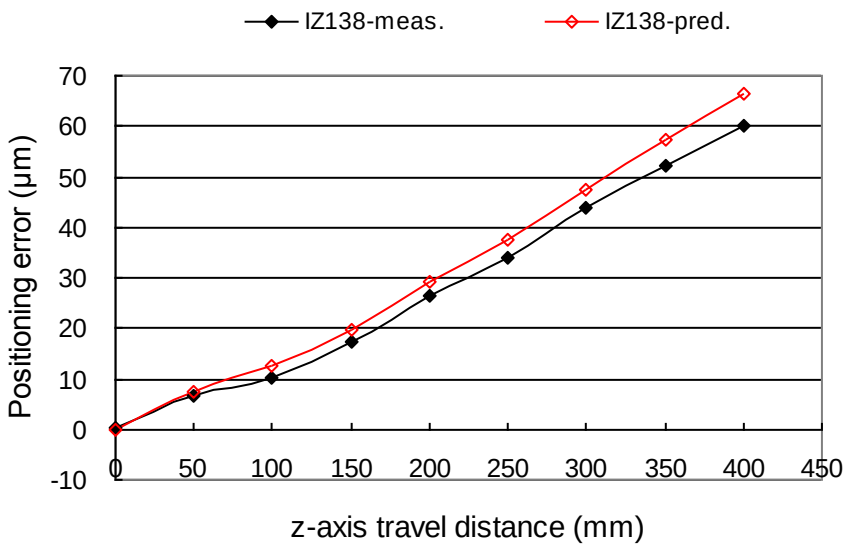

Figure 5.52: Comparison of Measured and Predicted Positioning Errors (*z*-axis, 26.1°C)

Table 5.4: Relative Difference between Measured and Predicted Errors (*x*-axis)

Position (mm)	IX50 (23°C)			IX185 (26°C)		
	Predicted Error (μm)	Measured Error (μm)	Difference* (%)	Predicted Error (μm)	Measured Error (μm)	Difference* (%)
150	7.62	6.73	13.30	15.10	15.51	-2.64
200	10.08	9.05	13.57	20.24	20.38	-0.67
250	13.64	12.43	9.67	26.09	25.99	0.38
300	16.38	14.97	9.44	31.33	31.07	0.85
350	19.80	17.84	11.04	37.24	37.64	-1.06
400	23.24	20.92	11.11	43.17	42.89	0.66
450	26.52	24.15	9.84	48.94	48.72	0.45
500	29.57	26.57	11.29	54.48	55.14	-1.18
550	32.62	29.64	10.07	60.03	60.80	-1.27
600	37.38	33.43	11.83	67.28	67.51	-0.35
650	40.00	36.63	9.21	72.39	72.68	-0.40
700	43.55	39.47	10.34	78.42	78.27	0.19
750	44.55	40.56	9.82	81.92	81.51	0.50
*Difference =100 x (predicted error – measured error)/measured error						

Table 5.5: Relative Difference between Measured and Predicted Errors (*y*-axis)

Position (mm)	IY18 (21.7°C)			IY136 (24.9°C)		
	Predicted Error (μm)	Measured Error (μm)	Difference* (%)	Predicted Error (μm)	Measured Error (μm)	Difference* (%)
100	5.86	7.21	-18.70	12.12	11.51	5.32
150	10.86	11.94	-9.07	20.24	19.50	3.81
200	16.37	18.67	-12.30	28.88	29.36	-1.61
250	20.30	22.92	-11.42	35.94	37.10	-3.13
300	26.49	29.82	-11.18	45.25	47.01	-3.74
350	33.59	37.19	-9.69	55.48	57.35	-3.26
400	39.00	41.96	-7.06	64.02	64.48	-0.71
*Difference =100 x (predicted error – measured error)/measured error						

Table 5.6: Relative Difference between Measured and Predicted Errors (*z*-axis)

Position (mm)	IZ16 (23.6°C)			IZ75 (25.3°C)		
	Predicted Error (μm)	Measured Error (μm)	Difference* (%)	Predicted Error (μm)	Measured Error (μm)	Difference* (%)
100	4.26	3.66	16.18	9.51	9.02	5.35
150	7.04	7.35	-4.26	14.91	14.94	-0.20
200	12.36	13.32	-7.24	22.85	22.36	2.22
250	16.37	18.02	-9.15	29.49	29.38	0.38
300	22.29	24.58	-9.32	38.04	38.17	-0.35
350	28.09	31.47	-10.73	46.46	46.41	0.12
400	32.92	36.46	-9.69	53.92	53.56	0.68
*Difference =100 x (predicted error – measured error)/measured error						

5.5 Concluding Remarks

On the basis of the analysis presented in this chapter, the following conclusions can be made:

- Thermally-induced positioning errors are closely related to ball screw nut temperature. They increase significantly for an initial period of time, typically for 1.5 h, and then the rate of error increase gradually slows down.
- Thermally-induced positioning errors are linearly proportional to travel distance.

- The thermal condition of a machine tool significantly affects the error hysteresis of non-vertical axes. This hysteresis also depends on the structure of the axis. Vertical axis hysteresis is close to zero at any thermal state.
- The errors generated in milling operations can be simulated by those produced in high-feed rate idle runs. At high temperatures, the errors generated in drilling operations are slightly lower.

Chapter 6

Model Application

6.1 Introduction

Improving the dimensional accuracy of parts has increasingly drawn the attention of manufacturers who desire to be competitive in modern industry. From the literature review conducted in Chapter 2, it has been established that temperature-induced error has the most significant effects on dimensional accuracy of machined parts after continuous usage of the machine tool. These errors can be predicted and compensated for by using mathematical models. A new model for calculating thermally-induced volumetric error has been developed in Chapter 4 and verified in Chapter 5. The aim of this chapter is to demonstrate through a number of cutting experiments how the proposed thermally-induced volumetric error compensation model can be applied to improve the dimensional accuracy of parts.

Two types of experiments were conducted: a test without compensation termed as *initial test* and a test with compensation termed as *compensation test*. To monitor the effects of temperature, both tests were conducted at the cold stage and the thermal stable stage of the machine tool. Finally, component parts were measured for their dimensional accuracy, and comparisons are made between the dimensional accuracy of parts produced with and without compensation at two thermal stages of the machine tool.

6.2 Accuracy, Repeatability and Resolution

A machine tool's performance is frequently assessed by three specifications: accuracy, repeatability and resolution.

Accuracy is the ability of a machine to move to a commanded position. Its value demonstrates how close an attempted position is to the true position; therefore, it can be represented as the difference between average measurements to the true value.

Repeatability is the ability of the machine to re-visit a location. Its value shows

how close a number of successive attempts are to each other. Repeatability (R_p) can be calculated by using the following Eq. 6.1 – Eq. 6.3.

$$X_{avg} = \frac{1}{N}\sum_{i=1}^{N}(X_i - X_d) \tag{6.1}$$

$$S = \sqrt{\frac{1}{N-1}\sum_{i=1}^{N}(X_i - X_{avg})^2} \tag{6.2}$$

$$R_p = \pm\ t \cdot S \tag{6.3}$$

where X_i denotes the measured position;
X_d denotes the designed position (nominal value);
X_{avg} is the average position deviation from the designed position;
S is the standard position deviation; and
the coefficient t (Student's t) depends on the confidence level and the number of observations [119].

Resolution is the least increment of movement that the machine is capable of making. The least count of resolution will affect both accuracy and repeatability. High resolution is subsequently easy to accomplish, so the actual effect on accuracy and repeatability is generally small.

6.3 Experimental Work

6.3.1 Component design

A test component (Fig. 6.1) was designed to monitor the positioning accuracy of the centres of a number of drilled holes. A drilling operation was chosen because it is relatively simple to compensate for positioning errors of drilled hole centres. The datum planes B and C were machined with care to assure the uniformity of reference surfaces for the co-ordinate measuring machine (CMM) inspection. A 12 mm diameter HSS drill mill combo cutter was employed to machine datum planes B and C and the five holes to reduce tool setup error. Sufficient space was left before hole

H1 (100 mm) and after hole H5 (102 mm) for clamping the workpiece. Aluminium alloy 6061 was chosen as the work material.

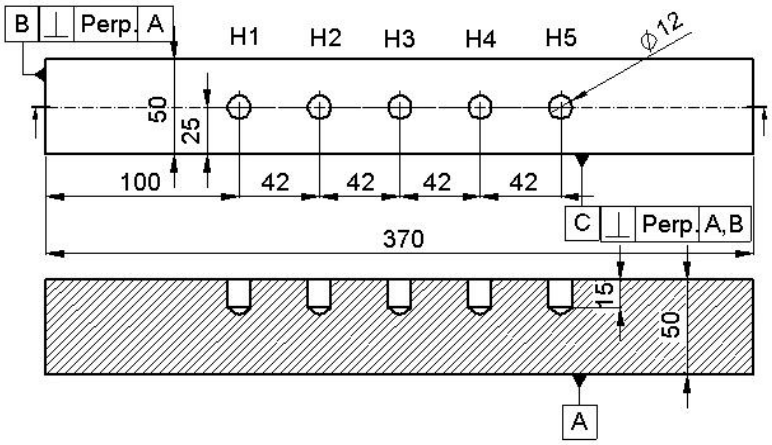

Figure 6.1: Test Component

6.3.2 Cutting conditions

All of the experiments were performed under the same cutting conditions. Coolant was applied through the entire cutting process. The cutting parameters used for milling the datum planes were: cutting speed, 151 m/min; feed rate, 417mm/min; and depth of cut, 0.5 mm. The cutting parameters used for drilling the holes were: cutting speed, 162 m/min; and feed per revolution, 0.04 mm/rev.

6.3.3 Experimental design

The aim of experiments conducted in this chapter was to evaluate the positioning accuracy of drilled hole centres with and without the application of the newly developed thermally-induced volumetric error compensation model (Eq. 5.1). Therefore, the experiments were divided into two categories: the first was an initial test (IT) in which the workpiece was machined according to the designed dimension without any compensation; the second was a compensation test (CT), in which the test was conducted in exactly the same way as the initial test, but with compensated values. A total of 30 components were machined, 20 during the initial test and the remaining 10 during the compensation test (see Table 6.1 for details).

In the initial test, 10 of the 20 components were machined using identical cutting conditions and design dimensions at the cold stage (22.5°C) of the machine tool.

These components were marked as ITCS1–ITCS10 (ITCS; initial test in cold stage). The remaining 10 components were machined using the same cutting conditions and design dimensions at the thermal stable stage (24.5°C) of the machine tool. These components were marked as ITSS1–ITSS10 (ITSS; initial test at thermal stable stage).

Table 6.1: Details of Experiments

Test	Test type	Temperature (°C)
ITCS1-10	Initial	22.5
ITSS1-10	Initial	24.5
CTCS1-5	Compensation	22.5
CTSS1-5	Compensation	24.5

In the compensation test, five of the 10 components were machined using identical cutting conditions, with compensated values for the dimensions at the cold stage (22.5°C) of the machine tool, which were marked as CTCS1–CTCS 5 (CTCS; compensation test in cold stage). The remaining five components were machined using identical cutting conditions and compensated dimensions for the thermal stable stage (24.5°C) of the machine tool, which were marked as CTSS1–CTSS 5 (CTSS; compensation test at thermal stable stage).

The temperatures (22.5°C and 24.5°C) refer to the nut temperature along the *x*-axis, which is the optimum temperature point when calculating the expansion of the lead screw used (Fig. 4.3 – Fig. 4.4). The reason for choosing these two temperatures is that when the test machine is used for only a short period of time it works at 22.5°C (the room temperature in our laboratory is controlled at 21°C); however, when the machine runs continually for normal machining over several hours, the *x*-axis nut temperature might increase to 24.5°C (Chapter 5).

6.3.4 Experimental procedure

The experiments were conducted on the Leadwell V30 CNC machining centre that was also used in the model verification tests performed in Chapter 5. A laser thermometer was used to measure the *x*-axis nut temperature. The measuring point was at the motor end and was as close as possible to the contact surface between the lead screw and the nut (as shown in Fig. 5.1). The details of the experimental procedure for the initial test and compensation test are as follows.

Initial test. The initial test components ITCS1–ITCS10 were machined at

22.5°C to examine the repeatability of the machine tool at its cold stage. Each experiment was performed on a different day to ensure that all the tests were conducted at 22.5°C. The blank material was initially clamped onto the machine table, according to the work co-ordinate system (WCS), and the machine was switched on (cold start). The relationship between the machine co-ordinate system (MCS) and the WCS is shown in Fig. 6.2. The blank material was secured at the same nominal position on the machine table for all of the conducted tests, and the *x* work offset was 350 mm for the convenience of loading and unloading the workpiece. The machine was then warmed up to 22.5°C by moving the table along the *x*-axis, which took approximately 20 minutes, after which the machine was moved back to the origin of the MCS. At last, the drilling process started with following the cutter path shown in Fig. 6.3. The reason for moving the table back to the origin of the MCS before starting the cutting process was to ensure that all the tests had exactly the same tool path.

The initial test components ITSS1–ITSS10 were machined at 24.5°C to assess the machine tool's repeatability at its thermal stable stage. The test procedure followed was the same as that which was used for ITCS1–ITCS10, with an exception being that the machine was warmed up to 24.5°C. This took approximately 100 minutes.

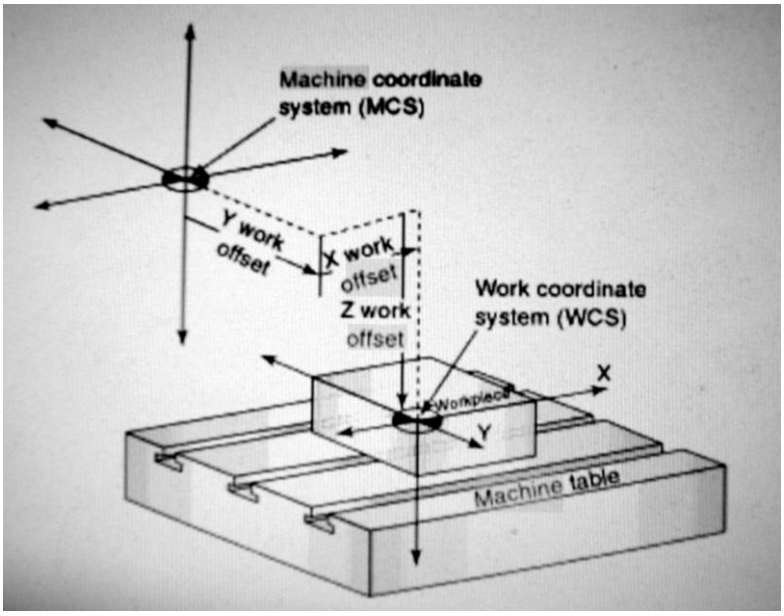

Figure 6.2: Machine Co-ordinate System and Work Co-ordinate System [120]

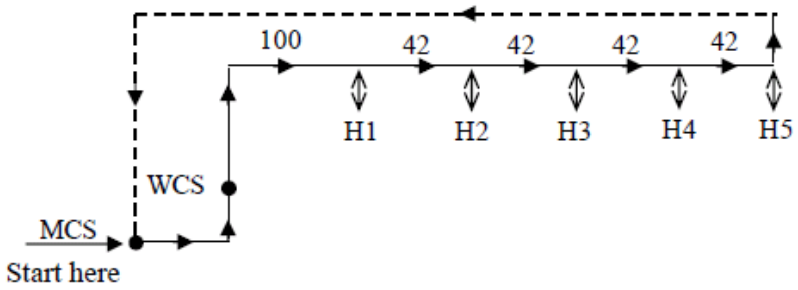

Figure 6.3: Cutter Path

Compensation test. The compensation test components CTCS1–CTCS5 and CTSS1–CTSS5 were machined at 22.5°C and 24.5°C, respectively, to assess the improvement of hole positioning accuracy after applying the proposed volumetric error compensation model. The same procedures were followed as for ITCS–ITCS10 and ITSS1–ITSS10, respectively, with the exception being that the drill tip was moved according to the compensated values instead of the designed values. The calculation of compensation value is explained in the results and analysis section.

The machined parts were inspected by the Discovery Model D-8 CMM that was also employed in Chapter 3 for dimensional measurements. With regard to the components machined in this chapter, measurements were taken from datum planes B and C, respectively, along the *x*-axis and *y*-axis, and 10 points were probed at each height level (five levels per hole) to determine the centre position of the hole.

6.4 Results and Analysis

6.4.1 Analysis of initial test results

The positioning errors of holes in the *x*-axis at the cold stage of the initial test (ITCS1–ITCS10) are shown in Fig. 6.4. The measurement refers to datum plane B, which is the origin of the WCS. A positioning error is defined as the measured position minus the designed position. As shown, all of the positioning errors were negative, and the positioning errors for different workpieces had significant variations, although they were machined in similar thermal conditions (22.5°C).

The positioning errors of holes in the *x*-axis at the thermal stable stage of the

initial test (ITSS1–ITSS10) are shown in Fig. 6.5. As demonstrated, all the positioning errors remain negative; however, there is less variation between the components of the positioning error, compared to the workpiece machined at 22.5°C. Fig. 6.6 compares the holes' average positioning error and the error distribution (plus/minus three standard deviation) between tests ITCS and ITSS. The comparison between these two tests reveals that the average positioning errors increased in a negative direction as the temperature increased to the thermal stable stage. Nevertheless, the components machined at the thermal stable stage produced improved repeatability of positioning accuracy compared to the workpiece machined at the cold stage. The explanation for the increase in positioning errors in a negative direction is outlined below.

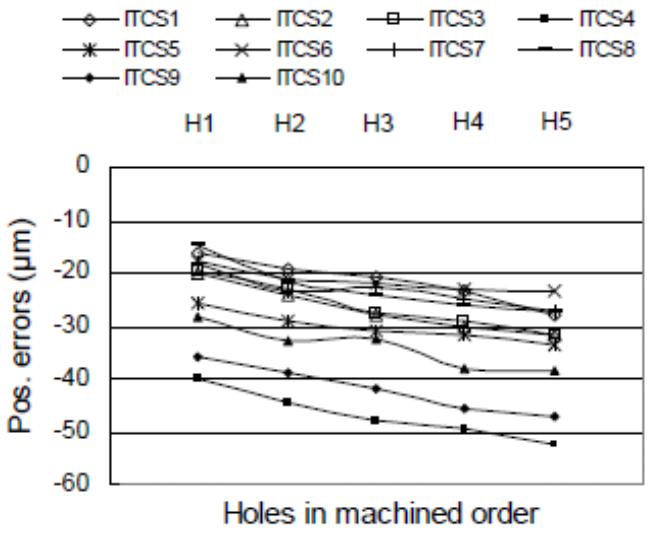

Figure 6.4: Positioning Errors of Holes for Initial Test at Cold Stage (ITCS1–ITCS10)

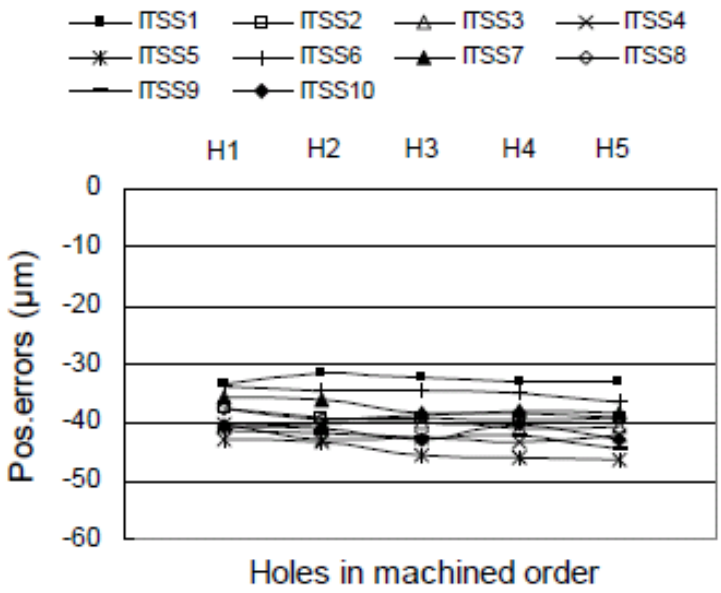

Figure 6.5: Positioning Errors of Holes for Initial Test at Thermal Stable Stage (ITSS1–ITSS10)

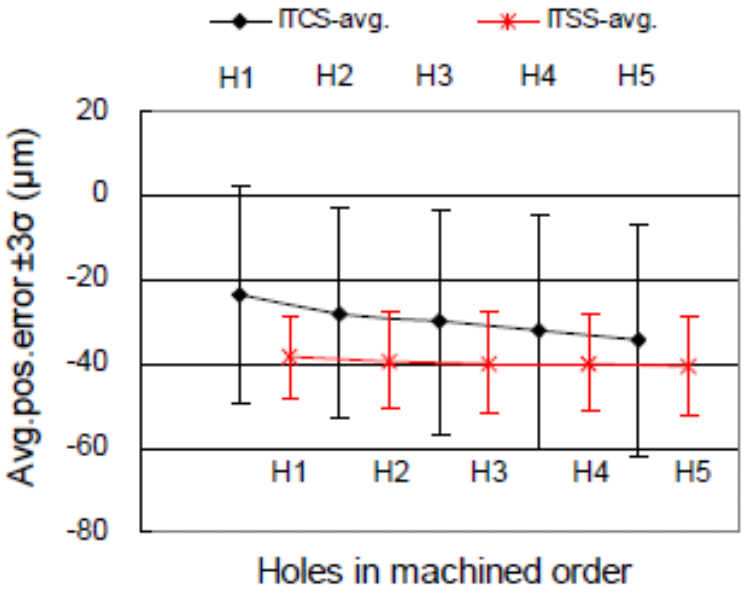

Figure 6.6: The Comparison of Holes' Average Positioning Error and the Error Distribution (±3σ) between Tests ITCS and ITSS

With regard to the structure of the lead screw of the test machine used (*x*-axis), one end of the lead screw was connected to the driving motor and supported by a thrust bearing. This end can be considered as fixed. The other end, where the *x*-axis for the test machine originates, was supported by a ball-bearing and can be considered as the free end. Therefore, when the temperature increased, the origin of the MCS drifted in a negative direction (point P, as shown in Fig. 6.7), due to the

thermal expansion of the lead screw. When the drill tip moved 350 mm from the origin of the MCS to reach the origin of the WCS as designed, the drill tip could not actually reach the precise origin of the WCS because of the negative thermal drifts Δx, even though the travel produces positive travelling errors E_{mw} (Chapter 5). In fact, the real machining started from plane B_1 rather than datum plane B; i.e., the origin of the WCS had negative deviations caused by thermal drifts of the origin of the MCS. This is the primary reason behind significant negative positioning errors.

On the basis of the above analysis and the machining procedure performed in the workpiece (Fig. 6.1), the positioning error of the drilled hole (along the *x*-axis) calculation model can be modified from Eq. 5.1 to the following form:

$$\begin{cases} Err_x(x,T_{xnut}) = O_x + RErr_x(x,T_{xnut}) \\ RErr_x(x,T_{xnut}) = RErr_x(x,T_{x0}) + \beta_x \cdot \alpha \cdot x \cdot (T_{xnut} - T_{x0}) \end{cases} \tag{6.4}$$

where *x*: designed position on the *x*-axis with respect to the origin of the WCS;

O_x: origin thermal deviations of the WCS, $O_x = \Delta x + E_{mw}$ (see Fig. 6.7);

Δx: thermal drifts of the origin of the MCS; its variations with the temperature can be measured and stored in the machine's databank;

E_{mw}: travelling error when the drill tip moves 350 mm from the origin of the MCS to the origin of WCS; its value can be determined from Eq. 5.1, as has been verified in Chapter 5;

$RErr_x(x,T_{xnut})$: relative positioning error when the machine travels from the origin of the WCS to the target position at temperature T_{xnut};

$RErr_x(x,T_{x0})$: relative positioning error when the machine travels from the origin of the WCS to the target position at the cold start (T_{x0}) of the machine; its value can be determined from the measured results (Chapter 5);

β_x: multiplication factor in the *x*-axis; its calculation is explained in Chapter 4.

The compensation value is calculated by the nominal position of the hole minus the positioning error. For example, the nominal position of the first hole H1 is 100 mm, and this will be substituted with a compensation value x_{comp} when drilling the first hole H1 in the compensation test (CTCS and CTSS). x_{comp} is calculated by:

$$x_{comp} = 100 - Err_x(x,T_{xnut}) \tag{6.5}$$

where $Err_x(x, T_{xnut})$ can be calculated from Eq. 6.4.

The positioning error ($Err_x(x, T_{xnut})$) calculation program is composed using Excel-based Microsoft Visual Basic (VB). The advantage of using the Excel-based VB is that the calculation program can be embedded in the Excel document as macros and the three main input variables—the workpiece's absolute position in MCS, the hole's position in WCS, and the ball screw nut temperature—can be arranged in the same worksheet in which a RUN button can be assigned to the related macros. The output results also present in the same worksheet. This makes the compensation procedure simple and quick.

6.4.2 Analysis of compensation test results

As explained above, the components machined in the initial test stage (ITCS and ITSS) are the components without compensation, while the components machined in the compensation test stage (CTCS and CTSS) are the components with compensation. The results are summarized in Fig. 6.8 – Fig. 6.11. Fig. 6.8 shows the positioning errors of holes for compensation tests at the cold stage (CTCS1–CTCS5). Fig. 6.9 shows the positioning errors of holes for compensation test at the thermal stable stage (CTSS1–CTSS5). It can be observed that the negative positioning errors are reduced after applying the proposed thermally-induced volumetric error compensation model for both thermal stages. Fig. 6.10 compares the positioning errors and their distributions between machining with and without compensation at the cold stage. Fig. 6.11 compares the positioning errors and their distributions between machining with and without compensation at the thermal stable stage. As shown, after application of the proposed thermally-induced volumetric error compensation model, the average positioning errors of machined holes are improved significantly; however, there was little variability in the error distribution range.

Although the amount of negative positioning errors was reduced significantly after application of the thermally-induced volumetric error model, some negative errors still remained. This is because some of the factors that have important effects on the positioning accuracy of the drill tip, such as spindle tilt caused by continuous rotating and column bending, workpiece thermal deformation, and natural variation of the drilling process, were not considered during the course of this research.

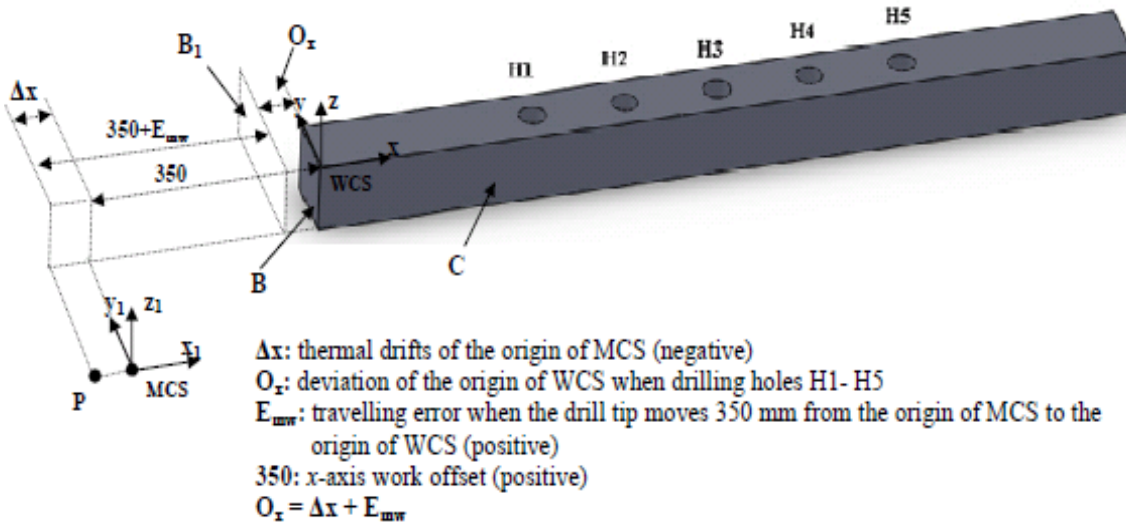

Figure 6.7: Thermal Drifts of the Origin of the Machine Co-ordinate System

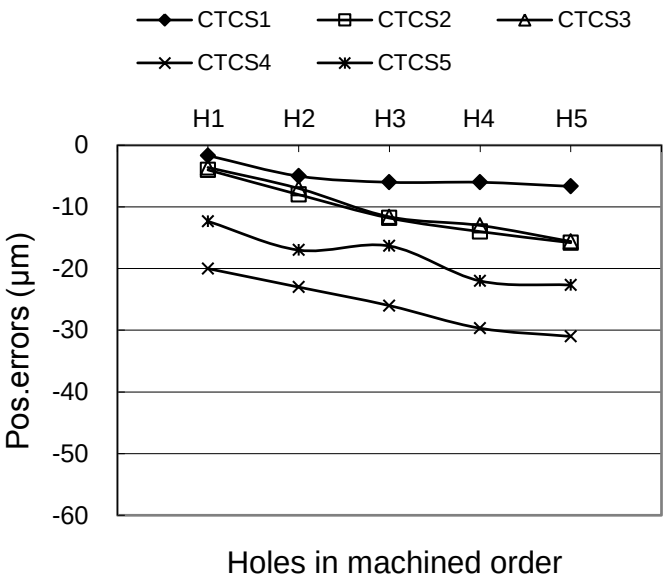

Figure 6.8: Positioning Errors of Holes for Compensation Test at Cold Stage (CTCS1–CTCS5)

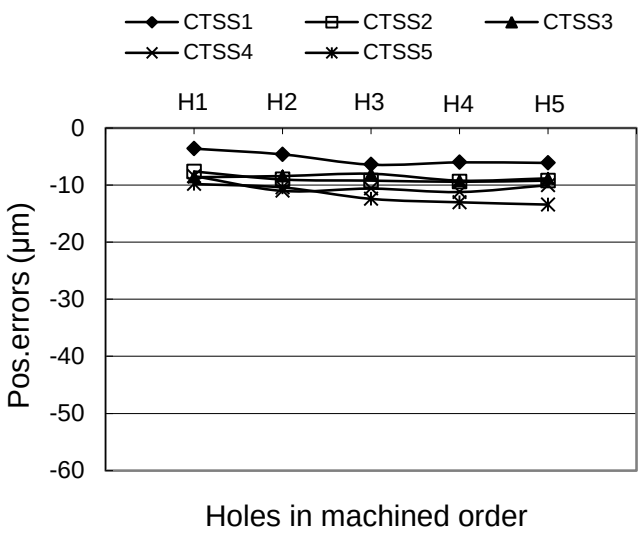

Figure 6.9: Positioning Errors of Holes for Compensation Test at Thermal Stable Stage (CTSS1–CTSS5)

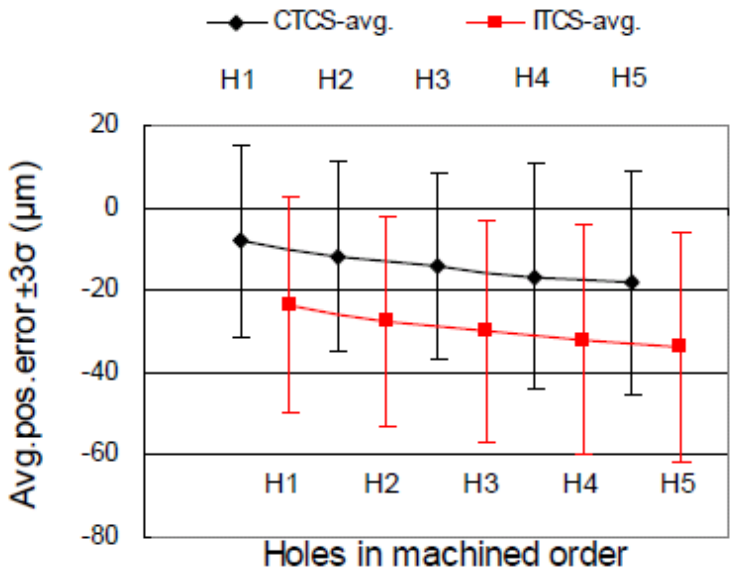

Figure 6.10: Comparison of Average Positioning Errors (±3σ) between Machining with Compensation (CTCS) and without Compensation (ITCS) at Cold Stage

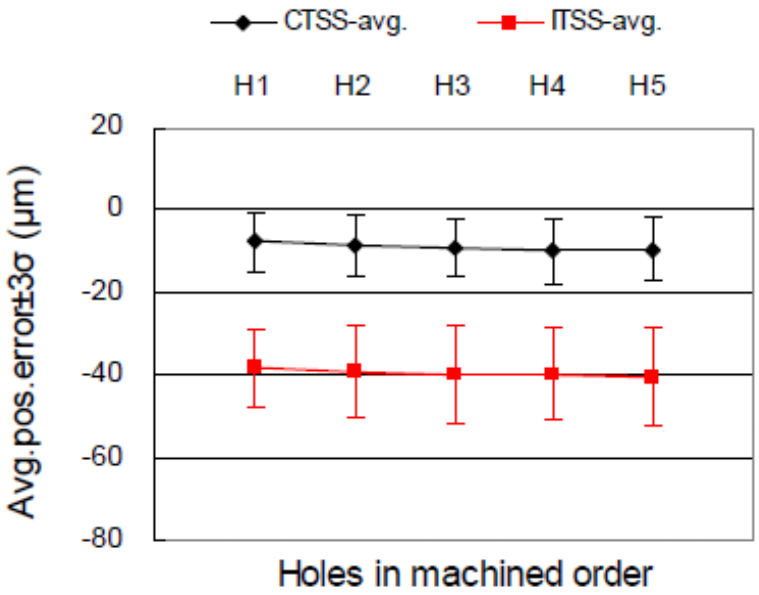

Figure 6.11: Comparison of Average Positioning Errors (±3σ) between Machining with Compensation (CTSS) and without Compensation (ITSS) at Thermal Stable Stage

Despite these limitations, the proposed thermally–induced volumetric error compensation method significantly improved the positioning accuracy of drilled hole centres. The reduction of positioning errors by compensation is summarised in Table 6.2. The average absolute reduction of the positioning errors of drilled holes was 15.50 μm at the cold stage (22.5°C) and 30.44 μm at the thermal stable stage (24.5°C), while the average relative reduction ratio of these positioning errors was 53% at the cold stage (22.5°C) and 77% at the thermal stable stage (24.5°C).

Table 6.2: Positioning Error Reduction after Compensation

Holes		Without compensation (μm; IT--)	With compensation (μm; CT--)	Absolute reduction (μm)+	Relative reduction (%)++
22.5-avg* (--CS)	1	-23.61	-8.32	15.29	65
	2	-27.76	-12.00	15.76	57
	3	-29.82	-14.35	15.47	52
	4	-32.13	-16.93	15.19	47
	5	-34.11	-18.35	15.77	46
	Average**	**-29.49**	**-13.99**	**15.50**	**53**
24.5-avg* (--SS)	1	-38.42	-7.60	30.82	80
	2	-39.04	-8.68	30.36	78
	3	-39.64	-9.32	30.32	76
	4	-39.64	-9.76	29.88	75
	5	-40.30	-9.50	30.80	76
	Average**	**-39.41**	**-8.97**	**30.44**	**77**

+ Absolute reduction = abs (error without compensation) – abs (error with compensation)
++ Relative reduction = 100*absolute reduction/abs (error without compensation)
* Average of holes in different workpiece and the same *x* position, such as H1 in ITCS1–ITCS10
** Average of all holes in the same type of test, such as all holes in ITCS

6.4.3 Calculation of accuracy and repeatability

The *x*-axis linear positioning accuracy in test ITCS (or ITSS) is calculated from position readings of 50 holes drilled in test ITCS (or ITSS) using average deviations of the measured position from the designed position ($Acc = X_{avg}$; X_{avg} is calculated from Eq. 6.1, $N = 50$), while the *x*-axis linear positioning accuracy in test CTCS (or CTSS) is calculated from position readings of 25 holes drilled in test CTCS (or CTSS) using the same method ($Acc = X_{avg}$; X_{avg} is calculated from Eq. 6.1, N = 25).

The machining repeatability in test ITCS (or ITSS) is calculated from position readings of 50 holes drilled in test ITCS (or ITSS) using Eq. 6.2 and Eq. 6.3 (N = 50). The coefficient *t* is selected as 2.011 according to the Student's *t* table [119] when the number of observations is 50 and the expected confidence level is 95%, while the machining repeatability in test CTCS (or CTSS) is calculated from position readings of 25 holes drilled in test CTCS (or CTSS) using the same method (Eq. 6.2 – Eq. 6.3; N = 25; $t = 2.060$).

The calculation results are shown in Fig. 6.12. It can be observed that machining accuracy and repeatability demonstrate different aspects of machining performance.

The machining repeatability could be high (the magnitude of R_p is small) although the machining accuracy is low (the deviation value is large), such as the machining performed in ITSS in which the repeatability range is as narrow as ± 7.42 μm, although the accuracy is low at -39.41 μm. Sometimes the machining repeatability is low although the accuracy is high, such as the machining performed in CTCS in which the accuracy is increased (-13.99 μm) in comparison with test ITSS, but the repeatability range is much wider (± 17.22 μm).

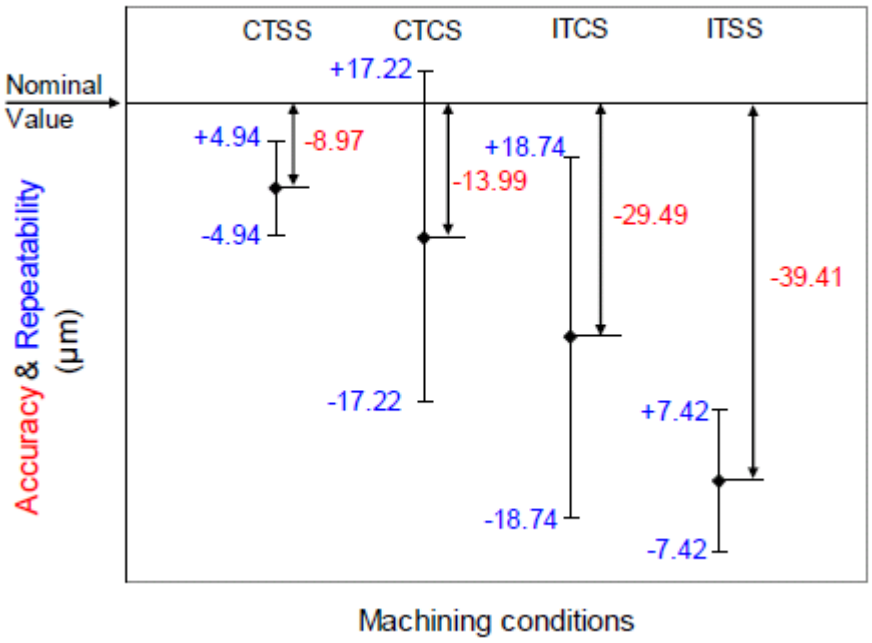

Figure 6.12: Accuracy and Repeatability of Different Machining Processes

The results shown in Fig. 6.12 also indicate that the machining accuracy is really improved after applying the proposed thermally-induced volumetric error compensation model (compare CTSS with ITSS and CTCS with ITCS); however, the repeatability shows less improvement when comparing the accuracy. It is also worth pointing out that the thermal stable stage is a better stage for repeatable machining and thermal error compensation. The repeatability range in the thermal stable stage (ITSS) is ± 7.42 μm instead of ± 18.74 μm in the cold stage (ITCS). After applying the proposed thermal error compensation model, the machining accuracy improves 77% in the thermal stable stage ((ITSS – CTSS)/ITSS = 77%) as compared with 53% in the cold stage ((ITCS – CTCS)/ITCS = 53%).

6.4.4 Application of proposed method in real machining

Fig. 6.13 outlines the structure of the proposed compensation method. The compensation procedure should be performed in the following steps.

Preparation of the databank. LDDM and a 3D sensor are used in this stage. LDDM is employed to calibrate the three positioning errors that do not have to been calibrated for each machining. It is recommended to check them every two years depending on the machine tool's condition. The details of positioning error calibration using LDDM are demonstrated in Chapter 5. The calibration results can be stored in the databank to modify the compensation model.

A 3D sensor is employed to determine the machine tool's origin thermal drifts. The 3D sensor is a new generation of edge finder for accurate tool setting. Its measuring accuracy can achieve measurements of 1 μm. Determining the origin thermal drifts using a 3D sensor is a simple and cheap method; therefore, it can be performed any time it is needed, such as every one year or two years depending on the machine's condition. The results can be stored in the databank to modify the compensation model.

The procedure of measuring the origin thermal drifts using a 3D sensor is as follows:

- Set up a fine machined (the application of a 3D sensor requires that all surfaces are in good condition) prismatic workpiece on the machine table in the machine's cold stage; find the origin of the workpiece (origin of WCS) using the 3D sensor and record the origin of the *x*-axis in WCS as x_0; move the machine back to the machine origin (origin of MCS); then move the machine to the origin of WCS again; and check the *x*-axis nut temperature (T_1) and the co-ordinate of the origin of WCS over again (symbolized as x_1) using the 3D sensor. The difference between x_0 and x_1 is the origin thermal drifts at temperature T_1 ($\Delta x_1 = x_0 - x_1$).
- Idle run the machine along the *x*-axis full stroke for ten minutes; move the machine to the origin of WCS; record the nut temperature (T_2); and check the co-ordinate of the origin of WCS (x_2) using the 3D sensor. The difference between x_0 and x_2 is the origin thermal drifts at temperature T_2 ($\Delta x_2 = x_0 - x_2$).
- Idle run the machine to 20, 30, 60, 120 and 180 minutes, respectively; and measure the origin thermal drifts Δx_3, Δx_4, Δx_5, … following the same

procedure.

- Save the origin thermal drifts and their corresponding temperatures in the databank. These values can be automatically collected while running the compensation program.

Before each machining. When the databank is ready, there are still some parameters required by the compensation program before each machining. Take the drilling as an example. The procedure for determining these parameters should follow the order listed below:

- Set up the work on the table and find the co-ordinate of the origin of WCS using a 3D sensor;
- Input the co-ordinate value and the hole's designed position (in WCS) into the compensation program;
- Collect the nut temperature from the data logger and input it into the compensation program;
- Run the compensation program and use the results (compensation value for each designed hole) to modify the CNC operating program; and
- Load the CNC operating program onto the CNC controller and start the machining.

This compensation method recommends starting each job from the machine tool's cold stage as the measurement of origin thermal drifts are based on the machine tool's cold start. However, it costs a lot of time for the real industry to wait for the machine to cool down. Solving this problem needs more testing; therefore, it should be our future research focus.

6.4.5 Comparison of application of traditional method and proposed method

The proposed thermally-induced volumetric error compensation method not only improves the dimensional accuracy of machined parts but also simplifies the compensation procedure and subsequently brings considerable cost savings to the industry. Table 6.3 compares the application of the traditional method and the proposed method. Researchers who employed the traditional model for thermal error compensation have used different compensation procedures. In Table 6.3, the method applied by Chen et al. [97] is considered as the traditional method that followed the outline shown in Fig. 2.3. A laser interferometer, model HP-5526A, was used for the

error measurement which is capable of measuring 18 geometric error components: three positioning errors, six straightness errors, three yaw errors, three pitch errors and three squareness errors. For the measurement of the three roll errors, an electronic level was needed. A laser interferometer is an expensive piece of equipment; as such, it is hard to obtain at its current price. The price quoted in Table 6.3 is for an older model made in 1976. Table 6.3 shows that the proposed method is considerably cheaper with marginally lower accuracy improvement capabilities.

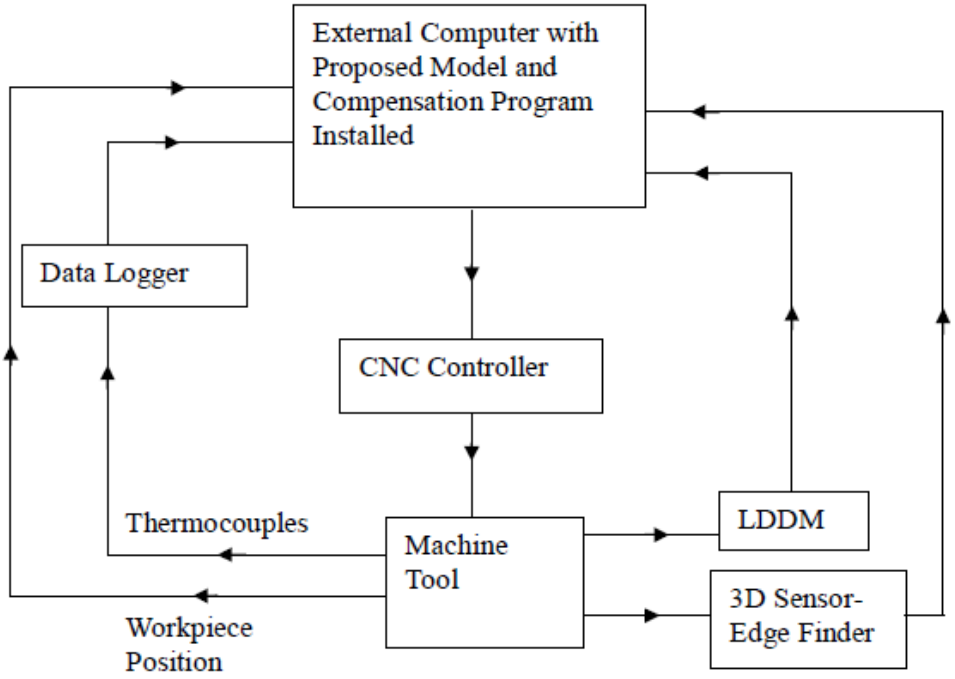

Figure 6.13: Structure of Proposed Compensation Method

Table 6.3: Comparison of Application of Traditional Method and Proposed Method

Compensation method	Traditional method		Proposed method	
Model employed	Eq. 4.18 and Eq. 4.11		Eq. 4.28	
Error components involved	21		3	
Number of temperature inspection locations required	17 [97]		3	
Compensation outline	Fig. 2.3 [97]		Fig. 6.13	
Equipment required and their costs (USD)	17 Thermocouples	$426	3 Thermocouples	$75
	Laser interferometer	$62,880*	LDDM	$16,003
	Electronic level	$2,520	3D sensor	$400
	External computer	$949	External computer	$949
	3–8 channel data logger	$1,095	1–8 channel data logger	$365
	Total costs	$67,870	Total costs	$17,784
Accuracy improves	80% [97]		77%	

USD [121]: 1 USD = 0.9488 AUD, 1 USD = 6.249 Chinese Yuan;
Thermocouple [122]: PFA T/C with miniature plug, K-type, 5 metres;
Laser interferometer [123]: HP-5526A;
LDDM [124]: LICS-100;
Electronic level [125]: Digi-Pas DWL3500XY;
3D sensor [126]: Haimer 3D sensor universal;
Computer [127]: HP ENVY Phoenix h9-1315t Desktop PC;
Data logger [128]: PICO USB TC-08, 8-channel thermocouple data logger;
*$62,880: a reference price for HP-5526A made in 1976.

6.5 Concluding Remarks

Based on the experiments and subsequent analysis, the following conclusions are drawn:

- Thermally-induced positioning errors include two key components: thermally-induced origin drifts and relative or travelling positioning errors. Although a travelling positioning error for the test machine is positive and proportional to the travel distance, the test machine used for the present study has a considerable negative origin thermal drift, which significantly affected the dimensional accuracy of the machined workpiece.
- For a small-sized workpiece, the thermal origin drifts could dominate the positioning error, so it is essential to avoid, or compensate for, the origin thermal drifts when planning the machining procedure.
- A machine tool produces reliably high dimensional replication at the thermal stable stage, so this stage is the optimal stage at which to conduct thermal error compensation.
- After application of the proposed thermally-induced volumetric error compensation model, the positioning accuracy of drilled holes improved significantly. The absolute reduction of the positioning errors of drilled holes was an average 30.44 μm at the thermal stable stage, while the average relative reduction ratio of these errors was 77%.
- Comparing with the traditional method, the proposed thermally-induced volumetric error compensation method is a simple and cost-effective way to enhance the existing machine tool's machining accuracy.

Chapter 7

Conclusion

7.1 Introduction

The thermal condition of machine tools can profoundly affect the dimensional accuracy of machined parts; consequently, the reduction of its influence has become increasingly important to modern machining. One of the most convenient and effective ways to reduce the thermal error of a machine tool and increase its working accuracy is volumetric error compensation, especially for CNC machine tools. However, currently available compensation methods based on the traditional volumetric error model do not consider thermal errors. In addition, they are complicated and difficult to apply in industry. They require a high-precision laser interferometer to measure the 21 geometric error components, which is costly and time-consuming; additionally, the large number of thermocouples employed by the traditional model to monitor temperature variations could obstruct the machine tool's routine work.

The objective of this project is to investigate the effects of thermal errors of a machine tool on the dimensional accuracy of machined parts and develop a new model for calculating thermally-induced volumetric error suitable for industrial applications. It has been achieved by combining the dominant thermal error components into the traditional geometric error-based volumetric error model to develop a synthesized model for thermally-induced volumetric error calculation. Subsequently, the model has been simplified by ignoring the error components which show insignificant variations with the temperature. As a result, the final model does not require an expensive laser interferometer or a large number of thermocouples for error measurement.

This chapter examines the success of this project in achieving the above-stated

objectives and then outlines possible improvements in the proposed methodology as well as future research interests on this topic.

7.2 Achievement

The main achievement of this thesis is the development of a new model for calculating thermally-induced volumetric error suitable for industrial applications. This goal has been achieved by integrating major thermally-induced error components into the traditional volumetric error model. The newly developed model has been verified experimentally and efficiently applied in real machining. The detailed conclusions drawn from this research are as follows:

- The machine tool has a warm-up period. During the warm-up period, the positioning error of the machine tool deteriorates significantly, which has detrimental effects on the accuracy and repeatability of machined parts, especially in the first hour after starting a machine. For a typical machine tool, it takes around two-and-a-half hours to get to its thermal stable stage, which is the optimum stage to improve the positioning accuracy and increase the repeatability of machined workpieces by the compensation technique (Chapter 3).
- A thermally-induced volumetric error compensation model (TIVEM) has been developed. Instead of using 21 measured geometric errors and their variations with the temperature to calculate the volumetric error, the newly developed model consider the thermal effects on only three axial positioning errors; the remaining 18 error components are assumed to remain the same as the pre-calibrated cold start value. The proposed model has been tested by simulated machining jobs. The total reduction of distance error between holes could be up to 99% (Chapter 4).
- The TIVEM is further simplified by ignoring all 18 geometric error components so that the simplified model includes the axial positioning error components only. The simplified model has been testified by simulated

machining jobs which indicate that only a negligible amount of total dimensional accuracy will be sacrificed by adopting the simplified compensation model instead of the full-error model comprised of 21 error components (Chapter 4).

- The simplified thermally-induced volumetric error compensation model has been verified experimentally on a vertical machining centre typically used in the industry. The thermally-induced positioning error under different operating conditions (idle running, milling and drilling) has been measured, predicted and analysed. The results show that the predicted positioning errors agree well with the measured values; errors generated in the milling operation can be simulated by errors generated in high-feed rate idle running. However, in high temperatures, errors generated in the drilling operation are a little bit lower (Chapter 5).
- The thermally-induced volumetric error compensation model has been applied on a vertical machining centre by compensating centre positions of a number of holes. The results show the position accuracy of drilled holes is significantly improved after compensation. The positioning error decrease ratio is up to 77% (Chapter 6).

7.3 Suggested Improvements and Future Research Interests

- Spindle drifts caused by spindle rotation and column bending affect the cutting tip's positioning accuracy, but they are not included in the proposed model due to time constraints. It is worth investigating the spindle drifts (six error components; see Table 1.1 for details) with the temperature variations, finding the dominant drifts, modelling the drifts as functions of a key temperature, and lastly, modifying the proposed model (TIVEM) by this model (spindle drifts with the temperature).
- A machine tool's thermal origin offsets make the major part of the positioning error. Further investigations are needed to understand the thermal behaviours

of origin offsets; then the proposed model can be modified according to the research findings.

- Thermal expansion of a workpiece is another factor which affects the dimensional accuracy of machined workpiece accuracy. Future research on the effect of workpiece thermal expansion is suggested.
- The three major elements that have significant influence on the positioning accuracy of a machine tool are: the lead screws, the spindle and the column. Therefore, individual numerical models for these elements can be developed and integrated into the overall error model of the system.
- A simple on-line volumetric error compensation scheme suggested in Chapter 4 needs further development. In the future, it can be an economical method for enhancing the machining accuracy of existing machine tools used in today's manufacturing industry.

References

[1] Trent, E. M., and Wright, P. K., 2000, *Metal Cutting*, 4th ed., Butterworth-Heinemann, Boston, USA.

[2] Metal Working Insider's Report, Feb. 2012, "The 2012 World Machine-Tool Output & Consumption Survey," Gardner Publications Inc., Cincinnati, USA.

[3] The Association for Manufacturing Technology, "13-June, 2011, USMTC News Release for April Manufacturing Technology Consumption," Home Page, www.amtonline.org/newsroom/AMTpressroom/, (5/11/2012).

[4] Groover, M. P., 2010, *Fundamentals of Modern Manufacturing*, 4th ed., John Wiley & Sons, New Jersey, USA.

[5] Farmer, L. E., 1999, *Dimensioning and Tolerancing for Function and Economic Manufacture*, Blueprint Publications, Sydney, Australia.

[6] Bryan, J., 1990, "International Status of Thermal Error Research," Annals of the CIRP, 39 (2), pp. 645-656.

[7] Mekid, S., 2009, *Introduction to Precision Machine Design and Error Assessment*, Tayler & Francis Group, Florida, USA.

[8] "Australian Standard (1984) AS1100, Technical Drawing, Part 201-1984, Mechanical Drawing," The Standard Association of Australia, Sydney.

[9] Bryan, J. B., 1971, "Closer Tolerance - Economic Sense," Annals of the CIRP, 19 (2), pp. 115-120.

[10] Nakazawa, H., 1994, *Principles of Precision Engineering*, Oxford University Press Inc., New York, USA.

[11] Ramesh, R., Mannan, M. A., and Poo, A. N., 2000, "Error Compensation in Machine Tools -- A Review: Part I: Geometric, Cutting-Force Induced and Fixture-Dependent Errors," International Journal of Machine Tools and Manufacture, 40 (9), pp. 1235-1256.

[12] Chen, L., and Tsutsumi, M., 1996, "Measurement and Compensation of Corner-Tracking Errors of CNC Machine Tools," International Journal of Japan Society of Precision Engineering, 30 (4), pp. 331-336.

[13] Lee, E. S., Suh, S. H., and Shon, J. W., 1998, "A Comprehensive Method for Calibration of Volumetric Positioning Accuracy of CNC Machines," International Journal of Advanced Manufacturing Technology, 14 (1), pp. 43-49.

[14] Ni, J., and Wu, S. M., 1993, "An on-Line Measurement Technique for Machine Volumetric Error Compensation," ASME Trans. Journal of Engineering for Industry, 115 (1), pp. 85-92.

[15] Tarng, Y. S., Huang, H. Y., and Hsu, W. T., 1997, "An Optimisation Approach to the Contour Error Control of CNC Machine Tools Using Genetic Algorithms," International Journal of Advanced Manufacturing Technology, 13 (5), pp. 359-366.

[16] Tarng, Y. S., Kao, J. Y., and Lim, Y. S., 1997, "Identification and Compensation for Backlash on the Contouring Accuracy of CNC Machining Centres," International Journal of Advanced Manufacturing Technology, 13 (2), pp. 77-85.

[17] Wilhelm, R. G., Srinivasan, N., and Farabaugh, F., 1997, "Part-Form Errors Predicted From Machine Tool Performance Measurements," Annals of the CIRP, 46 (1), pp. 471-475.

[18] Schultschik, R., 1977, "The Components of the Volumetric Accuracy," Annals

of the CIRP, 25 (1), pp. 223-228.

[19] Ferreira, P. M., and Liu, C. R., 1986, "A Contribution to the Analysis and Compensation of the Geometric Error of A Machining Centre" Annals of the CIRP, 35 (1), pp. 259-262.

[20] Oya, M., Hokari, H., and Tanura, H., 1987, "A Study on Improvement of the Accuracy of A Three-Coordinate Measuring Machine (A Method of Error Compensation)," JSME International Journal, 30 (260), pp. 344-349.

[21] Postlethwaite, S. R., and Ford, D. G., 1997, "Geometric Error Analysis Software for CNC Machine Tools," Proc. 3rd Int. Conf. on Laser Metrology and Machine Performance LAMDAMAP, pp. 305-316.

[22] Soons, J. A., 1997, "Error Analysis of A Hexapod Machine Tool," Proc. 3rd Int. Conf. on Laser Metrology and Machine Performance LAMDAMAP, pp. 347-358.

[23] Fan, K. C., and Burdekin, M., 1986, "Development of a Computer Software Package for Positioning Accuracy Calibration and Analysis on NC Machine Tools," Proc. 26th Int. MTDR Conf. 17 Manchester, pp. 107-113.

[24] Freeman, J. M., and Ford, D. G., 1997, "The Analysis of Geometric and Thermal Errors of Non-Cartesian Structures," Proc. 3rd Int. Conf. on Laser Metrology and Machine Performance - LAMDAMAP, pp. 371-379.

[25] Holsa, J., 1997, "Utilising CMM Measurements in the Evaluation of Machine Tool Accuracy," Proc. 3rd Int. Conf. on Laser Metrology and Machine Performance - LAMDAMAP, pp. 487-496.

[26] Yang, S., Yuan, J., and Ni, J., 1997, "Real-Time Cutting Force Induced Error Compensation on A Turning Centre," International Journal of Machine Tools and Manufacture, 37 (11), pp. 1597-1610.

[27] Ramesh, R., Mannan, M. A., and Poo, A. N., 2000, "Error Compensation in Machine Tools -- A Review: Part II: Thermal Errors," International Journal of Machine Tools and Manufacture, 40 (9), pp. 1257-1284.

[28] Bryan, J., 1968, "International Status of Thermal Error Research," Annals of the CIRP, 16, pp. 203-215.

[29] Okushima, K., Kakino, Y., Sawai, H., and Kikuchi, T., 1972, "Thermal Deformation of Machine Tools (1st Report), Thermal Deformation of Column in Steady-State," Journal of the Japan Society of Precision Engineering, 38, pp.283-288.

[30] Okushima, K., Kakino, Y., and Kikuchi, T., 1972, "Thermal Deformation of Machine Tools (2nd Report), Unsteady State Thermal Deformation Due To Inner Heat Sources," Journal of the Japan Society of Precision Engineering, 38, pp. 565-571.

[31] Okushima, K., Kakino, Y., and Kikuchi, T., 1973, "Thermal Deformation of Machine Tools (3rd Report), Effects of the Circulation of Fluids," Journal of the Japan Society of Precision Engineering, 39, pp. 230-236.

[32] Moore, R., and Victory, F., 1955, *Holes, Contours and Surfaces: Located, Machined, Ground, and Inspected by Precision Methods,* Moore Special Tool Co., Bridgeport, USA.

[33] Tlusty, J., and Mutch, G. F., 1974, "Testing and Evaluating Thermal Deformations of Machine Tools", Proc. 14th International Machine Tool Design and Research Conference, 1973, Macmillan, London, pp. 285-297.

[34] Sata, T., Y. Takeuchi, Y., and Okubo, N., 1975, "Control of the Thermal Deformation of a Machine Tool", MTDR Conference Proceedings, 16, pp. 203-208.

[35] Weck, M., and Zangs, L., 1975, "Computing the Thermal Behaviour of Machine Tools Using the Finite Element Method-Possibilities and Limitations," 16th MTDR, 16, pp. 185-194.

[36] Breev, B. T., 1956, "Thermal Deformations in Machine Tools and Their Reduction," Stanki i Instrument, 3 (4), pp. 14-15.

[37] Smirnov, V. E., 1963, "The Effect of the Thermal Deformations on the Accuracy of Machine Tools," Stanki i Instrument, 52 (1), p.15.

[38] Sata, T., Takeuchi, Y., Sato, N., and Okubo, N., 1974, "Analysis of Thermal Deformation of Machine Tool Structure and Its Application," Proc. 14th International Machine Tool Design and Research Conference, 1973, Macmillan, London, pp. 275-280.

[39] DeBra, D. B., Victor, R. A., and Bryan, J. B., 1986, "Shower and High Pressure Oil Temperature Contro1," Annals of the CIRP, 35(1), pp. 359-363.

[40] Chou, C., and DeBra, D. B., 1990, "Liquid Temperature Control for Precision Tools," Annals of the CIRP, 39 (1), pp. 535-543.

[41] Kaebernick, H., 1986, "Thermal Behaviour of Machine Tools: Summarized Report of Work at Technical University of Berlin, Germany: 1986," CSIRO Division of Manufacturing Technology, Woodville North, SA.

[42] Okushima, K., Kakino, Y., and Higashimoto, A., 1975, "Compensation of Thermal Displacement by Coordinate System Correction," Annals of the CIRP, 24 (1), pp. 327-331.

[43] McClure, E. R., 1969, "Manufacturing Accuracy through the Control of Thermal Effects," Thesis, in Engineering, University of California, Berkeley and LLNL.

[44] Attia, M. H., and Kops, L., 1978, "On the Role of Fixed Joints in Thermal Deformation of Machine-Tool Structures," Annals of the CIRP, 27 (1), pp. 305-310.

[45] Camera, A., Favareto, M., Militano, L., and D' Aprile, F., 1976, "Analysis of the Thermal Behaviour of a Machine Tool Table Using the Finite Element Method," Annals of the CIRP, 25(1), p. 297.

[46] Bryan, J., Donaldson, R., McClure, E., and Clouser, R., 1972, "A Practical Solution to the Thermal Stability Problem in Machine Tools," S.M.E Technical Report, MR 72-138, UCRL 73577.

[47] Bryan, J., 1979, "Design and Construction of an Ultra Precision 84 Inch Diamond Turning Machine," Precision Engineering, 1 (1), pp. 13-17.

[48] Modern Machine Shop, Home Page, www.mmsonline.com/articles/gearing--up-to-make-big-gears, (11/05/2012).

[49] Trapet, E., and Waldele, F., 1989, "Coordinate Measuring Machines in the Production Line: Influence of Temperature and Measuring Uncertainties," Proceedings of the IV Congress International Metrologic Industrial, Zaragoza (Spain), pp. 229-242.

[50] Kim, H. S., Jeong, K. S., and Lee, D. G., 1997, "Design and Manufacture of A Three-Axis Ultra-Precision CNC Grinding Machine," ASME Trans. Journal of Materials Processing Technology, 71 (2), pp. 258-266.

[51] Kim, J. D., and Kin, D. S., 1997, "Development and Application of an Ultra-Precision Lathe," International Journal of Advanced Manufacturing Technology, 13, pp. 164-171.

[52] Spur, G., and Fischer, H., 1969, "Thermal Behaviour of Machine Tools," Proc. 10th Int. MTDR Conf. Manchester, UK, pp. 147-160.

[53] Sugishita, H., Nishiyama, H., Nagayasu, O., Shinnou, T., Sato, H., and O-hori, M., 1988, "Development of a Concrete Machining Centre and Identification of the Dynamic and Thermal Structural Behaviour," Annals of the CIRP, 37 (1), pp. 377-380.

[54] Takada, K., and Tanabe, I., 1987, "Basic Study on Thermal Deformation of Machine Tool Structure Composed of Epoxy Resin Concrete and Cast iron," Bulletin of JSPE, 21 (3), pp. 173-178.

[55] Spur, G., and DeHaas, P., 1974, "Thermal Behaviour of NC Machine Tools," Proc. 14th International Machine Tool Design and Research Conference, 1973, Macmillan, London, pp. 267-273.

[56] McClure, E. R., 1967, "Significance of Thermal Effect in Manufacturing and Metrology," Annals of the CIRP, 15 (1), pp. 61-66.

[57] Spur, G., Hoffmann, E., Paluncic, Z., Benzinger, K., and Nymoen, H., 1988, "Thermal Behaviour Optimisation of Machine Tools," Annals of the CIRP, 37 (1), pp. 401-405.

[58] Attia, M. H., and Kops, L., 1979, "Calculation of Thermal Deformation of Machine Tools in Transient State with the Effect of Structural Joints Taken into Account," Annals of the CIRP, 28 (1), pp. 247-251.

[59] Murty, R. L., 1980, "Thermal Deformation of A Semi-Automatic Machine: A Case Study," Precision Engineering, 2 (1), pp. 17-21.

[60] Moriwaki, T., 1988, "Thermal Deformation and Its On-Line Compensation of Hydrostatically Supported Precision Spindle," Annals of the CIRP, Manufacturing Technology, 37 (1), pp. 393-396.

[61] Jedrzejewski, J., 1988, "Effect of the Thermal Contact Resistance on Thermal Behavior of the Spindle Radial Bearings," International Journal of Machine

Tools and Manufacture, 28 (4), pp. 409-416.

[62] Balsamo, A., Marques, D., and Sartori, S., 1990, "A Method for Thermal Deformation Corrections of CMMs," Annals of the CIRP, 39 (1), pp.557-560.

[63] Jedrzejewski, J., and Modrzycki, W., 1992, "A New Approach to Modelling Thermal Behaviour of A Machine Tool under Service Conditions," Annals of the CIRP, 41 (1), pp. 455-458.

[64] Hatamura, Y., Nagao, T., Mitsuishi, M., Kato, K., Taguchi, S., Okumura, T., Nakagawa, G., and Sugishita, H., 1993, "Development of An Intelligent Machining Centre Incorporating Active Compensation For Thermal Distortion," Annals of the CIRP, 42 (1), pp. 549-552.

[65] Stephenson, D. A., Barone, M. R., and Dargush, G. F., 1995, "Thermal Expansion of the Workpiece in Turning," Transaction of the ASME, Journal of Engineering for Industry, 117, pp. 542-550.

[66] Bryan, J. B., Carter, D. L., Clouser, R. W., and Hamilton, J. H., 1982, "An Order of Magnitude Improvement in Thermal Stability with Use of Liquid Shower on A General Purpose Measuring Machine," ASME Technical Paper, IQ82-936.

[67] Srinivasa, N., Ziegert, J. C., and Mize, C. D., 1996, "Spindle Thermal Drift Measurement Using the Laser Ball Bar," Precision Engineering, 18, pp.118-128.

[68] Huang, P. S., and Ni, J., 1995, "On-Line Error Compensation of Coordinate Measuring Machines", International Journal of Machine Tools and Manufacture, 35 (5), pp. 725-738.

[69] Lo, C. H., Yuan, J., and Ni, J., 1995, "An Application of Real-Time Error Compensation on A Turning Centre," International Journal of Machine Tools

and Manufacture, 35 (12), pp. 1669-1682.

[70] Attia, M. H., and Kops, L., 1993, "Thermometric Design Considerations for Temperature Monitoring in Machine Tools and CMM Structures," International Journal of Advanced Manufacturing Technology, 8 (5), pp. 311-319.

[71] Mou, J., Donmez, M. A., and Cetinkunt, S., 1995, "An Adaptive Error Correction Method Using Feature-Based Analysis Techniques for Machine Performance Improvement, Part I: Theory Derivation," Journal of Engineering for Industry, 117 (4), pp. 584-590.

[72] Kim, S. K., and Cho, D. W., 1997, "Real-Time Estimation of Temperature Distribution in A Ball-Screw System," International Journal of Machine Tools and Manufacture, 37 (4), pp. 451-464.

[73] Zhao, H., Yang, J., and Shen, J., 2007, "Simulation of Thermal Behaviour of A CNC Machine Tool Spindle," International Journal of Machine Tools and Manufacture, 47 (6), pp. 1003-1010.

[74] Lin, J., 1995, "Inverse Estimation of the Tool-Work Interface Temperature in End Milling," International Journal of Machine Tools and Manufacture, 35 (5), pp. 751-760.

[75] Chen, J. S., 1996, "A Study of Thermally Induced Machine Tool Errors in Real Cutting Conditions," International Journal of Machine Tools and Manufacture, 36 (12), pp. 1401-1411.

[76] Yang, M., and Lee, J., 1998, "Measurement and Prediction of Thermal Errors of A CNC Machining Centre Using Two Spherical Balls," ASME Trans. Journal of Materials Processing Technology, 75, pp. 180-189.

[77] Jedrzejewski, J., and Modrzycki, W., 1997, "Intelligent Supervision of

Thermal Deformations in High Precision Machine Tools," Proc. 32nd Int. MATADOR Conference, Manchester, UK, pp. 457-462.

[78] Yoshida, Y., Honda, F., and Kubota, M., 1969, "Effects of Thermal Deformation on the Cylindrical Accuracy in A Grinding Process", Proc. 10th Int. MTDR Conf., Manchester, UK, pp. 161-170.

[79] Venugopal, R., 1985, "Thermal Effects on the Accuracy of Numerically Controlled Machine Tools," Thesis, Purdue University, USA.

[80] Mou, J., Donmez, M. A., and Cetinkunt, S., 1995, "An Adaptive Error Correction Method Using Feature-Based Analysis Techniques for Machine Performance Improvement, Part II: Experimental Verification," Journal of Engineering for Industry, 117 (4), pp. 591-600.

[81] Huang, S. C., 1995, "Analysis of a Model to Forecast Thermal Deformation of Ball Screw Feed Drive System," International Journal of Machine Tools and Manufacture, 35 (8), pp. 1099-1104.

[82] Chen, J. S., 1997, "Fast Calibration and Modelling of Thermally-Induced Machine Tool Errors in Real Machining," International Journal of Machine Tools and Manufacture, 37 (2), pp. 159-169.

[83] Yun, W. S., Kim, S. K., and Cho, D. W., 1999, "Thermal Error Analysis for a CNC Lathe Feed Drive System," International Journal of Machine Tools and Manufacture, 39 (7), pp. 1087-1101.

[84] Yang, J., Yuan, J., and Ni, J., 1999, "Thermal Error Mode Analysis and Robust Modelling for Error Compensation on a CNC Turning Centre," International Journal of Machine Tools and Manufacture, 39 (9), pp. 1367-1381.

[85] Choi, J. P., Lee, S. J., and Kwon, H. D, 2003, "Roundness Error Prediction

with a Volumetric Error Model Including Spindle Error Motions of a Machine Tool," International Journal of Advanced Manufacturing Technology, 21, pp. 923–928.

[86] Lee, J. H., and Yang, S. H., 2002, "Statistical Optimization and Assessment Of a Thermal Error Model for CNC Machine Tools," International Journal of Machine Tools and Manufacture, 42 (1), pp. 147-155.

[87] Tae, J. K., Gim, T. W., and Ha, J. Y., 2003, "Particular Behaviour of Spindle Thermal Deformation by Thermal Bending," International Journal of Machine Tools and Manufacture, 43 (1), pp. 17-23.

[88] Wu, C. H., and Kung, Y. T., 2003, "Thermal Analysis for the Feed Drive System of a CNC Machine Centre," International Journal of Machine tools and Manufacture, 43 (15), pp. 1521-1528.

[89] Kim, J. J., Jeong, Y. H., and Cho, D. W., 2004, "Thermal Behaviour of a Machine Tool Equipped With Linear Motors," International Journal of Machine Tools and Manufacture, 44, pp. 749-758.

[90] Chen, J. S., 1997, "Fast Calibration and Modelling of Thermally Induced Machine Tool Errors in Real Machining," International Journal of Machine Tools and Manufacture, 37 (2), pp. 159-169.

[91] Chen, J. S., and Ling, C. C., 1996, "Improving the Machine Tool Accuracy Through Machine Tool Metrology and Error Correction," International Journal of Advanced Manufacturing Technology, 11 (3), pp. 198-205.

[92] Ahn, K. G., and Cho, D. W., 1999, "In-Process Modelling and Estimation of Thermally Induced Errors of a Machine Tool during Cutting," International Journal of Advanced Manufacturing Technology, 15 (4), pp. 299-304.

[93] Ramesh, R., Mannan, M. A., and Poo, A. N., 2003, "Thermal Error

Measurement and Modelling in Machine Tools. Part I: Influence of Varying Operating Conditions," International Journal of Machine Tools and Manufacture, 43 (4), pp. 391-404.

[94] Ramesh, R., Mannan, M. A., Poo, A. N., and Keerthi, S. S., 2003, "Thermal Error Measurement and Modelling in Machine Tools. Part II: Hybrid Bayesian Network Support Vector Machine Model," International Journal of Machine Tools and Manufacture, 43 (4), pp. 405-419.

[95] Lovett, C. D., 1989, "Progress report of the quality in automation," NISTIR 89-4045, National Institute of Standards and Technology.

[96] Koliskor, A. S., 1971, "Compensating for Automatic-Cycle Machining Errors," Machines and Tooling, 41 (5), pp. 11-44.

[97] Chen, J. S., Yuan, J. X., Ni, J., and Wu, S. M., 1993, "Real-time Compensation for Time-Variant Volumetric Errors on a Matching Centre," Journal of Engineering for Industry, 115 (4), pp. 472-479.

[98] Chen, J. S., 1995, "Computer-Aided Accuracy Enhancement for Multi-Axis CNC Machine Tool," International Journal of Machine Tools and Manufacture, 35 (4), pp. 593-605.

[99] Lo, C. H., Yuan, J., and Ni, J., 1995, "An Application of Real Time Error Compensation on a Turning Centre," International Journal of Machine Tools and Manufacture, 35 (12), pp.1669-1682.

[100] Yuan, J., and Ni, J., 1998, "The Real Time Error Compensation Technique for CNC Machining Systems," Mechatronics, 8(3), pp.359-380.

[101] Liang, J. C., Li, H. F., Yuan, J. X., and NI, J., 1997, "A Comprehensive Error Compensation System for Correcting Geometric, Thermal and Cutting Force Induced Errors," International Journal of Advanced Manufacturing

Technology, 13 (10), pp. 708-712.

[102] Mekid, S. and Ogedengbe, T., 2010, "A Review of Machine Tool Accuracy Enhancement through Error Compensation in Serial and Parallel Kinematic Machines," International Journal of Precision Technology, 1 (3/4), pp. 251-286.

[103] Yang, H. and Ni, J., 2005, "Adaptive Model Estimation of Machine-Tool Thermal Errors Based on Recursive Dynamic Modelling Strategy," International Journal of Machine Tools and Manufacture, 45, pp. 1-11.

[104] Yang, H. and Ni, J., 2005, "Dynamic Neural Network Modelling for Non-Linear, Non-Stationary Machine Tool Thermally Induced Error," International Journal of Machine Tools and Manufacture, 45, pp. 455-465.

[105] Wang, S. M., Yu, H. J. and Liao, H. W., 2006, "A New High- Efficiency Error Compensation System for CNC Multi-Axis Machine Tools," International Journal of Advanced Manufacturing Technology, 28, pp. 518-528.

[106] Kang, Y., Chang, C. W., Huang, Y., Hsu, C. L. and Nieh, I. F., 2007, "Modification of a Neural Network Utilizing Hybrid Filters for the Compensation of Thermal Deformation in Machine Tools," International Journal of Machine Tools and Manufacture, 4792), pp. 376-387.

[107] Du, Z. C., Yang, J. G.., Yao, Z. Q. and Xue, B. Y., 2002, "Modelling Approach for Regression Orthogonal Experiment Design for the Thermal Error Compensation of a CNC Turning Center," Journal of Materials Processing technology, 129, pp. 619-623.

[108] Mian, N. S., 2010, "Efficient Machine Tool Thermal Error Modelling Strategy for Accurate Offline Assessment," Thesis, University of Huddersfield, UK.

[109] Gao, Q., Yang, J. and Wu, H., 2010, "Application of ACO-BPN to Thermal Error Modelling of NC Machine Tool," International Journal of Advanced Manufacturing Technology, 50(5-8), pp. 667-675.

[110] Mayr, J., Ess, M., Weikert, S. and Wegener, K., 2009, "Compensation of Thermal Effects on Machine Tools Using a FDEM Simulation Approach," Proceedings of the 9th Lamdamap Conference, pp. 38-47.

[111] Pahk, H. and Lee, S. W., 2002, "Thermal Error Measurement and Real Time Compensation System for the CNC Machine Tools Incorporating the Spindle Thermal Error and the Feed Axis Thermal Error," International Journal of Advanced Manufacturing Technology, 20(7), pp. 487-494.

[112] Hexagon Metrology, "Sheffield Discovery II.pdf", Home Page, www.sheffieldmeasurement.com, (21/05/2009).

[113] Drozda, T., Wick, C., Bendict, J. T., and Veilleux, P. F., 1983, *Tool and Manufacturing Engineers Handbook, Vol. 4, Quality Control and Assembly*, 4th, ed., SME, Dearborn, Michigan, USA.

[114] Doiron, T., 2007, "20 °C—A Short History of the Standard Reference Temperature for Industrial Dimensional Measurements," Journal of Research of the National Institute of Standards and Technology, 112 (1), pp. 1-23.

[115] Conway, H. G., 1966, *Engineering Tolerances*, 3rd ed. Sir Isaac Pitman & Sons Ltd., London.

[116] Gladman, C. A., 1972, *Geometric analysis of engineering designs*, 2nd ed. Australian Trad Publ. Pty. Ltd., Sydney.

[117] Leadwell Taiwan, User's Guide of Leadwell V30 (hold by the CNC machining center at the CAD/CAM lab of Department of Mechanical Engineering, Curtin University).

[118] Optodyne Inc., User's Guide of LICS-100, Home Page, www.optodyne.com, (12/06/2011).

[119] Hayward, Alan T. J., 1977, *Repeatability and Accuracy: an Introduction to the Subject, and a Proposed Standard Procedure for Measuring the Repeatability and Estimating the Accuracy of Industrial Measuring Instruments.* Mechanical Engineering Publications Ltd., London.

[120] Hoffman, P. J., Hopewell, E. S., Janes, B., and Sharp, J. K. M., 2011, *Precision Machining Technology*, Delmar Cengage Learning, New York, USA.

[121] OzForex, Home Page, www.ozforex.com.au, (12/12/2012).

[122] TC Direct, Home Page, www.tcdirect.net.au, (10/12/2012).

[123] The Dave Meier Web Page, Home Page, www.n4mw.com, (11/12/2012).

[124] New Maker, Home Page, www.cn.newmaker.com, (11/12/2012).

[125] Amazon, Home Page, www.amazon.com, (11/12/2012).

[126] Just Tools, Home Page, www.justtools.com.au, (11/12/2012).

[127] HP Home and Home Office Store, Home Page, www.shopping.hp.com, (11/12/2012).

[128] Saelig Unique Electronics, Home Page, www.saelig.com, (11/12/2012).

APPENDIX A

Specifications of Leadwell V30 [117]

MACHINE SIZE:		
Length	mm (inch)	2250 (88.5)
Width	mm (inch)	2100 (82.7)
Height	mm (inch)	2368 (93)
Weight	kg (lb)	4500 (9900)
TABLE:		
Table size	mm (inch)	890 x 400 (35 x 15.7)
Table height	mm (inch)	780 (30.7)
Max. load capacity	kg (lb)	300 (660)
TRAVEL:		
X/Y/Z axes travel	mm (inch)	760/410/410+110 (30/16/20)
Spindle centre to column	mm (inch)	438 (17)
Spindle nose to table surface	mm (inch)	130-540 (5-21)
SPINDLE:		
Spindle motor	kw (hp)	5.5(7.4)-continue, 7.5(10)-30min
Spindle speed (Fanuc)	rpm	80-8000
Spindle taper		7/24 (Mas-bt40)
Gear ratio		1:1
FEED MOTOR:		
X/Y/Z axes (Fanuc)	kw (hp)	1.0/1.0/2.1 (1.3/1.3/2.8)
X/Y/Z motor type (Fanuc)		AC *a*-6/AC *a*-6/AC *a*-12
FEED RATE:		
X/Y/Z rapid feed rate	m/min(in/min)	20/20/15 (787/787/590)
Feed rate X/Y/Z	m/min(in/min)	0-5(0-196)
AUTOMATIC TOOL CHANGER:		
Tool shank type		BT-40
Pull stud type		Mas 407-T40-1
ATC type		Armless (drum)
Tool capacity		20
Max. tool diameter (adjacent)		80mm (3.1inch)
Max. tool length		250mm (9.8inch)
Max. tool weight		7kg (15lb)
ATC tool to tool		8sec
ATC chip to chip		14sec
Tool pocket pitch		95mm (3.74inch)
ACCURACY:		
Positioning		±0.01mm/full travel
Repeatability		±0.005mm
Power requirement		20KVA

APPENDIX B

Technical Specifications of LICS-100 [118]

Laser				
Stability:	0.1	ppm		
Resolution:	1 (0.01)	μin (μm)		
Range:	0-50 (0-15)	ft (meters)		
Rate (max.):	40 (1000)	inch/sec. (mm/sec.)		
ATC Probe				
Pressure:	2	mmHg		
Sensitivity:	0.2	degree, C		
Outputs	Computer interface, USB			
Operating Environment				
Temperature:	50-95°F (10-35°C))			
Altitude:	0-10,000 feet (0-3000 m)			
Humidity:	0-95 percent (non-condensing)			
Components	Width (in)	Height (in)	Length (in)	Weight (lb)
Laser head	5 (127mm)	2.43(61.7mm)	8.5(215.9mm)	5(2.3kg)
Retroreflector	Φ0.5 (12.7mm)	---	0.35(8.9mm)	0.1(90gm)
Interconnection				
Cables number:	1 or 2			
Length (USB cable)	12 ft (3.6m)			
Power Requirements:	85-264 VAC, 50-60HZ, 100W			

APPENDIX C

X-Axis Positioning Errors

Unit: μm Bi-direction measuring
Machine: Leadwell V30 Date: 15/06/2011
Air Temp = 21.5ºC, Air Pressure = 765mmHg, Humidity = 50

Position （mm）	IX0	IX50	IX105	IX145	IX185	IX225	IX285
0	0.13	0.42	0.02	0.25	-0.02	0.02	0.20
50	4.20	3.51	4.78	7.33	5.33	6.67	7.30
100	7.52	7.58	10.67	13.28	11.95	13.89	14.54
150	8.40	9.10	12.86	16.78	15.42	18.02	20.51
200	11.23	11.89	17.55	22.69	21.14	23.97	26.50
250	14.65	15.35	22.88	28.96	28.03	30.87	33.41
300	16.63	18.03	26.35	33.50	33.63	36.52	39.29
350	19.64	20.71	31.30	39.42	40.54	43.19	46.43
400	22.48	23.76	36.39	45.40	45.67	49.21	52.90
450	25.29	26.78	40.48	50.75	51.54	55.29	59.64
500	28.04	29.30	44.56	56.09	57.36	60.65	66.21
550	30.22	32.12	49.09	61.45	62.70	66.58	72.28
600	34.31	35.64	54.55	67.54	69.32	73.18	80.04
650	36.52	38.70	58.39	72.80	74.66	78.56	85.92
700	39.94	41.74	62.71	78.14	80.15	85.13	92.17
750	40.84	42.78	64.89	81.00	83.56	89.23	96.29
750	35.80	38.35	60.48	76.59	79.45	84.80	92.45
700	35.53	37.19	58.91	74.00	76.39	81.06	88.38
650	32.69	34.56	54.23	68.81	70.69	75.35	82.08
600	30.49	31.22	50.16	63.82	65.70	70.01	76.35
550	25.90	27.16	44.81	57.64	58.90	62.44	68.58
500	22.80	23.84	39.49	51.69	52.91	56.11	62.48
450	20.28	21.51	36.01	46.89	45.91	50.78	56.13
400	17.36	18.08	31.34	41.58	40.11	44.78	49.55
350	14.15	14.96	26.63	36.31	34.75	38.65	43.22
300	11.16	11.92	21.91	30.33	28.51	32.31	36.42
250	8.47	9.52	18.46	25.54	23.96	27.43	30.65
200	6.01	6.21	13.76	20.71	19.62	21.19	25.12
150	4.35	4.35	10.33	16.16	15.59	16.71	19.27
100	2.46	2.51	7.54	12.87	12.06	12.84	14.68
50	-0.86	-0.93	2.83	7.25	6.14	6.40	8.52
0	-3.81	-3.77	-1.87	2.52	0.59	0.65	2.01

APPENDIX D

Y-Axis Positioning Errors

Units: μm, Bi-direction measuring
Machine: Leadwell V30 Date: 16/06/2011
Air Temp = 22°C, Ai r Pressure = 768mmHg, Humidity = 50

Position (mm)	IY0	IY18	IY51	IY85	IY136	IY194
0	-0.15	0.22	-0.42	-0.69	0.00	0.00
50	2.15	5.43	5.02	6.43	7.45	8.51
100	3.69	9.92	9.94	13.09	14.92	16.48
150	7.17	14.59	15.33	20.31	22.26	25.92
200	11.45	21.85	25.04	29.85	32.62	36.96
250	13.61	25.68	30.57	38.59	40.72	45.51
300	17.96	32.45	38.13	47.75	49.64	55.38
350	23.90	39.15	47.17	56.28	59.43	66.15
400	28.57	43.89	53.86	63.80	66.86	75.34
400	24.41	40.03	49.48	60.33	62.10	70.93
350	21.38	35.23	43.52	53.63	55.27	62.64
300	16.25	27.19	33.91	44.32	44.39	51.43
250	11.36	20.17	25.32	32.50	33.49	39.80
200	8.78	15.49	20.04	24.02	26.10	30.77
150	5.16	9.29	10.90	15.05	16.73	20.95
100	1.78	4.50	4.29	6.84	8.09	10.97
50	-0.91	0.33	-1.00	-0.43	1.51	2.75
0	-3.97	-5.23	-7.55	-8.27	-6.33	-6.22

APPENDIX E

Z-Axis Positioning Errors

Units: μm, Bi-direction measuring
Machine: Leadwell V30 Date: 16/06/2011
Air Temp = 22°C, Air Pressure = 768mmHg, Humidity = 50

Position (mm)	**IZ0**	**IZ16**	**IZ45**	**IZ75**	**IZ138**
0	-0.01	0.01	-0.01	0.01	-0.01
50	0.26	3.33	5.29	5.98	6.57
100	-1.43	3.65	6.84	9.34	10.02
150	-1.16	7.14	11.51	15.88	17.79
200	1.02	12.99	18.10	22.50	26.28
250	2.81	18.20	24.72	30.07	34.36
300	5.83	24.24	32.46	38.17	43.88
350	9.32	31.48	39.70	46.67	52.36
400	11.47	36.78	45.66	53.83	60.20
400	11.47	36.14	45.02	53.29	60.16
350	9.32	31.45	39.69	46.15	52.14
300	6.57	24.92	32.49	38.17	43.88
250	3.11	17.83	24.62	28.70	33.51
200	2.24	13.65	18.71	22.22	26.25
150	-0.85	7.56	11.01	14.00	17.19
100	-0.79	3.68	6.50	8.71	10.62
50	0.88	2.98	4.01	5.93	6.57
0	0.01	0.63	0.08	0.70	0.63

APPENDIX F

List of Supporting Papers

Journal Papers

1. Lu, Y. X. and Islam, M. N., 2011, "A New Approach to Thermally Induced Volumetric Error Compensation," International Journal of Advanced Manufacturing Technology, DOI 10.1007/s00170-011-3849-6, available online.
2. Lu, Y. X. and Islam, M. N., 2011, "A Simplified Method for Thermally Induced Volumetric Error Compensation," International Review of Mechanical Engineering (IREME), **5**(5), pp. 1006-1012.
3. Lu, Y. X. and Islam, M. N., 2011, "The Effects of the Thermal Behaviour of a Machine Tool on the Dimensional Accuracy of Parts," International Review of Mechanical Engineering (IREME), **5**(1), pp. 79-87.

Conference Papers

1. Lu, Y. X. and Islam, M. N., 2012, "Application of a Newly Developed Thermally Induced Volumetric Error Compensation Model in Improving Dimensional Accuracy of Parts," *International Conference on Engineering Materials ICEM2012*, 30th-31st December, 2012, Singapore.
2. Lu, Y. X. and Islam, M. N., 2012, "Prediction and Analysis of Thermal Effects on Dimensional Accuracy of Machined Parts," *Proceeding of the International Conference on Mechanical Engineering and Mechatronics*, August 15th-17th, 2012, Ottawa, Canada, Paper No 31, pp.1-8.
3. Lu, Y. X. and Islam, M. N., 2010, "An Experimental Investigation of Thermal Effects on the Dimensional Accuracy of Machined Parts," *Proceeding of 2010 2nd International Conference on Computer Engineering and Technology,* Chengdu, China, 16th-18th April, 2010, v. 5, pp.455-459.

Paper under Review

1. Lu, Y. X. and Islam, M. N., *under review*, "An Investigation of Thermal Behaviour of a Machine Tool on the Dimensional Accuracy of Machined Parts," International Journal of Mechanical Engineering and Mechatronics.